ON-LINE CONTROL OF PROCESS UNIFORMITY USING CATEGORIZED VARIABILITIES

by

SUNGDO HA

B.S., SEOUL NATIONAL UNIVERSITY, 1983
M.S., KOREA ADVANCED INSTITUTE OF SCIENCE & TECHNOLOGY, 1985

Submitted to the Department of Mechanical Engineering
in Partial Fulfillment of the Requirements for the Degree of
DOCTOR OF PHILOSOPHY IN MECHANICAL ENGINEERING

at the
MASSACHUSETTS INSTITUTE OF TECHNOLOGY

June 1993

Signature of Author _____
Department of Mechanical Engineering
May 12, 1993

Certified by _____
Emanuel Sachs
Professor of Mechanical Engineering
Thesis Supervisor

Accepted by _____
Ain Sonin
Chairman, Departmental Committee on Graduate Students

ON-LINE CONTROL OF PROCESS UNIFORMITY USING CATEGORIZED VARIABILITIES

by

SUNGDO HA

Submitted to the Department of Mechanical Engineering
on May 12, 1993, in partial fulfillment of the requirements
for the Degree of Doctor of Philosophy in Mechanical Engineering

ABSTRACT

The uniformity of process output characteristics is a critical problem in improving process quality. Because of the difficulties of modeling, uniformity has been optimized using off-line methods. However, off-line methods cannot respond to changes of process conditions and compensate for incoming material variations. This work is aimed at developing a new *on-line* control methodology of process uniformity.

This methodology extends the robust design method to support the on-line control of processes. Process variabilities are categorized into *non-tunable* and *tunable*. Process parameters are classified according to their effects on non-tunable and tunable variabilities, respectively. *Robustness factors* are used in off-line optimization to minimize the non-tunable variability due to stochastic disturbances and highly nonlinear effects. *Tuning factors* are used for the on-line control of tunable variabilities in the face of process condition changes and incoming material variations. *Adjustment factors* are used to adjust the process mean to target. Since only the tunable variability is controlled on-line, the risk of applying on-line control of uniformity is reduced, and simple control algorithms are applied effectively.

The methodology is applied to single wafer plasma etching processes for the improvement of within-a-wafer uniformity. The radial component of the uniformity is categorized as a tunable variability, and the circumferential component is categorized as a non-tunable variability by considering the axisymmetry of the single wafer plasma etching equipment. It is shown that radial uniformity is improved by on-line control using single or multiple tuning factors while also maintaining the circumferential uniformity as optimized off-line. This on-line control methodology results in higher within-a-wafer uniformity compared with off-line optimization alone.

Thesis Supervisor: Emanuel Sachs

Title: Associate Professor of Mechanical Engineering

TO JEONGHYUN, MYUNGHYUN, MY PARENTS,
& KEASOOK

ACKNOWLEDGMENTS

My sincere gratitude goes to Professor Emanuel Sachs, who has provided guidance and counseling throughout the course of my stay at MIT. This work would not have been possible without him. His insight and perspective on the project have always inspired me. I learned very much from him in every aspect. I thank him deeply. Also, I thank the other committee members, Professors Don Clausing and Herbert Sawin, for their valuable advice.

I would like to thank Dr. Genichi Taguchi and Dr. Madhav Phadke for their constructive remarks on this work.

I wish to thank my colleagues working on the process optimization and control project. Special thanks go to Andy Guo and Albert Hu for their help from the beginning of my stay at MIT. I thank Armann Ingolfsson, Stefan Thomke, Ka Shun Wong, Octavio Marenzi, and Jay Ochoco for the useful insights. Also, I would like to thank Tim Dalton especially for his time and effort in performing the polysilicon etching experiments.

I am also grateful to all the members of the staff at Microsystems Technology Laboratories who taught me how to use the clean room equipment and helped me with the experiments. Among them are Joe Walsh, Brian Foley, Velma McClure, Paul Tierney, Tim Tyson, and Rob Cuikay. Without their help, I could not have completed the experiments successfully.

A very special thank goes to my family. My lovely wife, Keasook, has been a great supporter. During my studies at MIT, Keasook and I have been blessed with two sons, Jeonghyun and Myunghyun. Although they keep us busy, they give us great pleasure of being their parents. I love you. Love and care from my parents, parents-in-law, brothers, and sisters made this endeavor possible. Their encouragement and support are sincerely cherished. Again I thank them all.

Finally, I would like to thank the SEMATECH Massachusetts Center of Excellence under contract 88MC503 for its support.

CONTENTS

LIST OF FIGURES

LIST OF TABLES

CHAPTER 1

INTRODUCTION

1.1 Motivation

Process quality has been controlled by statistical process control (SPC) methods since control charts were introduced by Shewhart in the late 1920s and promoted by Deming in the 1950s [1]. In mass production systems of the past, the SPC method was an effective tool for process quality control, because the number of one kind of products was large enough to render the statistical modeling of processes meaningful. When a mass production system is *in control*, the process conditions of the system are believed to remain invariant, and the characteristics of the products are assumed to have a stable distribution with constant means and constant variances. Once the distribution of process output characteristics is statistically modeled, the models are used to monitor process conditions by comparing the measured values of product characteristics with model predictions in order to detect if there is an *out of control* status. It is only when the process output characteristics show the out of control status that process engineers are called upon to check and tune the process [2].

Production systems have evolved from mass production systems to flexible manufacturing systems that produce many kinds of products with a low quantity of products, and each product is produced in small quantities [3]. In flexible

manufacturing systems, product specifications change frequently, and process conditions are adjusted accordingly. Processes are no longer stable in a statistical sense, and the SPC method should be modified to monitor process quality properly [4]. In pursuit of higher quality, it is imperative not only to monitor process quality using the SPC method but also to control it actively. Hence, it becomes necessary to develop a new methodology for quality control in flexible manufacturing systems.

Quality control during actual production is referred to as *on-line*, control whereas quality control during product and process designs is referred to as *off-line* control [5]. On-line control has the possibility of achieving higher quality since it controls the process while the actual products are being manufactured. Every process experiences process condition changes whether they are slow or abrupt. On-line control can compensate for the changes so that higher process quality may be achieved. On-line control can also maintain high quality by compensating for incoming material variations. Since on-line quality control requires on-line measurements of the product characteristics, it is now possible to accomplish on-line control with the development of automated measurement devices. In flexible manufacturing systems, process conditions change frequently in order to manufacture products with different specifications, which makes on-line control a critical control methodology for higher quality.

Even though on-line process control has advantages over off-line process control for flexible manufacturing systems, there are still some problems to be solved. On-line control is based on on-line measurements that cannot cover all the characteristics of a product. Characteristics such as product reliability, product life time, and end-product performance, for example, may not be measured on-line but may affect the process quality. Therefore, on-line control based only on on-line measurable characteristics has the potential to degrade those characteristics that cannot be measured on-line. Also, some product characteristics may be too complex for on-line control. For example, when product characteristics have a very highly non-linear relationship with the process parameters, it is difficult to control them on-line.

This thesis is motivated by the need to develop an effective and a simple methodology for on-line process quality control. Among many process characteristics, the uniformity of the process output characteristics is important for higher quality.

However, uniformity is very difficult to model because of its stochastic nature and highly non-linear dependency on process parameters. This thesis is an attempt to develop a new on-line control methodology of process uniformity.

1.2 Process Quality Control

1.2.1 Process Quality

In manufacturing systems, *quality* is determined by how closely process outputs meet the target values such as the physical dimensions of the parts, the material properties of the products (e.g., mechanical, electrical, chemical, etc.), and the material characteristics of the products (e.g., surface finish, color, shape, etc.). Process outputs usually have some distribution of their characteristics, and the distribution is often found to be normal as expected by the central limit theorem [6].

Figure 1.1 shows the normal distributions of output characteristics from three different processes with the same target value. It shows that the output characteristics of process C have a mean value that deviates from the target value, and the output characteristic mean of process B is the same as the target. Processes B and C have the same output characteristic variances. Process A has the same mean as process B but has smaller variance. From the comparisons of the mean values and variances, process A is the best in terms of quality since it has more products with output characteristics closer to the target, and process C is the worst since it has only a small number of products with output characteristics close to the target.

In order to improve process quality, it is necessary not only to adjust the mean values of the output characteristics to the target (from process C to process B in Figure 1.1) but also to minimize the variances of the output characteristics (from process B to process A in Figure 1.1). Control of the mean values has been applied by using the methods explained in Section 1.2.3, and the mean values are controlled to meet the target by tuning process parameters. After the mean values are adjusted to the target, reducing the variances is the key to improving quality. Hence, it is necessary to measure appropriately the quality loss caused by the variances.

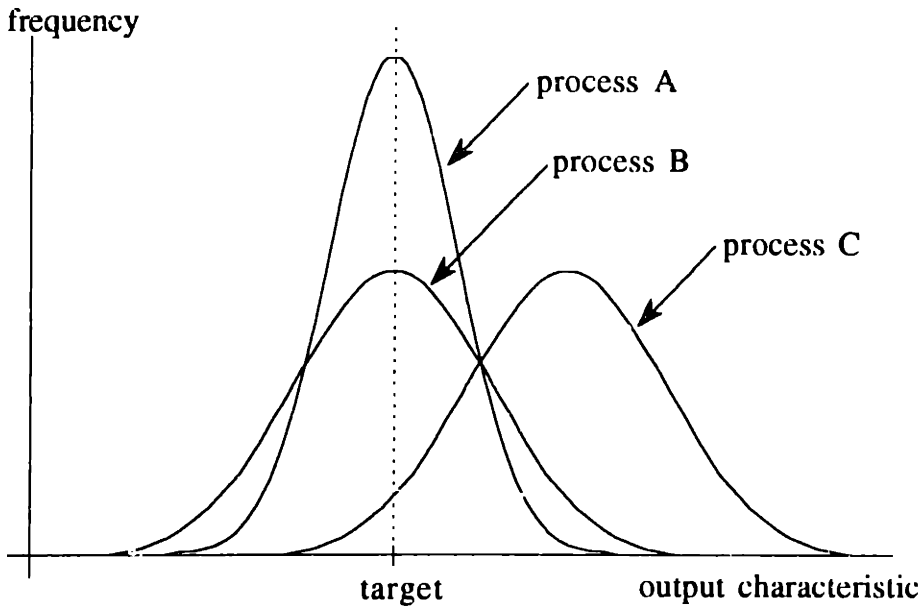

Figure 1.1 Output characteristic distributions

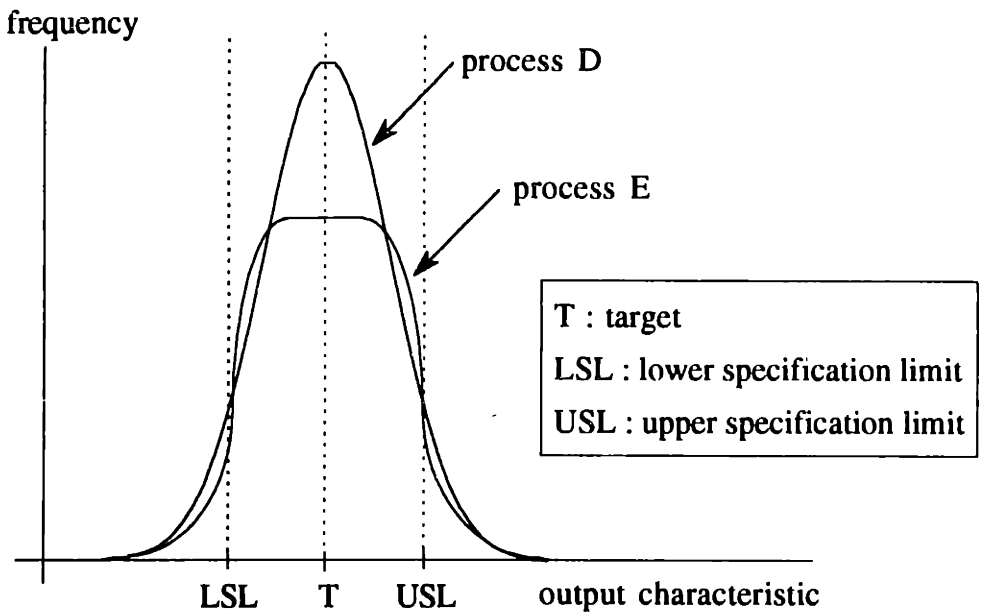

Figure 1.2 Comparison of processes using the fraction defective method

The quality of a process is usually measured by the fraction of the products whose output characteristics are out of the specification limits. Processes with the same fraction of defective products, however, can have a significantly different

distribution of their output characteristics as shown in Figure 1.2. The figure illustrates that process D and process E have the same mean values that meet the target exactly and a similar fraction of defective products. However, when the products within the specification limits are compared, process D has a larger percentage of products whose output characteristics are closer to the target value than process E; hence, process D is a better process.

The fraction defective method explained above does not appropriately measure the quality of the processes due to the variances, because the products within the specification limits are treated equally regardless of the magnitude of deviations from the target. The quality loss increases stepwise as the output characteristic crosses the specification limits as shown in Figure 1.3.A, which is not realistic. Instead, a continuous function is proposed for measuring the quality of a process [7].

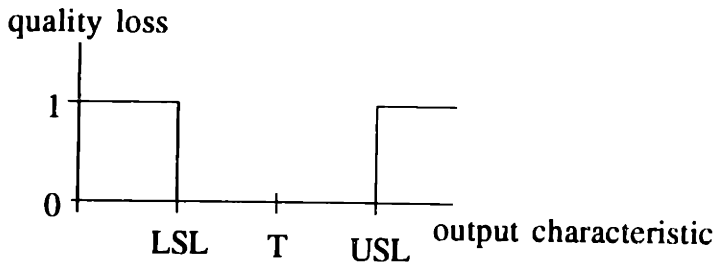

A. fraction defective quality loss function

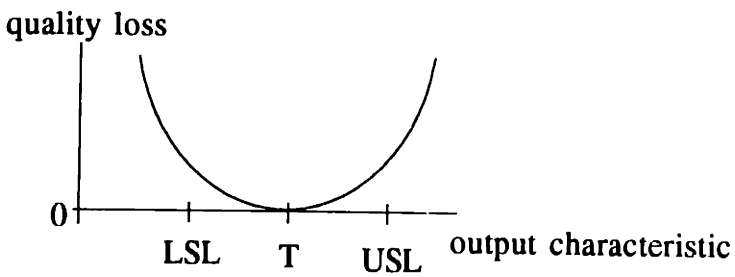

B. quadratic quality loss function

Figure 1.3 Quality loss functions

A quality loss function, QL(y), is defined as a continuous function of the output characteristic, y, in order to calculate quality loss due to the variations. The function is

expressed by the Taylor series approximation around the target of the output characteristic, T, as follows:

$$QL(y) = C_0 + C_1 \times (y - T) + C_2 \times (y - T)^2 + C_3 \times (y - T)^3 + \cdots . \qquad \text{(Eq. 1.1)}$$

In the above expression of the quality loss function, coefficient C_0 is zero since the quality loss is zero when y meets the target T, and coefficient C_1 is also zero since the quality loss is minimum when y = T, i.e.,

$$QL(T) = 0 , \text{ and } \left[\frac{\partial (QL)}{\partial y} \right]_{y=T} = 0 .$$

Disregarding the higher-order terms, the quality loss function can be represented as a quadratic function as follows:

$$QL(y) = K \times (y - T)^2 , \qquad \text{(Eq. 1.2)}$$

where K is the quality loss coefficient [8]. The quality loss coefficient is obtained by comparing the magnitudes of specification limits with the magnitudes of actual loss (often in dollar value) when the product is out of specification limits. Figure 1.3.B shows the quadratic quality loss function.

1.2.2 MIT Process Control System

A modular framework of a process control system is under development at MIT [9]. The MIT process control system is being developed for an application to VLSI (very large scale integration) fabrication processes, but the algorithms of the control system are general enough to be applicable to other manufacturing processes. The objective of the control system is to improve process quality by applying optimization and control. Figure 1.4 is the schematic block diagram of the system.

For the effective control of processes, the process control system has three main modules: the flexible recipe generator (FRG), the run by run (RbR) controller, and the real time controller (RTC). The modules cover different ranges of process parameter space respectively, and have different strategies for optimization and control. FRG is for the off-line optimization of processes using the equipment models when new specifications or new designs are given. FRG covers the widest range of

process parameter space and generates the initial recipe (process parameter value) that is considered to be in the region of global optimization according to the equipment models inside. The equipment models of FRG are usually constructed using the data from off-line designed experiments. FRG is also invoked later when it is indicated that the processes need a new parallel optimization.

The RbR controller is for the optimization and control of the processes on a run by run basis. The RbR controller uses pre-process measurement data for feed-forward control and post-process measurement data and summarized *in situ* measurement data for feedback control. The RbR controller covers the region of global optimization that is around the initial recipe. First, the optimization of the processes is performed sequentially, starting with the initial recipe from FRG and continuing until optimization is no longer necessary. Sequential optimization improves the quality of the processes further because it explores the region of global optimization thoroughly. After the optimization, on-line control maintains the optimized quality by generating updated recipes for each run. The recipes are determined by the equipment models that reside in the RbR controller and that are updated on a run by run basis. The model adaptation is performed in two ways: gradual model modification and rapid model modification. The gradual model modification is aimed to compensate for slow changes of process conditions such as aging, tool wear, material buildup, process condition drifts, etc., and the rapid model modification is for sudden changes such as cleaning, material change, preventive maintenance, equipment part replacement, etc. [10]. The RbR controller is also responsible for determining which type of modification is necessary [11].

RTC accepts *in situ* measurement data as inputs and controls the process parameter values while the processes are being run. RTC controls the processes real time by making minor changes to the process parameters; hence, it covers the smallest range of the process parameters that is closer to the updated recipe determined by the RbR controller. Since *in situ* measurement data are used for real time control, any differences of the process output characteristics from the target can be controlled even when they are unknown to the RbR controller. Finally, RTC has the responsibility for controlling the processes so the target may be satisfied.

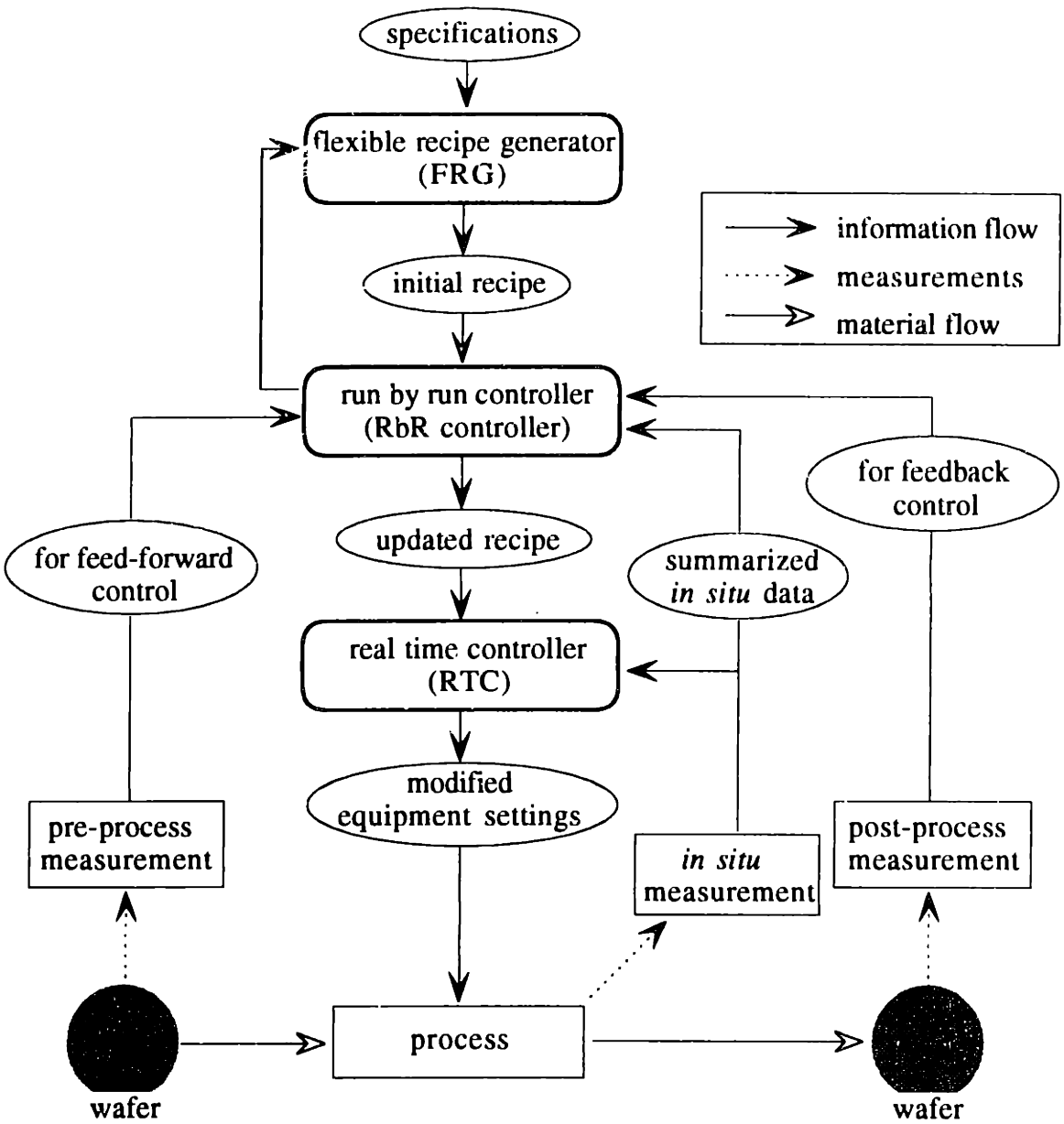

Figure 1.4 Schematic block diagram of the MIT process control system for VLSI fabrications

By dividing the control actions into the terms of time scales and the process parameter ranges, the control system has more flexibility and efficiency. Algorithms appropriate for each module either have been developed or are under development. Several algorithms have been implemented and the application examples are as follows: modeling and optimization of an LPCVD (low pressure chemical vapor

deposition) process, uniformity control of a silicon epitaxy process, a tungsten CVD (chemical vapor deposition) process, single wafer plasma etching processes, etc. The developed process control system will also be incorporated in the MIT CAFE (computer aided fabrication environment) System [12].

1.2.3 Related Works

This section introduces existing process optimization and control methods such as the traditional SPC method, the generalized SPC method, the sequential optimization method, the multiple response surface method, the method combining the automatic control and the traditional SPC method, and the multivariate SPC method.

The SPC method begins with the idea that every process has a certain amount of inherent variability no matter how well it is designed and no matter how carefully it is controlled. In the SPC method, a process is regarded in statistical control as long as the magnitude of process variability is within certain limits. These limits are determined by the magnitude of inherent variability. When process variability becomes large enough to make process performance unacceptable, it is regarded that the source of variability is not a so-called *chance cause* but a special cause or an *assignable cause*. The objective of the SPC method is to detect the presence of assignable causes as quickly as possible so corrective actions may be taken to reduce the number of non-conforming products during the manufacturing process. However, the SPC method alone does not provide the guidance on how to correct the process conditions in order to restore process variability when the assignable causes are detected.

The traditional SPC method assumes that the processes are statistically stable with inherent variabilities when they are in control. Process conditions should not be changed for processes to remain statistically stable. Hence, this method is not appropriate for processes that are being controlled, since controlling action changes the process conditions and makes the processes no longer statistically stable. In order to make it possible to detect the presence of assignable causes while the processes are controlled, a generalized version of a traditional SPC method was developed by combining traditional control charts and the regression analysis method [11][13]. In the generalized SPC method, regression models of processes are used

to predict process output characteristics when the control inputs change. The differences between the model predictions and the measured output characteristics are monitored: only the measured output characteristics are monitored in the traditional SPC method. By monitoring the differences, the effects of the controlling actions are accounted for of and only the true variability of the processes is measured.

Control charts from the traditional SPC method and the generalized SPC method are compared in Figure 1.5. Figure 1.5.A is an individual control chart of a statistically stable process by the traditional SPC method. The figure shows the center value of output measurements as well as the upper control limit (UCL) and the lower control limit (LCL). No output is beyond the control limits, which means the process is in control.

Figure 1.5.B is a plot of the process output characteristic versus the control input when the control inputs are increased from x_1 to x_{19}; the output characteristic is modeled as a linear regression function of the control input. The differences between the measurements and the model predictions are due to either model errors or inherent variabilities of the process. All the actual output characteristics are within the confidence limits, which shows that the process is statistically stable. However, if the traditional SPC method is applied, false alarms will occur as shown in Figure 1.5.C. The figure shows that measurements of runs 14, 15, 16, and 17 are beyond the control limits when the traditional SPC method is used. They are caused by control actions not by assignable causes, which means that the process is not out of control. The figure also shows the control chart when the generalized SPC method is applied; it is plotted as open circles. These represent the differences between the model predictions and the measured output characteristics and show no false alarms. The generalized SPC method was implemented in the RbR controller of the MIT process control system to detect sudden changes and to invoke accordingly the rapid model modification algorithm.

In manufacturing systems, it is often required to improve process performances while the actual production continues. Sequential optimization methods are applied during actual production to enhance process quality. Also, experiments are designed in a small range around the current process parameter value to reduce the risk of producing scraps.

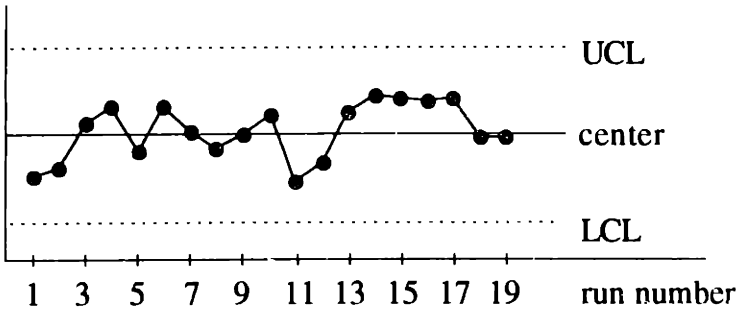

A. an individual control chart of a statistically stable process

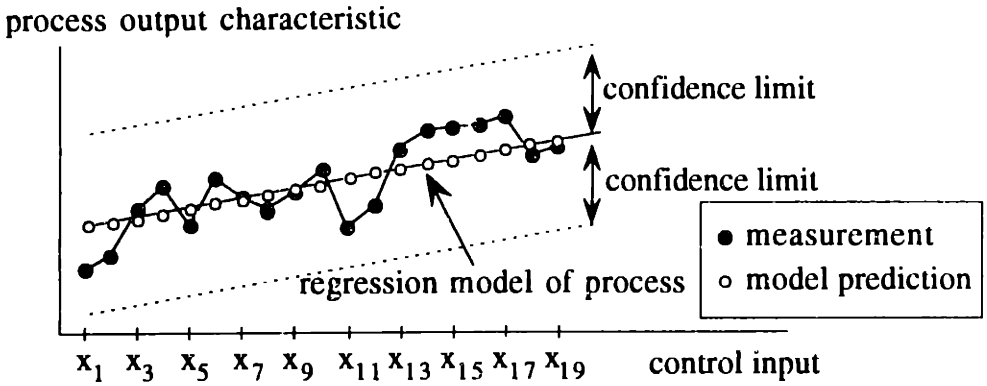

B. process output changes due to control

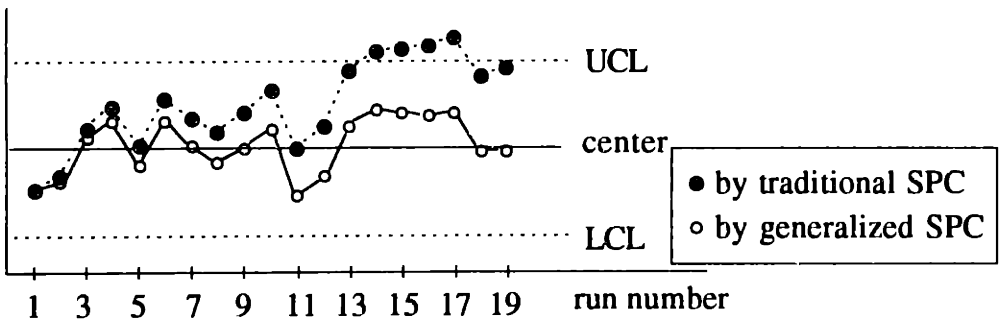

C. control charts of the process shown in B

Figure 1.5 Traditional SPC method vs. generalized SPC method

Figure 1.6 shows how the sequential optimization of a process is performed. The process performance, Y, is shown to be optimized using one process parameter, X, for simplicity. Figure 1.6.A shows experimental data around the current process

parameter value X_0. The entire performance response is unknown yet but is drawn for illustration purposes. Using the current experimental data, a quadratic model of the process performance is constructed as shown in Figure 1.6.B. Note that the quadratic model is valid only in the vicinity of the current process parameter value. Then the performance is optimized using the currently available model by determining the optimizing process parameter value. Figure 1.6.C shows the current model and its optimizing process parameter value X_1. It is noted that the moving distance from X_0 to X_1 is confined because of the uncertainty of the model.

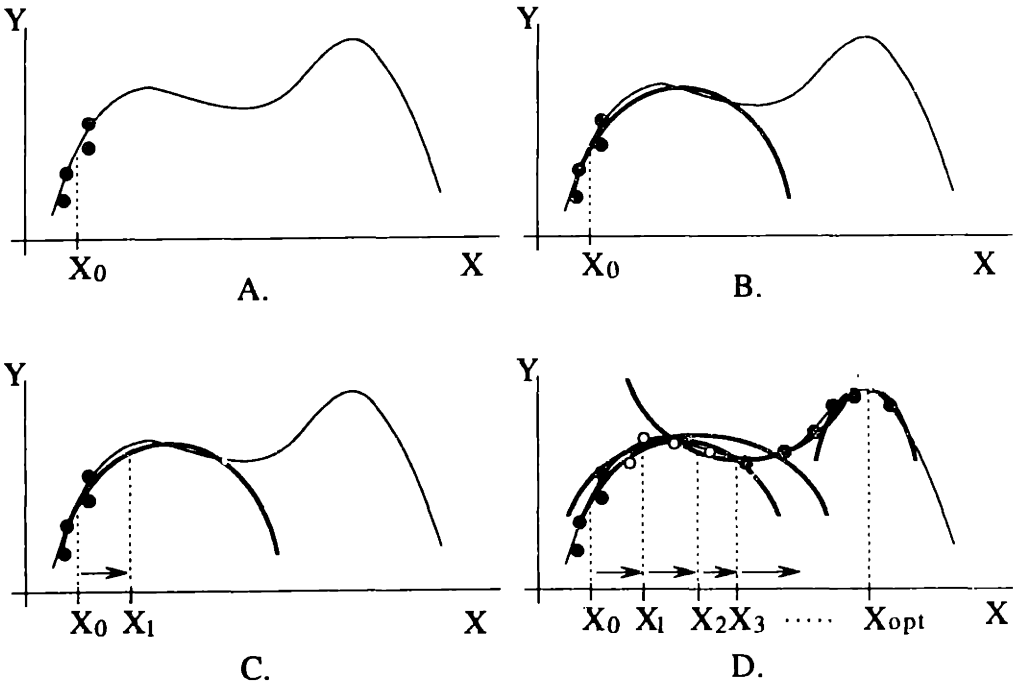

Figure 1.6 Illustration of sequential optimization

Other experiments are then designed around X_1 and a new model is constructed. A new optimizing process parameter value X_2 is determined using the new model and other experiments are designed again around X_2. These sequences continue until the true global optimizing process parameter value, X_{opt}, is found as shown in Figure 1.6.D. The figure also shows that the local models are different from the other local models since they are based on the local experimental data.

Evolutionary operation (EVOP) is one of the sequential optimization methods [14]. In EVOP, the improvement of process performances is achieved gradually by changing the process parameter values in the direction of the increasing process performances. These are determined by the experimental results that are performed in the vicinity of the current operating process parameter value. Well-organized worksheets are prepared so the procedure may be performed easily on manufacturing floors.

Another sequential optimization algorithm is implemented by a commercial software package called Ultramax® [15]. In Ultramax®, the data from the previous experiments as well as all the historical data are used for building process models. The data are weighted according to their age, i.e., larger weights are given to more recent data. The sequential optimizer also has the capability of exploring the process parameter space when designing the next experiments so the process can be modeled more accurately [16]. The models become more precise around the optimum point as more runs are performed as suggested by the optimizer, which increases the performance of optimization over the parallel optimization methods.

The on-line control of processes requires the capability of rapid model adaptation for higher performance. A new modeling methodology called the multiple response surface method was developed, and spatial uniformity of processes was modeled effectively [17]. In the methodology, multiple, low-order polynomials are used to model the output characteristics at each of the measurement sites within a batch of products. Process performance models are then obtained by combining these multiple models. Using the combined process performance models, process performance is optimized and controlled. The advantages are effective modeling using a small number of data, rapid adaptation of the models for the process condition changes, and better immunity against process noises.

Besides the MIT process control system, other approaches were to combine the traditional SPC method and the automatic feed-forward/feedback control theory to exploit the strengths of both [18][19]. Automatic control theory concepts are used to minimize the deviations from the target by making frequent process adjustments while fundamental improvements are gained by using SPC concepts that detect changes from past performances and lead to the identification of their root causes. Dynamic

behaviors of processes, for example, are modeled using a time series analysis method, and appropriate control actions are determined based on the model. When changes in process performances are so large that the automatic control cannot compensate, their root causes are identified by the SPC methods and are eliminated.

Process quality is often determined by more than a single process output characteristic. When multiple process output characteristics are measured, it is possible that they are cross-correlated. In such cases, univariate approaches for the process quality measurement are not appropriate and can be misleading, since the control limits of each output characteristic are affected by the correlation with others. Multivariate statistical process control methods have been developed to monitor process conditions using multiple *in situ* process condition measurements or multiple post-process measurements of process output characteristics [20][21]. Multiple measurements are combined to calculate a statistic, such as Hotelling's T^2 statistic or Mahalanobis's D^2 statistic, and the statistic is monitored in a single control chart to detect process condition changes.

1.2.4 Robust Design Method

As stated in Section 1.2.1, the adjustment of the mean values of the output characteristics to the target as well as the minimization of variations are necessary to improve process quality. The method of *robust design* has been developed to meet such twofold goals [22][23]. In this method, variances of output characteristics are considered the effects of process disturbances and are minimized by finding the process parameter values that make the processes *robust* against process disturbances. The magnitude of the effects of the process disturbances is measured by a defined quantity called the SN ratio [24]. The mean values are then adjusted to the target using a process parameter called an adjustment factor. Based on the experimental results, the adjustment factor is selected among the process parameters to change the mean value without changing the robustness of the process.

The following example illustrates how the robustness of a process is optimized [19]. Output characteristics are usually non-linear over a wide range of process parameters. Because of the non-linearity, output characteristics have different sensitivities to process parameter variances at different process parameter values.

The variances are often due to stochastic noise, disturbances from the environment, aging of the equipment, etc. In order to optimize the robustness, proper values of the process parameters are determined so that the process has the minimum sensitivity.

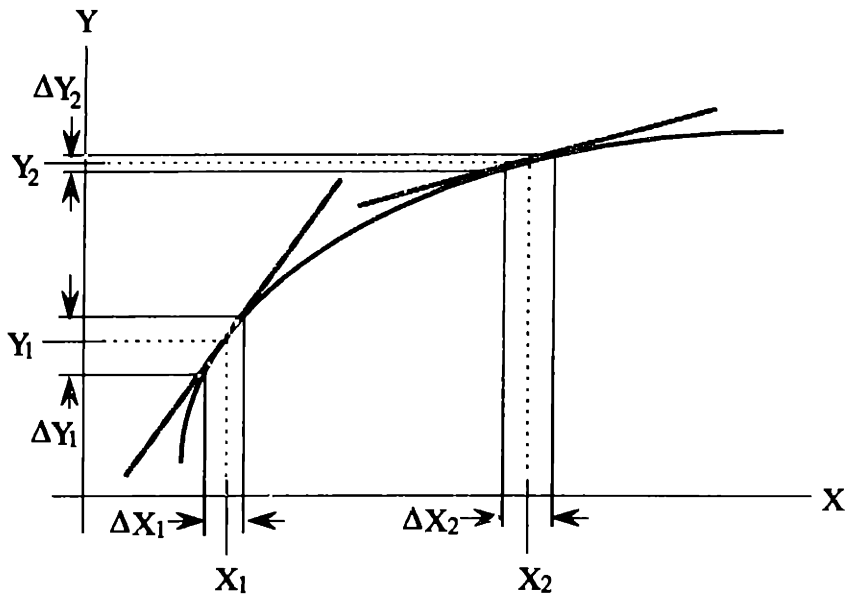

Figure 1.7 Illustration of robustness optimization

In Figure 1.7, an output characteristic, Y, which has a non-linear relationship with a process parameter X, is considered for simplicity. Because of the non-linearity, the output characteristic sensitivity at process parameter value X_1 is different from the sensitivity at process parameter value X_2. The sensitivities are represented as the slopes of two tangential lines to the output characteristic response curve in the figure. When the process parameter is set at X_1, the output characteristic has a larger sensitivity to the process parameter variations than when the process parameter is set at X_2. For the same magnitude of process parameter variations, ΔX_1 and ΔX_2, variations in the output characteristic have different magnitudes. ΔY_1, the output characteristic variation at X_1, is larger than ΔY_2, the output characteristic variation at X_2. Therefore, X_2 is more effective than X_1 for optimizing robustness. The mean output characteristic value Y_2 is to be adjusted to the target value using the adjustment factor in a following procedure.

In the example above, the variation of the process parameter is considered a disturbance to the process. The concept of disturbances may be extended to the different kinds of causes. For example, when spatial uniformity is of concern, the disturbance is the difference of the product positions. Due to the position differences, the products experience different process conditions, which causes non-uniformity. Such process condition disturbances are represented as ΔX in Figure 1.7. Since the sensitivities vary for different X values, the effect of the same magnitude of disturbances resulting from positional dependence can be minimized by selecting the proper process parameter values.

SN ratios are used for the measurement of process robustness. They are defined according to the characteristics of each process. For example, when there is a target value for the process output characteristics, the SN ratio is defined as follows: Total quality loss, QL, due to the deviations of n products from the target, T, is

$$QL = K \sum_{i=1}^{n} (Y_i - T)^2 = K\left[(\mu - T)^2 + \sigma^2\right] , \qquad \text{(Eq. 1.3)}$$

where K is the quality loss coefficient, μ is the mean, and σ^2 is the variance. When the mean is adjusted to the target, the total quality loss becomes as follows:

$$QL_a = K\, T^2 \left[\frac{\sigma}{\mu}\right]^2 , \qquad \text{(Eq. 1.4)}$$

where QL_a is the total quality loss after adjustment.

The SN ratio is defined from the total quality loss after adjustment by taking log transforms of $\left[\frac{\sigma}{\mu}\right]^2$ as follows:

$$\text{SN ratio} = -10 \log_{10}\left[\frac{\sigma}{\mu}\right]^2 = 10 \log_{10}\left[\frac{\mu}{\sigma}\right]^2 . \qquad \text{(Eq. 1.5)}$$

The total quality loss after adjustment is to be minimized by maximizing the SN ratio. The adjustment factor is a process parameter that has little effect on the SN ratio so the mean can be adjusted without changing the process robustness.

The SN ratio above is derived from the quadratic quality loss function under the assumption that the standard deviation of the output characteristics changes proportionally to the mean of the output characteristics. Another performance

measure called PerMIA (performance measures independent of adjustment) is also proposed as an extension of the SN ratio [25]. PerMIA's can be used when the assumption of proportionality between the mean and the standard deviation is not valid.

In the case of dynamic systems, where process output characteristics are expected to follow signal factor values, a scaling factor is selected to tune the proportionality between the signal factor value and the process output characteristic value, just as the adjustment factor is selected to adjust the mean to the target in the above static process. In dynamic systems, the SN ratio is defined as follows:

$$\text{SN ratio} = 10 \log_{10} \left[\frac{\beta}{\sigma_e} \right]^2 , \qquad \text{(Eq. 1.6)}$$

where β is the slope of the regression line in the process output characteristic and signal factor space, and σ_e is the regression error variance. Maximizing the SN ratio leads to a reduction in sensitivity to noise factors as well as to the non-linearity of the relationship of the process output characteristic and the signal factor. The scaling factor is selected as a process parameter that has little effect on the SN ratio.

In the robust design method, experiments are designed using orthogonal arrays [26]. The orthogonal arrays facilitate the calculation of the main effects of the process control parameters on the SN ratios, reduce the number of experiments, and make the experiments economical.

In the robust design method, process quality is optimized in two steps: a robustness optimization step and a mean adjustment step [27]. In this method, optimization is an unconstrained problem because the mean adjustment is decoupled from robustness optimization, which is much simpler than the constrained optimization problems of the classical statistical experiment design methods. In the classical statistical experiment design methods, robustness is optimized under the constraint that the mean must meet the target.

Even though the robust design method shares the principles of planning experiments and data analysis with the classical statistical experiment design methods, the fundamental differences are as follows [8][28]. In the classical statistical experiment design methods, mathematical equations of the mean responses

are derived assuming that the variances are constant over the process parameter ranges. When the variances are not constant, techniques such as blocking, randomization, and transformation of variables are tried to control the variances to increase the model predictability. Hence, the classical statistical experiment design methods are not appropriate for improving process quality by both adjusting the mean and minimizing the variances. The robust design method attempts to model the effects of process parameters on process robustness and to determine the proper process parameter values for the maximum robustness. The maximum robustness corresponds to the minimum variance; hence, high process quality. Accurate modeling of the mean response is not critical in the robust design method, since the mean is easily controlled by the adjustment factor after the robustness optimization.

1.3 Background and Approach

The goal of process control systems, including the MIT process control system, is to increase process quality by controlling the process output characteristics so the target values can be met. In order to control the process output characteristics, it is necessary to have accurate models that describe their behavior, which is a function of the process parameters that are available for control. Several methods have been developed in order to model process output characteristics. For example, physically based modeling methods are used to accurately model process output characteristics and to determine the process parameter values in order to achieve the desired output characteristic values. Response surface modeling methods can also be used to construct process output characteristics models using experimental data when the underlying physics is too complicated or not readily understood.

To improve process quality, the means as well as the variances of the process output characteristics should be controlled as explained in Section 1.2.1. Process output characteristic variances are not easily modeled and, therefore, are difficult to control. They are often caused by stochastic noise in the process, disturbances from the environment, variability of incoming materials. Therefore, the physically based modeling of variances is almost unrealistic. Response surface modeling of variances is also not practical, because the variances have a wide spread in their distribution (χ^2 distribution) even when the process output characteristics have a purely normal

distribution. Hence, a large amount of data are required in order to model the process output characteristics with sufficient confidence.

Several methods have been developed to improve the process quality by controlling the process output characteristic variances; for example, the multiple response surface (MRS) method [17]. In the MRS method, spatial uniformity is modeled first by constructing models for each measurement and then by combining the multiple models. The spatial uniformity is equivalent to the process output characteristic variance.

For example, in a batch-type LPCVD process of VLSI fabrication processes, where a batch of wafers are put into the furnace in a row and processed simultaneously, uniformity of the deposited film thickness down the tube (within-a-batch uniformity) is modeled by first making multiple thickness models for each wafer and then by combining the multiple models. Control or optimization or both that is based on the MRS method still does not deal with the variability that is not modeled, i.e., within-a-wafer uniformity and batch-to-batch uniformity. It is unknown how the control or optimization or both of the modeled uniformity affects the unmodeled uniformity.

The robust design method explained in Section 1.2.4 deals with the process output characteristic variances by maximizing process robustness. This method decouples the mean control from the robustness optimization and allows on-line control of the process output characteristic mean. However, it is not sufficient to control only the process output characteristic mean on-line for higher quality of the processes. Another difficulty is that parts of the process robustness may vary due to the process condition changes, even though it is claimed that the process robustness includes all kinds of process variability and just the optimization of the process robustness can make processes robust enough. Also, it is often necessary to change the robustness (the uniformity in more understandable terms) because of specification changes.

For example, in a single wafer VLSI fabrication process where one wafer is processed at a time, within-a-wafer uniformity is important. With robust design method, the within-a-wafer uniformity combined with the run-to-run uniformity is treated as a robustness problem. Then, only the process output characteristic mean is

controlled on-line. The method does not provide how to control parts of the within-a-wafer uniformity, i.e., the radial uniformity that is often observed as a so-called bull's eye pattern when the process condition changes. Also, the method does not provide how to compensate for the incoming non-uniformity that can be measured before the process step.

One interesting observation from the MRS modeling is that the model fitness is better when the group mean values of multiple measurements are modeled than when all the measurements are modeled separately. Hence, it is possible that the uniformity can be grouped according to process output characteristics. The differences among the group means can be modeled and controlled while the uniformity within each group is treated as a robustness problem.

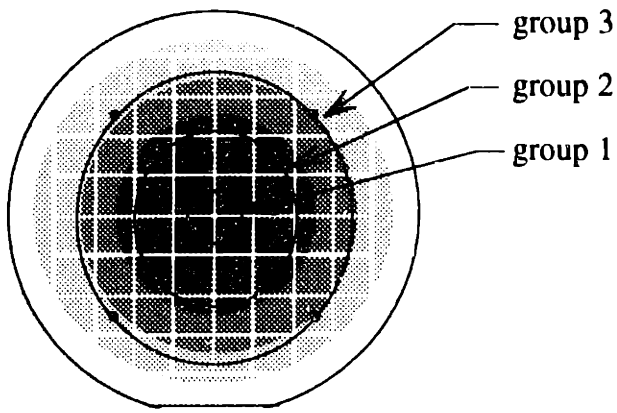

Figure 1.8 Grouped measurement sites of a wafer

For example, in the case of single wafer processes where the bull's eye pattern is a typical non-uniformity pattern, the multiple measurements are grouped according to the radial distances from the wafer center as shown in Figure 1.8. The differences among the group means represent the radial uniformity, and the variabilities within each group represent the circumferential uniformity. As can be seen from the results of Appendix F, sequential optimization of only the radial uniformity did not improve the overall within-a-wafer uniformity since the circumferential uniformity was degraded while the radial uniformity was optimized. Hence, it was shown that the

circumferential uniformity needs to be optimized off-line by the robust design method while the radial uniformity is modeled and controlled on-line.

A new methodology of on-line process quality control is contributed in this thesis. First, the process variability is categorized so that one part of the variability can be treated as a robustness problem and the other part can be modeled and controlled on-line. Several questions are then posed on how to define the robustness appropriately, how to decide which process parameter is appropriate for on-line control while maintaining the robustness as optimized, how to define the on-line controllable process variability, and how to perform on-line control effectively. This thesis proposes solutions to these questions. A new methodology for process optimization and control is developed and applied to some examples, which will be explained in the following chapters.

1.4 Outline

In chapter 2, the on-line control methodology developed in this work is discussed. It is explained how to categorize process variabilities by using some examples of several processes and how to classify process parameters. It is also explained how to define process robustness and on-line controllable variability. Procedures of robustness optimization, parameter identification, and on-line control are also described in detail.

Examples of applying the methodology to the on-line control of the within-a-wafer uniformity in single wafer plasma etching processes are shown in Chapter 3. Robustness optimization and the on-line control of uniformity of the oxide etching processes were performed with different numbers of process parameters. The results of the on-line control experiments are compared with the results of optimization-only experiments. The polysilicon etching process was also optimized and controlled on-line, and the results are compared.

In Chapter 4, the results of the sequential optimization of within-a-batch uniformity in an LPCVD process simulation are described. The sequential optimization of the categorized process variability was performed with a tuning factor

after the robustness optimization. The effectiveness of using a tuning factor for the optimization of categorized process variability is discussed.

Chapter 5 includes discussions on the work. Conclusions and future works are discussed in Chapter 6.

Experimental data of Chapters 4 and 5 are listed in Appendices B, C, and D. In Appendix E, on-line control using multiple site models is discussed. The results of the on-line control of an oxide etching process are compared with the results of the experiments without control. Appendix F shows the results of sequential optimization using all process parameters.

CHAPTER 2
ON-LINE CONTROL METHODOLOGY

2.1 Overview

Process quality controls are divided into on-line control and off-line control, according to when they are performed. On-line control is performed during the actual production, whereas off-line control is accomplished before the actual production begins. In batch production systems, on-line control is performed both on a run by run basis and in real time. The run by run process control is based the measurements of the process output characteristics both before the process and after the process. Using the pre-process measurements, incoming material variability is detected and compensated for by the process parameter controls. Using the post-process measurements, the process conditions are monitored and the process parameter values for the next run are decided accordingly. Real time control varies process parameter values during a run based on real time measurements. In this chapter, a new methodology is developed for the on-line control of process uniformity, which is to be implemented for both the run by run control and the real time control of process uniformity.

An equipment model is the basis for control of a process. An equipment model is defined as a forward simulation of a manufacturing process and related equipment [9]. In the equipment model, the process and the equipment are treated as one unit as

shown in Figure 2.1, which shows a generic model of a manufacturing process and related equipment.

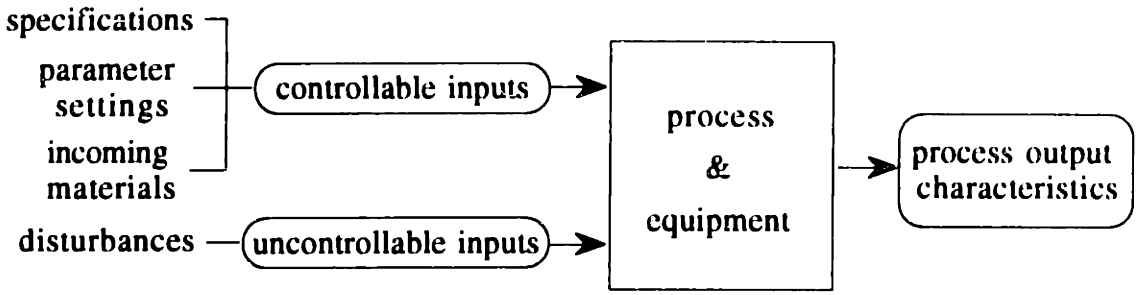

Figure 2.1 Generic model of manufacturing process and related equipment

There are two types of inputs in the manufacturing processes: controllable inputs and uncontrollable inputs. The controllable inputs include the specifications of the products, process parameter settings, and incoming materials. The uncontrollable inputs are stochastic disturbances to the process or to the equipment. The outputs of the manufacturing processes are the process output characteristics of interest. The equipment model represents the functional relationship between controllable inputs and process output characteristics as shown in Figure 2.2. The equipment model of a process is suited for process control, since the controllable input values are determined to get the desired process output characteristics.

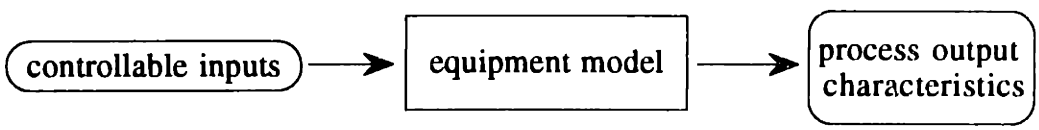

Figure 2.2 An equipment model

An equipment model may be constructed in a mechanistic way, or in an empirical way, or as a combination of both. Mechanistic models are derived from understanding of the underlying physics and are expressed in closed forms or via numerical solution. It often takes too much time and effort to develop mechanistic models because the underlying physics is not easy to model, especially when the process output characteristics are not readily understandable. Also, developed mechanistic models may be too complex for on-line control purposes. Empirical

models are derived from analyzing experimental data and are usually polynomial regression models [29]. The experimental data are best obtained through experiments that are designed systematically. Empirical models are generally faster to construct than mechanistic models. Low-order polynomial regressions are usually used as empirical models, because they are simple and appropriate for on-line control. In on-line control, process parameter ranges are usually small enough to make low-order polynomial approximations effective.

The combination of mechanistic modeling and empirical modeling results in semi-empirical models. The semi-empirical models combine the advantages of mechanistic and empirical models and are possible even when the underlying physics is not completely understood. For example, unknown coefficients of the mechanistic models can be calibrated using data from designed experiments [30][31]. The semi-empirical modeling method can be more effective than the empirical modeling method in designing experiments and utilizing experimental data, because the effects of the process parameters are qualitatively understood in advance. For example, the process parameters are transformed into grouped parameters based on the dimensional analysis of the process, and the regression model can have better modeling accuracy using the grouped parameters [32]-[34].

In this thesis, on-line controllable variabilities are modeled using empirical models because their dependency on process parameters is either not readily understandable or very complicated. For the purpose of the on-line control of an on-line controllable variability, regression models of the on-line controllable variability, as simple as first-order linear models, are used to approximate the behavior of the on-line controllable variability in small process parameter ranges.

When it is guaranteed that a process does not experience any changes in the process conditions, the off-line control method is best suited. A one time process optimization performed before the actual production is enough, and it is not necessary to intervene to check and control the process conditions during production. All processes, however, experience changes in process conditions and variations in incoming materials. Changes of process conditions may be slow, such as the changes due to tool wear, aging, material deposition, etc., as well as abrupt, such as the changes due to tool change, cleaning, preventive maintenance operation, etc. When

such changes occur, it is necessary to compensate for them by re-setting the process parameters. This re-setting procedure is called *tweaking* the process parameters.

On-line control is a procedure for modifying equipment settings so the desired target values of the process output characteristics can be satisfied even when there are changes in process conditions and incoming materials. Changes in the process conditions are detected by measuring process output characteristics after the process and comparing the post-process measurements with the predicted values, providing a feedback control loop. By measuring the incoming material characteristics, proper parameter values can be determined to compensate for the incoming material variations. This pre-process measurement enables feed-forward control. Figure 2.3 illustrates feed-forward and feedback paradigm of an on-line control system.

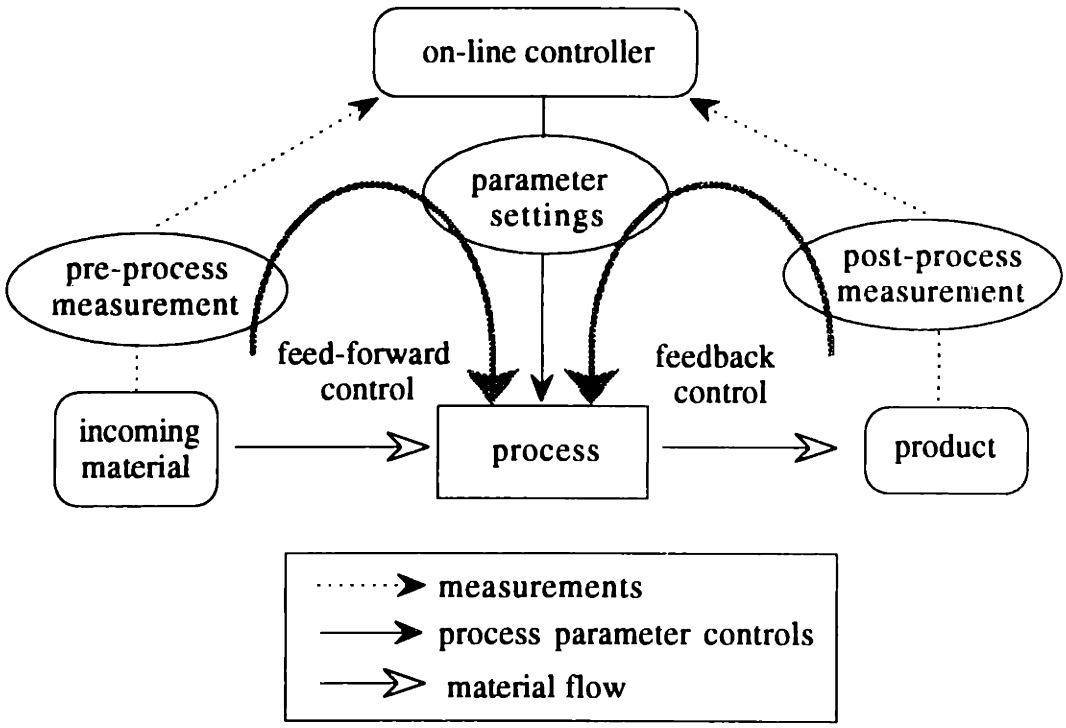

Figure 2.3 Feed-forward and feedback control in on-line control system

By combining the feed-forward and feedback control schemes, on-line control can properly tweak process parameters in order to achieve the maximum quality all the time. Since the control action is based on the equipment model of a process, the equipment model needs to be adapted in order to catch up with any changes that may

have occurred in the process conditions during production. Effective model adaptation algorithms are critical for an on-line control of the processes.

On-line control is based on on-line measurements that includes both pre-process and post-process measurements. On-line measurements, however, cannot cover all the aspects of process output characteristics. Some of the process output characteristics may not be measured on-line. On-line control based only on the on-line measurable characteristics has a risk of degrading the other characteristics that are not measured on-line.

Actual manufacturing environments require a simple and an effective control algorithm. Some of the process output characteristics, however, may be too complex to be controlled on-line. When a process output characteristic has a highly non-linear relationship to the process parameters or has complex interactions with other process output characteristics, the control scheme should be very elaborate, which may not be appropriate for on-line control in actual manufacturing environments.

In this thesis, a new methodology for the on-line control of process uniformity is developed. Process uniformity has been regarded as difficult to control because of its stochastic nature and highly non-linear dependency on the process parameters. It is critical, however, to control the uniformity since it is closely related to process quality. The on-line control of uniformity is considered an effective way to achieve higher process quality, because it can handle both process condition changes and incoming material variations.

2.2 Process Variability

2.2.1 Categorization of Process Variabilities

Variability of processes is defined as the difference between designed values and the actual measurement values of the process output characteristics. Examples of process output characteristics are the physical dimensions of the products, functionality of the products, and material properties such as mechanical, electrical, physical, chemical, etc. In manufacturing processes, designed process output characteristic values are targets to be satisfied when processing incoming materials or workpieces. Process quality is determined by the magnitude of process variability and

should be improved by reducing the process variability. Process quality is evaluated by *quality loss* caused by the process variability as explained in Section 1.2.1.

Process variabilities are inevitable in actual manufacturing processes. They come from stochastic disturbances to process conditions, variability in incoming materials or workpieces, imperfect equipment conditions, environmental variations, etc. The goal of process optimization and control is to reduce the quality loss by minimizing the process variabilities even though it is impossible to eliminate them.

In this thesis, process variabilities are categorized into non-tunable variability and tunable variability according to their characteristics. *Non-tunable variability* is defined as process variability that is difficult to model and control since it is due to stochastic disturbances or the effects of process parameters that are not readily understood to model and control. *Tunable variability* is defined as on-line controllable process variability that is relatively easy to model and control. Hence, it is the degree of difficulty of modeling and controlling that categorizes non-tunable and tunable variabilities. The categorization of variabilities is specific to each process and needs knowledge and experience on the process and equipment.

Tunable variability consists of two components: the deviation of the mean process output characteristic from the target and tunable uniformity. The process output characteristic mean is often the easiest to model and control. Many methods have been developed for modeling process output characteristic mean values. For example, process output characteristic means are often modeled by understanding the underlying physics of the processes. Tunable uniformity is defined as the process uniformity that is to be modeled and controlled. The parts of tunable variability other than the mean deviation are tunable uniformity. When uniformity is considered in many processes, multiple measurement sites are selected to measure the characteristics, and uniformity is calculated from them. It is difficult to model all the multiple measurements of product characteristics, but the multiple measurements can be grouped so that the means of each group may be modeled. Multiple measurements can be grouped so that measurement sites in a group have similar process conditions. For example, many kind of equipment are designed to have symmetry in order to increase uniformity, and the measurements at the symmetric positions can be grouped. Figure 2.4 shows the categories of process variabilities.

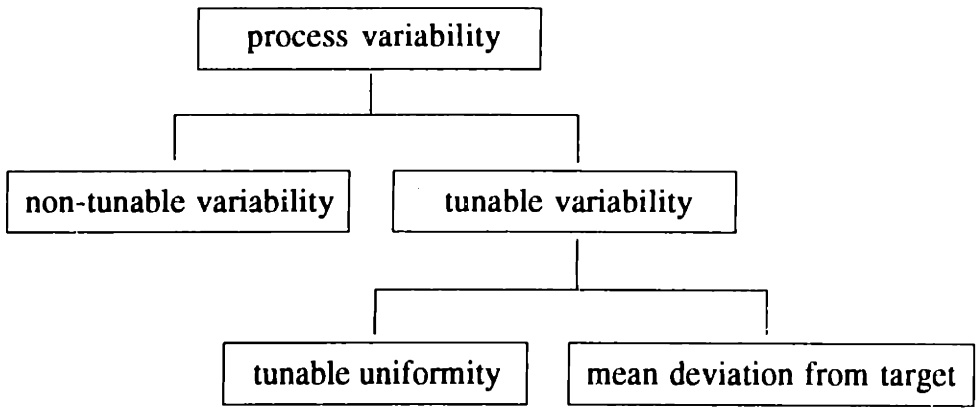

Figure 2.4 Categories of process variabilities

Non-tunable variability is to be optimized off-line, where the most favorable process parameter values for the minimum non-tunable variability are determined. The optimal process parameter values are expected to bring the processes to a position of process parameter space so that the effects of stochastic disturbances may be minimized. Also, the effects of controlling other process parameters are expected to be small in the position.

Tunable uniformity and mean are controlled on-line based on the models that are obtained either mechanistically or empirically. It is only through on-line control that changes of both process conditions and incoming materials or workpieces can be compensated for.

2.2.2 Examples

The categorization of process variabilities is illustrated in this section by using examples of several processes: a straight turning process, an injection molding process, and a single wafer process and a batch process in VLSI fabrication processes.

In the straight turning process, goal of process control is to obtain perfect circular cross sections of a designed diameter along the axis of a workpiece by machining the workpiece using a tool as shown in Figure 2.5 [35]. It is assumed that the diameters are measured in m positions along the axis of the workpiece and n measurements are performed along the periphery of the cross section at each position.

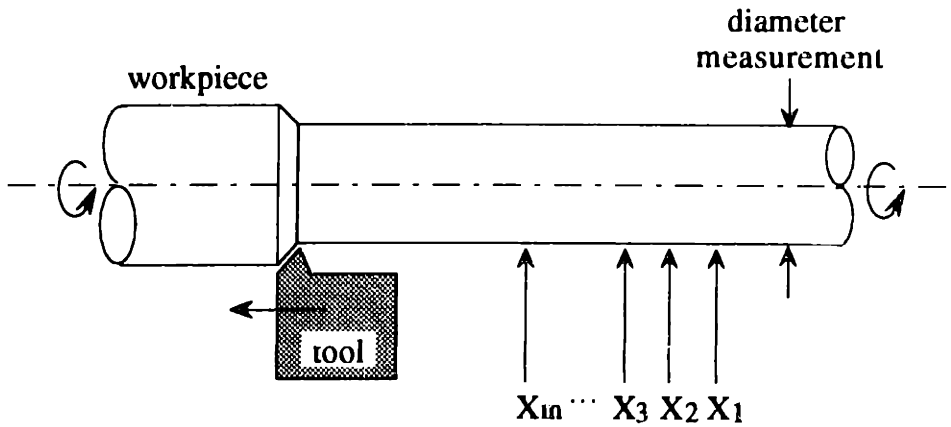

m measurements position along the axis

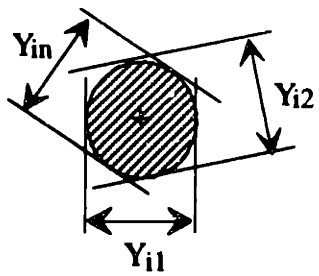

n measurements in X_i cross section

Figure 2.5 Straight turning process and measurements of diameter

The process variabilities of this example are categorized as follows. The differences between the n measured diameters at each cross section are categorized as non-tunable variability because they are due to stochastic disturbances, such as vibrations and chattering. The n measurements of the diameters at each cross section are averaged. The differences between the m average diameters are categorized as tunable uniformity since they are on-line controllable by changing the distance between the tool tip and the center line of the workpiece as the tool moves. The overall average diameter of m×n measurements is calculated, and the deviation from the target diameter is defined as the mean deviation.

In the injection molding process with multiple cavity molds, the goal of process control is to obtain the correct dimensions of the parts from all the cavities. The dimensions are measured at several points on each part, and the differences between

the measurement and the designed value are the variabilities. The process variabilities in this example are categorized as follows. The variability within a part is categorized as non-tunable variability, since control of local process conditions of the mold is difficult. The variability between the parts is categorized as tunable variability, since global process conditions of the mold, such as the temperature distribution, is on-line controllable. The overall average of the differences is the mean deviation from the target.

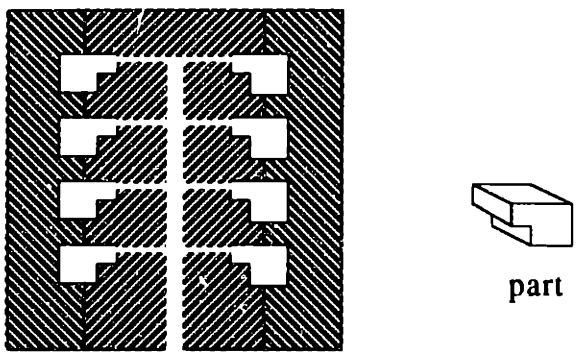

Figure 2.6 Multiple cavity mold of injection molding process

In single wafer processes in the VLSI fabrication, within-a-wafer uniformity is critical for process quality. It is known that more than 70% of single wafer process equipment has axisymmetry in their configurations in order to increase process quality [36]. Figure 2.7 shows the examples of axisymmetric configurations. Even in those instances when the equipment does not have axisymmetry, the wafer is rotated in order to provide an axisymmetric process condition to the wafer as shown in Figure 2.8.

Axisymmetry provides similar process conditions around the circumference of a wafer. The result of the axisymmetric process condition is often shown as a so-called bull's eye pattern, which is caused by the dominant radial non-uniformity of the process. Figure 2.9 shows an example of the bull's eye pattern, where the thickness of the etched film has radial non-uniformity. The thickness variation is represented by the different gradations of darkness in the figure. Because of axisymmetry, the process conditions in the radial direction are easier to control than the circumferential

process conditions. Variations in the circumferential direction are categorized as non-tunable variability and variations in the radial direction as tunable uniformity.

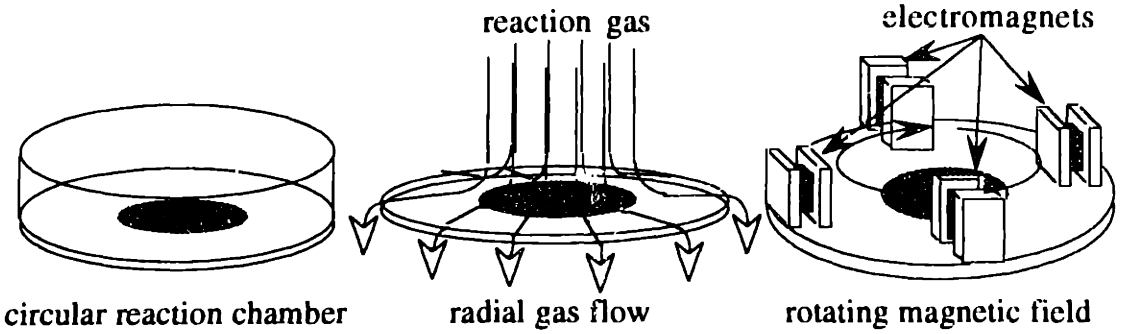

Figure 2.7 Examples of axisymmetric configuration in single wafer process equipment

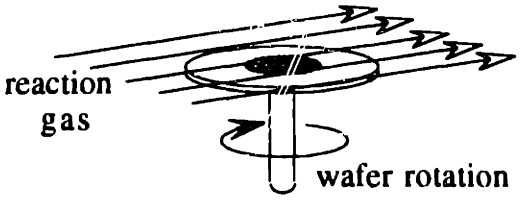

Figure 2.8 Rotating wafer in single wafer process equipment

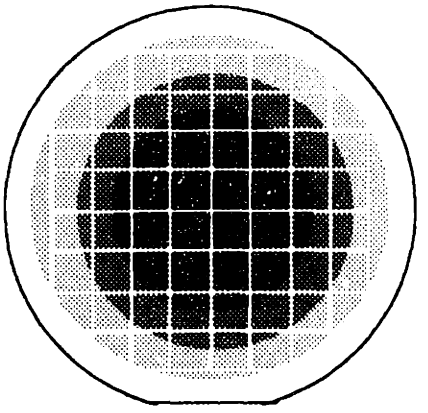

Figure 2.9 Bull's eye pattern of single wafer plasma etching processes

In batch VLSI fabrication processes, a batch of wafers experience different process conditions since they are located at different positions within a machine. The process conditions at each wafer position are controlled by using multiple control devices such as temperature controllers and gas injectors. Hence, the wafer-to-wafer variation is categorized as tunable uniformity. Variations within each wafer or variations of the wafers at the same positions from different batches are categorized as non-tunable variability, since they are due to the non-uniform process conditions over the wafer or stochastic disturbances, both of which are difficult to model.

2.3 Process Parameters

Process parameters are controllable inputs to processes by which process conditions are controlled. Examples of the process parameters are the set values of temperature, pressure, power, feed rate, spindle speed, gas flow rates, process time, etc. Process output characteristics are optimized and controlled by setting the process parameters to proper values. The effects of varying process parameters on process output characteristics are often difficult to model, because the configurations of the equipment as well as the underlying physics of the processes must be understood clearly.

For the effective optimization and control of the process variabilities, process parameters are classified into robustness factors, tuning factors and adjustment factors in this thesis. A *robustness factor* is defined as a process parameter that has a large effect on the non-tunable variability and a small effect on the tunable variability. A *tuning factor* is defined as a process parameter that has a small effect on the non-tunable variability but a large effect on the tunable uniformity. An *adjustment factor* is defined as a process parameter that has a small effect on both the non-tunable variability and the tunable uniformity but a large effect on the mean. The effects of each factor are summarized in Table 2.1.

	effects on		
	non-tunable variability	tunable uniformity	mean
robustness factor	large	*	*
tuning factor	small	large	*
adjustment factor	small	small	large

(* : irrelevant)

Table 2.1 Effects of process parameters on categorized variabilities

The purpose of classifying process parameters is to enable the on-line control of the tunable variability. One of the difficulties of on-line control is the degradation of the non-tunable variability due to the control action. The classified process parameters can properly handle both the non-tunable and tunable variabilities and reduce the risk of applying the control. The use of each classified process parameter in the optimization and control of process is shown in Figure 2.10. The following sections will explain how the process parameters are classified and used for the optimization of non-tunable variability and the control of tunable variability.

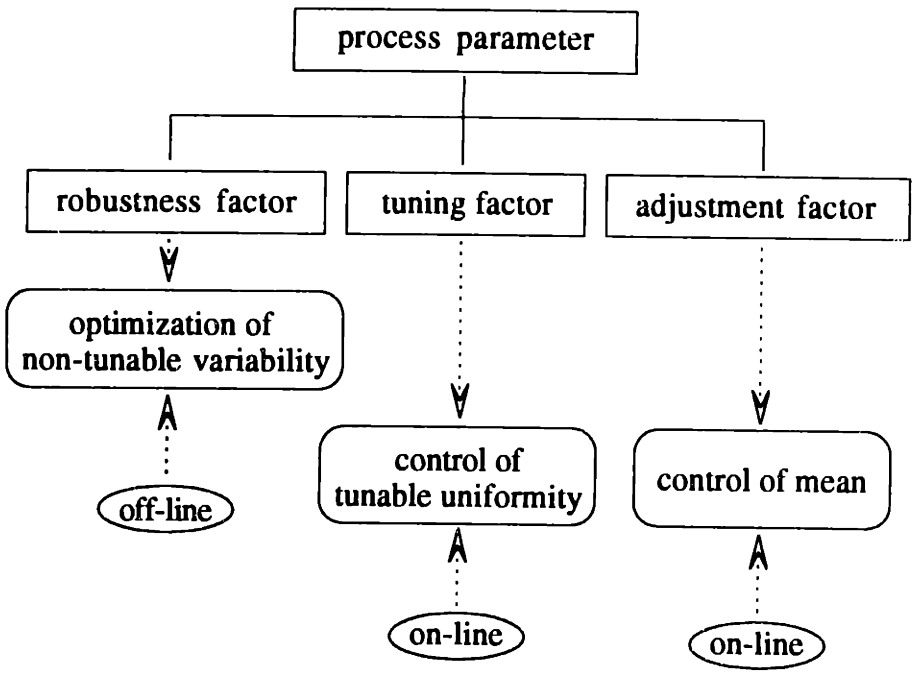

Figure 2.10 Process parameter classification and their use

2.4 Definition of Robustness

In order to minimize the non-tunable variability of processes, it is necessary to define a quantity that measures properly the magnitude of non-tunable variability. In this thesis, a quantity called *robustness* is defined to measure the magnitude of non-tunable variability. Robustness is to be used to optimize non-tunable variability as well as to identify the tuning factor and adjustment factor, which will be explained in the following sections.

Consider a batch process in which the process output characteristics are measured at multiple measurement sites. The purpose of process control in this case is to make the process output characteristics as uniform as possible. The process output characteristics can be grouped according to the process conditions as explained in Section 2.2. Each group has group means and group variances. It is assumed that it is relatively easy to model and control the group means on-line using the process parameters, i.e., the differences of the group means are tunable variabilities. However, the variabilities of the measurements within each group are assumed to be non-tunable, i.e., they are difficult to model and control on-line. Let m be the number of the groups and n be the number of the measurements within each group. The groups may have different numbers of process output characteristic measurements within each group, but for simplicity it is assumed here that each group has the same number of measurements.

In Figure 2.11, the m×n measurements of a process output characteristic to be controlled are plotted along the horizontal axis. The measurements are scattered around the target value of the product characteristic, T. It is this scattering that causes poor quality of the process. The measurements are grouped according to the process conditions, and the groups are indicated in the figure.

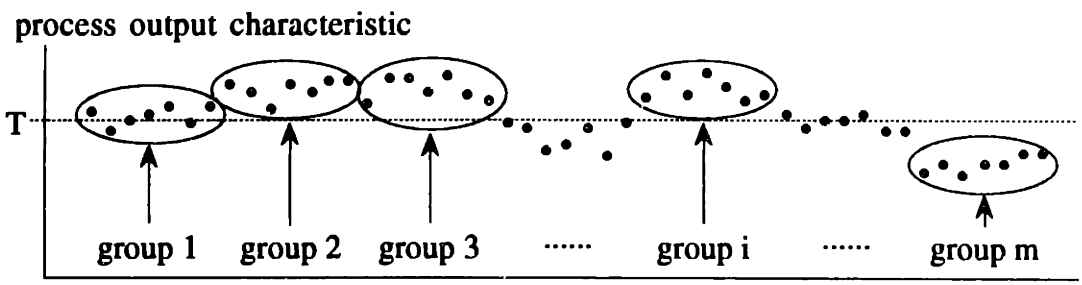

Figure 2.11 Process output characteristic measurements from a batch process

In Figure 2.12, the group means and group variances of each group are shown; the open circles represent the group means and the error bars represent the magnitude of the group variances.

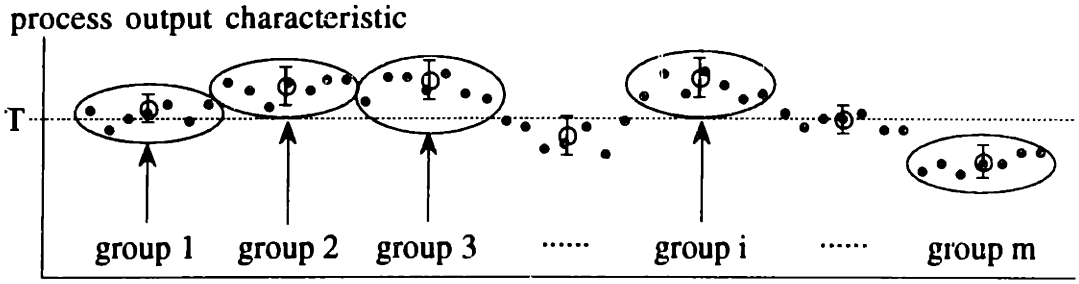

Figure 2.12 Group means and group variances for each grouped measurements

In Section 1.2.1, the quality loss of a process is defined as a quadratic function of the deviation from the target (Eq. 1.2). In this example, total quality loss, QL, due to the deviations of the process output characteristics from target value, T, is

$$QL = K \sum_{i=1}^{m} \sum_{j=1}^{n} (Y_{ij} - T)^2 , \qquad \text{(Eq. 2.1)}$$

where Y_{ij} is the process output characteristic measurements of the j-th measurement points in the i-th group, and K is the quality loss coefficient.

After the measurements are grouped as shown in the figures above, the total quality loss can be expressed using the group means and the group variances as follows:

$$QL = n K \left[\{ \sum_{i=1}^{m} [\sigma_{i\bullet}^2 + (\overline{Y}_{i\bullet} - \overline{Y}_{\bullet\bullet})^2] \} + \{ m (\overline{Y}_{\bullet\bullet} - T)^2 \} \right] , \qquad \text{(Eq. 2.2)}$$

where $\overline{Y}_{\bullet\bullet}$ is the grand mean of all the measurements, and $\overline{Y}_{i\bullet}$ and $\sigma_{i\bullet}^2$ are the group mean and the group variance of the i-th group, respectively, i.e.,

$$\overline{Y}_{\bullet\bullet} = \frac{1}{mn} \sum_{i=1}^{m} \sum_{j=1}^{n} Y_{ij} , \qquad \text{(Eq. 2.3)}$$

$$\overline{Y}_{i\bullet} = \frac{1}{n} \sum_{j=1}^{n} Y_{ij} , \qquad \text{(Eq. 2.4)}$$

and

$$\sigma_{i\bullet}^2 = \frac{1}{n} \sum_{j=1}^{n} (Y_{ij} - \overline{Y}_{i\bullet})^2 . \qquad \text{(Eq. 2.5)}$$

Refer to Appendix A for the derivation of Eq. 2.2.

In Eq. 2.2, the first summation term corresponds to the quality losses due to the non-tunable variability (the group variances) and the tunable uniformity (the group mean deviation from the grand mean). The second term is the quality loss due to the grand mean deviation from the target.

In the methodology developed in this thesis, the on-line control of the tunable variability is decoupled from the off-line optimization of non-tunable variability. The optimized non-tunable variability is not to be affected while the on-line control is performed. On-line control includes both the tuning of the tunable uniformity and the adjustment of the mean. Therefore, it is necessary to define the robustness so that it can anticipate the magnitude of the non-tunable variability after the tuning and adjustment procedures. By optimizing the defined robustness in the off-line optimization procedure, the non-tunable variability is minimized ahead of the tuning and adjustment procedures.

Since both the tuning and adjustment factors are the process parameters that control the tunable uniformity and the mean, respectively, without affecting the non-tunable variability, they are identified by comparing the amount of the robustness change corresponding to the process parameter changes. The smaller the robustness change is when a process parameter varies, the better candidate for use as a tuning factor or adjustment factor the process parameter is.

A number of tuning factors can be used in the on-line tuning of the tunable uniformity. In the simplest case, it can be performed with one tuning factor. On the other hand, it can be performed with as many tuning factors as the number of the differences among the group means, (m-1).

In the former case, one quantity representing the tunable uniformity is to be controlled. In order to explain tunable uniformity with one quantity, a linear regression of the group means is performed with the group numbers as explanatory variables [37]-[40]. The slope of the linear regression line is used to represent the magnitude of the tunable uniformity and is tuned to zero on-line to minimize the differences among the group means. Figure 2.13 shows the procedure of tuning of the slope with one tuning factor.

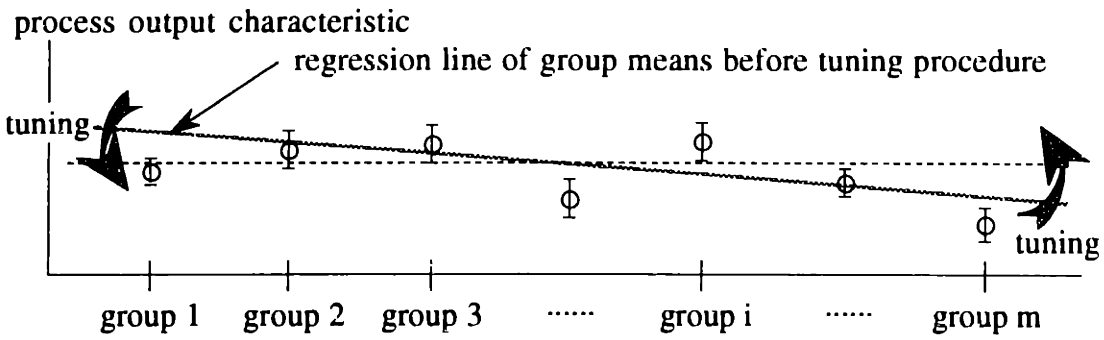

A. before tuning procedure

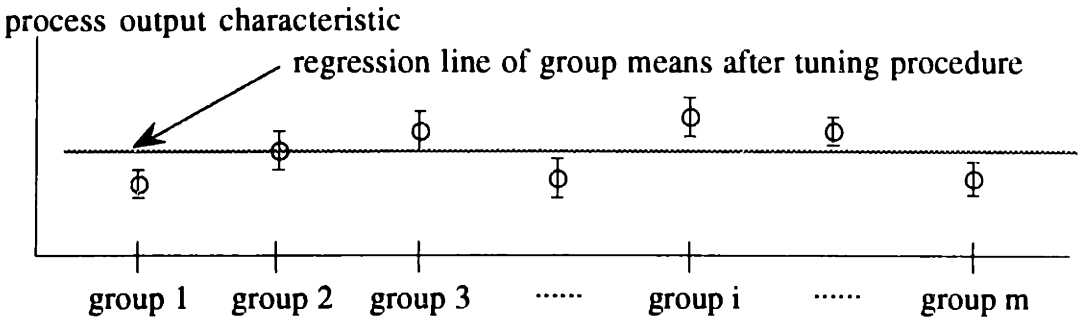

B. after tuning procedure

Figure 2.13 Tuning procedure with one tuning factor

In the latter case, (m-1) quantities are to be controlled using (m-1) tuning factors. The (m-1) quantities are the (m-1) differences of m group means. When the tuning of (m-1) differences is perfectly performed, all the differences are made zero as shown in Figure 2.14. In the figures, only the group means and the group variances are plotted for simplicity.

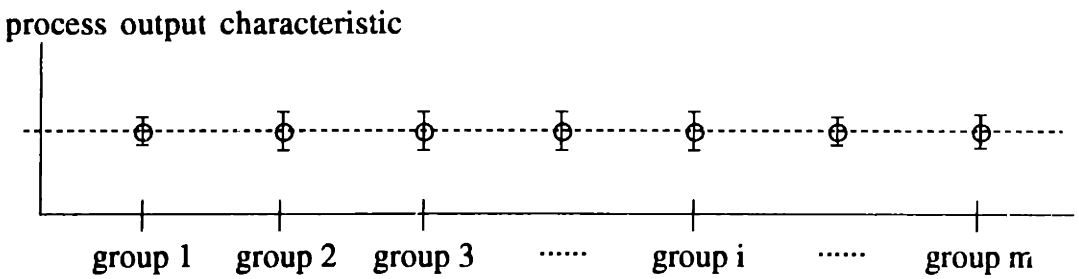

Figure 2.14 Group means after tuning procedure with (m-1) tuning factors

The number of tuning factors is between one and (m-1) when there are m groups in the process. It is determined by the number of available process parameters, the interaction among the process parameters, and by how tunable uniformity is defined. According to the numbers of the group means and tuning factors, robustness is defined accordingly as follows.

First, assume that we have (m-1) tuning factors so that all the group means, $\overline{Y}_{i\bullet}$, may be made identical, i.e., the tunable uniformity is completely controlled. The total quality loss after the tuning procedure, QL_t, is as follows:

$$QL_t = n K \left[\{ \sum_{i=1}^{m} (\frac{\overline{Y}^{*}_{\bullet\bullet}}{\overline{Y}_{i\bullet}} \sigma_{i\bullet})^2 \} + \{ m (\overline{Y}^{*}_{\bullet\bullet} - T)^2 \} \right] , \qquad \text{(Eq. 2.6)}$$

which is derived from Eq. 2.2, assuming that the group standard deviations, $\sigma_{i\bullet}$'s, change proportionally to the changes of group means. $\overline{Y}^{*}_{\bullet\bullet}$ is a new grand mean after the tuning procedure. In the equation, the first summation term is the quality loss due to the non-tunable variability, and the second term is the quality loss due to the grand mean deviation from the target. Note that the quality loss due to the tunable uniformity has disappeared since the tunable variability was tuned. Figure 2.15 shows the process output characteristics that are obtained after the tuning procedure. In the figure, it is noted that there is a difference between the new grand mean, $\overline{Y}^{*}_{\bullet\bullet}$, and the target value, T, after the tuning procedure.

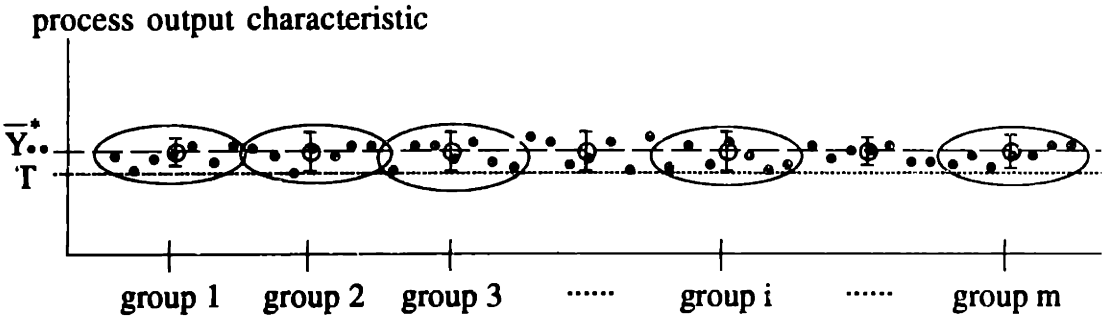

Figure 2.15 Process output characteristic measurements after perfect tuning

After the tuning procedure, the new grand mean, $\overline{Y}^{*}_{\bullet\bullet}$, is adjusted to the target value using the adjustment factor to minimize quality loss. The quality loss after

the tuning and adjustment procedures, QL_{ta}, is

$$QL_{ta} = n\,K\,T^2\left[\sum_{i=1}^{m}\left(\frac{\sigma_{i\bullet}}{\overline{Y}_{i\bullet}}\right)^2\right]. \qquad \text{(Eq. 2.7)}$$

The quality loss is now due to only the non-tunable variability. The product characteristics after the tuning and adjustment procedures are shown in Figure 2.16, where the grand mean meets the target value.

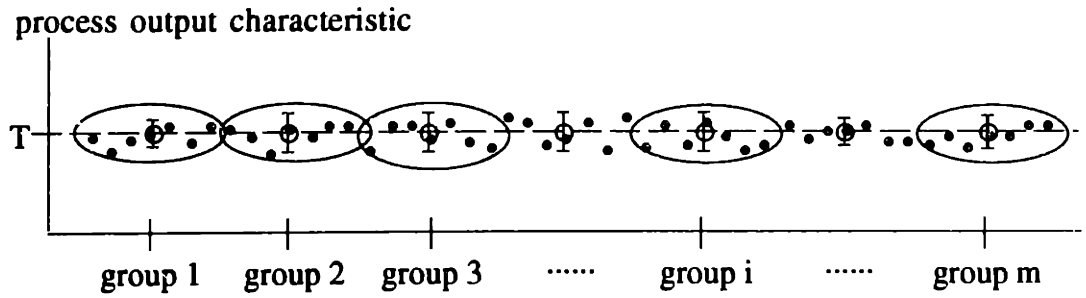

Figure 2.16 Process output characteristic measurements after perfect tuning and adjustment

Now assume that we have one tuning factor and the tuning of tunable uniformity is performed by making the regression line slope zero as shown in Figure 2.13. From the linear regression of the group means, we get the regression predictions of the group means, $\hat{\overline{Y}}_{i\bullet}$'s, for each $\overline{Y}_{i\bullet}$ as shown in Figure 2.17. In the figure, only the group means and the regression predictions are plotted for simplicity.

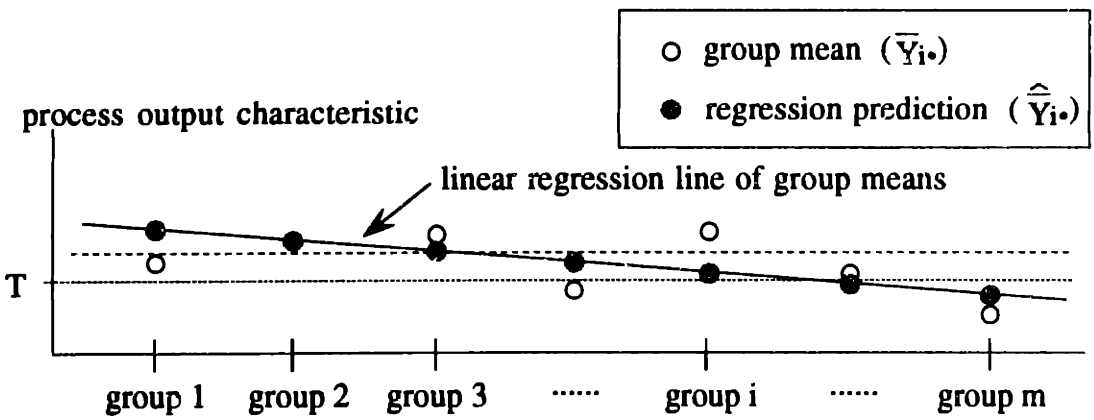

Figure 2.17 Group means and regression predictions for single tuning factor

When the tuning is performed with one tuning factor, the slope of the linear regression line is controlled to be zero to minimize the differences between the group means. After the tuning procedure, all the regression predictions become identical to the new grand mean, $\overline{Y}^{*}_{\bullet\bullet}$, as shown in Figure 2.18. The total quality loss after the tuning procedure, QL_t, is as follows:

$$QL_t = n K \left[\{ \sum_{i=1}^{m} (\frac{\overline{Y}^{*}_{\bullet\bullet}}{\hat{\overline{Y}}_{i\bullet}} \sigma_{i\bullet})^2 + (\frac{\overline{Y}^{*}_{\bullet\bullet}}{\hat{\overline{Y}}_{i\bullet}} \overline{Y}_{i\bullet} - \overline{Y}^{*}_{\bullet\bullet})^2 \} + \{ m (\overline{Y}^{*}_{\bullet\bullet} - T)^2 \} \right] , \quad \text{(Eq. 2.8)}$$

which is derived from Eq. 2.2, assuming that the group standard deviations, $\sigma_{i\bullet}$'s, and the group means, $\overline{Y}_{i\bullet}$'s, change proportionally to the changes of the regression predictions. In the equation, the first part of the summation is the quality loss due to the non-tunable variability, and the second part is the quality loss due to the deviation of the group means from the grand mean after the tuning procedure. The last term in the equation is the quality loss due to the grand mean deviation from the target.

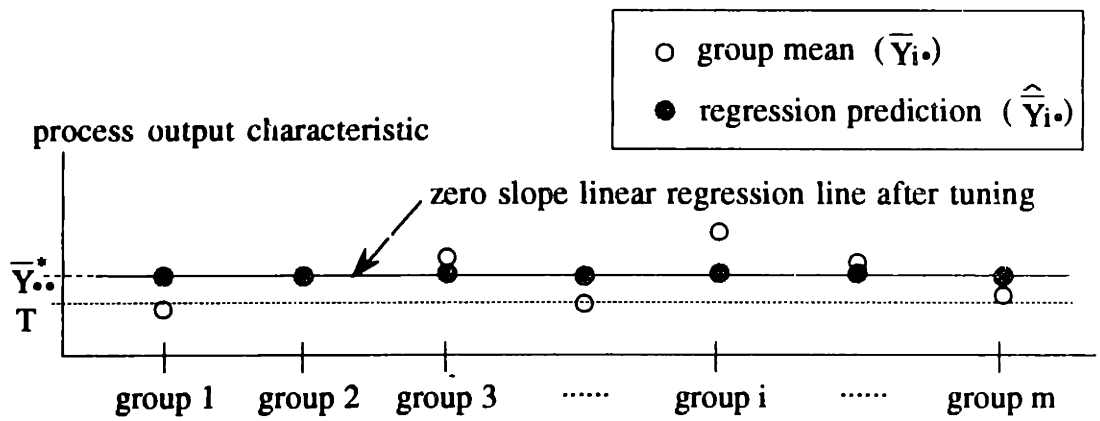

Figure 2.18 Group means and regression predictions after tuning with single tuning factor

After the tuning procedure, the new grand mean, $\overline{Y}^{*}_{\bullet\bullet}$, is adjusted to meet the target value, T. The total quality loss after the tuning and adjustment procedures, QL_{ta}, is

$$QL_{ta} = n K T^2 \left[\sum_{i=1}^{m} \{ (\frac{\sigma_{i\bullet}}{\hat{\bar{Y}}_{i\bullet}})^2 + (\frac{\bar{Y}_{i\bullet} - \hat{\bar{Y}}_{i\bullet}}{\hat{\bar{Y}}_{i\bullet}})^2 \} \right] . \qquad \text{(Eq. 2.9)}$$

In the equation above, the quality loss due to the grand mean deviation from the target is eliminated since the mean was adjusted to target.

Note that QL_{ta} with one tuning factor (Eq. 2.9) becomes the same as QL_{ta} with (m-1) tuning factors (Eq. 2.7), if the group means, $\bar{Y}_{i\bullet}$, coincide with the regression predictions, $\hat{\bar{Y}}_{i\bullet}$. It means that tuning with one tuning factor has the same effect as tuning with (m-1) tuning factors, when the group means are exactly aligned in a straight line as shown in Figure 2.13.

When the number of tuning factors is between 1 and (m-1), the total quality loss is defined according to how tunable uniformity is defined. The magnitude of the total quality loss is between QL_{ta} with one tuning factor (Eq. 2.9) and QL_{ta} with (m-1) tuning factors (Eq. 2.7).

Using QL_{ta}'s (Eqs. 2.7 and 2.9), robustness is defined as follows:

$$\text{robustness} = \left[\sum_{i=1}^{m} (\frac{\sigma_{i\bullet}}{\bar{Y}_{i\bullet}})^2 \right]^{-1} \qquad \text{(Eq. 2.10)}$$

for the (m-1) tuning factor case and

$$\text{robustness} = \left[\sum_{i=1}^{m} \{ (\frac{\sigma_{i\bullet}}{\hat{\bar{Y}}_{i\bullet}})^2 + (\frac{\bar{Y}_{i\bullet} - \hat{\bar{Y}}_{i\bullet}}{\hat{\bar{Y}}_{i\bullet}})^2 \} \right]^{-1} \qquad \text{(Eq. 2.11)}$$

for one tuning factor case.

The inverse of the quality loss is taken in the above definition of robustness above so that small quality loss corresponds to high robustness.

2.5 Definition of Tunable Variability

Whereas non-tunable variability is characterized as the process variability due to stochastic disturbances on the process conditions and stochastic non-uniformity of the process conditions, tunable variability is characterized as the process variability

that is relatively easily controlled, because it is due to the deviation of the process output characteristic mean from the target value and the controllable uniformity of the process conditions.

When underlying physics of the processes and equipment is well understood, tunable variability is modeled as a function of the process parameters in a mechanistic way. When underlying physics of the processes and equipment is too complicated to be modeled mechanistically, statistical methods are used for the modeling of tunable variability.

The process output characteristic mean is one of the tunable variabilities and should be controlled to meet target value. Often, it is simple to model the process output characteristic mean using the process parameters. Process time, for example, is the main parameter for controlling the process output characteristic mean in many processes where the rate of the process is constant or can be approximated as constant [41]. Once the rate of a process is determined, the process output characteristic mean is easily controlled to meet the target value by selecting the proper process time.

When non-uniformity of the process output characteristics is due to controllable variability of the process conditions, it is considered tunable uniformity. The equipment of batch processes is designed to increase the spatial uniformity of process conditions for the product. For example, the equipment is designed to have symmetric configurations and to rotate the products in order to generate axisymmetric process conditions. However, it is difficult to get a complete spatial uniformity of process conditions. For example, reaction chemicals deplete as they flow in chemical processes, uniform temperature distribution is difficult to achieve in thermal processes, and stiffness of the structure changes as the configuration changes in mechanical processes. Hence, it is necessary to model the spatial uniformity as tunable uniformity and to tune it on-line by proper process parameters.

Tunable uniformity is specific to the process output characteristics and equipment configurations being considered. Hence, it must be defined according to the specific problem. Tunable uniformity is modeled as a function of the process parameters in either a mechanistic or an empirical way. Even though mechanistic modeling is possible, the empirical modeling method is often used because the tunable

uniformity has a complex relationship with the process parameters. For the purpose of on-line control, the most effective parameter for controlling tunable uniformity is identified as the tuning factor and then the tunable uniformity is modeled as a function of the tuning factor. The on-line control of tunable uniformity is performed based on the constructed model. In on-line control, models are adapted in order to catch up with any changes in the process conditions whenever necessary.

2.6 Robustness Optimization and Parameter Identification

2.6.1 Designed Experiments

Process variabilities are categorized specifically according to the characteristics of the processes being controlled. As explained in the previous sections, robustness is defined to measure the magnitude of non-tunable variability, and tunable uniformity is defined specifically according to process characteristics and equipment configurations. After the robustness and tunable uniformity are defined, the tuning factor and adjustment factor are identified through a set of designed experiments.

In order to be used for optimization and control, process parameters should be easy to set and there should be no extra cost in changing them. Since on-line control requires tweaking the process parameters between or during the process, the process parameters that are used for on-line control should be easy to set.

The operating ranges of the process parameters are usually determined according to the process characteristics. Since the purpose of performing designed experiments is to measure the effects of the process parameters on robustness and tunable uniformity, it is preferred to use a large range of the process parameter.. The ranges, however, should not be so large to include the process parameter ranges where the process is in a different condition from its normal state. For the purpose of identifying tuning factors and adjustment factors, measuring first-order or second-order effects is sufficient in most problems. Hence, two or three factor levels are used in designing experiments.

Once the parameters and their levels have been determined, orthogonal arrays are used because of simplicity in application. Orthogonal arrays can evaluate the

effects of several process parameters in a small number of experiments [25]. Orthogonal arrays evolved from Plackett and Burman designs, and were rearranged by Taguchi [42][43]. Even though orthogonal arrays are used primarily to analyze the main effects of the process parameters, the effects of interactions between the process parameters can also be evaluated.

Using orthogonal arrays with two levels for each process parameter, first-order effects are evaluated by averaging the results of the experiments. For example, Table 2.2 shows an L8 orthogonal array for up to seven process parameters with two levels. The main effects of process parameter 1, $\overline{m}_{1,low}$ for the low level, and $\overline{m}_{1,high}$ for the high level are obtained by averaging the results from experiments 1, 2, 3, and 4, and the results from experiments 5, 6, 7, and 8, respectively, as follows:

$$\overline{m}_{1,low} = \frac{m_1 + m_2 + m_3 + m_4}{4} , \qquad \text{(Eq. 2.12)}$$

and

$$\overline{m}_{1,high} = \frac{m_5 + m_6 + m_7 + m_8}{4} . \qquad \text{(Eq. 2.13)}$$

experiment number	parameter							measurement
	1	2	3	4	5	6	7	
1	low	low	low	low	low	low	low	m_1
2	low	low	low	high	high	high	high	m_2
3	low	high	high	low	low	high	high	m_3
4	low	high	high	high	high	low	low	m_4
5	high	low	high	low	high	low	high	m_5
6	high	low	high	high	low	high	low	m_6
7	high	high	low	low	high	high	low	m_7
8	high	high	low	high	low	low	high	m_8

Table 2.2 L8 orthogonal array for up to seven parameters with two levels

Because of orthogonality, other process parameters are evenly included in the calculation of the main effects of process parameter 1, and their effects are averaged

when calculating the main effects of process parameter 1, which are plotted in Figure 2.19. The main effects of the other process parameters are similarly calculated.

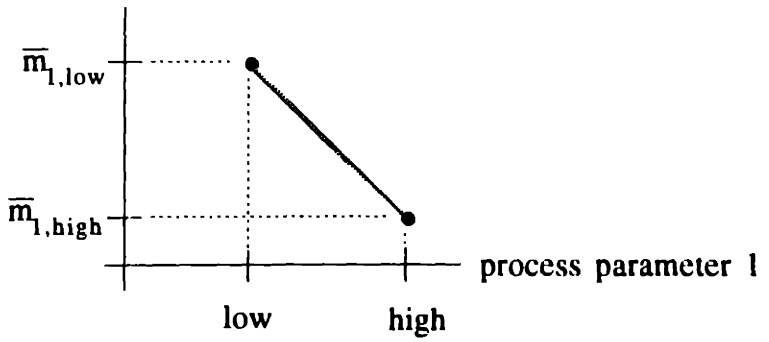

Figure 2.19 Main effect analysis of process parameter 1 for two-level design

When three levels are used, the first-order effect as well as the second-order effect are analyzed. By calculating three main effects for each level, quadratic fitting is performed, as shown in Figure 2.20. In the figure, the main effects of process parameter 1 and the corresponding second-order curve are plotted.

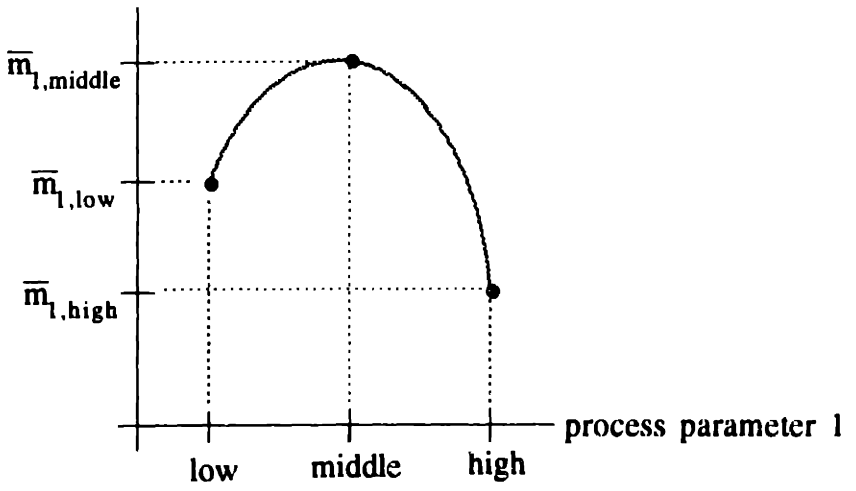

Figure 2.20 Main effect analysis of process parameter 1 for three-level design

2.6.2 Robustness Optimization

From the results of designed experiments, robustness is maximized by determining the process parameter values called the *maximum robustness operating points*. When no interactions are included in the orthogonal array design, the maximum robustness operating points for each process parameter can be determined independently for each process parameter. When interactions are included as high-order terms, non-linear optimizers are used to calculate the maximum robustness operating points [44].

Robustness measures the magnitude of non-tunable variability, which is not easily modeled. Hence, only the low-order effects of the process parameters on robustness are evaluated by using the data from designed experiments. When two levels are used in designed experiments, only the first-order effects of the process parameters are analyzed, and the maximum robustness operating points are one of the levels used in the experiments. When a three-level design is used, second-order effects are analyzed, and the maximum robustness operating points are determined by finding the process parameter values that maximize quadratic models within the operating ranges.

The higher-order effects of the process parameters are not considered because of the difficulties of modeling robustness.

2.6.3. Parameter Identification

Using the results of designed experiments, the tuning factors and adjustment factors are also identified among the process parameters. To identify the tuning factor and adjustment factor, the effects of the process parameters on robustness, tunable uniformity, and mean are evaluated. The magnitude of changes and the average values of robustness, tunable uniformity, and mean are measured respectively when each process parameter changes from its lowest value to highest value within the operating ranges while the other process parameters are fixed at their maximum robustness operating points. Using the measurements, index values are defined for each process parameter as follows:

$$\text{index}_t = \left| \frac{\left[\dfrac{\Delta \text{ robustness}}{\text{average of robustness}}\right]}{\left[\dfrac{\Delta \text{ tunable uniformity}}{\text{average of tunable uniformity}}\right]} \right| , \qquad \text{(Eq. 2.14)}$$

and

$$\text{index}_a = \left| \frac{\left[\dfrac{\Delta \text{ tunable uniformity}}{\text{average of tunable uniformity}}\right]}{\left[\dfrac{\Delta \text{ mean}}{\text{average of mean}}\right]} \right| . \qquad \text{(Eq. 2.15)}$$

Index_t (Eq. 2.14) represents the ratio of the relative change of robustness to the relative change of tunable uniformity. Index_a (Eq. 2.15) represents the ratio of the relative change of tunable uniformity to the relative change of mean. An ideal tuning factor can control tunable uniformity without changing robustness; hence, it has a zero value of index_t. An ideal adjustment factor can control mean without changing robustness and tunable uniformity; hence, it has zero values of both index_t and index_a.

In real problems, it is unusual to have ideal tuning factors and adjustment factors. Therefore, the process parameters whose index_t values are small are identified as the tuning factors. The process parameter with the smallest index_a among the process parameters whose index_t's are small is identified as an adjustment factor. The number of tuning factors depends on the number of tunable uniformities as explained in Section 2.4. In order to control the mean, one adjustment factor is necessary. Because of the way in which tuning factors and adjustment factors are defined, the tuning of tunable uniformity is decoupled from the robustness optimization, and the adjustment of mean is decoupled from both the robustness optimization and the tuning of tunable uniformity.

2.7 On-line Control of Tunable Variability

2.7.1 Modeling of Tunable Variability

The tunable variability is controlled on-line while the robustness is optimized off-line. The differences between on-line control and off-line optimization are as follows: on-line control is being performed during production, while off-line optimization

is completed before production begins; it is necessary to explore small ranges of the process parameters for on-line control to avoid scraps; and on-line control needs models that are updated continuously to describe the current process conditions correctly. Since the tunable variability is characterized as the process variability, which is relatively easy to model and control, it is readily modeled as a function of the tuning factor and adjustment factor. The tunable uniformity is modeled as a function of the tuning factors, and the mean is modeled as a function of the adjustment factor.

Although the mechanistic modeling of tunable variability is not impossible, the empirical modeling is preferred because it is simple and appropriate for on-line control. Since on-line control is usually performed in small ranges of the tuning factor and adjustment factor, the tunable variability is modeled with a low-order approximation. For example, the mean is modeled as a first order linear function of the adjustment factor as follows:

$$\text{mean} = C_0 + C_1 \times (\text{adjustment factor}), \qquad \text{(Eq. 2.16)}$$

where C_0 and C_1 are the constant and first-order coefficient, respectively. C_0 and C_1 are determined by fitting experimental data and are updated when necessary.

The tunable uniformity is defined specifically according to the process and equipment characteristics. For example, the tunable uniformity might be represented by a quantity such as the slope of the regression line of group means as explained in Section 2.4, where one tuning factor is necessary to control the slope. In such a case, the goal of on-line control of the tunable uniformity is to make the slope zero. For the purpose of on-line control, the slope is modeled as a first-order linear function of the tuning factor as follows:

$$\text{slope} = D_0 + D_1 \times (\text{tuning factor}), \qquad \text{(Eq. 2.17)}$$

where D_0 and D_1 are the constant and first-order coefficient, respectively. D_0 and D_1 are also determined by fitting experimental data and are updated when necessary. When more than one tunable uniformity is considered, appropriate quantities are defined to explain the magnitude of the tunable uniformities, and multiple tuning factors are identified. The appropriate quantities are then modeled as functions of multiple tuning factors.

As explained in Section 2.6.1, while robustness optimization uses a non-linear characteristic of the processes to maximize the robustness by exploring wide ranges of the process parameters, on-line control of tunable variability is performed in small ranges of the tuning factors and adjustment factor based on local models. The models are first-order approximations of the mean and the tunable uniformity as functions of the adjustment factor and tuning factors, respectively, as shown in Eqs. 2.16 and 2.17. First-order approximations of the mean and the tunable uniformity are considered appropriate for the purpose of on-line control.

2.7.2 Control Algorithms

In the on-line control of the tunable variabilities, values of the tuning factors and adjustment factor are determined for the next process so the tunable uniformity may be maximized and the mean may be adjusted to the target value. In calculating the control values of the tuning factors and adjustment factor, the models described in the previous section are used. The use of first-order linear models for the tunable uniformity and the mean simplifies the determination of the control values of the tuning factors and the adjustment factor. For example, when the tunable uniformity is represented by the slope of the regression line of group means, the slope is modeled as shown in Eq. 2.17, and the control value of the tuning factor is determined as follows:

$$\text{tuning factor control value} = -\frac{D_0}{D_1}\ , \qquad \text{(Eq. 2.18)}$$

since zero slope is required for the maximum uniformity. Similarly, the control value of the adjustment factor is determined as follows:

$$\text{adjustment factor control value} = \frac{\text{target value} - C_0}{C_1}\ . \qquad \text{(Eq. 2.19)}$$

On-line control uses the feedback of the post-process measurement data in order to adapt models for the tunable uniformity and the mean. When a process experiences changes in its conditions, it is necessary to adapt models to accurately describe the process. Since first-order linear models are used for the tunable

variability, two coefficients, i.e., constant and first-order coefficient, must be updated for model adaptation.

Algorithms have been developed to adapt models when processes experience either gradual changes or abrupt changes in process conditions. When there are gradual changes such as drifts in process conditions, an EWMA (exponentially weighted moving average) algorithm is used to weight historical data for proper model adaptation [45][46]. In the EWMA algorithm, historical data are weighted with exponentially decaying weights: the data from the previous run have the largest weight and the weights decrease exponentially as the data become dated. Figure 2.21 shows the weights in the EWMA algorithm, which are calculated as follows:

$$\text{weight for i-th data} = w\,(1-w)^{t-i} \qquad (\text{for } i = 1, 2, \ldots, t), \qquad \text{(Eq. 2.20)}$$

where t is the current run number. In the figure, value of 0.1 is used for w. The calculated weights are used for the modification of model coefficients in order to control (t+1)th run.

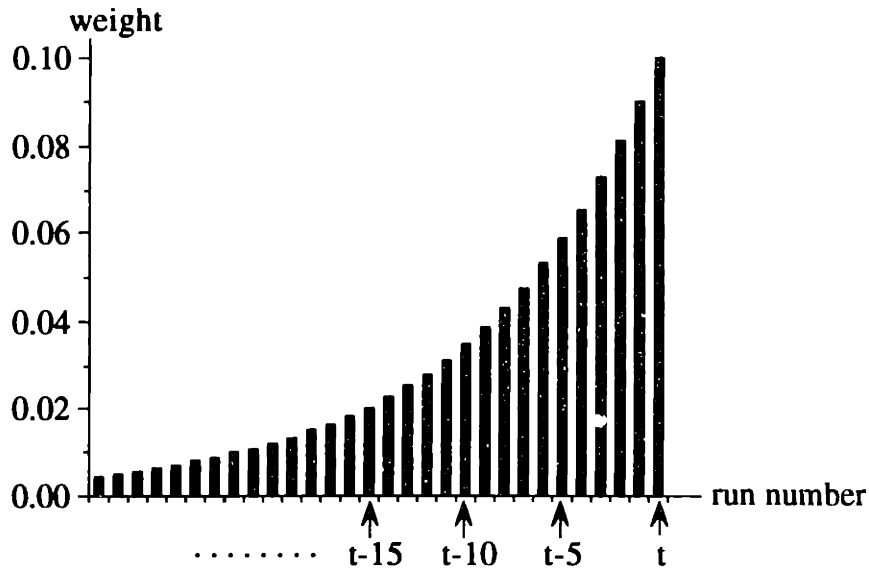

Figure 2.21 Weight values for calculation of t-th model coefficient

Consider the example where the model of the slope (Eq. 2.17) is being updated by modifying the constant, D_0, using the EWMA algorithm. When the historical data

up to the t-th run are available, the updated constant after t-th run, $D_{0,t}$, is calculated as follows:

$$D_{0,t} = \sum_{i=1}^{t} \left[w(1-w)^{t-i} \times \{(\text{slope})_i - D_1 \times (\text{tuning factor})_i\} \right] + D_{0,0} \times (1-w)^t \ , \quad \text{(Eq. 2.21)}$$

where w is the weight value, $(\text{slope})_i$ is the i-th measured slope value, and $D_{0,0}$ is the initial constant.

When there are sudden changes such as shifts in process conditions due to maintenance operations, it is necessary to adapt models based on the differences between the model prediction and the current measurement. Because there is a degree of uncertainty in measuring the magnitude of the change, compensation factors are used to reduce the risk of incorrectly modifying the models. For example, the compensation factor can be calculated using Bayesian inferences [10][11].

When a process shows periodic behavior due to cyclic environment changes, a time series analysis method can be applied to estimate the model coefficients. The cyclic environment changes are often due to daily temperature changes, periodic maintenance operations, seasonal changes, etc. Seasonal time series analysis can detect periodic changes of the processes and construct seasonal ARIMA (autoregressive integrated moving average) models [47][48]. The seasonal ARIMA model is used to forecast future process conditions, which enables the adaptation of model coefficients and control parameter values.

2.8 Summary and Illustration

The procedures of the off-line optimization of the robustness and the on-line control of the tunable variability are summarized as follows. Figure 2.22 illustrates the procedures.

Given a process, process variabilities are categorized into tunable variability and non-tunable variability based on the unique characteristics of the process and equipment. Tunable variability is easier to control than non-tunable variability and

includes the tunable uniformity and the mean. The robustness of a process is defined depending on how the tunable uniformity is characterized.

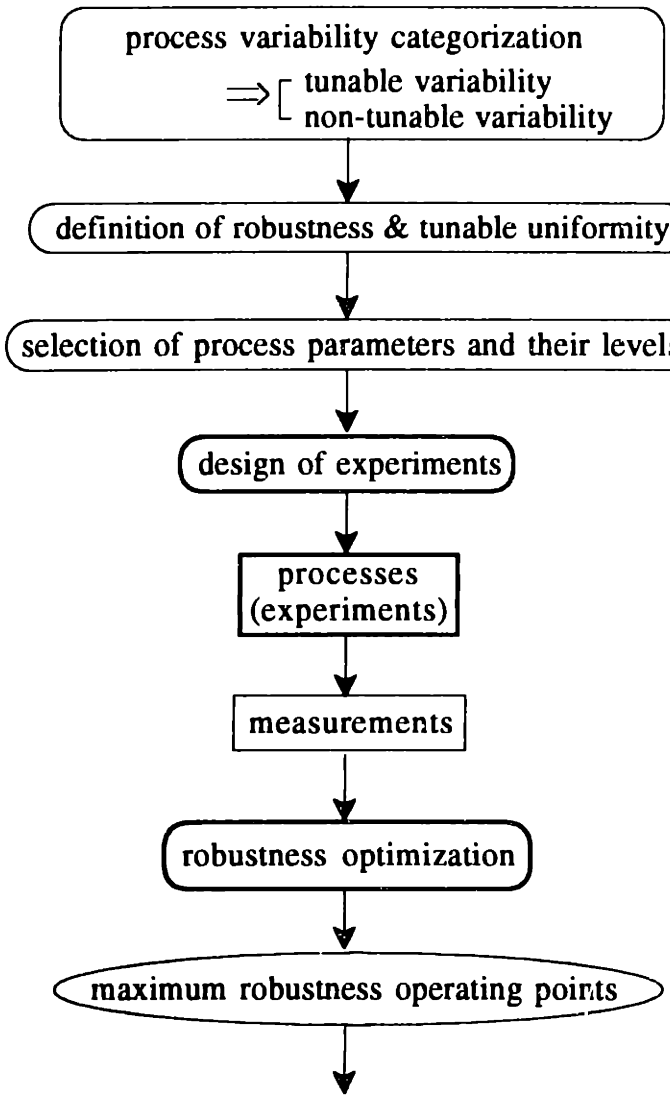

Figure 2.22 Procedures of methodology

The process parameters that will be used in the optimization and control are selected next. Considering the magnitude of process parameter ranges, the levels of the process parameters are determined in order to design experiments. In designing experiments, two or three levels are usually used, and orthogonal arrays are often used in designing experiments.

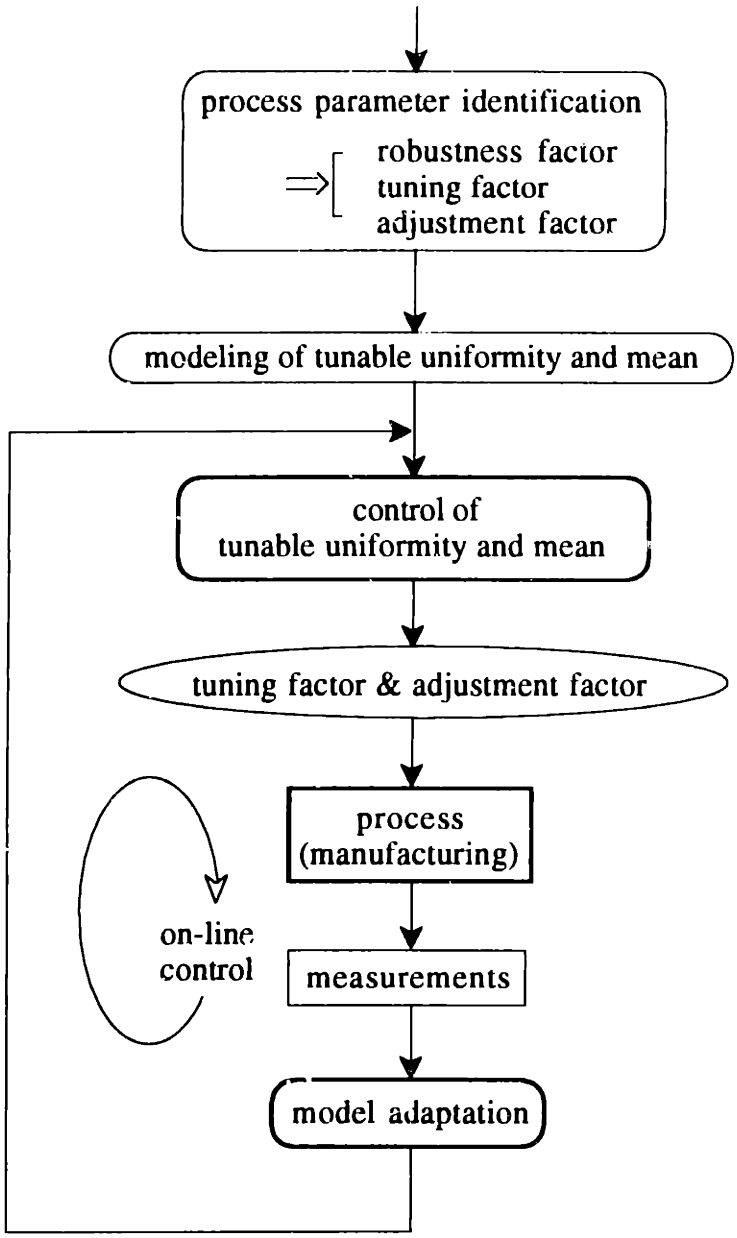

Figure 2.22 Procedures of methodology (continued)

The robustness is optimized with the analysis of experimental data from the designed experiments. It is maximized by determining the process parameter values called the maximum robustness operating points. Among the process parameters used in optimization, the tuning factors and the adjustment factor are identified based on the analysis of experimental data. The magnitude of the changes of the robustness, the tunable uniformity, and the mean are measured, and indices are calculated to

explain the effects of the process parameters on the robustness change, the tunable uniformity change, and the mean change. According to the index values, the tuning factors and adjustment factor are identified.

After the tuning factor and adjustment factor are identified, the tunable uniformity and mean are modeled as functions of the tuning factors and the adjustment factor, respectively. Usually simple first-order linear models are used to approximate the tunable uniformity and mean. The control value of the tuning factor for the maximum tunable uniformity and the control value of the adjustment factor for bringing the mean to the target value are determined using models of the tunable uniformity and mean.

After a process is run using the control values of the tuning factor and the adjustment factor, product characteristics are measured. The post-process measurement data are used to update the tunable uniformity model and the mean model. By adapting the models, the controller compensates for changes that have occurred to the process. Model adaptation and the determination of the control values of the tuning factor and adjustment factor are performed on a run by run basis, which keeps the process tunable variability at a minimum at all times.

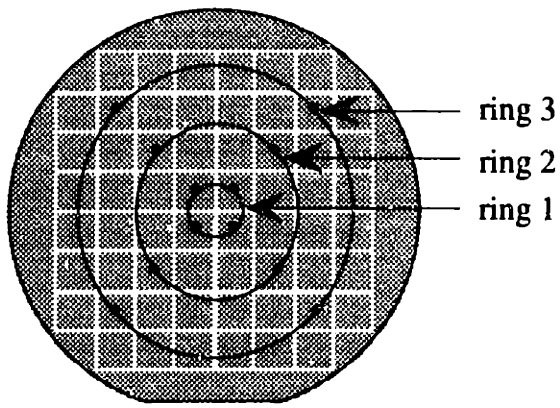

Figure 2.23 Measurement points grouped as ring 1, ring 2, and ring 3

The procedures are illustrated using a single wafer etching process of the VLSI fabrication processes. As explained in Section 2.2.2, process variabilities of single wafer processes can be divided into radial uniformity and circumferential uniformity.

The radial uniformity is categorized as tunable variability and the circumferential uniformity as non-tunable variability. In other words, the radial uniformity can be modeled and controlled on-line.

Figure 2.23 shows a wafer with the measurement sites. In the figure, 12 measurement sites are grouped as three rings. Differences between the group means correspond to the radial uniformity, and variations within each group correspond to the circumferential uniformity. Within-a-wafer uniformity of etching depths is controlled in this example for the purpose of illustration, and it is assumed that a target etching depth is given.

In Figure 2.24, the etching depth profile of the initial state is drawn as a response surface over the wafer, and the 12 measurements of the etching depths are plotted as grouped in three rings. The radial uniformity is represented by the slopes of the lines connecting group means. For the maximum radial uniformity, the slopes should be controlled to be zero. In Figure 2.24.A, the initial state of the etching depth uniformity is shown, which needs to be controlled to increase process quality. In the figure, both the radial and circumferential uniformities are shown to be poor.

Figure 2.24.B illustrates the result of off-line robustness optimization. The circumferential uniformity is optimized off-line by determining the maximum robustness operating points through designed experiments. Improved circumferential uniformity is shown as the reduced variations within each group. Note that the radial uniformity is not improved during the robustness optimization.

In Figure 2.24.C, the result of controlling the radial uniformity is shown. In this illustration, it is assumed that the ideal tuning factors exist. With ideal tuning factors, the radial uniformity can be controlled without degrading the optimized circumferential uniformity. Zero slopes of the lines connecting the group means show that radial uniformity is maximized. Note, however, that there is still a discrepancy between the grand mean of etching depths and the target value.

In Figure 2.24.D, where the grand mean is adjusted on-line to the target value using an adjustment factor, it is shown that all the measurements are made close to the target value; hence, the overall uniformity is maximized. Note that the mean adjustment is performed without degrading the optimized circumferential uniformity and the tuned radial uniformity.

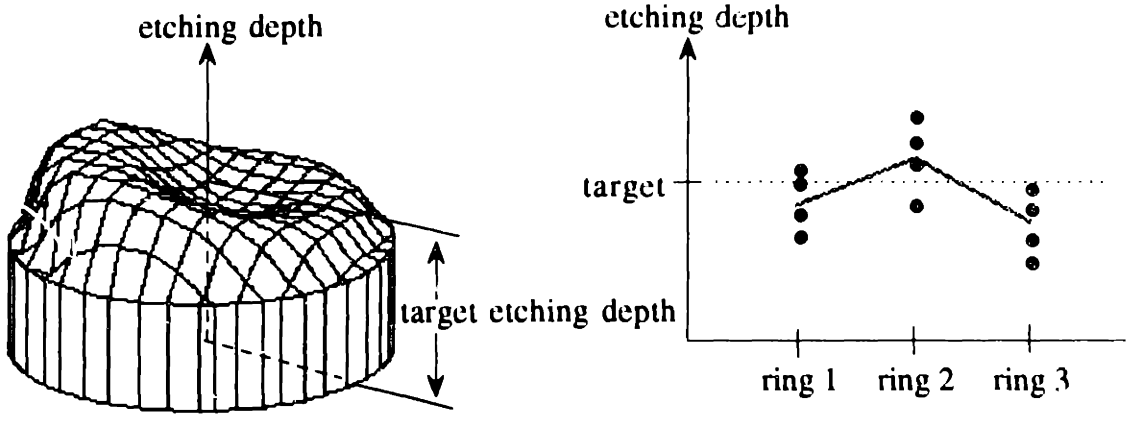

A. initial state

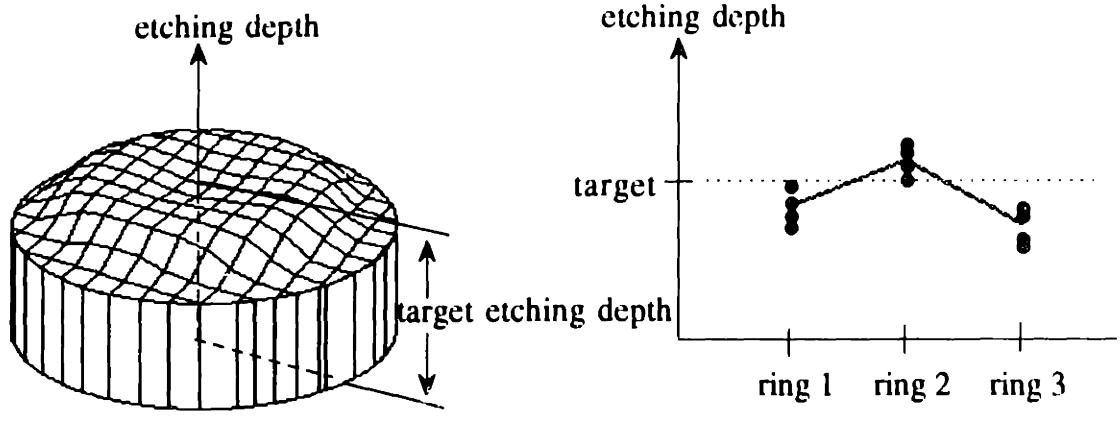

B. after off-line robustness optimization

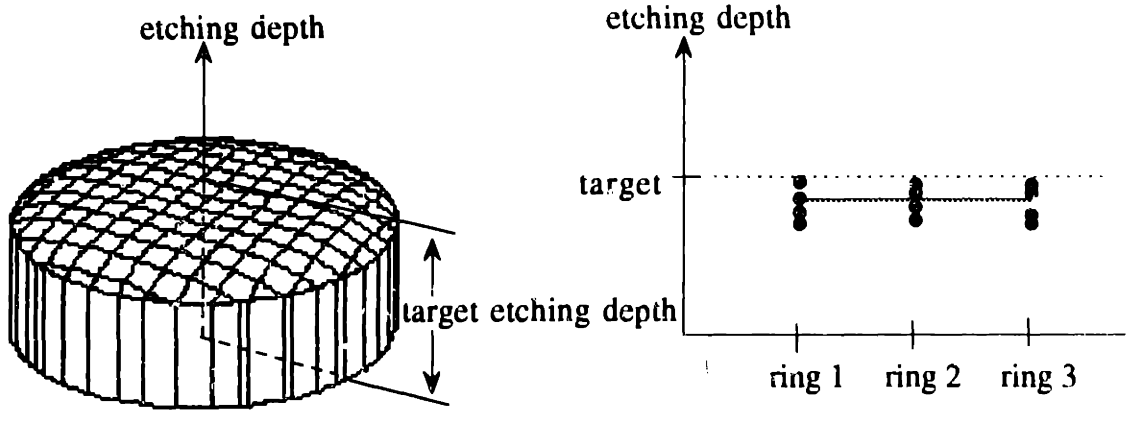

C. after on-line tunable uniformity tuning

Figure 2.24 Illustration using a single wafer etching process example

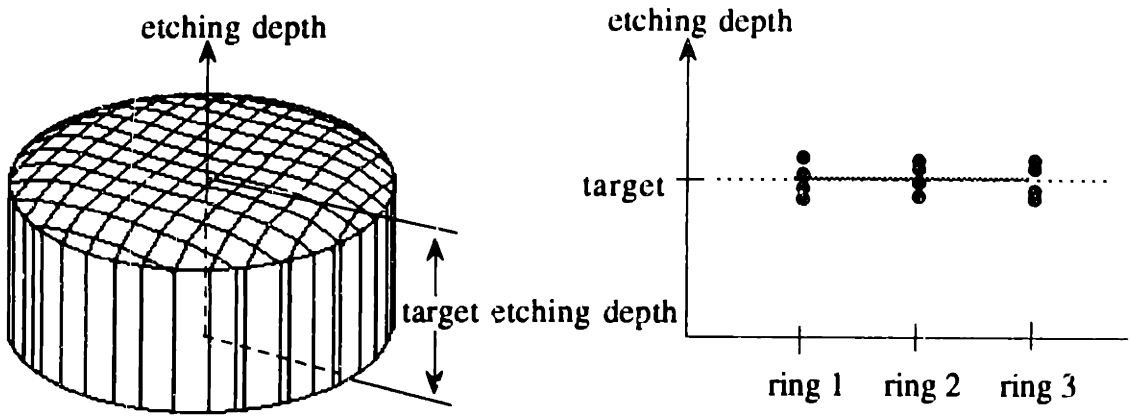

D. after on-line mean adjustment

Figure 2.24 Illustration using a single wafer etching process example (continued)

2.9 Discussions

The characteristics of the on-line control methodology developed in this work are as follows: The methodology is based on categorized process variabilities, it classifies the process parameters and uses them for different purposes, it decouples the procedures of robustness optimization and tunable variability control, and it increases process quality by the on-line control of tunable variability without degrading the process robustness.

The categorization of process variabilities requires an understanding of the process and equipment to be optimized and controlled. Understanding the underlying physical phenomena is helpful but a thorough understanding is not required since empirical modeling methods are usually used to approximate process responses.

Process parameters are classified into the robustness factor, the tuning factor and the adjustment factor. In many traditional methods of process optimization and modeling, all the available process parameters are used, with the expectation that the more process parameters are used, the more accurately process responses are explained. In real processes, however, disturbances to the processes as well as measurement noises cause large variabilities in the process responses, and the use of all the process parameters in modeling may be misleading. In this work, the tuning

factor and adjustment factor are selected as the most effective process parameters for modeling and control of tunable variabilities. By limiting the number of process parameters to be used in on-line control, modeling is simple and effective and adaptation of the model is fast, which is important for a rapid recovery from the deteriorated process performance due to the step changes in the process conditions.

The tuning factors and adjustment factors are selected so they do not degrade the process uniformity that has been optimized or controlled in previous steps. The tuning factors should control the tunable uniformity on-line without changing the robustness that has been optimized before on-line control begins. The adjustment factor should control the process mean on-line without degrading the robustness and the tunable uniformity. Therefore, the sequence of off-line robustness optimization, on-line control of the tunable uniformity, and on-line control of the mean improves process quality further without the deterioration of the preceding results. Hence, the risk of increasing process variability by tampering is reduced by using the tuning factors and adjustment factor.

The on-line control methodology contributed in this work can be compared with the robust design method. In robust design, process quality is optimized by two steps: robustness optimization and mean adjustment. The robust design method is based on the assumption that the process is so stable that the off-line optimization of process robustness is enough. In real manufacturing environments, however, process conditions change, and off-line optimization is not able to anticipate all the possible changes. In order to deal with any changes in process conditions, on-line control is necessary and can result in better process performance.

The algorithm developed in this work fits into the structure of the MIT process control system. The robustness optimization is performed off-line by FRG, and the on-line controls are performed by the RbR controller and RTC. It is expected that the implementation of the developed algorithm will enhance the system by enabling the on-line control of the process output characteristic mean as well as the process output variance.

CHAPTER 3
ON-LINE CONTROL EXAMPLES

The on-line control methodology developed in this thesis was applied to the uniformity control of single wafer plasma etching processes. Within-a-wafer uniformity of the etching processes was optimized and controlled on-line to improve quality of the etching processes.

3.1 Single Water Plasma Etching Process

Etching processes are used to make patterns of windows and holes on the film of various materials that are deposited on the wafer surfaces. The film functions as a barrier to the diffusion or implantation of impurities, and the windows define the area through which the impurities pass. The holes are used to make electrical connections to the underlying film [49]. The mask patterns are transferred from the masks to the photoresist by using a process called photolithography. The photoresist is light-sensitive material which is evenly coated on top of the wafer surface by a spinning process. After the photoresist is exposed and developed, mask patterns of the photoresist are formed on top of the film.

Patterns of the film are formed by etching parts of the film that are exposed through the windows of the photoresist mask pattern. After the etching process, the

photoresist pattern is removed, and the film patterning process is accomplished. Figure 3.1 shows the initial state of the film, which is evenly deposited on a wafer, the patterned photoresist mask on top of the film, and the final result of the etching process after the photoresist mask pattern is removed. It is shown that the pattern of the photoresist mask is transferred to the film.

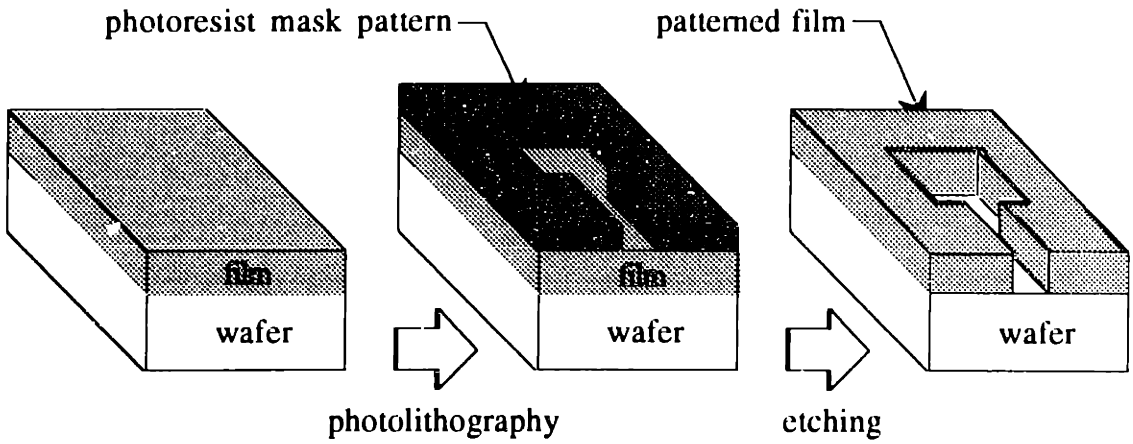

Figure 3.1 Pattern transfer to film by etching processes

A plasma etching process is a dry etching process that reduces particulate contamination, safety hazards and treatment of waste compared with the wet etching process that uses liquid chemicals such as acids; hence, the plasma etching process is preferred for VLSI fabrication processes. The plasma etching process generates etchant species using glow discharges. The plasma serves as a source of etchant species such as atoms, free radicals, and ions which are created from reactant gases at room temperature [50]. The reactant gases are selected so the etchant species can react chemically with the materials to be etched. The etchant species diffuse to the film surface and are adsorbed on the surface. A chemical reaction occurs between the etchant species and the film material and volatile byproduct is produced. The byproduct is desorbed from the surfaces, diffuse into the bulk of gas, and is carried away, which concludes the etching process [51]. The steps of the plasma etching process are shown in Figure 3.2.

The plasma etching process has the capability of replicating precisely lithographic mask patterns to underlying thin film by anisotropic etching. An electric

field created by the plasma directs ion bombardment along the normal to the wafer surface and the directionality of the ion flux causes a larger etching rates in a vertical direction, which results in anisotropic etching. Figure 3.3 compares isotropic etching used in the wet etching process and anisotropic etching in the plasma etching process.

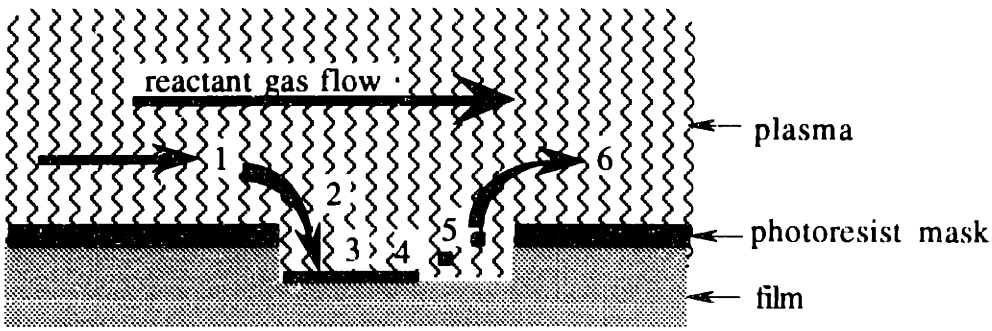

process steps:

1. generation of etchant species → 2. diffusion to surface of film → 3. adsorption → 4. chemical reaction → 5. desorption → 6. diffusion into bulk of gas

Figure 3.2 Process steps in plasma etching processes

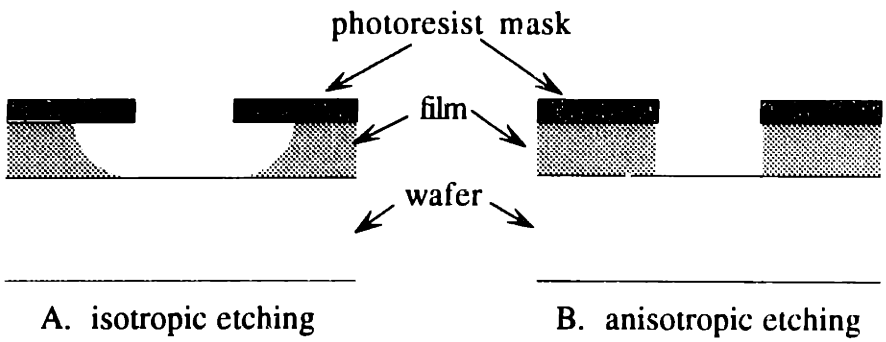

Figure 3.3 Isotropic etching vs. anisotropic etching

Etching equipment is classified into single wafer etchers and batch etchers according to the number of wafers in a process. Single wafer etchers have several advantages over batch etchers: the etching uniformity is well controlled, the end point detection is more accurate, and automation and load-locking is easier to implement.

However, single wafer etchers have lower throughput rates than batch etchers. In order to increase the throughput of single wafer etchers, the wafer size becomes larger. As the wafer size becomes larger, within-a-wafer uniformity becomes more critical. In the plasma etching process, the rate of etching is diffusion-limited, i.e., the etching rate is controlled by the rate of diffusion of etchant gases to the wafer surfaces [52]. Therefore, in the case of single wafer plasma etchers, a uniform concentration of etchant gases should be maintained over the wafer surface to produce high within-a-wafer uniformity.

In the experiments of this thesis, two single wafer plasma etchers were used: AutoEtch™ 590 by Lam Research Corp. for oxide etching experiments and Precision 5000 by Applied Materials, Inc., for polysilicon etching experiments.

AutoEtch™ 590 is an automated single wafer plasma etching equipment. It is equipped with two circular, parallel electrodes. A wafer is positioned on the bottom electrode, and the gap spacing between the top and bottom electrodes is controlled by a movement mechanism of the top electrode. Mixed reactant gases are injected onto the wafer surface from the top electrode through a shower head nozzle of more than 1,000 uniformly distributed holes and flow radially over the wafer surface. Operating pressure, RF plasma power, gap spacing, and gas flow rates are under automatic, closed-loop feedback control [53]. Figure 3.4 is a schematic diagram of the reaction chamber of AutoEtch™ 590.

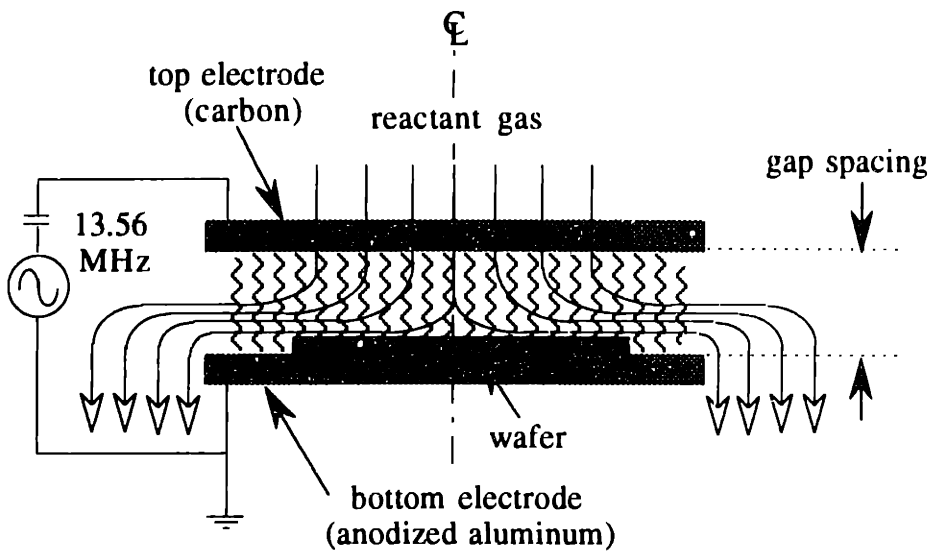

Figure 3.4 Schematic diagram of AutoEtch™ 590 single wafer plasma etcher

In the experiments, mixture of He, CHF_3, and CF_4 gases is used for oxide etching. A standard recipe for oxide etching is listed in Table 3.1.

parameter	value
pressure	3 torr
power	900 watts
gap spacing	0.36 cm
He flow rate	125 sccm
CHF_3 flow rate	30 sccm
CF_4 flow rate	90 sccm

Table 3.1 Standard recipe for oxide etching processes of AutoEtch™ 590

Precision 5000 is a magnetron ion etcher where a magnetic field is applied to enhance excitations by the electrons [54][55]. The magnetron ion etcher has high rates of both reactant species production and ion bombardment at low powers and pressures. It reduces some of the drawbacks of the single wafer plasma etcher such as bulk radiation damage and resist erosion due to the high power density and pressure. Hence, the magnetron ion etcher can maintain the high etch rates necessary for high throughputs in a single wafer plasma etcher.

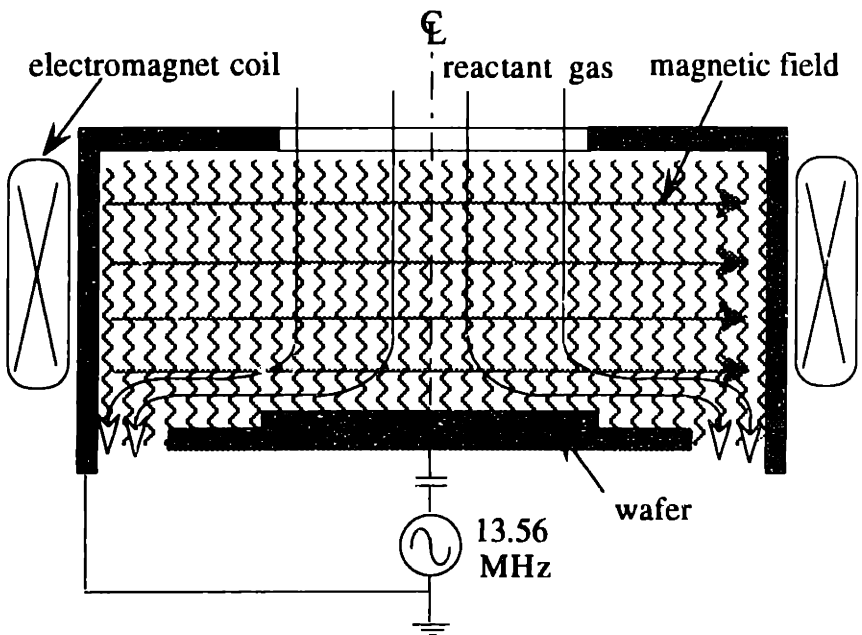

Figure 3.5 Schematic diagram of Precision 5000 single wafer plasma etcher

The magnetic field of the Precision 5000 is generated by two pairs of diagonally positioned electromagnets that create a rotating magnetic field orthogonal to the electric field of the RF discharge. The rotating magnetic field provides uniform process conditions over the wafer. The electrodes are of unequal areas, and a wafer is placed on the smaller electrode, which is powered, to expose it to the high energy ion flux. The reaction gases are injected downward into the reaction chamber through two rings of nozzle holes and flow radially over the wafer surface. The process parameters are operating pressure, RF plasma power, gas flow rates, magnetic field strength, and frequency of the rotating magnetic field. Figure 3.5 is a schematic diagram of the reaction chamber of the Precision 5000.

In the experiments, a mixture of HBr and Cl_2 gases is used for polysilicon etching. A standard recipe for polysilicon etching is listed in Table 3.2.

parameter	value
pressure	100 mtorr
power	250 watts
HBr/Cl_2 gas flow rates	10/30 sccm
magnetic field strength	75 G
magnetic field frequency	2 Hz

Table 3.2 Standard recipe for polysilicon etching processes of Precision 5000

Within-a-wafer uniformity of the single wafer etching processes was calculated using 12 measurement data of a wafer. Figure 3.6 shows 12 measurement sites of a wafer. The initial thickness of the film before the process is measured first. In the experiments, the etching procedures are stopped before the etching of the film is completed and the thickness of the remaining film is measured. The etching amounts are calculated by comparing the thickness differences before and after the process.

The thickness of the oxide film and polysilicon film were measured by using the Nanospec/AFT automatic film thickness measurement system by Nanometrics, Inc. which uses the optical interference method [56]. It measures the reflected light intensity in the wavelength range of 480-790 nm using a micro spectrophotometer and calculates the thickness of the film based on the interference [51]. In the case of oxide film thickness measurements, the interference occurs between the lights reflected from

the air/SiO_2 interface and the Si/SiO_2 interface. In the case of polysilicon film thickness measurements, there is an oxide layer of 1000 Å thickness underneath the polysilicon film; hence, the interference occurs between the lights reflected from the air/polysilicon interface and from the polysilicon/SiO_2 interface. The device has an accuracy of ±2% when it measures SiO_2 film thickness in the range of 400Å to 30,000Å.

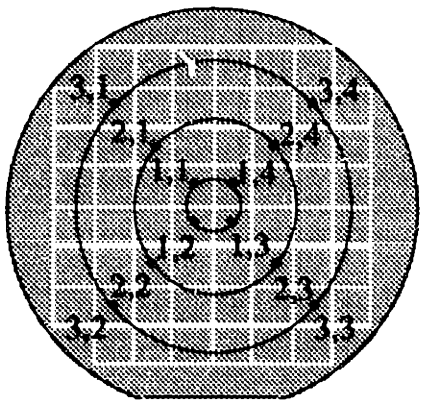

• : measurement site

Figure 3.6 Positions of 12 measurement sites on a wafer

3.2 Related Works on Plasma Etching Process

In plasma etching processes, many chemical reactions occur simultaneously: electron impact reactions to generate etchant species, gas-to-gas reactions, gas-to-wafer surface reactions, etc. Although the reactions can be modeled by understanding the creation, transport, and loss of species by the use of methods such as continuum approaches, Monte Carlo simulations, or finite element methods, the rate constants and the diffusion coefficients for most reactions need to be assumed, which makes the mechanistic modeling difficult [57]. Hence, statistical approaches to the modeling of plasma etching processes have been used instead.

Jenkins *et al.* showed that the response surface methodology can quantitatively and efficiently characterize the plasma etching processes [58]. The etching rate was modeled using polynomials of process parameters. They also observed three distinctive etching patterns and found that radial etching uniformity can be modeled and optimized.

Riley modeled etching rate and uniformity in a SiO_2 etching process using fully quadratic models with four process parameters [59]. The models have 15 coefficients to be fitted, and a Box-Behnken design was used for designing 27 experiments. He showed that fully quadratic models provide a significantly better fit to the experimental data than do linear models. From the models, it was found that SiO_2 etching uniformity is virtually insensitive to changes in pressure between 1,000 and 1,300 mtorr with reactant gases of either CHF_3 or C_2F_6.

May *et al.* modeled the etching rate, uniformity, selectivity, and anisotropy of a polysilicon etching process using the AutoEtch™ 490 single wafer plasma etcher [60]. Riley *et al.* also studied characteristics of the SF_6/He plasma of the AutoEtch™ 490 in Si_3N_4, thermal SiO_2, and photoresist etching processes using response surface methodology [61]. They showed that interelectrode spacing has significant effects on etching uniformity and modeled the etching uniformity with full quadratic polynomials.

The response surface methodology was also used to develop a new process and to identify new process parameter windows. The effects of the process parameters are first characterized through designed experiments, and then the optimum process parameter values are determined based on the model constructed from the experimental data. For example, Riley *et al.* used response surface methodology in developing a multi-step SiO_2 plasma etching process and a magnetron-enhanced plasma process for a tungsten etchback process [62][63]. Daniel *et al.* used response surface methodology to identify a new process parameter window for a single-wafer plasma etcher [64].

Real time monitoring of plasma etching processes was studied to detect problems. Barna monitored both an endpoint trace and the analog values of all the process control parameters [65]. Using the end point trace, it was determined whether the processed wafer had experienced any anomalous processing conditions. The analog values of all the process control parameters were monitored during the entire etching process for each wafer and were analyzed for only the misprocessed wafers. It was shown that the combination of two measurements enhanced significantly the reliability and the uptime of etchers .

Real time control was performed with multivariable control system analysis [66]. Linear dynamic models of process variables such as species concentrations, and

dc bias, were constructed as functions of manipulated variables such as pressure, power, gas flow compositions, etc. Since it is difficult to measure performance variables such as etching rate, selectivity, anisotropy, uniformity, etc., in real time, correlations of the process variables and the performance variables were modeled using regression analysis methods.

Multivariate statistical process control method was also applied to the plasma etching processes with real time measurements of process conditions [20]. The real time measurement data were filtered by time series models of the processes, and a multivariate statistical process control was performed on the filtered data to monitor the process conditions.

One example of the quantitative studies of the effects of the process parameters in the plasma etching process is an analysis of the effects of gas flow rates in the etching of silicon materials in fluorocarbon gases. Chapman *et al.* defined a utilization factor to describe the extent to which reaction gases are converted to volatile products and showed that many process characteristics can be explained using the utilization factor [67].

3.3 Process Variability in Single Wafer Plasma Etching Process

Non-uniformity in single wafer plasma etching processes is considered to be caused by reactant gas flow patterns, local concentration variations caused by the reactant recombination, wafer temperature uniformity, and electrode conditions such as polymeric film buildup and surface contamination. Single wafer plasma etchers are usually designed to have axisymmetry in their configurations to ensure the circumferential symmetry. Hence, within-a-wafer uniformity in single wafer plasma etching processes are divided into radial uniformity and circumferential uniformity. Because of the axisymmetry, control of circumferential uniformity cannot be easily accomplished. The radial uniformity, however, is readily controlled with process parameters. Hence, the radial uniformity is categorized as tunable variability, and the circumferential uniformity is categorized as non-tunable variability. Mean etch depth, another component of tunable variability, is easily controlled to meet the target thickness by changing process time. Therefore, process time is identified accordingly as the adjustment factor.

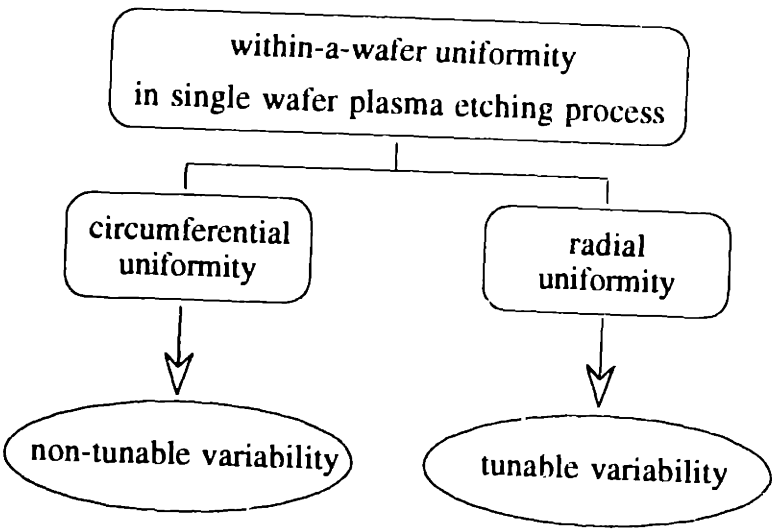

Figure 3.7 Process variabilities in single wafer plasma etching processes

Since the adjustment factor is clearly defined, the uniformity of etching rates is considered instead of the uniformity of etching depths. The etching rates of 12 measurement sites are calculated by dividing the etching depths by process time. The measurement sites are as shown in Figure 3.6. The 12 etching rate data are grouped into three rings, according to the distance from the center of the wafer, and each group mean, $\overline{Y}_{i\bullet}$, is calculated as follows:

$$\overline{Y}_{i\bullet} = \frac{1}{4}\sum_{j=1}^{4} Y_{ij} \qquad (\text{for } i = 1, 2, 3), \qquad \text{(Eq. 3.1)}$$

where Y_{ij} is the etching rate at j-th measurement site of i-th ring.

First, consider the case where the radial uniformity is controlled using a single tuning factor. The radial uniformity is represented by *slope* defined as the relative slope of the regression line of three group means as follows:

$$\text{slope} = 100 \times \left(\frac{\hat{\overline{Y}}_{3\bullet} - \hat{\overline{Y}}_{1\bullet}}{2\,\overline{Y}_{\bullet\bullet}}\right), \qquad \text{(Eq. 3.2)}$$

where $\hat{\overline{Y}}_{1\bullet}$ and $\hat{\overline{Y}}_{3\bullet}$ are regression predictions of the group means $\overline{Y}_{1\bullet}$ and $\overline{Y}_{3\bullet}$, respectively, and $\overline{Y}_{\bullet\bullet}$ is the grand mean of 12 measurements, i.e.,

$$\overline{Y}_{\bullet\bullet} = \frac{1}{12} \sum_{i=1}^{3} \sum_{j=1}^{4} Y_{ij} \quad . \qquad \text{(Eq. 3.3)}$$

Figure 3.8 shows 12 measured etching rates, each group mean, and the regression line. The zero value of slope corresponds to the maximum radial uniformity.

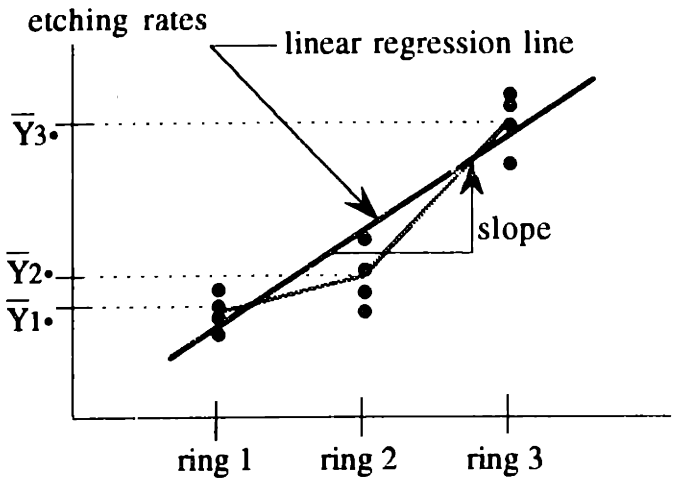

Figure 3.8 Slope for single tuning factor

The circumferential uniformity is represented by *robustness* defined in Eq. 2.11 as follows:

$$\text{robustness} = \left[\sum_{i=1}^{3} \left\{ \left(\frac{\sigma_{i\bullet}}{\hat{\overline{Y}}_{i\bullet}} \right)^2 + \left(\frac{\overline{Y}_{i\bullet} - \hat{\overline{Y}}_{i\bullet}}{\hat{\overline{Y}}_{i\bullet}} \right)^2 \right\} \right]^{-1} , \qquad \text{(Eq. 3.4)}$$

where $\sigma_{i\bullet}$'s are group standard deviations, i.e.,

$$\sigma_{i\bullet} = \sqrt{\frac{1}{4} \sum_{j=1}^{4} (Y_{ij} - \overline{Y}_{i\bullet})^2} \quad . \qquad \text{(Eq. 3.5)}$$

When the radial uniformity is controlled using two tuning factors so that all the group means may be identical, the radial uniformity is represented by not only the slope defined above but also the deviation of ring2 group mean, $\overline{Y}_{2\bullet}$, from the line connecting ring1 group mean, $\overline{Y}_{1\bullet}$, and ring3 group mean, $\overline{Y}_{3\bullet}$. The deviation explains

the radial profile of etching rates and is defined as *curvature*. The slope and curvature are calculated as follows:

$$\text{slope} = 100 \times \left(\frac{\bar{Y}_{3\bullet} - \bar{Y}_{1\bullet}}{2\,\bar{Y}_{\bullet\bullet}}\right) , \qquad \text{(Eq. 3.6)}$$

and

$$\text{curvature} = 100 \times \left[\frac{\bar{Y}_{2\bullet} - \frac{(\bar{Y}_{3\bullet}+\bar{Y}_{1\bullet})}{2}}{2\,\bar{Y}_{\bullet\bullet}}\right] . \qquad \text{(Eq. 3.7)}$$

Figure 3.9 shows 12 measured etching rates, each group mean, and the regression line. The zero values of both slope and curvature means the maximum radial uniformity.

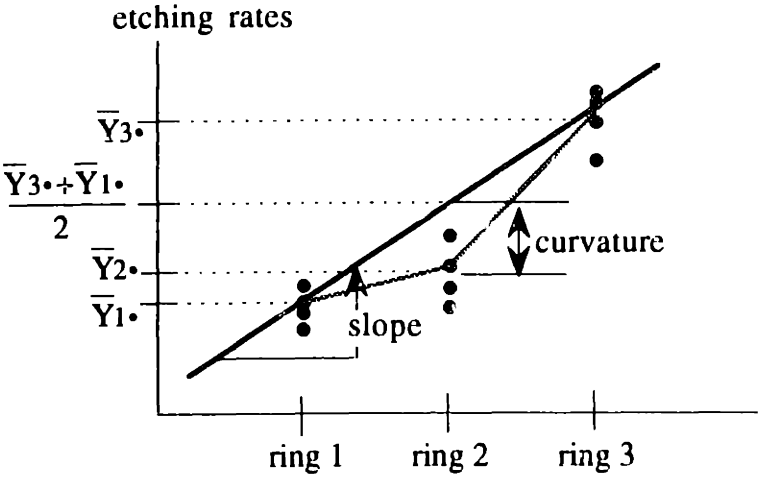

Figure 3.9 Slope and curvature for two tuning factors

When two tuning factors are used, the circumferential uniformity is represented by *robustness* defined in Eq. 2.10 as follows:

$$\text{robustness} = \left[\sum_{i=1}^{3} \left(\frac{\sigma_{i\bullet}}{\bar{Y}_{i\bullet}}\right)^2\right]^{-1} . \qquad \text{(Eq. 3.8)}$$

Note that the slopes of Eq. 3.2 and of Eq. 3.6 are identical since the regression is performed on 3 group means in this example.

Figure 3.10 shows compiled data of overall uniformity versus slope of the oxide etching experiments using the AutoEtch™ 590 over a long period of time and with a wide range of process parameter values. In order to represent the total quality of processes, *overall uniformity* is also defined as follows:

$$\text{overall uniformity } (\%) = 100 \times \frac{\sigma_{\bullet\bullet}}{\bar{Y}_{\bullet\bullet}} \quad , \qquad \text{(Eq. 3.9)}$$

where

$$\sigma_{\bullet\bullet} = \sqrt{\frac{1}{12} \sum_{i=1}^{3} \sum_{j=1}^{4} (Y_{ij} - \bar{Y}_{\bullet\bullet})^2} \quad . \qquad \text{(Eq. 3.10)}$$

Hence, the overall uniformity is directly related to the total quality of the processes.

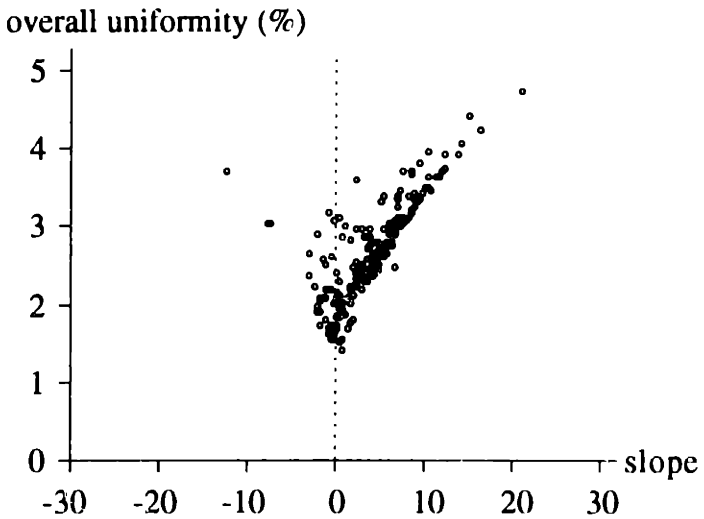

Figure 3.10 Overall uniformity vs. slope of AutoEtch™ 590 experimental data

It is shown that overall uniformity is improved by making slope zero. It is also shown that the zero slope is not enough to improve the overall uniformity, considering the wide spreads of overall uniformity at each slope value. The spreads are due to the magnitudes of the circumferential uniformity. Therefore, it is concluded that it is necessary to make slope zero as well as to control the circumferential uniformity to improve overall uniformity effectively.

3.4 Oxide Etching Process Experiments

3.4.1 Single Tuning Factor Experiments

The experimental results of applying on-line control using a single tuning factor to the oxide etching process are included in this section. Since one tuning factor was used, the slope defined in Eq. 3.2 was controlled on-line after the robustness defined in Eq. 3.4 was optimized off-line.

3.4.1.1 Robustness Optimization

Among the process parameters of the oxide etching process using the AutoEtch™ 590, gap spacing between the top and bottom electrodes (gap) and CHF_3 gas flow rate (CHF_3) were used as process parameters in the single tuning factor experiments. Two parameters were used to show the effects on robustness and slope as response surfaces in three dimensions. Gap and CHF_3 were selected among the process parameters since they were known to have significant effects on the slope and the robustness from the results of preliminary experiments.

In order to decide a tuning factor and a maximum robustness operating point between two process parameters, 2^2 full factorial experiments were designed as shown in Figure 3.11, using two levels of each parameter. The values of the other process parameters, which were fixed in the experiments, are also shown in the figure. Each experimental design was performed twice as replicates, and eight experiments were performed in total.

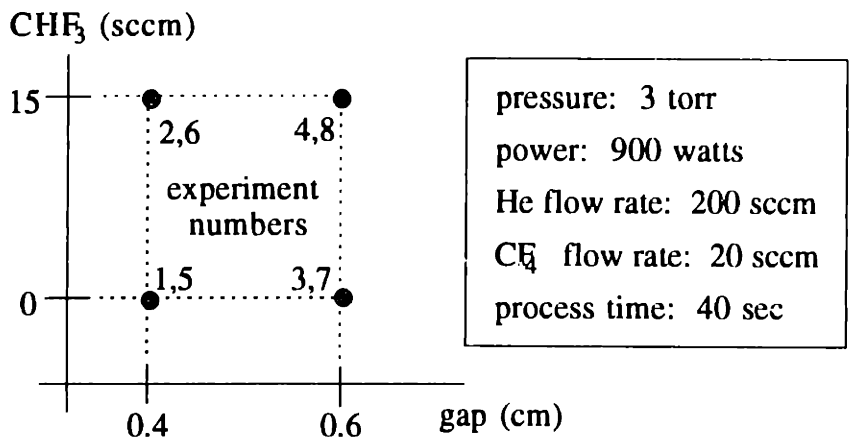

Figure 3.11 Process parameter values for 2^2 full factorial experiments

Using the experimental data listed in Appendix B.1.1, the robustness and slope were calculated as shown in Table 3.3. The robustness and slope were then modeled respectively as functions of gap and CHF_3 as follows:

$$\text{robustness} = 546.2 - 296.7\times(\text{gap}) - 388.6\times(CHF_3) + 310.0\times(\text{gap})\times(CHF_3), \quad \text{(Eq. 3.11)}$$

and

$$\text{slope} = -4.1488 - 1.0663\times(\text{gap}) - 2.7463\times(CHF_3) - 5.9988\times(\text{gap})\times(CHF_3). \quad \text{(Eq. 3.12)}$$

Being based on the 2^2 full factorial design experimental data, the models have first-order terms and an interaction term as shown in Eqs. 3.11 and 3.12. In the above equations, gap and CHF_3 are normalized to have values between -1 and 1. The standard errors of coefficients are 103.3 and 0.5074 in Eq. 3.11 and Eq. 3.12, respectively.

The response surfaces of the robustness and slope are plotted in Figures 3.12 and 3.13, respectively. It is shown that the low levels of both gap and CHF_3 are maximum robustness operating points since they results in high robustness.

experiment number	gap (cm)	CHF_3 (sccm)	robustness	slope
1	0.4	0	1154.5	-5.735
2	0.4	15	158.5	-1.531
3	0.6	0	202.5	4.448
4	0.6	15	100.2	-13.826
5	0.4	0	1928.4	-6.941
6	0.4	15	130.2	1.865
7	0.6	0	453.5	2.614
8	0.6	15	241.5	-14.086

Table 3.3 Results of 2^2 full factorial experiments

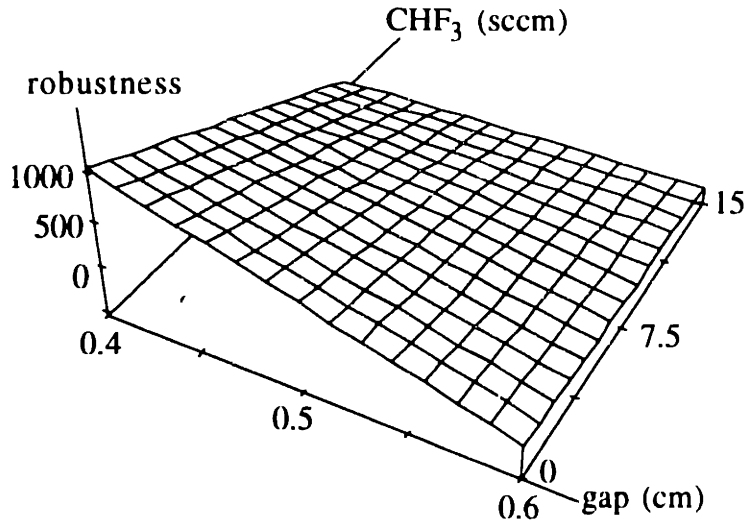

Figure 3.12 3D plot of robustness response surface

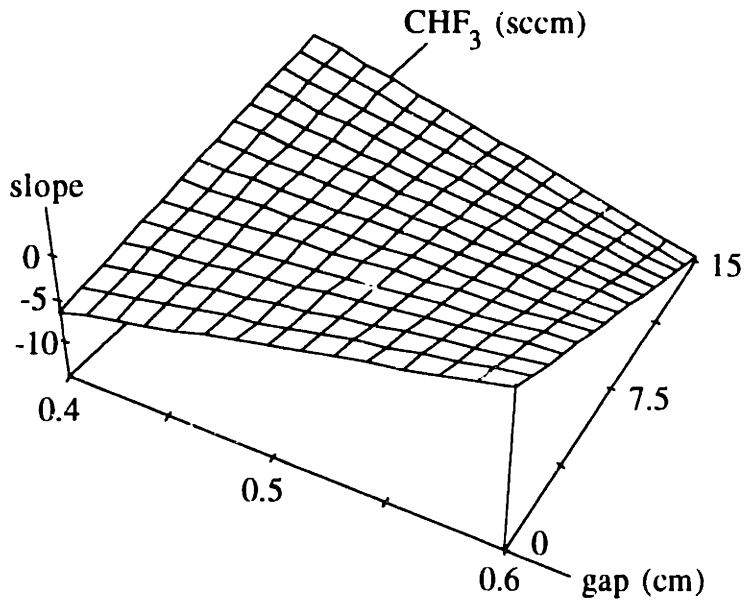

Figure 3.13 3D plot of slope response surface

In order to identify a tuning factor, indices (Eq. 2.14) for gap and CHF_3 at the maximum robustness operating points were calculated as follows:

$$\text{index}_t = \left| \frac{\left[\frac{\Delta \text{ robustness}}{\text{average of robustness}}\right]}{\left[\frac{\Delta \text{ slope}}{\text{average of slope}}\right]} \right| , \qquad \text{(Eq. 3.13)}$$

and their values are listed in Table 3.4.

		gap	CHF_3
robustness	average	934.8	842.9
	difference	1213.4	1397.2
slope	average	-1.403	-3.083
	difference	9.865	6.505
$index_t$		0.1846	0.7856

Table 3.4 Index values for gap and CHF_3

Since gap has the smaller index value, it was selected as a tuning factor, and CHF_3 was used as a robustness factor. Using the previous experimental data for low values of CHF_3, slope was modeled as a first-order linear function of gap as follows:

$$\text{slope} = -1.4025 + 4.9325\times(\text{gap}) \ , \qquad \text{(Eq. 3.14)}$$

where gap is normalized to have values between -1 and 1. The standard error of coefficient is 0.5487.

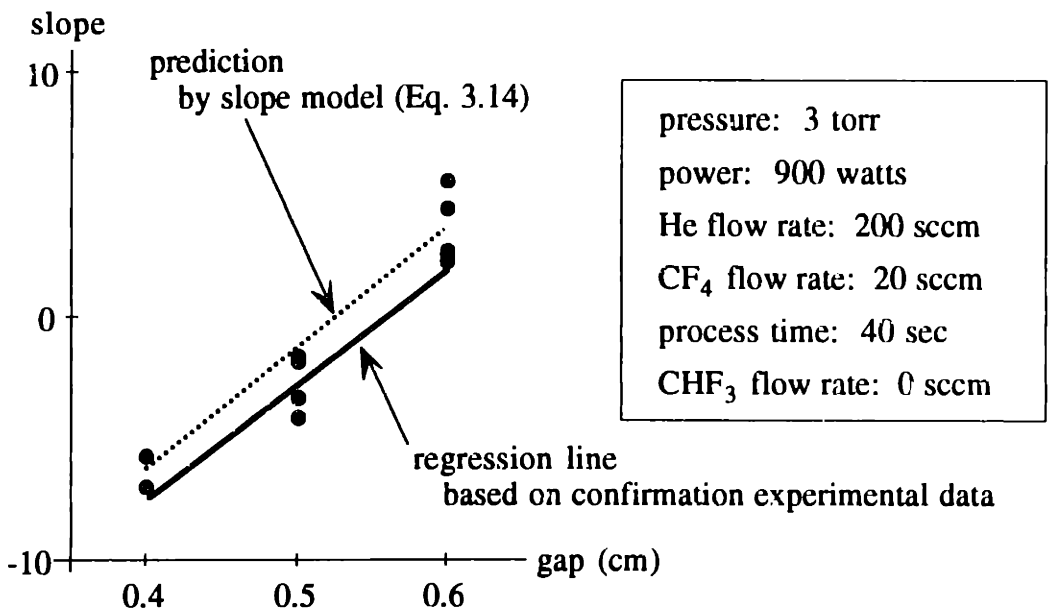

Figure 3.14 Results of confirmation experiments

After the slope model was obtained, a set of experiments were performed in order to confirm the model. In the experiments, CHF_3 was set to its maximum

robustness operating point. Figure 3.14 shows the results of the confirmation experiments with the first-order regression line of the measurements.

The slope of the regression line is shown as similar to that of the slope model (Eq. 3.14). Therefore, it is concluded that the model needs to be adapted by updating only the constant term to compensate for the process condition differences between the two sets of experiments.

3.4.1.2 On-line Control

In Section 3.4.1.1, robustness was optimized by finding the maximum robustness operating point of CHF_3. After the robustness optimization, the slope was controlled on-line using the selected tuning factor. In order to compare the efficiency of on-line control, another experiments were performed without control at the same time and the results of both experiments were compared. The optimization-only experiments were performed with the process parameter values as determined by the robustness optimization; hence, the results of the optimization-only experiments are expected to have a good uniformity. On-line control is expected to compensate for any changes in the process conditions, which are to be reflected in the results of the optimization-only experiments.

Table 3.5 shows the process parameter values for the optimization-only experiments and the on-line control experiments, respectively. A series of parallel experiments were performed over several days so the process condition changes can be seen in the results of the optimization-only experiments.

	optimization-only	on-line control
pressure (torr)	3	3
power (watts)	900	900
gap (cm)	0.53	tuning factor
He flow rate (sccm)	200	200
CHF_3 flow rate (sccm)	0	0
CF_4 flow rate (sccm)	20	20
process time (sec)	40	40

Table 3.5 Process parameter values for experiments

For the on-line control experiments, the slope model (Eq. 3.14) was adapted by updating the constant term of the model. Figure 3.15 illustrates how the model adaptation algorithm works. Using the current slope model shown as ①, the gap value ② is determined to make the model prediction zero. After an experiment is performed, the slope is measured as ③. The slope is different from zero since either the model is not correct or there is a change in process conditions. The constant term of the model is the updated so the model can fit the measured value of the slope. The adapted model is shown as ④. By using the adapted model, the gap value for the next run ⑤ is calculated. This model adaptation algorithm is equivalent to the EWMA algorithm explained in Section 2.7.2, with a weight value of 1.

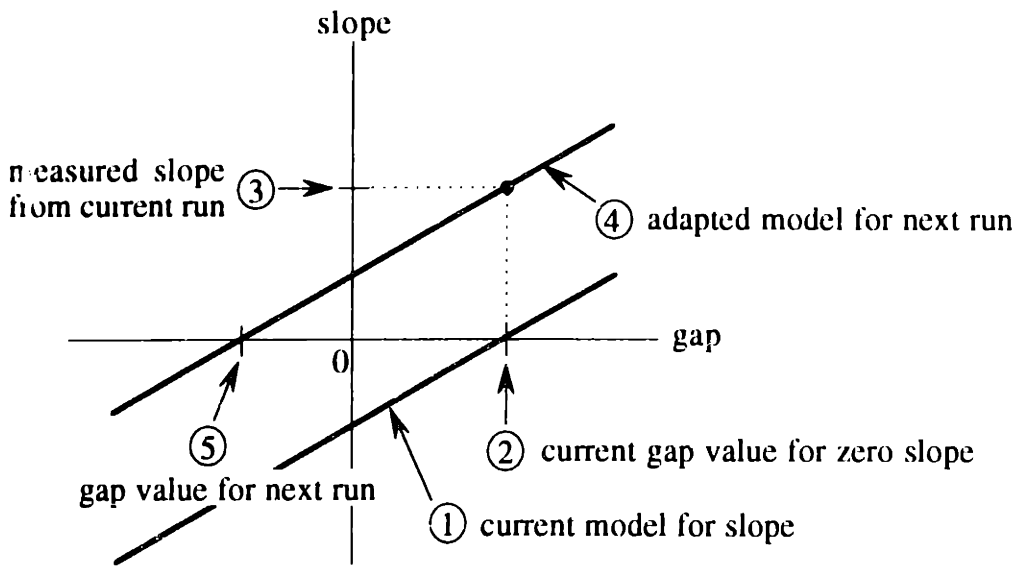

Figure 3.15 Illustration of model adaptation algorithm

15 runs of paired optimization-only and on-line control experiments were performed. A step change was introduced after the 9th run to check the performance of the on-line control. The process parameter values, other than the tuning factor and robustness factor, were changed after the 9th run so that the process conditions change stepwise. Table 3.6 shows the process parameter values before and after the step change.

	before	after
pressure (torr)	3	4
power (watts)	900	700
He flow rate (sccm)	200	125
CF_4 flow rate (sccm)	20	75
process time (sec)	40	40

Table 3.6 Process parameter shifts as a step change

Data of the experiments are listed in Appendix B.1.2. Table 3.7 shows the values of the constant term of the slope model and the gap values that were generated based on the model for each run. It is shown that the constant term value was updated from a negative to a positive value after the step change was introduced to compensate for the process condition changes.

run number	constant	gap (cm)
1	-1.4025	0.53
2	-3.0225	0.56
3	-1.2125	0.52
4	-2.7825	0.56
5	-0.5425	0.51
6	-1.6525	0.53
7	-5.3625	0.60
8	-5.9225	0.60
9	-5.4825	0.60
10	-5.4825	0.60
11	-1.9625	0.54
12	0.1370	0.50
13	1.7800	0.46
14	3.3730	0.43
15	5.3028	0.40

Table 3.7 Constants and gap values of on-line control

In Figure 3.16, the slope values of the optimization-only and on-line control experiments are plotted. The target value of slope is zero for the radial uniformity. The slopes are shown to be controlled by the on-line control algorithm so that they are close to the zero slope, while the slope values of the optimization-only experiments represent the process condition fluctuations.

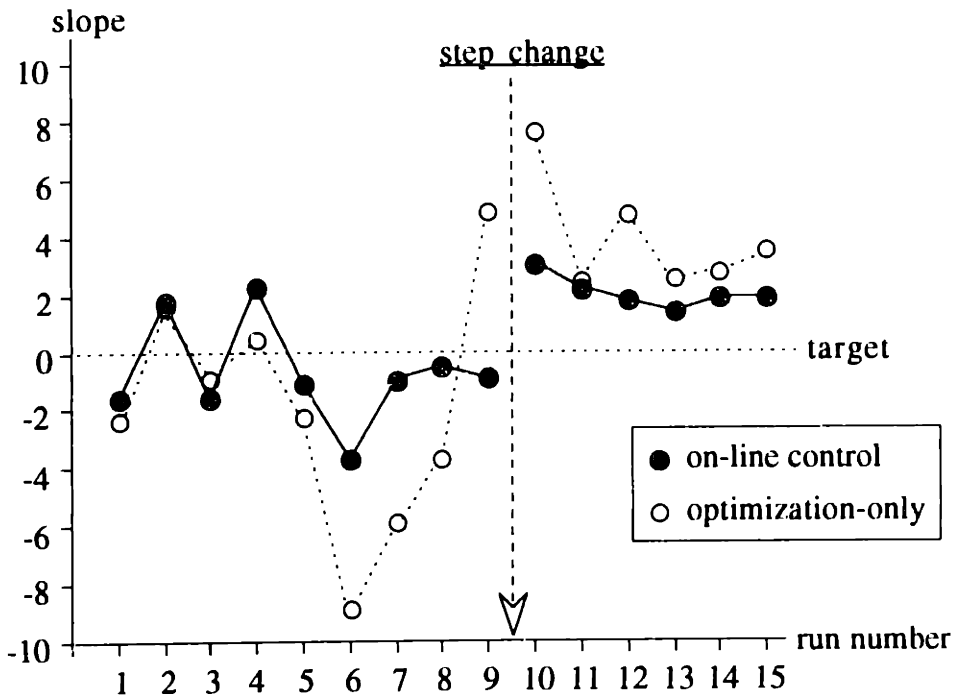

Figure 3.16 Historical data of the slope of single tuning factor experiments

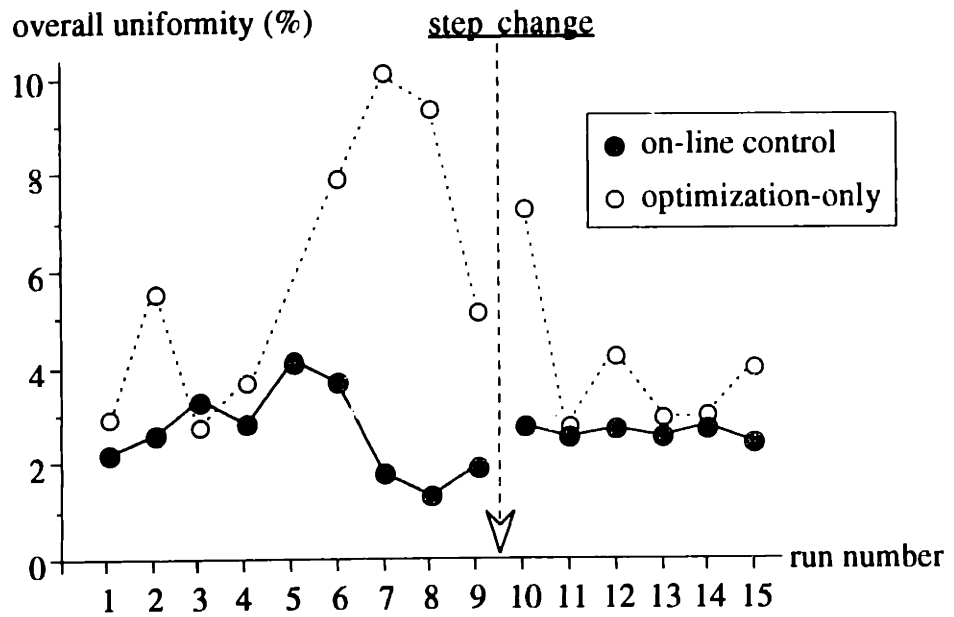

Figure 3.17 Historical data of the overall uniformity of single tuning factor experiments

Figure 3.17 shows the historical data of overall uniformity defined in Eq. 3.9. It is shown that overall uniformity of the on-line control experiments are better than that of the optimization-only experiments, which means that within-a-wafer uniformity was controlled effectively by on-line control of the slope.

3.4.1.3 Discussions

It was shown that the slope is controlled by using a first-order linear model and by applying the constant term update algorithm. By controlling the slope, the overall uniformity was improved when compared with the results of the optimization-only experiments. Even when a step change was introduced, the on-line control was able to compensate for the change, resulting in better within-a-wafer uniformity.

Figure 3.18 shows the average values of the slopes before and after the step change for the optimization-only experiments and on-line control experiments, respectively. The slopes of the on-line control experiments are shown to be closer to the zero slope which is the target slope for control. In the figure, the error bars represent the magnitude of two standard deviations of the average slope values.

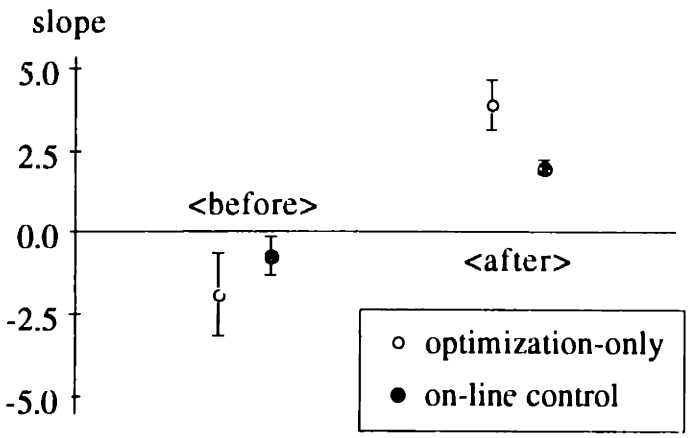

Figure 3.18 Average slopes before and after the step change

Figure 3.19 shows the averages of the overall uniformity before and after the step change for the optimization-only experiments and on-line control experiments, respectively. It is shown that on-line control improved the overall uniformity by a factor of 2.2 before the step change and by a factor of 1.5 after the step change. The

on-line control also kept overall uniformity at similar values before and after the step change. In the figure, the error bars represent the magnitude of two standard deviations of the average overall uniformity values.

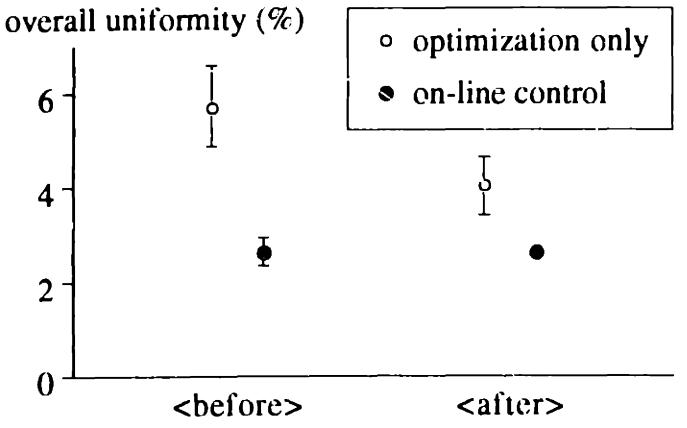

Figure 3.19 Average overall uniformity before and after the step change

One concern of using on-line control is whether the variability of a process is increased or not by tweaking process parameters. If the process conditions are stable enough, then the process variability may increase by tweaking [68].

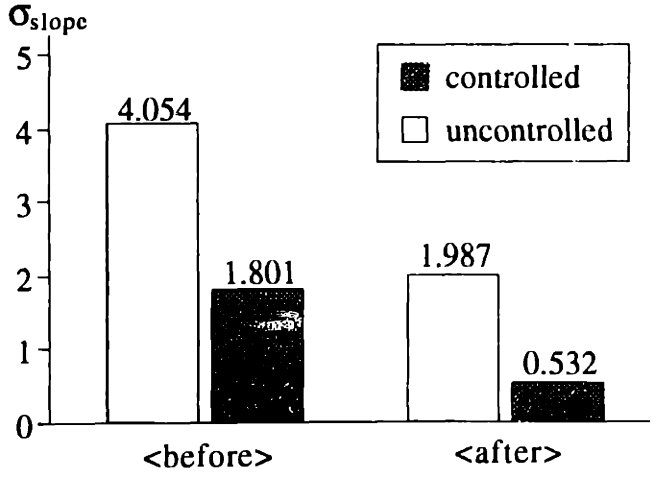

Figure 3.20 Standard deviations of the slopes before and after the step change

In Figure 3.20, the standard deviations of the slopes of the optimization-only and the on-line control experiments before and after the step change are compared. It

is shown that the standard deviations of the slopes were reduced by applying on-line control. Hence, it is concluded that the process conditions are not so stable that on-line control of the slope was actually necessary to improve overall uniformity. The effectiveness of on-line control is shown by the reduced standard deviation.

The overall uniformity consists of the radial uniformity and the circumferential uniformity. In the on-line control experiments, the radial uniformity was on-line controlled and the circumferential uniformity was off-line optimized and maintained as optimized during on-line control. Figure 3.21 shows the magnitudes of the radial and the circumferential uniformities for the on-line control experimental data. The fact that the circumferential non-uniformity became large for runs 7,8, and 9 means the tuning factor used in the experiment was not ideal. The tuning factor does have some effect on the robustness, even if the effect of the tuning factor was the smallest among the process parameters. Also, it is shown that the circumferential uniformity became degraded due to the process condition changes after the step change was introduced after the 9th run, while the radial uniformity was still well controlled.

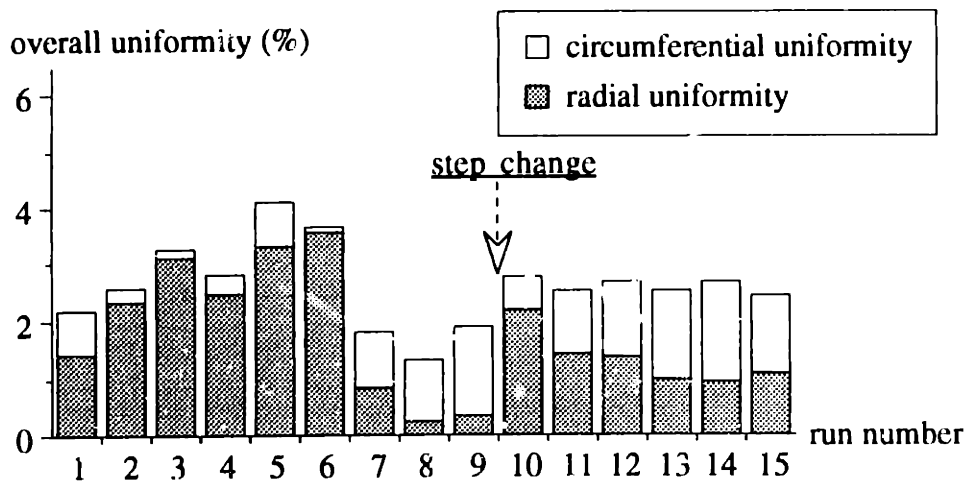

Figure 3.21 Portions of the radial and circumferential uniformities

3.4.2 Multiple Tuning Factor Experiments

The experimental results of applying on-line control using multiple tuning factors to the oxide etching process are included in this section. Since there are three group means, two tuning factors were used. The slope and curvature for two tuning

factors were defined in Eqs. 3.6 and 3.7, respectively. Both the slope and the curvature were controlled on-line using two selected tuning factors after the robustness was optimized off-line.

3.4.2.1 Robustness Optimization

In this example, all the process parameters of the oxide etching process using the AutoEtch™ 590 were used in robustness optimization except for process time, which was the adjustment factor. The process parameters are RF plasma power (power), pressure of the reaction chamber (pressure), gap spacing between the top and bottom electrodes (gap), He gas flow rate (He), CHF_3 gas flow rate (CHF_3), and CF_4 gas flow rate (CF_4). Three levels of each process parameter were decided for the experiments as shown in Table 3.8.

	low	medium	high
pressure (torr)	3	4	5
power (watts)	500	700	900
gap (cm)	0.4	0.5	0.6
He flow rate (sccm)	100	150	200
CHF_3 flow rate (sccm)	0	8	15
CF_4 flow rate (sccm)	40	95	135

Table 3.8 Levels of process parameters

Since there are six process parameters with three levels each, an L18 orthogonal array was used to analyze the main effects of each process parameter. The L18 orthogonal array is shown in Table 3.9.

According to the array, the experiments were designed as shown in Table 3.10. After the experiments were performed, the robustness, the slope and the curvature were calculated; these are also listed in the table. The robustness values were transformed using a logarithm function for ease of calculation. The experimental data are listed in Appendix B.2.1.

experiment number	level					
	pressure	power	gap	He	CHF_3	CF_4
1	1	1	1	1	1	1
2	2	1	2	2	2	2
3	3	1	3	3	3	3
4	1	2	1	2	2	3
5	2	2	2	3	3	1
6	3	2	3	1	1	2
7	1	3	2	1	3	2
8	2	3	3	2	1	3
9	3	3	1	3	2	1
10	1	1	3	3	2	2
11	2	1	1	1	3	3
12	3	1	2	2	1	1
13	1	2	2	3	1	3
14	2	2	3	1	2	1
15	3	2	1	2	3	2
16	1	3	3	2	3	1
17	2	3	1	3	1	2
18	3	3	2	1	2	3

Table 3.9 L18 orthogonal array for designed experiments

exp number	pressure (torr)	power (watts)	gap (cm)	He (sccm)	CHF_3 (sccm)	CF_4 (sccm)	robustness	slope	curvature
1	3	500	0.4	100	0	45	29.280	0.326	1.056
2	4	500	0.5	150	8	90	8.427	30.016	-1.802
3	5	500	0.6	200	15	135	18.500	13.228	0.742
4	3	700	0.4	150	8	135	26.249	3.600	0.324
5	4	700	0.5	200	15	45	26.522	8.928	1.026
6	5	700	0.6	100	0	90	25.044	8.605	0.612
7	3	900	0.5	100	15	90	26.813	6.880	0.521
8	4	900	0.6	150	0	135	19.788	-1.650	1.474
9	5	900	0.4	200	8	45	25.429	7.284	0.889
10	3	500	0.6	200	8	90	30.041	0.574	0.342
11	4	500	0.4	100	15	135	19.386	11.877	-0.544
12	5	500	0.5	150	0	45	27.035	2.097	0.257
13	3	700	0.5	200	0	135	30.991	0.062	1.923
14	4	700	0.6	100	8	45	20.543	5.792	-0.016
15	5	700	0.4	150	15	90	19.461	14.352	1.383
16	3	900	0.6	150	15	45	29.242	0.569	1.714
17	4	900	0.4	200	0	90	28.756	-0.356	0.902
18	5	900	0.5	100	8	135	29.695	8.899	0.377

Table 3.10 Designs and results of experiments

Using the experimental results shown in Table 3.10, robustness, slope, and curvature were modeled as second-order polynomials without interaction terms as follows:

$$\begin{aligned}\text{robustness} = {} & 16.0273 - 2.2877\times(\text{pressure}) + 5.9113\times(\text{pressure})^2 \\ & + 2.2545\times(\text{power}) - 0.4357\times(\text{power})^2 - 0.4503\times(\text{gap}) \\ & - 0.6039\times(\text{gap})^2 + 0.7898\times(\text{He}) + 4.2163\times(\text{He})^2 \\ & - 1.7475\times(CHF_3) + 1.5613\times(CHF_3)^2 - 1.1202\times(CF_4) \\ & + 2.1313\times(CF_4)^2 , \end{aligned} \qquad \text{(Eq. 3.15)}$$

$$\begin{aligned}\text{slope} = {} & 19.1306 + 3.5378\times(\text{pressure}) - 3.5615\times(\text{pressure})^2 \\ & - 3.0410\times(\text{power}) - 0.2445\times(\text{power})^2 - 0.8304\times(\text{gap}) \\ & - 4.1303\times(\text{gap})^2 - 1.0549\times(\text{He}) - 2.1558\times(\text{He})^2 + 3.8958\times(CHF_3) \\ & - 3.7078\times(CHF_3)^2 + 0.9183\times(CF_4) - 4.9275\times(CF_4)^2 , \end{aligned} \qquad \text{(Eq. 3.16)}$$

and

$$\begin{aligned}\text{curvature} = {} & -0.7659 - 0.1350\times(\text{pressure}) + 0.6717\times(\text{pressure})^2 \\ & + 0.4855\times(\text{power}) - 0.3813\times(\text{power})^2 + 0.0715\times(\text{gap}) \\ & + 0.3562\times(\text{gap})^2 + 0.3182\times(\text{He}) + 0.0942\times(\text{He})^2 - 0.1152\times(CHF_3) \\ & + 0.8995\times(CHF_3)^2 - 0.0525\times(CF_4) + 0.4422\times(CF_4)^2 . \end{aligned} \qquad \text{(Eq. 3.17)}$$

The functions above were obtained by quadratic curve fitting of the experimental data using normalized parameter values. Each parameter value is normalized to have values between -1 and 1. In Eq. 3.15, the standard errors of coefficients for constant, 1st-order term coefficients, and 2nd-order term coefficients are 4.491, 1.523, and 2.639, respectively. Similarly the standard errors of coefficients are 5.696, 1.932, and 3.347, respectively in Eq. 3.16, and 0.422, 0.143, and 0.248, respectively in Eq. 3.17.

The robustness was maximized using the model above (Eq. 3.15). Process parameter values for the maximum robustness can be determined independently with other parameters, since the robustness model does not include interaction terms. The

calculated maximum robustness operating points, the process parameter values that maximize the robustness, are listed in Table 3.11.

parameter	maximum robustness operating points
pressure (torr)	3
power (watts)	900
gap (cm)	0.46
He flow rate (sccm)	200
CHF_3 flow rate (sccm)	0
CF_4 flow rate (sccm)	45

Table 3.11 Maximum robustness operating points

The effect of each process parameter on the robustness, the slope, and the curvature were investigated to identify tuning factors. The changes of the robustness, the slope, and the curvature corresponding to the changes of each process parameter are plotted in Figure 3.22. In the figures, each response is obtained with the other process parameters fixed at their maximum robustness operating points.

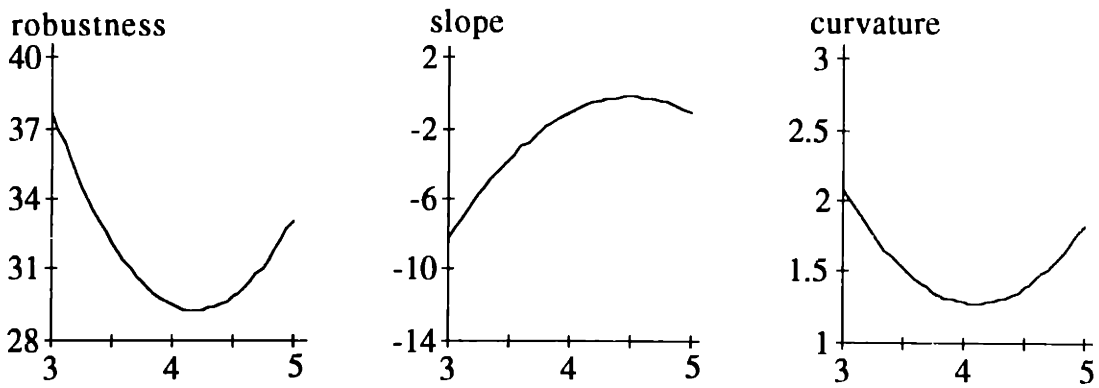

A. pressure (torr)

Figure 3.22 Robustness, slope, and curvature at maximum robustness operating points

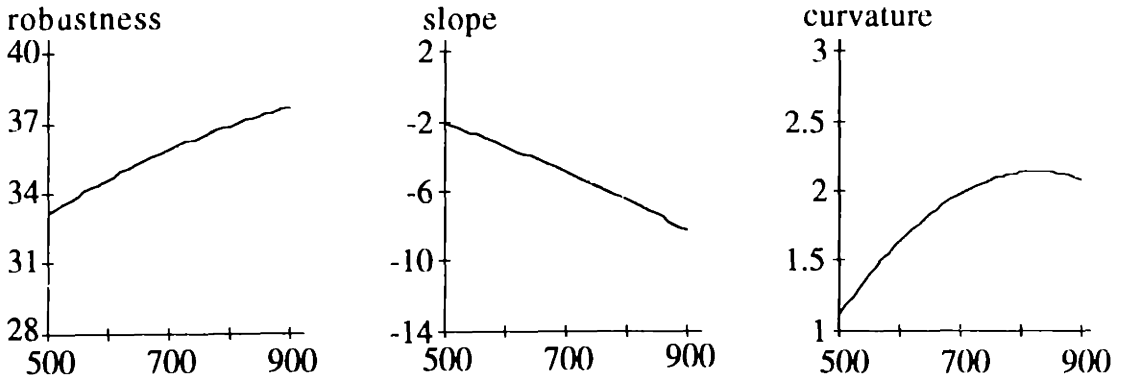

B. power (watts)

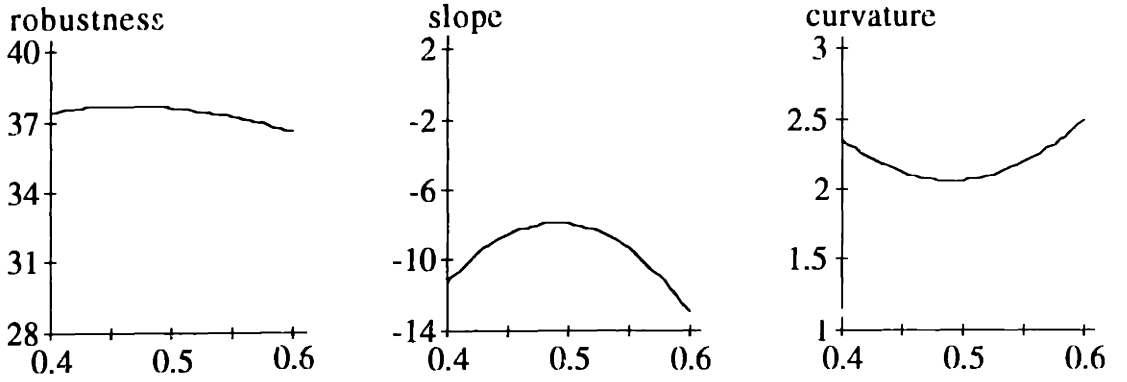

C. gap (cm)

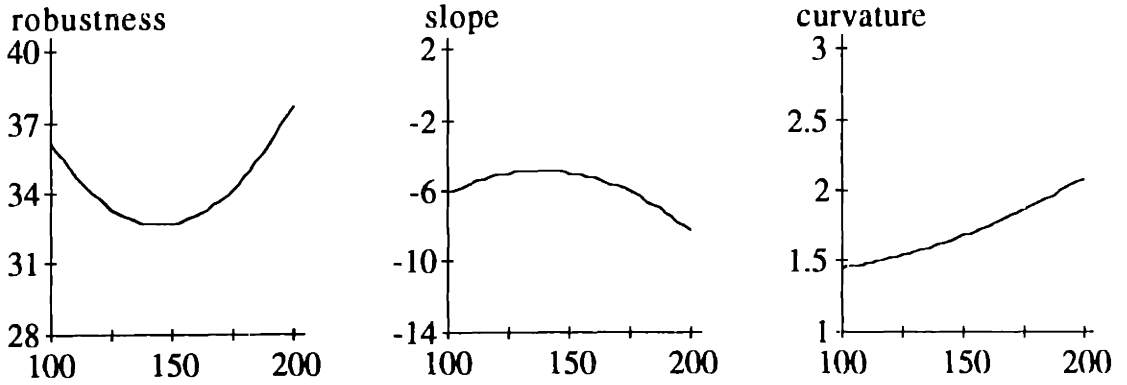

D. He flow rate (sccm)

Figure 3.22 Robustness, slope, and curvature at maximum robustness operating points (continued)

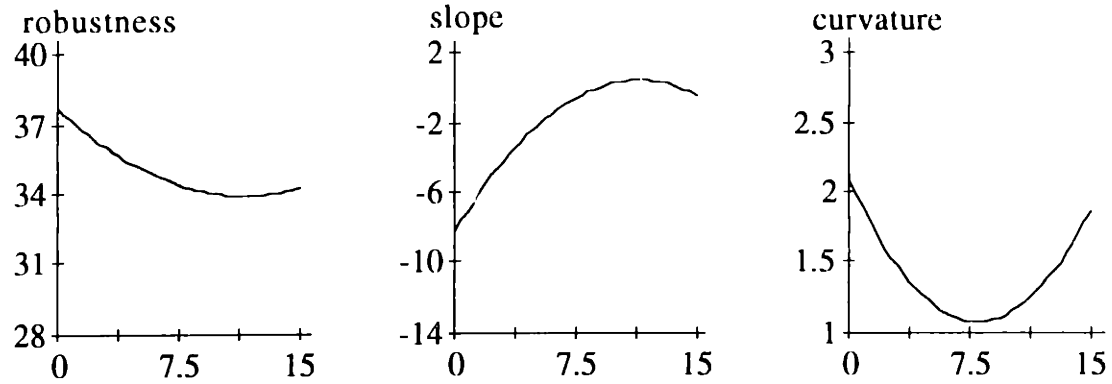

E. CHF_3 flow rate (sccm)

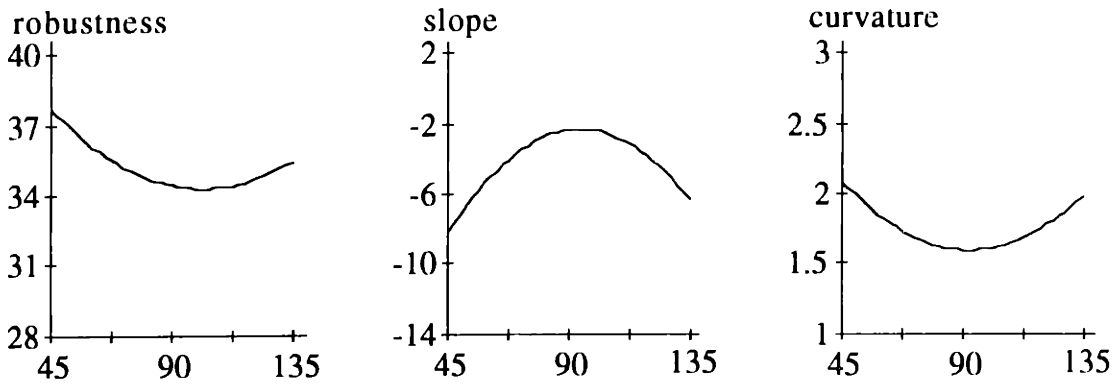

F. CF_4 flow rate (sccm)

Figure 3.22 Robustness, slope, and curvature at maximum robustness operating points (continued)

In order to identify two tuning factors among the process parameters, indices were calculated for each process parameter. $Index_t$ (Eq. 2.14) was defined in this example as follows:

$$index_t = \left| \frac{\left[\frac{\Delta \text{ robustness}}{\text{average of robustness}}\right]}{\left[\frac{\Delta \text{ slope}}{\text{average of slope}}\right]} \right| + \left| \frac{\left[\frac{\Delta \text{ robustness}}{\text{average of robustness}}\right]}{\left[\frac{\Delta \text{ curvature}}{\text{average of curvature}}\right]} \right|, \quad \text{(Eq. 3.18)}$$

which includes effects on both the slope changes and the curvature changes.

In Table 3.12, index values at the maximum robustness operating points for each process parameter are listed. By comparing the values, CHF_3 and gap were identified as the tuning factors since they have small index values. The other process parameters were then classified as the robustness factors, and their values are fixed at the maximum robustness operating points during on-line control.

		pressure	power	gap	He	CHF_3	CF_4
robustness	average	31.467	35.731	37.410	34.095	34.907	35.154
	difference	8.42	4.509	1.138	5.043	3.798	2.810
slope	average	-2.266	-4.974	-9.290	-5.686	-1.810	-3.975
	difference	7.978	6.082	5.002	3.340	8.627	5.889
curvature	average	1.507	1.858	2.186	1.709	1.375	1.742
	difference	0.813	1.022	0.431	0.636	1.018	0.496
$index_t$		0.572	0.3326	0.2108	0.6493	0.1698	0.3347

Table 3.12 Index values for each parameter

Both the slope and curvature need to be modeled as functions of the tuning factors to be controlled on-line. In order to make the models, parallel experiments of 2^2 full factorial design were performed with the robustness factors at their maximum robustness operating points. Figure 3.23 shows the experiment points with the robustness factor values, and Table 3.13 lists the results of the experiments. Experimental data are listed in Appendix B.2.2.

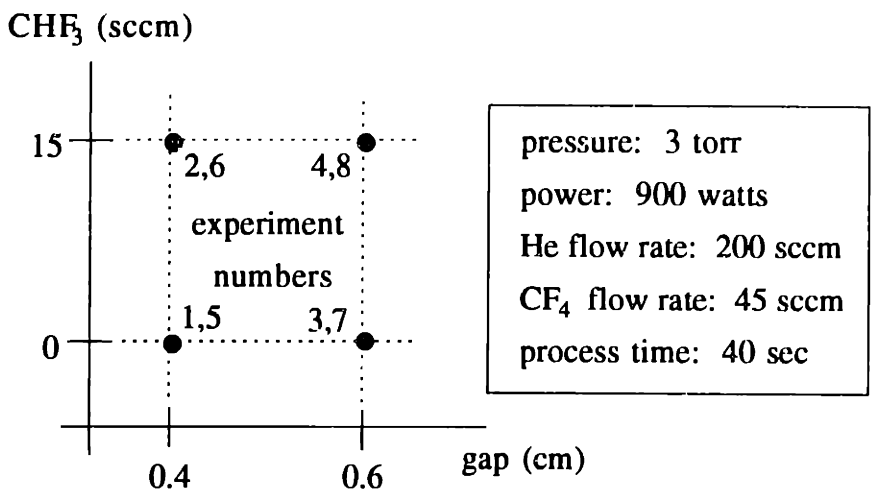

Figure 3.23 Process parameter values for 2^2 experiments

experiment number	gap (cm)	CHF_3 (sccm)	slope	curvature
1	0.4	0	-3.427	-2.921
2	0.4	15	-9.213	3.069
3	0.6	0	4.004	-2.135
4	0.6	15	-4.533	4.037
5	0.4	0	-3.833	-2.537
6	0.4	15	-9.631	3.987
7	0.6	0	4.093	-1.598
8	0.6	15	-5.464	3.864

Table 3.13 Results of 2^2 experiments

Using the experimental data, the slope and curvature were modeled as functions of CHF_3 and gap as follows:

$$\text{slope} = -3.5005 + 3.0255\times(\text{gap}) - 3.7098\times(CHF_3) - 0.8138\times(\text{gap})\times(CHF_3) \ , \qquad \text{(Eq. 3.19)}$$

and

$$\text{curvature} = 0.7208 + 0.3214\times(\text{gap}) + 3.0184\times(CHF_3) - 0.1100\times(\text{gap})\times(CHF_3) \ , \qquad \text{(Eq. 3.20)}$$

where CHF_3 and gap are normalized to have values between -1 and 1. The models include first-order terms as well as an interaction term. The standard errors of coefficients of Eqs. 3.19 and 3.20 are 0.1377 and 0.1430, respectively.

The response surfaces of the slope and curvature are plotted in Figs. 3.24 and 3.25, respectively. As can be seen from the figures, the interaction of CHF_3 and gap is small and the effects of gap on the curvature are small, which was also verified by the t-ratio test of the regression model. Hence, the interaction term was deleted in both of the models, and gap was excluded from the curvature model as follows:

$$\text{slope} = -3.5005 + 3.0255\times(\text{gap}) - 3.7098\times(CHF_3) \ , \qquad \text{(Eq. 3.21)}$$

and

$$\text{curvature} = 0.7208 + 3.0184\times(CHF_3) \ , \qquad \text{(Eq. 3.22)}$$

where CHF_3 and gap were normalized to have values between -1 and 1. The models have the standard errors of coefficients of 0.3842 and 0.3626, respectively. The above models were used in on-line control of the slope and curvature.

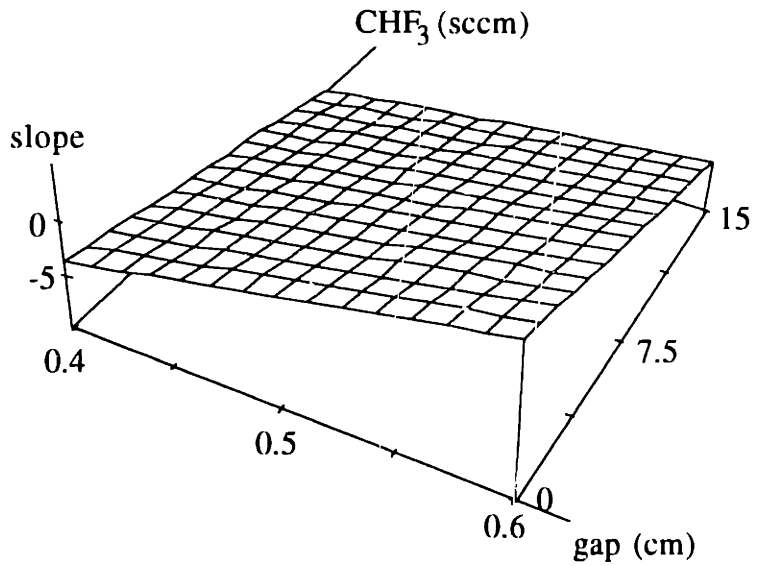

Figure 3.24 3D plot of slope response surface

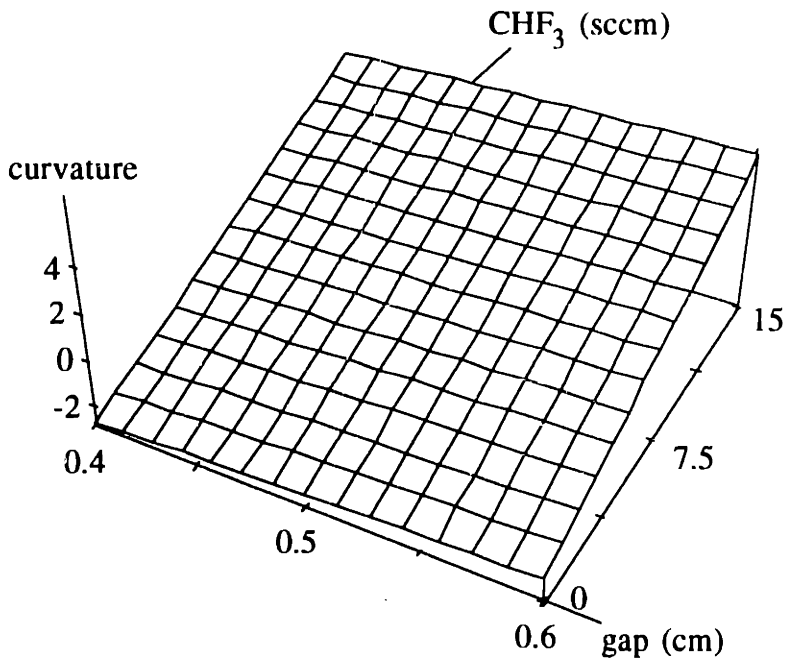

Figure 3.25 3D plot of curvature response surface

3.4.2.2 On-line Control

In Section 3.4.2.1, robustness was optimized by finding the maximum robustness operating points of the robustness factors. CHF_3 and gap were also selected as tuning factors. After the robustness optimization, the slope and the curvature were controlled on-line using the selected tuning factors. In order to compare the efficiency of on-line control, another experiments were performed without on-line control at the same time and the results of both experiments were compared. The optimization-only experiments were performed with the process parameter values as determined by the robustness optimization. On-line control is expected to compensate for any changes in the process conditions, which are to be reflected in the results of the optimization-only experiments.

Table 3.14 shows the process parameter values for the optimization-only experiments and the on-line control experiments, respectively. A series of paired experiments were performed over several days so the process condition changes can be seen in the results of the optimization-only experiments.

	optimization-only	on-line control
pressure (torr)	3	3
power (watts)	900	900
gap (cm)	0.58	tuning factor
He flow rate (sccm)	200	200
CHF_3 flow rate (sccm)	6	tuning factor
CF_4 flow rate (sccm)	45	45
process time (sec)	40	40

Table 3.14 Process parameter values for experiments

On-line control was performed by adapting the constant terms of the slope model (Eq. 3.21) and the curvature model (Eq. 3.22) using the model adaptation algorithm as explained in Section 3.4.1.2. 15 runs of the paired optimization-only and on-line control experiments were performed. A step change was introduced after the 8th run to see the performance of on-line control. The process parameter values, other than the tuning factors, were changed after the 8th run so that the process conditions

change stepwise. Table 3.15 shows the process parameter values before and after the step change.

	before	after
pressure (torr)	3	4
power (watts)	900	700
He flow rate (sccm)	200	125
CF_4 flow rate (sccm)	45	75
process time (sec)	40	40

Table 3.15 Process parameter shifts as a step change

The experimental data are listed in Appendix B.2.3. Table 3.16 shows the values of the constant terms of the slope model and of the curvature model, respectively, and the values of gap and CHF_3 that were generated based on the models for each run. It is shown that the constant term values changed by large amounts before and after the step change, which is due to the compensating function of the on-line control algorithm.

run number	slope model constant	curvature model constant	gap (cm)	CHF_3 (sccm)
1	-8.738	0.529	0.60	6
2	-5.190	0.408	0.60	6
3	-4.568	0.577	0.60	6
4	-4.597	-0.589	0.60	5
5	-5.470	-0.018	0.60	8
6	-4.515	0.999	0.60	3
7	-5.012	0.128	0.60	7
8	-6.269	-0.069	0.60	8
9	-6.269	-0.069	0.60	8
10	2.399	0.333	0.43	4
11	3.954	1.925	0.40	3
12	5.407	2.298	0.28	0
13	2.415	3.253	0.29	0
14	3.803	3.319	0.25	0
15	2.185	3.130	0.25	0

Table 3.16 Constants and tuning factor values of on-line control

In Figure 3.26, the slope values of the optimization-only and on-line control experiments are plotted. Before the step change, the slope values were controlled to be close to the zero slope. After the step change was introduced, on-line control was able to the bring the deviated slope value back to zero slope in a couple of runs.

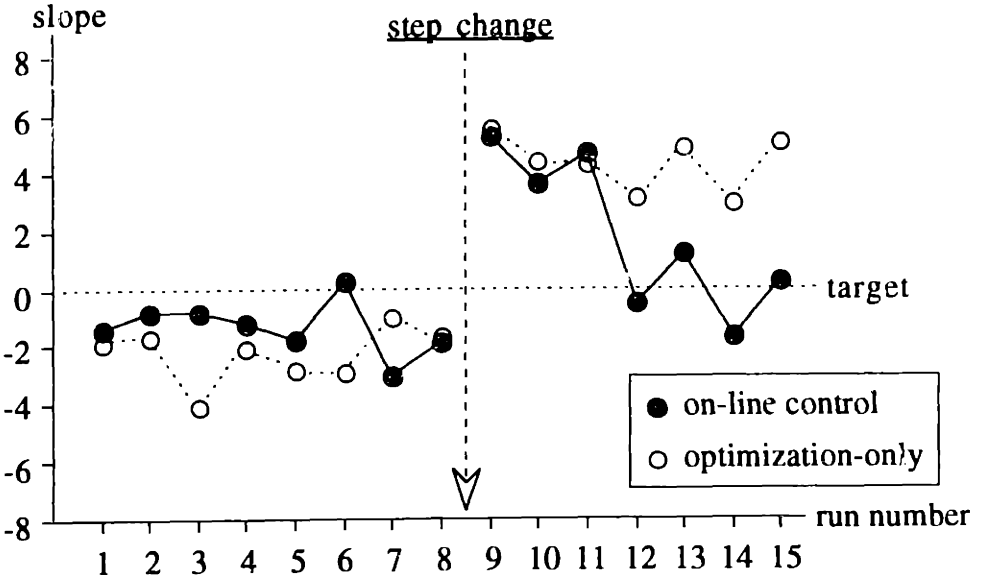

Figure 3.26 Historical data of the slope of multiple tuning factor experiments

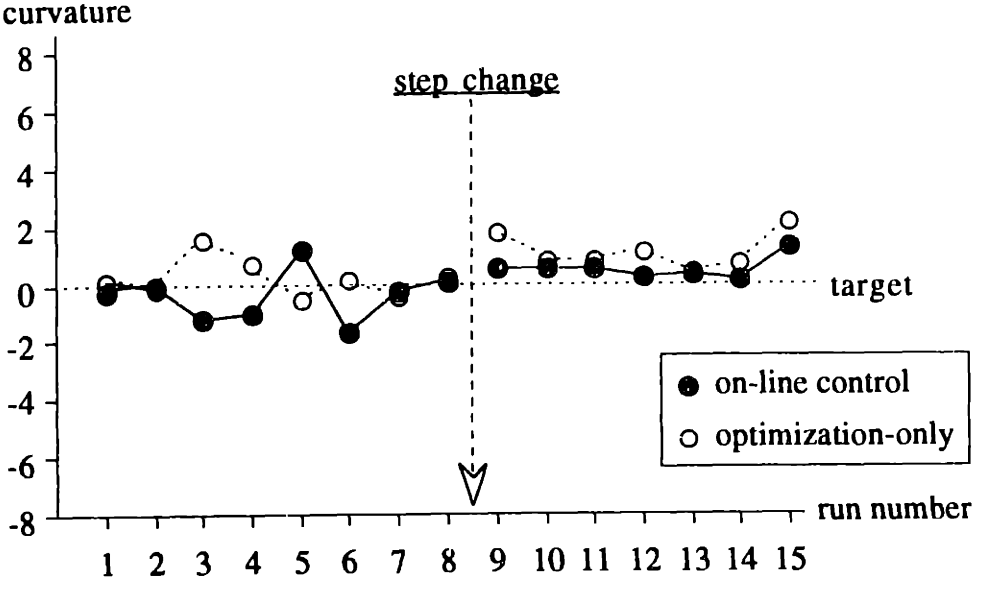

Figure 3.27 Historical data of the curvature of multiple tuning factor experiments

In Figure 3.27, the curvature values of the optimization-only and on-line control experiments are plotted. Before the step change, the curvature values of the on-line control experiments showed the same magnitude of fluctuations as the optimization-only experiment curvature values. After the step change, however, the curvature values of the on-line control experiments were improved, resulting in closer values to zero curvature.

Figure 3.28 shows the historical data of the overall uniformity defined in Eq. 3.9. It is shown that the overall uniformity of the on-line control experiments is better than that of the optimization-only experiments, which means that within-a-wafer uniformity was controlled effectively by on-line control of the slope and curvature.

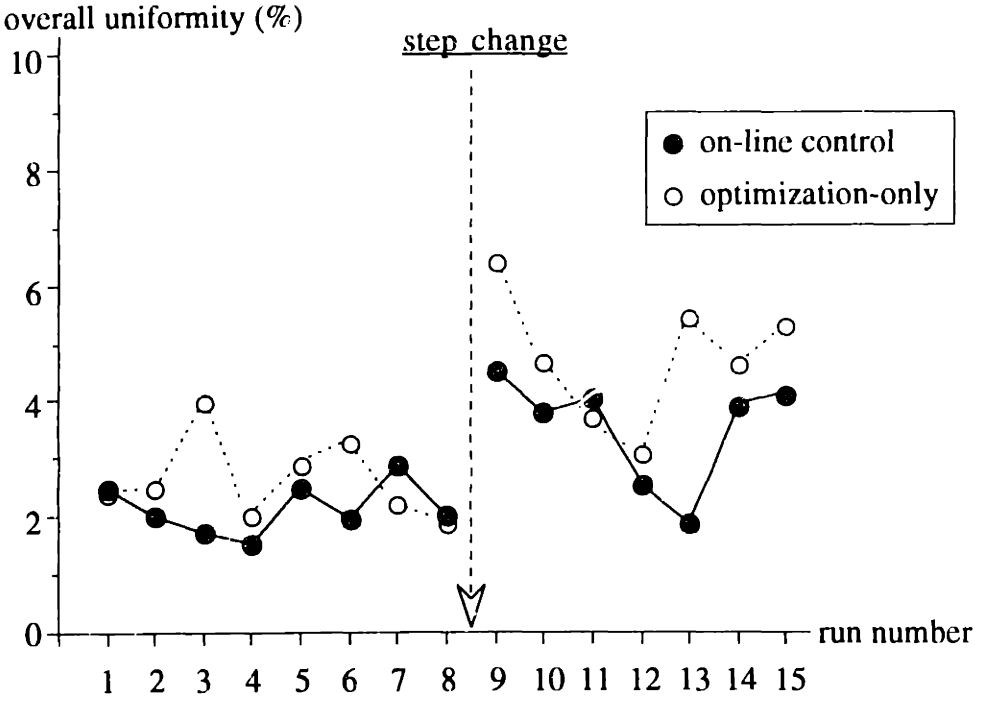

Figure 3.28 Historical data of the overall uniformity of multiple tuning factor experiments

3.4.2.3 Discussions

It was shown that the slope and curvature were controlled by using first-order linear models and by applying the constant term update algorithm. By controlling the slope and curvature, the overall uniformity was improved when compared with the results of the optimization-only experiments. Even when a step change was

introduced, on-line control was able to compensate for the change, resulting in better uniformity.

The average values of slopes and curvatures before and after the step change for the optimization-only experiments and the on-line control experiments are shown in Figures 3.29 and 3.30, respectively. In the figures, the error bars represent the magnitudes of two standard deviations of the average values. It is noted that the slope was controlled both before and after the step change, but the curvature was controlled only after the step change. The curvature values before the step change of both the optimization-only and the on-line control experiments were close to zero, which means the process parameter values before the step change were already optimized and resulted in good curvatures. It was only after the step change was introduced that the on-line control of curvature showed an improvement.

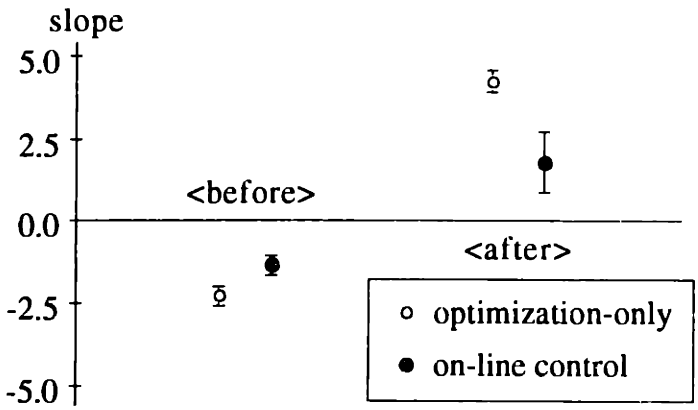

Figure 3.29 Average slopes before and after the step change

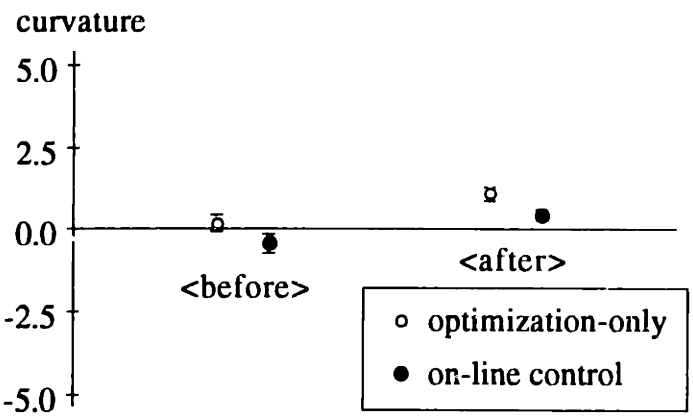

Figure 3.30 Average curvatures before and after the step change

Figure 3.31 shows the averages of the overall uniformity before and after the step change for the optimization-only experiments and on-line control experiments, respectively. The error bars in the figure represent the magnitudes of two standard deviations of the average overall uniformity. The on-line control improved overall uniformity by a factor of 1.2 before the step change and by a factor of 1.3 after the step change.

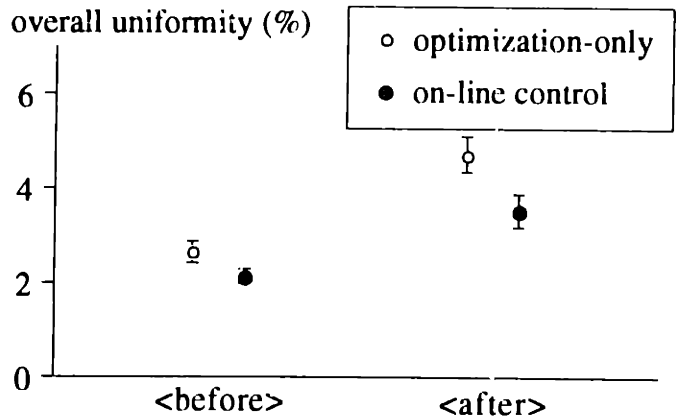

Figure 3.31 Average overall uniformity before and after the step change

Figure 3.32 shows the magnitudes of the radial and the circumferential uniformities for the on-line control experimental data. When compared with the results of the single tuning factor on-line control experiments (Figure 3.21), it is noted that the radial uniformity portion is generally smaller, which indicates that the radial uniformity was controlled more effectively with multiple tuning factors. However, the circumferential non-uniformity portion is larger when compared with the single tuning factor experiments, because the process robustness variation becomes larger when the process is controlled by tuning factors that are not ideal. The improvement of the radial uniformity is offset by the degradation of the circumferential uniformity, resulting in similar overall uniformity in both experiments. Therefore, it is concluded that as small as possible number of tuning factors is recommended for an effective control of tunable variability without degrading non-tunable variability when the tuning factors are not ideal.

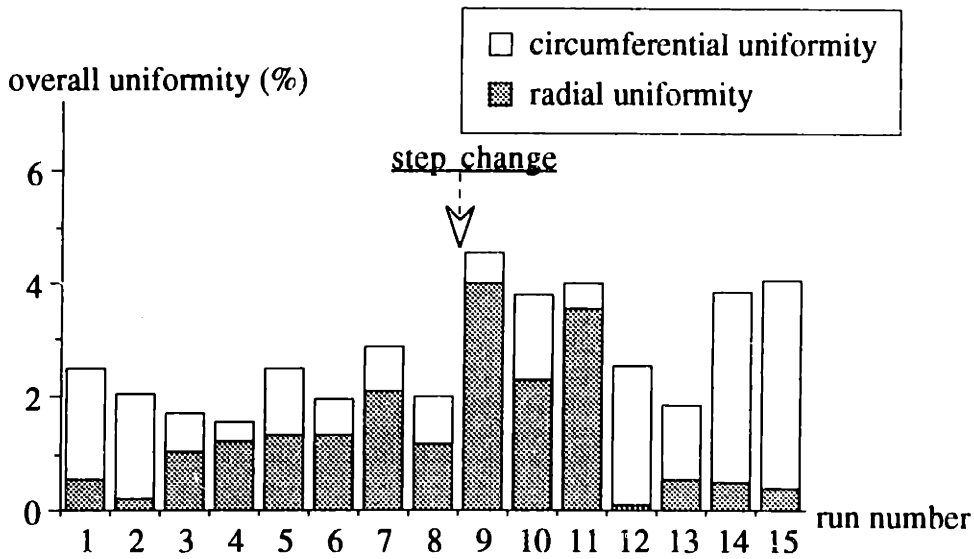

Figure 3.32 Portions of radial and circumferential uniformities

3.5 Polysilicon Etching Process Experiments

The experimental results of applying on-line control using a single tuning factor to the polysilicon etching process are included in this section. One tuning factor was selected from the analysis of the slope defined in Eq. 3.2 and the robustness defined in Eq. 3.4. The on-line control of the slope was performed with a tuning factor to increase the within-a-wafer uniformity.

3.5.1 Robustness Optimization

Among the process parameters of the polysilicon etching process using the Precision 5000, magnetic field strength (field) and RF plasma power (power) were used as process parameters in the experiments. They are selected since it was found from the preliminary experiments that both have significant effects on the slope and robustness. In order to decide a tuning factor and a maximum robustness operating point from two process parameters, 2^2 full factorial experiments were designed as shown in Figure 3.33 using two levels of each parameter. The values of the other process parameters, which were fixed in the experiments, are also shown in the figure. Each experimental design was performed twice as replicates and eight experiments were performed in total.

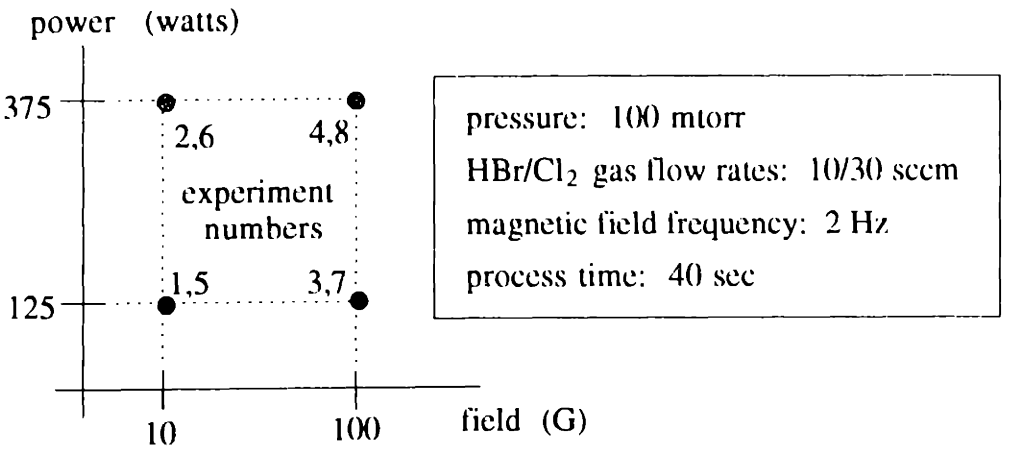

Figure 3.33 Process parameter values for 2^2 full factorial experiments

Using the experimental data listed in Appendix C.1, the robustness and slope were calculated as shown in Table 3.17. The robustness and slope were then modeled respectively as functions of field and power as follows:

$$\text{robustness} = 1155.3 - 78.3\times(\text{field}) + 739.8\times(\text{power}) - 291.1\times(\text{field})\times(\text{power}), \quad \text{(Eq. 3.23)}$$

and

$$\text{slope} = 1.1251 - 4.2791\times(\text{field}) - 0.9551\times(\text{power}) + 1.8101\times(\text{field})\times(\text{power}). \quad \text{(Eq. 3.24)}$$

Being based on the 2^2 full factorial design experimental data, the models have first-order terms and an interaction term as shown in Eqs. 3.23 and 3.24, respectively. In the above equations, field and power were normalized to have values between -1 and 1. The standard errors of coefficients of models in Eqs. 3.23 and 3.24 are 99.27 and 0.9377, respectively. The response surfaces of robustness and slope are plotted in Figures 3.34 and 3.35, respectively. It is shown that the high levels of both field and power are maximum robustness operating points since they corresponds to high robustness.

experiment number	field (G)	power (watts)	robustness	slope
1	10	125	81.9	4.496
2	10	375	1911.4	2.552
3	100	125	753.3	-3.465
4	100	375	1473.4	-2.820
5	10	125	323.6	11.843
6	10	375	2617.7	2.726
7	100	125	503.3	-4.553
8	100	375	1578.1	-1.778

Table 3.17 Results of 2^2 full factorial experiments

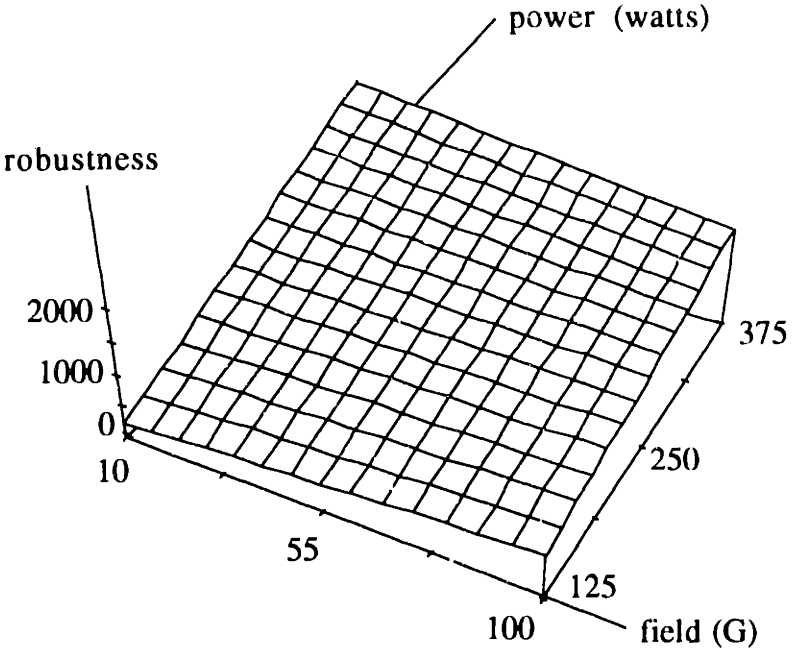

Figure 3.34 3D plot of robustness response surface

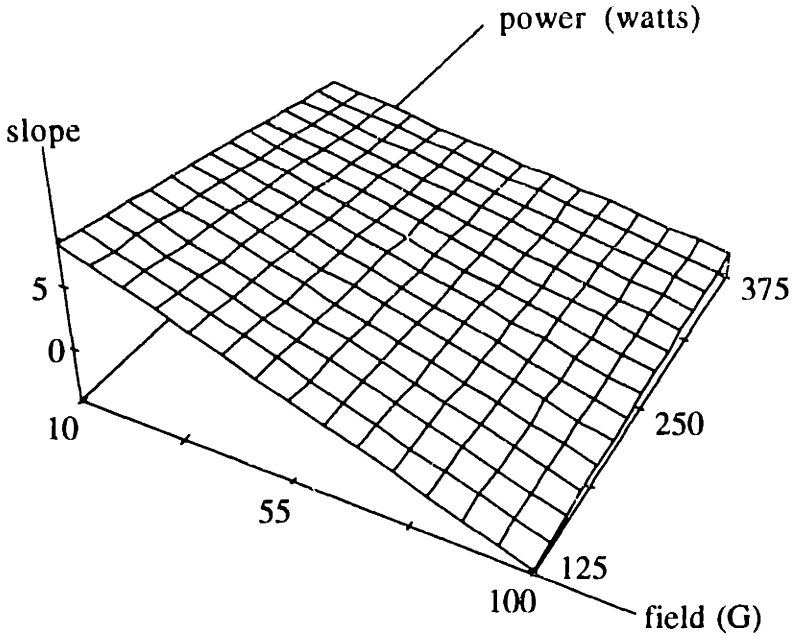

Figure 3.35 3D plot of slope response surface

In order to identify the tuning factor, indices for field and power were calculated using Eq. 3.13 and are shown in Table 3.18.

		field	power
robustness	average	1895.1	1077.0
	difference	425.6	897.4
slope	average	0.170	-3.154
	difference	4.938	1.710
$index_t$		0.0077	1.5369

Table 3.18 Index values for field and power

Since field has the smaller index value, it was selected as a tuning factor, and power was used as a robustness factor. Using the previous experimental data for high values of power, the slope was modeled as a first-order linear function of field as follows:

$$\text{slope} = 0.17 - 2.47\times(\text{field}) \ , \qquad \text{(Eq. 3.25)}$$

where field is normalized to have values between -1 and 1. The standard error of coefficients is 0.2641 in the model.

After the slope model was obtained, a set of experiments were performed to confirm the model. In the experiments, power was set to its maximum robustness operating point. Figure 3.36 shows the results of the confirmation experiments with the first-order regression line of the measurements. The slope of the regression line is shown as similar to that of the slope model (Eq. 3.25), which means the slope has the same sensitivity to field even if the process condition has been changed due to time interval between two sets of experiments.

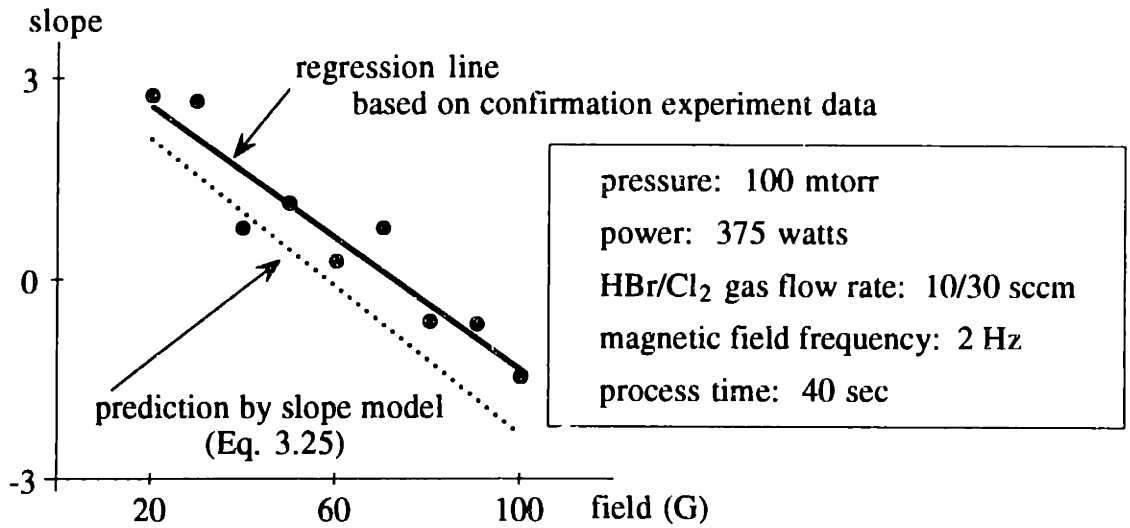

Figure 3.36 Results of confirmation experiments

3.5.2 On-line Control

In Section 3.5.1, the tuning factor was identified and the robustness was optimized by finding the high level of power as the maximum robustness operating point. The slope is controlled on-line to maximize the process uniformity even when the process condition drifts. In order to see the effectiveness of on-line control, another experiments were performed without on-line control at the same time, and the results were compared as in Section 3.4.1.2. Note that the process parameter values of the optimization-only experiments are also the maximum robustness operating points; hence, uniformity was already optimized.

Taole 3.19 shows the process parameter values for the optimization-only experiments and the on-line control experiments, respectively.

	optimization-only	on-line control
pressure (mtorr)	100	100
power (watts)	375	375
HBr/Cl_2 gas flow rates (sccm)	10/30	10/30
magnetic field strength (G)	75	tuning factor
magnetic field frequency (Hz)	2	2

Table 3.19 Process parameter values for experiments

For the on-line control of the slope, the slope model (Eq. 3.25) was adapted by updating the constant term using the algorithm explained in Section 3.4.1.2. 12 runs of the paired optimization-only and on-line control experiments were performed. After six runs, it was assumed that the incoming wafers have non-uniform radial thickness; therefore, it was necessary to compensate for the initial non-uniformity by controlling the slope. The value of 2 was set as a new target slope after the 6th run.

The experimental data are listed in Appendix C.2. Table 3.20 shows the values of field for each run.

run number	field (G)
1	58.0
2	60.7
3	77.9
4	89.2
5	84.6
6	68.8
7	27.6
8	21.4
9	46.7
10	19.0
11	31.0
12	25.9

Table 3.20 Magnetic field strength values of on-line control

In Figure 3.37, the slope values of the optimization-only and the on-line control experiments are plotted. It is shown that slopes are controlled so that they are close to the zero slope before the target change and are approaching to the slope of 2 that is a new target after the target change. An overshoot in the slope values was observed just after the target change.

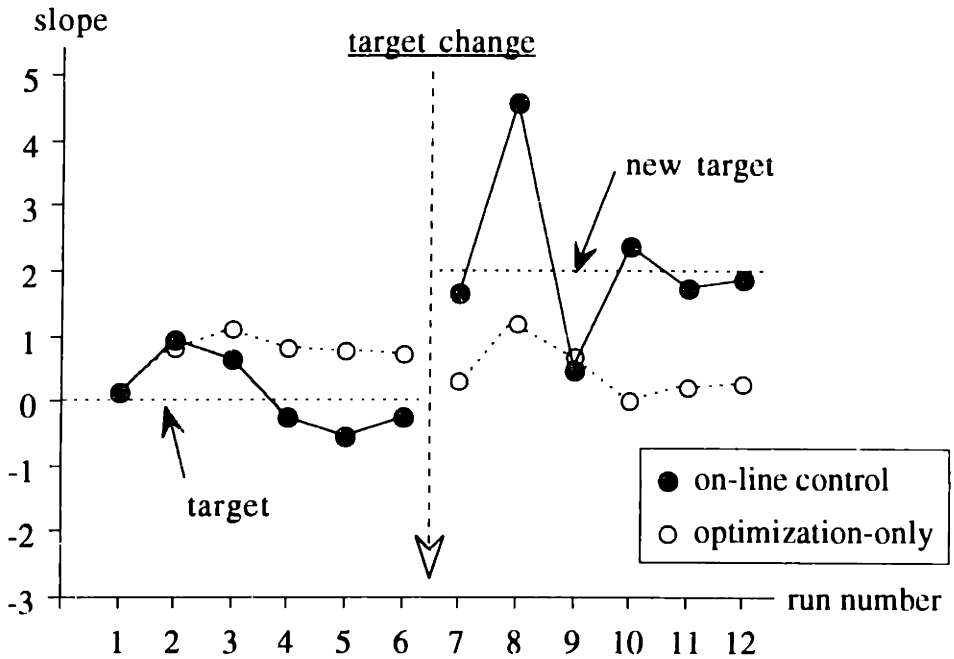

Figure 3.37 Historical data of the slope of single tuning factor experiments

3.5.3 Discussions

Figure 3.38 shows the average values of slope before and after the target change for the optimization-only experiments and the on-line control experiments, respectively. The error bars in the figure represent the magnitudes of two standard deviations of the average slope values. It is noted that slope of the on-line control experiments is closer to the target value both before and after the target change, which illustrates the effectiveness of on-line control.

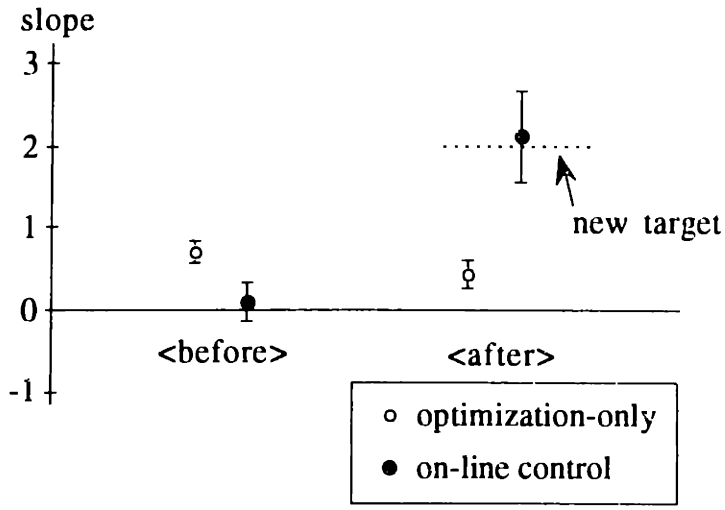

Figure 3.38 Average slopes before and after the target change

Before the target change, the goal was achieve a uniform etching rate all over the wafer surface. Figure 3.39 compares the overall uniformities defined in Eq. 3.9 for the optimization-only experiments and the on-line control experiments, respectively. The error bars in the figure represent the magnitudes of two standard deviations of the average overall uniformity values. Although the slope was well controlled to be close to the zero slope value, overall uniformity was not improved by on-line control as shown in the figure.

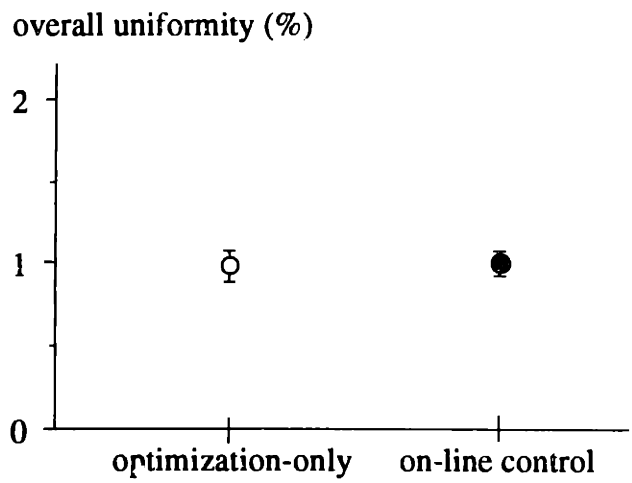

Figure 3.39 Overall uniformity comparison

In Figure 3.40, the portions of the radial uniformity and the circumferential uniformity of the on-line control experiments are shown. It is noted that the radial uniformity was controlled as the slope was controlled but that the circumferential uniformity was degraded as well. Therefore, it is concluded that on-line control of this example was not effective in improving the overall uniformity since the circumferential uniformity was not preserved. The average overall uniformity, however, is equivalent to the results of the optimization-only experiments.

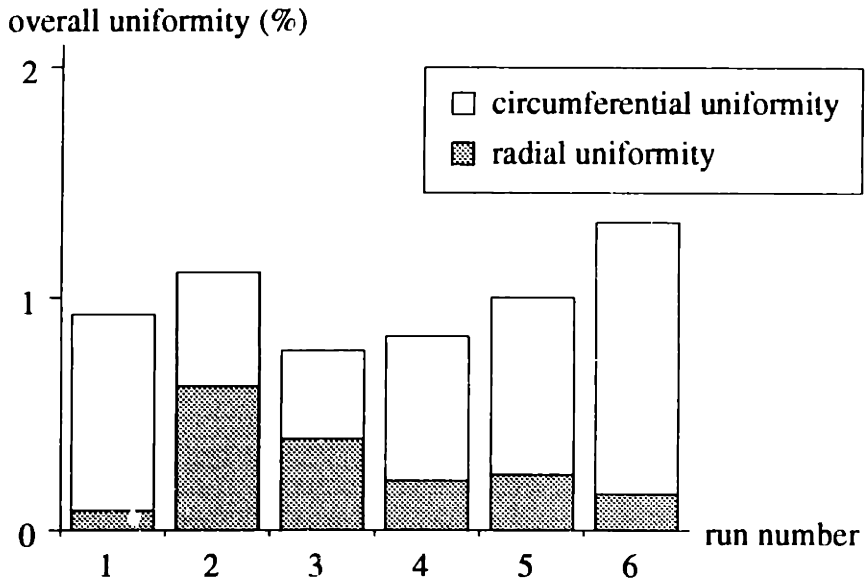

Figure 3.40 Portions of radial and circumferential uniformities

After the target was changed to the slope value of 2, the on-line control experimental results show that the target was achieved after four runs. Hence, it is shown in this example that on-line control can compensate for the incoming material variations by meeting new target values so that the quality of the processes may be maximized at all times.

CHAPTER 4
A SEQUENTIAL OPTIMIZATION EXAMPLE

4.1 Introduction

The uniformity of film thickness in a low pressure chemical vapor deposition (LPCVD) process was optimized by categorizing the process variabilities into tunable variability and non-tunable variability. Optimization was performed in two steps: the parallel optimization of the non-tunable uniformity and the sequential optimization of the tunable uniformity. After the robustness factor and tuning factor were identified through parallel designed experiments, the non-tunable uniformity was optimized by setting the robustness factors to their maximum robustness operating points. In the sequential optimization step, the tuning factor was used to optimize tunable uniformity. The sequential optimization of the tunable uniformity is expected to improve overall uniformity further when compared with the overall uniformity of only parallel optimization, because the process parameter space of the tuning factor is explored more closely in the vicinity of optimum points.

In the LPCVD process, desired materials contained in reactant gases are deposited onto the wafer surface by adsorption. In a typical LPCVD reactor, a batch of wafers is placed in a low pressure furnace and heated by radiation, and reactant gases are injected into the furnace through nozzles. Reaction occurs on the wafer surface and the desired material is adsorbed on the wafer surface, the result of which

is a deposition of film. Figure 4.1 is a schematic diagram of a LPCVD furnace, where the quartz tube, liner, wafers sitting on wafer boats, load injector, center injector, source injector, and thermocouple sheath are shown.

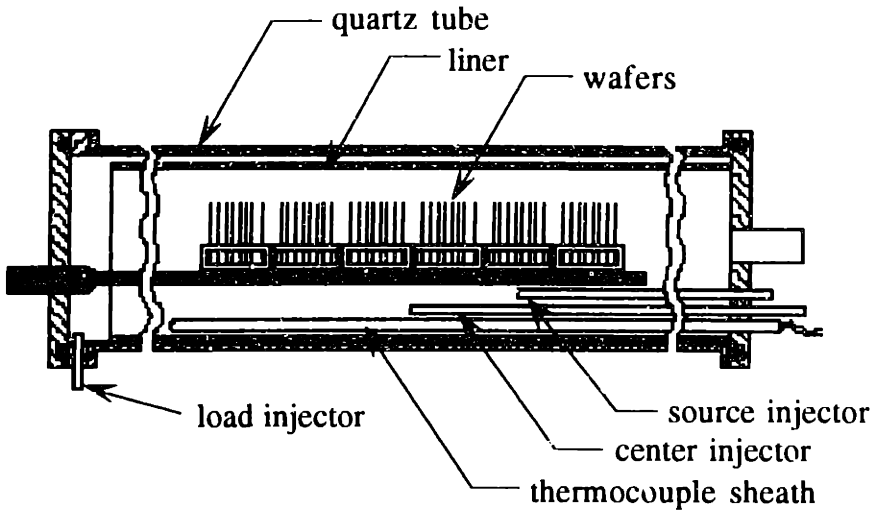

Figure 4.1 Schematic diagram of a LPCVD furnace

The LPCVD process of polysilicon deposition using silane (SiH_4) gas as the reactant gas is considered in this example. Silane gas breaks down inside the furnace and solidifies as polysilicon crystals on the hot wafer surfaces [49][69]. Concentration of silane gas is not uniform inside the furnace due to the depletion of reactant gas as it flows and the generation of byproduct gas (H_2 gas in this example). This non-uniformity of silane gas concentration along the furnace causes non-uniform deposition rates of polysilicon for the wafers along the tube. As shown in Figure 4.1, multiple injectors are equipped in order to increase the reaction gas concentration uniformity.

A simulation program of the polysilicon LPCVD process was developed based on the equipment modeling of the process [30]. Inputs to the program are equipment settings such as pressure, temperature, gas flow rates, and injector positions. Outputs of the program are polysilicon deposition rates of each wafer along the furnace. In this example, the simulation program was used as a process to be optimized. In order to simulate real manufacturing conditions, random noises were

superimposed both on the equipment settings as input noises and on the calculated deposition rates as measurement noises.

4.2 Process Variability of LPCVD Process Simulation

The uniformity of film thickness in the polysilicon LPCVD simulation process has two components: within-a-batch uniformity and batch-to-batch uniformity. Within-a-batch uniformity is caused by the depletion effect as explained in the previous section, and batch-to-batch uniformity is due to disturbances to the process conditions. The within-a-batch uniformity is considered to be controlled easily, because the process is equipped with multiple injectors. Hence, the within-a-batch uniformity is categorized as tunable variability. The batch-to-batch uniformity, however, is difficult to control and categorized as non-tunable variability. Figure 4.2 shows the categories of process variabilities.

The mean thickness of polysilicon film, another component of tunable variability, can be easily controlled to meet the target thickness by changing the process time since the deposition rates are assumed constant. Therefore, process time is identified as the adjustment factor in this example. In optimization, the uniformity of the deposition rates was controlled instead of the uniformity of film thicknesses.

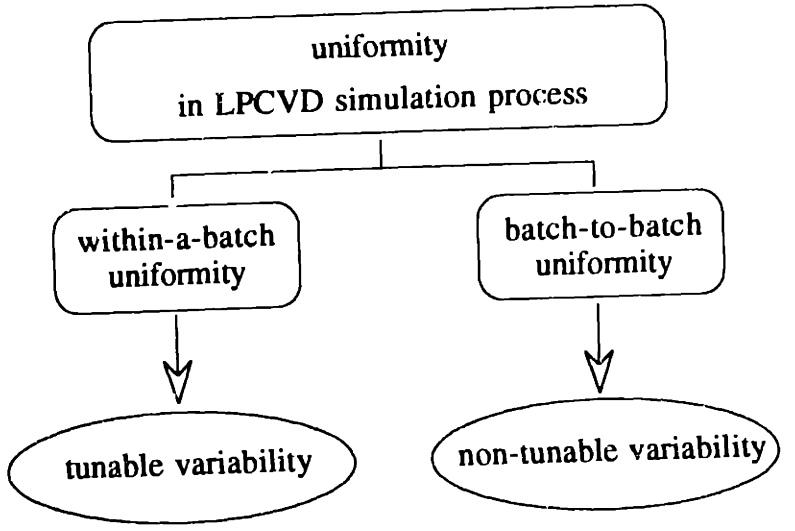

Figure 4.2 Process variabilities in LPCVD process simulation

Within-a-batch uniformity is calculated using the measurements of three wafers from a batch of wafers, and batch-to-batch uniformity is calculated using the variations of three measurement wafers from five batches. The positions of the measurement wafers from one batch and from five batches are shown in Figure 4.3. The deposition rates of three measurement wafers from five batches were measured. The measurement Y_{ij} represents the measured deposition rate of i-th wafer in j-th batch. The measurement wafers from five batches at the same position are grouped as shown in the figure. The differences between the group means are tunable uniformity, and the differences within each group are non-tunable uniformity.

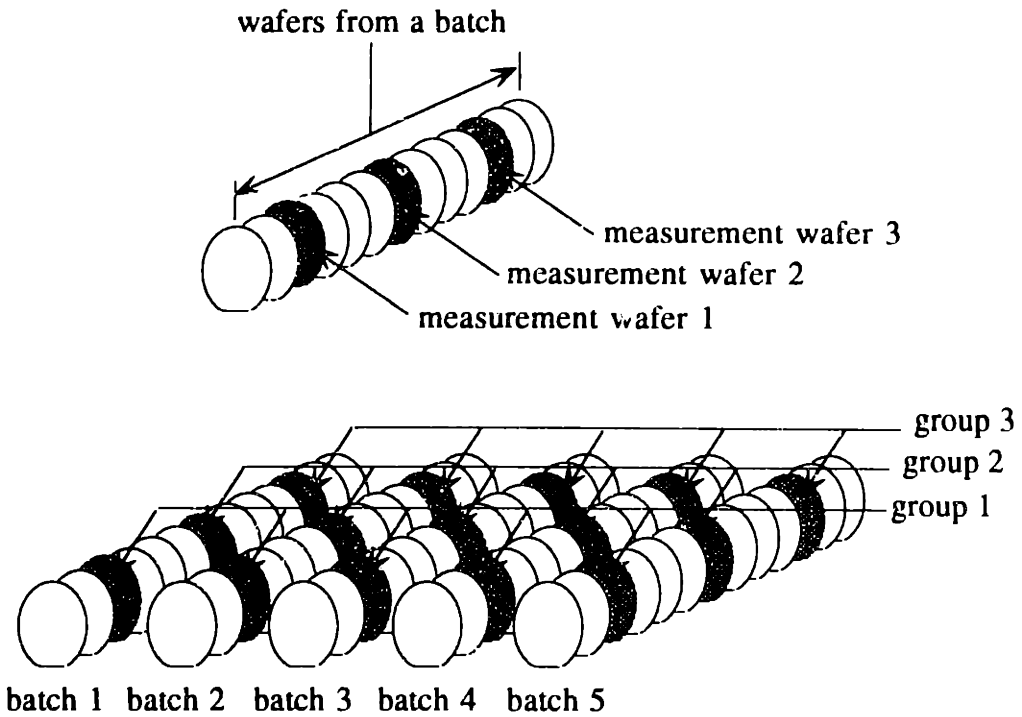

Figure 4.3 Process outputs of LPCVD process simulation

Figure 4.4 shows an example of the measurement data plotted in groups. In the figure, measurements of three measurement wafers from five batches are plotted together, respectively.

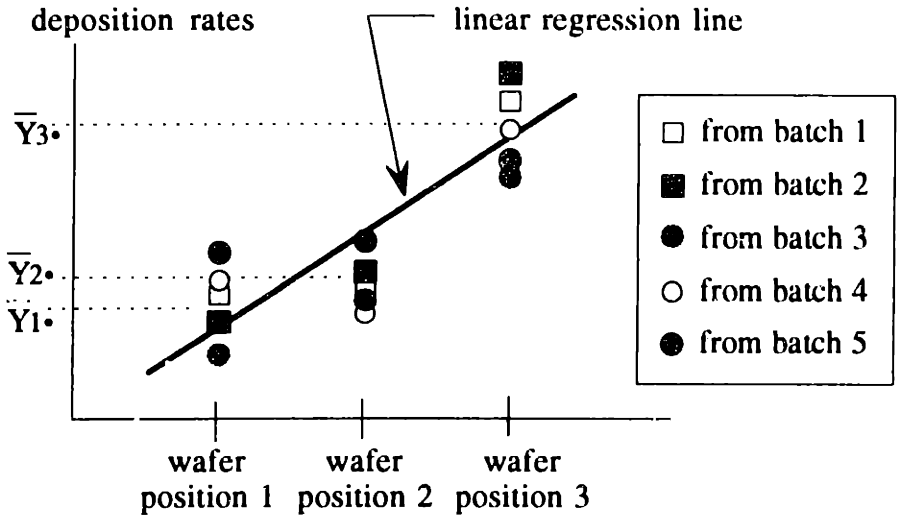

Figure 4.4 Grouped measurement data and regression line

The i-th group mean, $\overline{Y}_{i\bullet}$, shown in the figure is defined as follows:

$$\overline{Y}_{i\bullet} = \frac{1}{5}\sum_{j=1}^{5} Y_{ij} \qquad \text{(for } i = 1, 2, 3\text{)}. \qquad \text{(Eq. 4.1)}$$

Linear regression is performed on the group means, and the resulting regression line is also plotted in the figure. Tunable uniformity was represented by the slope of the linear regression line. In order to measure the magnitude of tunable uniformity, *slope* is defined as follows:

$$\text{slope} = 100 \times \left(\frac{\hat{\overline{Y}}_{3\bullet} - \hat{\overline{Y}}_{1\bullet}}{2\,\overline{Y}_{\bullet\bullet}}\right), \qquad \text{(Eq. 4.2)}$$

where $\hat{\overline{Y}}_{i\bullet}$ is the regression prediction of the i-th group mean $\overline{Y}_{i\bullet}$, and $\overline{Y}_{\bullet\bullet}$ is the grand mean of all the measurements, i.e.,

$$\overline{Y}_{\bullet\bullet} = \frac{1}{15}\sum_{i=1}^{3}\sum_{j=1}^{5} Y_{ij}. \qquad \text{(Eq. 4.3)}$$

The magnitude of non-tunable variability is represented by *robustness* defined in Eq. 2.11 as follows:

$$\text{robustness} = \left[\sum_{i=1}^{3} \left\{ \left(\frac{\sigma_{i\bullet}}{\hat{\bar{Y}}_{i\bullet}} \right)^2 + \left(\frac{\bar{Y}_{i\bullet} - \hat{\bar{Y}}_{i\bullet}}{\hat{\bar{Y}}_{i\bullet}} \right)^2 \right\} \right]^{-1}, \qquad \text{(Eq. 4.4)}$$

where $\sigma_{i\bullet}$ is the i-thi-th group standard deviation, i.e.,

$$\sigma_{i\bullet} = \sqrt{\frac{1}{5} \sum_{j=1}^{5} (Y_{ij} - \bar{Y}_{i\bullet})^2} \quad . \qquad \text{(Eq. 4.5)}$$

4.3 Robustness Optimization

Among the process parameters of the LPCVD process, pressure inside the furnace (P), gas flow rate from the load injector (Q_l), gas flow rate from the center injector (Q_c), and position of the source injector (X_s) were used for optimization of the process. Table 4.1 shows the levels of the process parameters used in the designed experiments.

	low	medium	high
P (torr)	0.20	0.25	0.35
Q_l (sccm)	30	45	60
Q_c (sccm)	40	55	70
X_s (cm)	118	124	130

Table 4.1 Levels of process parameters

Since there are four parameters with three levels each, an L9 orthogonal array was selected for the design of the experiments as shown in Table 4.2. Using the L9 orthogonal array for four parameters with three levels each, the main effects of each parameter were analyzed.

For a set of process parameter levels, the simulation program was executed five times each with random noises superimposed. Using the results of the deposition rates from the simulation program listed in Appendix D.1, the robustness and the slope were calculated. The results are listed in Table 4.3.

experiment number	level			
	P	Q_l	Q_c	X_s
1	1	1	1	1
2	1	2	2	2
3	1	3	3	3
4	2	1	2	3
5	2	2	3	1
6	2	3	1	2
7	3	1	3	2
8	3	2	1	3
9	3	3	2	1

Table 4.2 L9 orthogonal array for designed experiments

experiment number	P (torr)	Q_l (sccm)	Q_c (sccm)	X_s (cm)	robustness	slope
1	0.20	30	40	118	1568.9	5.550
2	0.20	45	55	124	585.3	-1.367
3	0.20	60	70	130	485.5	-9.305
4	0.25	30	55	130	1022.4	2.194
5	0.25	45	70	118	339.9	-2.419
6	0.25	60	40	124	1512.2	-4.043
7	0.35	30	70	124	238.0	2.458
8	0.35	45	40	130	964.1	-0.050
9	0.35	60	55	118	540.3	-6.424

Table 4.3 Results of designed experiments

The robustness and slope were modeled as functions of the process parameters using the experimental data listed in Table 4.3 as follows:

$$\text{robustness} = 663.6 - 149.6\times P - 227.8\times P^2 - 48.6\times Q_l + 264.8\times Q_l^2 - 497.0\times Q_c + 135.4\times Q_c^2 + 3.8\times X_s + 41.7\times X_s^2 \ , \qquad \text{(Eq. 4.6)}$$

and

$$\text{slope} = -1.0008 + 0.1867\times P - 0.1825\times P^2 - 4.9950\times Q_l - 0.3150\times Q_l^2 - 1.7883\times Q_c + 0.5650\times Q_c^2 - 0.6467\times X_s - 0.7600\times X_s^2 \ . \qquad \text{(Eq. 4.7)}$$

The functions above were obtained by quadratic curve fitting of the experimental data using normalized parameter values. Each parameter value is normalized to have values between -1 and 1.

After the robustness was modeled (as shown above) as a function of the process parameters, it was maximized by determination of the optimizing process parameter values. The optimizing process parameter values could be determined independently with the other parameters, because the robustness function does not include any interaction terms. Maximum robustness operating points, the process parameter values that maximize the robustness, are listed in Table 4.4.

parameter	maximum robustness operating points
P (torr)	0.24
Q_1 (sccm)	60
Q_c (sccm)	40
X_s (sccm)	130

Table 4.4 Maximum robustness operating points

After the maximum robustness operating points were determined, the effects of the process parameters on the robustness and the slope when they vary from a low to a high value were investigated to identify the tuning factor. The changes of robustness and slope corresponding to the changes of each process parameter are plotted in Figure 4.5. In the figure, each response was obtained with the other process parameters fixed at their maximum robustness operating points.

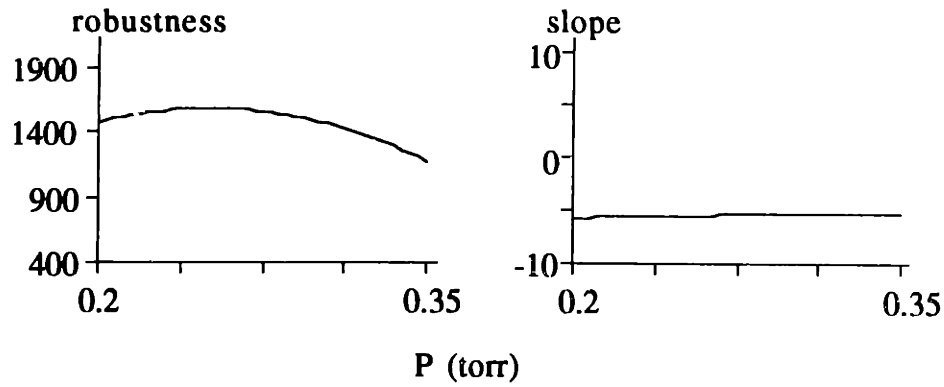

Figure 4.5 Robustness and slope at maximum robustness operating points

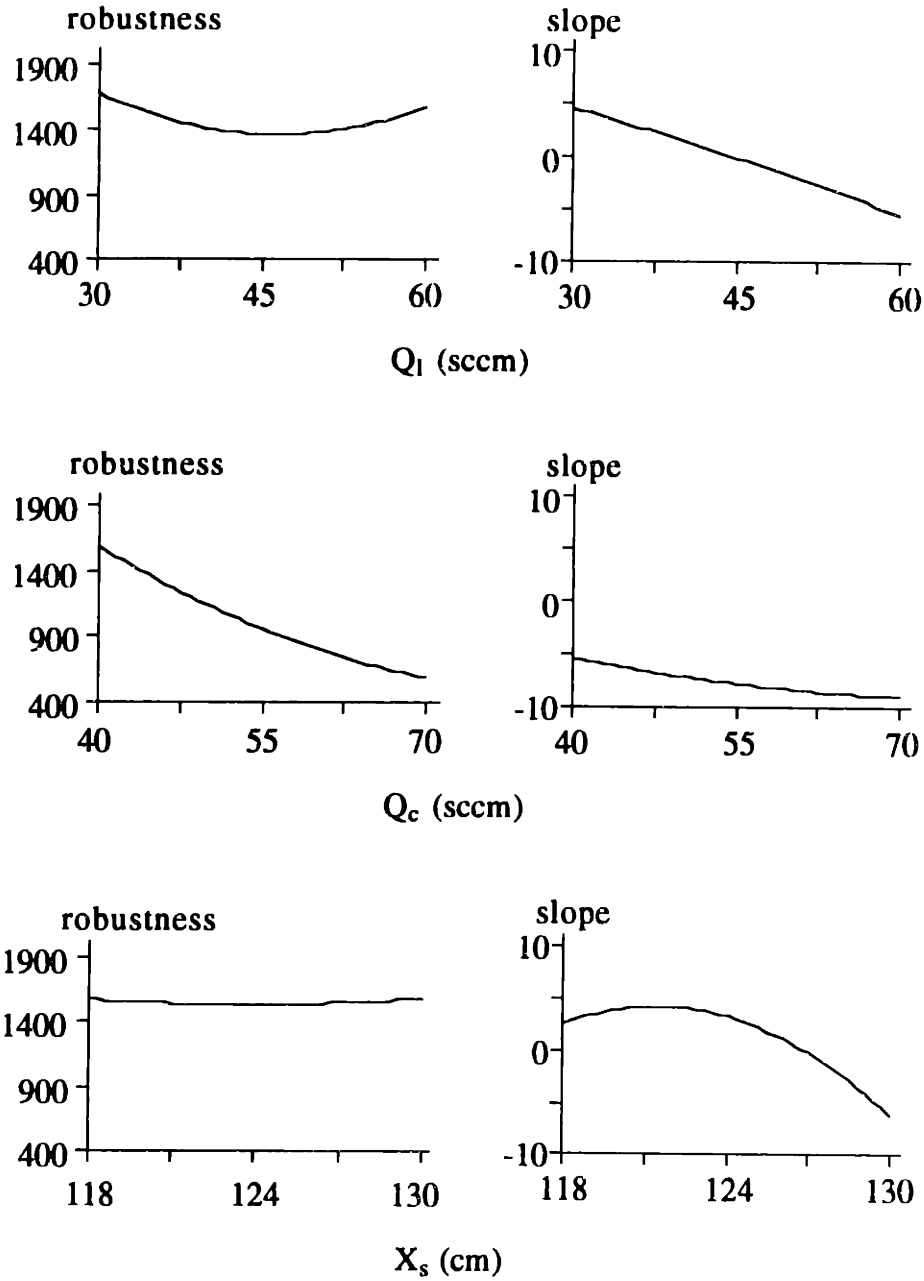

Figure 4.5 Robustness and slope at maximum robustness operating points (continued)

In order to identify the tuning factor among the process parameters, indices were calculated for each process parameter. $Index_t$ (Eq. 2.14) was defined as follows:

$$\text{index}_t = \left| \frac{\left[\frac{\Delta \text{ robustness}}{\text{average of robustness}}\right]}{\left[\frac{\Delta \text{ slope}}{\text{average of slope}}\right]} \right| . \qquad \text{(Eq. 4.8)}$$

In Table 4.5, index values for each process parameter are listed. By comparing the indices, Q_l was identified as the tuning factor because it has the smallest index value. The other process parameters were classified as robustness factors, and their values were fixed at the maximum robustness operating points during sequential optimization.

		P	Q_l	Q_c	X_s
robustness	average	1474.27	1446.73	987.39	1550.66
	difference	401.96	218.46	994	45.59
slope	average	-5.43	-0.11	-7.48	-4.15
	difference	0.42	9.99	3.58	1.54
index_t		3.5250	0.0017	2.1034	0.0792

Table 4.5 Index values for each parameter

4.4 Sequential Optimization

In Section 4.3, robustness was optimized by finding the maximum robustness operating points as shown in Table 4.4. After the robustness optimization, tunable uniformity was optimized using a sequential optimization method.

Sequential optimization was performed using a commercial software called Ultramax® [15]. In the sequential optimization method, a process is optimized sequentially using a model that is updated every time new data are available. With the updated model, the process is more precisely described, especially in the vicinity of the optimum point; hence, better optimization is expected.

In Section 4.2, tunable uniformity was represented by the slope of the linear regression line (Eq. 4.2). In order to perform sequential optimization of the tunable uniformity, a new performance index was defined as follows:

$$\text{performance index} = \sum_{i=1}^{3} \left(\frac{\overline{Y}_{i\bullet} - \overline{Y}_{\bullet\bullet}}{\overline{Y}_{\bullet\bullet}}\right)^2 \quad . \qquad \text{(Eq. 4.9)}$$

The performance index is the squared sum of relative deviations of each group mean from the grand mean, which includes the effect of group mean deviation from the regression line as well as the effect of the regression line slope. By minimizing the performance index, both the deviations and the regression line slope are minimized.

The performance index was modeled as a function of the tuning factor using the multiple response surface method. First, multiple response surfaces for each relative group mean deviation from the grand mean were modeled as a first-order function of the tuning factor (Eq. 4.10) and then combined to calculate the performance index (Eq. 4.11), i.e.,

$$\frac{\overline{Y}_{i\bullet} - \overline{Y}_{\bullet\bullet}}{\overline{Y}_{\bullet\bullet}} = C_{0i} + C_{1i}Ql \qquad (\text{for } i = 1,2,3) \ , \qquad \text{(Eq. 4.10)}$$

and

$$\text{performance index} = \sum_{i=1}^{3} (C_{0i} + C_{1i}Ql)^2 \ . \qquad \text{(Eq. 4.11)}$$

Since each response surface has only two coefficients, the model adaptation can be performed quickly with a small quantity of data, which increases the speed of optimization.

Figure 4.6 shows the results of sequential optimization of the performance index, which are listed in Appendix D.2. It is shown that the sequential optimizer explores the parameter space as well as minimizes the performance index further as more data become available. Because of the parameter space exploration, the performance index has some fluctuations. The performance index was optimized with orders of magnitude decrease by the sequential optimization.

The improvement of tunable uniformity by sequential optimization resulted in an increase of overall uniformity in conjunction with the optimized non-tunable uniformity. The non-tunable uniformity was not degraded during the sequential optimization of tunable uniformity. The overall uniformity defined in Eq. 3.9 is plotted in Figure 4.7.

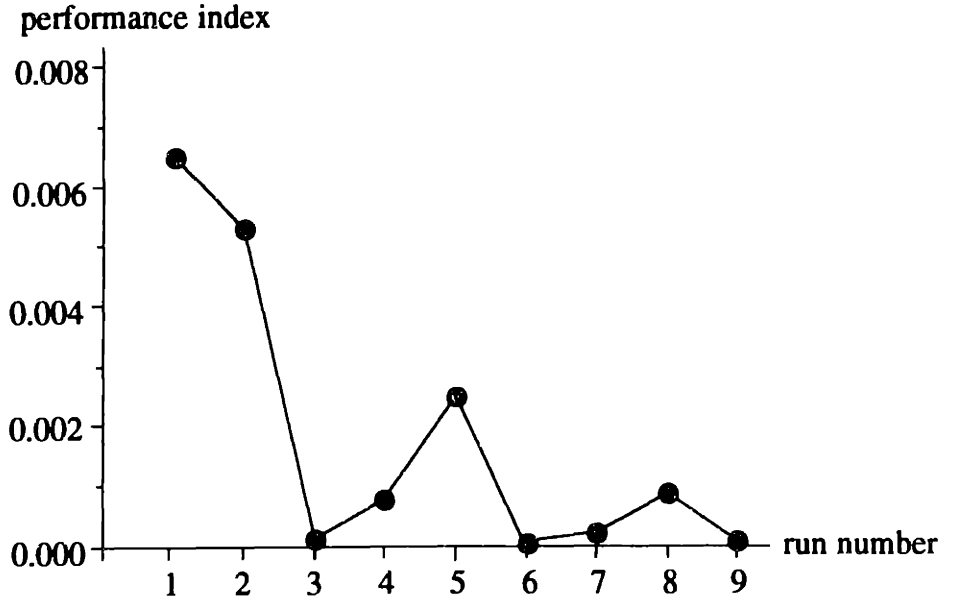

Figure 4.6 Performance index in sequential optimization

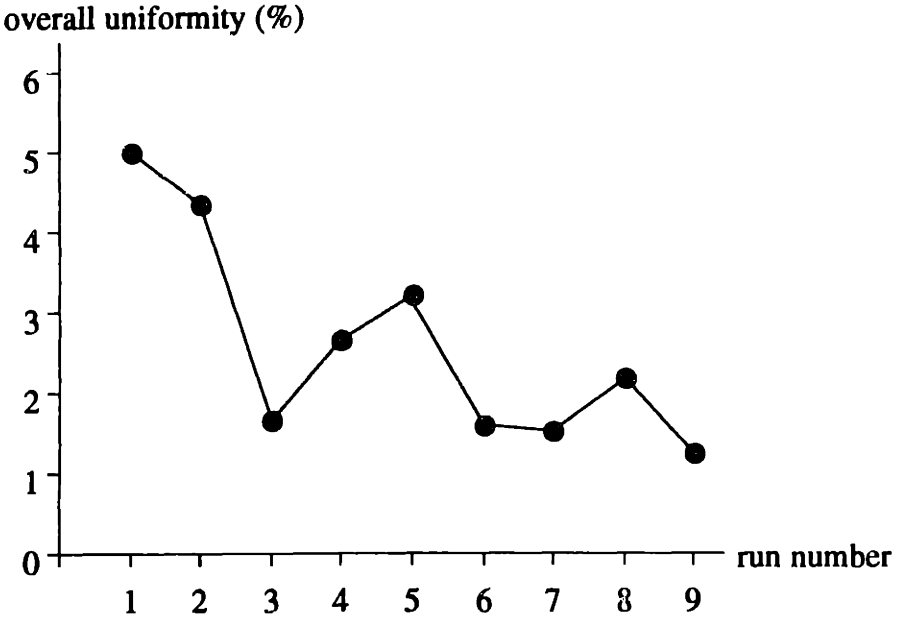

Figure 4.7 Overall uniformity in sequential optimization

4.5 Discussions

The uniformity of film thickness in the polysilicon LPCVD simulation process was improved by the robustness optimization that improved the batch-to-batch uniformity and by the sequential optimization of tunable uniformity that improved within-a-batch uniformity. Among the process parameters, gas flow rate from the load injector (Q_1) was identified as a tuning factor based on the analysis of index.

The results showed that the sequential optimization of tunable uniformity after parallel non-tunable uniformity optimization improves the overall uniformity more than only the parallel optimization of non-tunable uniformity. With sequential optimization, the overall uniformity was improved from 5% just after the non-tunable uniformity optimization to 1.3% in ten runs. The use of the tuning factor in sequential optimization enabled the optimization of tunable uniformity without degrading the non-tunable uniformity, which is indicated by similar decreasing patterns of the performance index (Figure 4.6) and the overall uniformity (Figure 4.7).

It is instructive to compare the results of sequential optimization using the tuning factor in this chapter with the results of sequential optimization using all the parameters in Appendix F. In Appendix F, all the process parameters were used to model and control the radial uniformity of a single wafer plasma etching process. The radial uniformity was considered to be tunable variability and was optimized sequentially. The performance index (Eq. F.4), which is similar to Eq. 4.9, was minimized sequentially as shown in Figure F.2. In this example, however, the non-tunable uniformity was not optimized, and all the process parameters were used for the optimization of only tunable uniformity. Circumferential uniformity, the non-tunable variability, was actually affected by the sequential optimization of tunable uniformity. Also the process parameters were not differentiated as tuning and robustness factors, and both were used in the sequential optimization of tunable uniformity. The result was that there was no improvement of the overall uniformity (shown in Figure F.3) even though the performance index was optimized.

CHAPTER 5

DISCUSSIONS

The application examples of Chapter 3 showed that the on-line control of process uniformity improves the within-a-wafer uniformity of single wafer plasma etching processes when it is combined with the optimization of non-tunable process variability. The example of Chapter 4 also showed that sequential optimization of tunable variability increases process uniformity more than the off-line parallel optimization result.

In the oxide etching process, on-line controls using single and multiple tuning factors were applied. The radial uniformity of wafers was categorized as tunable variability and circumferential uniformity as non-tunable variability. It was shown that both methods are effective in controlling the radial uniformity when compared with the optimization-only experiments that were performed simultaneously without on-line control. The selected tuning factors in the experiments were not ideal tuning factors, since the effects of the tuning factors on the robustness was not absolutely absent. As a result, on-line control with multiple tuning factors degraded circumferential uniformity more than on-line control with a single tuning factor, which can be shown by comparing Figs. 3.21 and 3.32. By comparing the results, it is suggested that as small as possible number of tuning factors are preferred to preserve the optimized non-tunable variability when the ideal tuning factors are not available in real processes.

In the polysilicon etching process, on-line control using a single tuning factor was applied. The robustness optimization resulted in high overall uniformity, and on-line control could not improve the overall uniformity substantially even though the tunable uniformity was well controlled. The effects of degraded non-tunable uniformity due to the control action offset the on-line controlled tunable uniformity, which resulted in no improvements in overall uniformity. However, it was shown that the radial uniformity can be controlled effectively to compensate for incoming material variations. A new target value for the slope, which represents the radial uniformity, was set to compensate for the radial non-uniformity of incoming wafers. On-line control using the tuning factor showed that the new target value was achieved quickly.

The concept of categorization of the process variability is useful for on-line control as well as optimization of the process uniformity as shown in Chapter 4. The sequential optimization result of Chapter 4 is compared with the results of Appendix F. In Appendix F, the sequential optimization of the defined performance index did not improve the overall uniformity due to the effects of process variability, which is not included in the definition of the performance index. In Chapter 4, it was shown that the sequential optimization of tunable variability using a tuning factor increased the overall uniformity effectively after the non-tunable variability was minimized by robustness optimization.

In Appendix E, the multiple response surface method was applied to the control of within-a-wafer uniformity. It was shown that the method is effective in controlling the overall uniformity on-line as long as the process is stable. When the process experiences a step change in process conditions, the multiple response surfaces were not able to predict the behavior of the process correctly, resulting in poor overall uniformity.

In the on-line control examples of this work, the simplest control algorithm was applied as explained in Section 3.4.1.2. Even though it was shown that the tunable variability is controlled well using the simplest control algorithm, more elaborate control algorithms that are now being developed for the MIT process control system are expected to increase the effectiveness. For example, when there is a long, slow drift in the process conditions, the EWMA algorithm, explained briefly in Section 2.7.2,

is appropriate, and when there is a sudden shift, such as step changes in process conditions, a control algorithm developed using Bayes's rule is appropriate [10].

On-line control was applied to examples of the plasma etching process, which is very complex and not fully understood. Control of the plasma etching process needs a very careful control scheme, since it is possible to introduce side effects that are not straightforward to understand [70]. The goal of the on-line control methodology developed in this work is to reduce the risk of applying on-line control to the process. In the developed methodology, the risk is reduced by confining the number of process parameters with which on-line control is performed. Therefore, it is very appropriate to apply the developed control methodology to the plasma etching process.

In many single wafer processes, efforts have been directed to increase the radial direction uniformity. For example, a circularly symmetric three-zone lamp system was developed for a single wafer rapid thermal process in order to control the temperature profile in the radial direction of a wafer [71]. In such a system, the circumferential uniformity is still necessary to optimize or control, and the methodology of this work is applicable for better process uniformity.

Process optimization and control may have different algorithms and methodologies according to how ideal the process is for optimization and control. Table 5.1 compares the ideal processes for optimization and control with the real processes. In dealing with real processes in manufacturing environments, a proper method should be developed accordingly.

When a process is stable, on-line control is not necessary. According to Deming [68]: "Action taken on a stable system in response to variation within the control limits, in an effort to compensate for this variation, is tampering, the results of which will inevitably increase the variation and increase costs." However, it is very difficult for manufacturing processes to be stable enough not to require on-line control or another off-line optimization [72]. The robust design method is known as an effective methodology for process quality improvements as long as the processes are stable [73][74]. The advantage of the methodology of this work is to improve the robust design method so that on-line control of process variability may be possible while keeping the optimized process robustness.

The methodology developed in this work is best suited for the processes whose process variability is readily categorized into tunable and non-tunable variabilities, whose process conditions are drifting and shifting, and whose incoming materials have variations.

	ideal processes	real processes
process physics	- process physics fully understood	- complex process physics
process variability	- tunable variability only	- tunable variability - non-tunable variability
process conditions	- stable or predictable change	- drifts and shifts
process modeling	- physically based modeling - dynamic modeling	- empirical or semi-empirical modeling - statistical modeling - response surface modeling - dynamic modeling is difficult
optimization	- global optimization	- sub-optimization within or near to process parameter window of experiments - robustness optimization
control	- control of process response using all available parameters - real time control: use of real time measured data	- SPC: monitoring of process conditions - control: using limited number of parameters for safe control - real time control: stochastic, adaptive control is required

Table 5.1 Ideal vs. real processes for optimization and control

CHAPTER 6
CONCLUSIONS & FUTURE WORKS

6.1 Conclusions

Motivated by the need for an effective and a simple methodology of on-line process quality control that can be implemented in a manufacturing environment, a new methodology of on-line control is developed. The characteristics of the developed methodology are: it is based on the categorization of process variabilities, it classifies process parameters and uses them for different purposes, it decouples the procedures of robustness optimization and on-line tunable variability control, and it increases process quality by on-line control of the tunable variability without degrading process robustness.

Process variability is categorized into non-tunable variability, defined as process variability that is difficult to model and control, and tunable variability, defined as on-line controllable process variability that is relatively easy to model and control. Process parameters are classified into the robustness factor, the tuning factor, and the adjustment factor according to the magnitudes of their effects on non-tunable and tunable variability. The robustness factor is for the optimization of non-tunable variability, the tuning factor is for the control of tunable uniformity, and the adjustment factor is for the control of mean. Non-tunable variability is optimized off-line, and tunable uniformity and mean are controlled on-line.

The procedures of the on-line control of tunable uniformity and mean are decoupled from the optimization of non-tunable variability due to the use of classified process parameters. It is this decoupling effect that enables on-line control with a reduced risk of tampering the process variability.

The developed methodology were applied to the examples of single wafer plasma etching processes and an LPCVD simulation process. The results showed that process uniformity was improved by applying on-line control of uniformity. On-line control was able to reduce the effects of natural variations in the process conditions as well as to make the process robust against step changes in the process conditions. Also, it was shown that on-line control can compensate for incoming material variations by controlling tunable uniformity accordingly.

The concept of categorizing process variability was also shown to be useful in optimizing process uniformity. The sequential optimization of tunable variability was successful in improving process uniformity more than the optimized uniformity with parallel designed experiments.

The categorization of process variability is concluded to be useful for both optimization and control of process uniformity. On-line control of process uniformity using categorized variability is shown as an effective control methodology that reduces the risk of tampering and the side effects without a complex and elaborated model of processes.

6.2 Future Works

In this work, only the uniformity of processes was considered. In real manufacturing processes, process optimization and control have multiple objectives. For example, in the plasma etching processes it is necessary not only the uniformity of etching depths but also selectivity, loss of critical dimensions, directionality, and throughput rates. Therefore, on-line control methodology should be extended so that it can handle more than one objectives.

Developments in sensor technology make it possible to measure many characteristics of processes in real time. The *in situ* measurement data are valuable, because they record the history of process condition changes during a process. When

on-line control is performed in a real time mode, an effective strategy on how to use *in situ* measurement data should be developed since the amount of *in situ* measurement data is usually large. On-line control performed both on a run by run basis and in real time is expected to enhance critically the process performance. The algorithms which can integrate pre-process and post-process measurements for the run by run control as well as the real time control should be developed.

A more elaborate control algorithm, other than the modification of the constant term that was used in this work, needs to be developed and applied to increase the effectiveness of on-line control. It is also necessary to decide how to select the best algorithm applicable for a given example appropriately.

The on-line control methodology developed in this work is to be integrated into the MIT process control system, and the integrated process control software is to be incorporated with the CAFE system at MIT.

REFERENCES

[1] L.P. Provost and C.L. Norman, "Variation Through the Ages," *Quality Progress*, pp.39-44, December 1990.

[2] H.M. Wadsworth, K.S. Stephens, and A.B. Godfrey, *Modern Methods for Quality Control and Improvement*, John Wiley & Sons, Inc., 1986.

[3] J.P. Womack, D.T. Jones, and D. Roos, *The Machine that Changed the World*, Harper Perennial, 1990.

[4] J.B. Keats and N.F. Hubele, *Statistical Process Control in Automated Manufacturing*, Marcel Dekker, Inc., 1989.

[5] G. Taguchi, E.A. Elsayed, and T. Hsiang, *Quality Engineering in Production Systems*, McGraw-Hill Book Co., 1989.

[6] D.C. Montgomery, *Introduction to Statistical Quality Control*, John Wiley & Sons, Inc., 1985.

[7] K. Dehnad, *Quality Control, Robust Design, and the Taguchi Method*, Wadsworth & Brooks/ Cole Advanced Books and Software, 1989.

[8] M.S. Phadke, *Quality Engineering using Robust Design*, Prentice-Hall, 1989.

[9] E.M. Sachs, R.S. Guo, S. Ha, and A. Hu, "Process Control System for VLSI Fabrication," *IEEE Transactions on Semiconductor Manufacturing*, vol.4, no.2, pp.134-144, May 1991.

[10] A.K. Hu, *An Optimal Bayesian Controller for Flexible Manufacturing Processes*, Ph.D. Thesis, Department of Mechanical Engineering, Massachusetts Institute of Technology, Cambridge, MA, 1992.

[11] A. Ingolfsson, *Run by Run Process Control*, M.S. Thesis, Department of Electrical Engineering and Computer Science, Massachusetts Institute of Technology, Cambridge, MA, 1991.

[12] D.S. Boning, D.E. Troxel, M.B. McIlrath, M.L. Heytens, D.A. Antoniadis, and P. Penfield, Jr., "CAFE: A System for VLSI Technology Complexity Management," *7th Annual SRC/DARPA CIM-IC Workshop*, Stanford, CA, August 1992.

[13] B.J. Mandel, "The Regression Control Chart," *Journal of Quality Technology*, vol.1, no.1, pp.1-9, January 1969.

[14] G.E.P. Box and N.R. Draper, *Evolutionary Operation: A Statistical Method for Process Improvement*, John Wiley & Sons, Inc., 1969.

[15] *Ultramax® software program*, Ultramax Corp., Cincinnati, OH, 1984.

[16] C.W. Moreno, "Self-learning Optimization Control Software," *Instrument Society of America, Robotics and Expert System Conference*, pp.371-377, Houston, TX, June 1986.

[17] R.S. Guo, "Modeling, Optimization, and Control of Spatial Uniformity in Manufacturing Processes," *IEEE Transactions on Semiconductor Manufacturing*, vol.6, no.1, pp.41-57, February 1993.

[18] S.V. Wiel, W.T. Tucker, F.W. Faltin, and N. Doganaksoy, "Algorithmic Statistical Process Control: Concepts and an Application," Unpublished Report, 1990.

[19] J.F. MacGregor, "Interfaces Between Process Control and On-line Statistical Process Control," *Computing and Systems Technology Division Communications*, pp.9-19, American Institute of Chemical Engineers, 1987.

[20] C.J. Spanos, H. Guo, A. Miller, and J. Levine-Parrill, "Real-Time Statistical Process Control Using Tool Data," *IEEE Transactions on Semiconductor Manufacturing*, vol.5, no.4, pp.308-318, November 1992.

[21] S.H. Thomke, *Multivariate Quality Control of Flexible Manufacturing Processes*, M.S. Thesis, Department of Electrical Engineering and Computer Science, Massachusetts Institute of Technology, Cambridge, MA, 1992.

[22] R.N. Kackar and A.C. Shoemaker, "Robust Design: A Cost-effective Method for Improving Manufacturing Processes," *AT&T Technical Journal*, vol.65, issue 2, pp.39-50, March/April 1986.

[23] R.N. Kackar, "Off-line Quality Control, Parameter Design, and the Taguchi Method," *Journal of Quality Technology*, vol.17, pp.176-209, 1985.

[24] W.C. Benton, "Statistical Process Control and the Taguchi Method: A Comparative Evaluation," *International Journal of Production Research*, vol.29, no.9, pp.1761-1770, 1991.

[25] R.V. Leon, A.C. Shoemaker, and R.N. Kackar, "Performance Measures Independent of Adjustment," *Technometrics*, vol.29, no.3, pp.253-265, 1987.

[26] G. Taguchi, *System of Experimental Design*, UNIPUB/Kraus International Publications, 1987.

[27] M.S. Phadke and K. Dehnad, "Optimization of Product and Process Design for Quality and Cost," *Quality and Reliability Engineering International*, vol.4, no.2, pp.105-112, 1988.

[28] G.E.P. Box, W.G. Hunter, and J.S. Hunter, *Statistics for Experiments*, John Wiley & Sons, Inc., 1978.

[29] G.E.P. Box and N.R. Draper, *Empirical Model-Building and Response Surfaces*, John Wiley & Sons Inc., 1987.

[30] E.M. Sachs, G. Prueger, and R. Guerrieri, "An Equipment Model for Polysilicon LPCVD," *IEEE Transactions on Semiconductor Manufacturing*, vol.5, no.1, pp.3-13, February 1992.

[31] E.M. Sachs and G. Prueger, "Equipment Models for Process Optimization and Control using Smart Response Surface," *Electrochemical Society Meeting Rec.*, Fall 1988.

[32] W.P. Wehrle, *Application of Dimensional Analysis to Statistical Process Modeling*, M.S. Thesis, Department of Mechanical Engineering, Massachusetts Institute of Technology, Cambridge, MA, 1989.

[33] K. Wong, *Sequential Optimization using Grouped Variables*, M.S. Thesis, Department of Mechanical Engineering, Massachusetts Institute of Technology, Cambridge, MA, 1990.

[34] R.H. McCafferty, "Dimensionless Parameters of Reactive Ion Etching," *Proceedings of 39th Electronic Components Conference*, Houston, TX, May 1989.

[35] S. Kalpakjian, *Manufacturing Engineering and Technology*, Addison-Wesley Publishing Co., 1992.

[36] R.H. McCafferty, Personal Communication, January 1993.

[37] R.V. Hogg and J. Ledolter, *Engineering Statistics*, Macmillan, 1987.

[38] N. Draper and H. Smith, *Applied Regression Analysis, 2nd Edition*, John Wiley & Sons, Inc., 1981.

[39] J.A. Rice, *Mathematical Statistics and Data Analysis*, Wadsworth & Brooks/ Cole Advanced Books and Software, 1988.

[40] J. Neter, W. Wasserman, and M. Kutner, *Applied Linear Regression Models*, Irwin Inc., 1983.

[41] R.L. Guldi, C.D. Jenkins, G.M. Damminga, T.A. Baum, and T.A. Foster, "Process Optimization Tweaking Tool (POTT) and its Application in Controlling Oxidation Thickness," *IEEE Transactions on Semiconductor Manufacturing*, vol.2, no.2, pp.54-59, May 1989.

[42] P.J. Ross, *Taguchi Techniques for Quality Engineering*, McGraw-Hill Book Co., 1988.

[43] R.L. Plackett and J.P. Burman, "The Design of Optimum Multifactorial Experiments," *Biometrika*, vol.33, pp.305-325, 1946.

[44] C. Moler, J. Little and S. Bangert, *PRO-MATLAB*, The MathWorks, Inc., 1990.

[45] J.M. Lucas and M.S. Saccucci, "Exponentially Weighted Moving Average Control Schemes," *Technometrics*, vol.32, no.1, pp.1-29, February 1990.

[46] J.S. Hunter, "The Exponentially Weighted Moving Average," *Journal of Quality Technology*, vol.18, no.4, pp.203-210, 1986.

[47] W.S. Wei, *Time Series Analysis: Univariate and Multivariate Methods*, Addison-Wesley Publishing Co., 1990.

[48] G.E.P. Box and G.M. Jenkins, *Time Series Analysis: Forecasting and Control*, Holden-Day Inc., 1976.

[49] R.C. Jaeger, *Introduction to Microelectronic Fabrication, Volume 5*, Addison-Wesley Publishing Co., 1988.

[50] H. H. Sawin and L. R. Reif, *Plasma Processing for Microelectronic Fabrication: Plasma Deposition, Etching, and Sputtering of Thin Films for VLSI*, Course Note, Massachusetts Institute of Technology, Cambridge, MA, 1991.

[51] S. Wolf and R.N. Tauber, *Silicon Processing for the VLSI Era, Volume 1 - Process Technology*, Lattice Press, 1986.

[52] W.M. Moreau, *Semiconductor Lithography: Principles, Practices, and Materials*, Plenum Press, 1988.

[53] *Operations and Maintenance Manual*, Lam Research Corp., Fremont, CA, 1989.

[54] D.C. Hinson *et al.*, "Magnetron-Enhanced Plasma Etching of Silicon and Silicon Dioxide," *Semiconductor International*, October 1983.

[55] A.J. van Roosmalen, J.A.G. Baggerman, and S.J.H. Brader, *Dry Etching for VLSI*, Plenum Press, 1991.

[56] *Operations Manual for Nanospec/AFT Model 200*, Nanometrics, Inc., Sunnyvale, CA, 1987.

[57] S. Park and D.J. Economou, "A Mathematical Model for Etching of Silicon Using CF_4 in a Radial Flow Plasma Reactor," *Journal of Electrochemical Society*, vol.138, no.5, pp.1499-1508, May 1991.

[58] M.W. Jenkins, M.T. Mocella, K.D. Allen, and H.H. Sawin, "The Modeling of Plasma Etching Processes Using Response Surface Methodology," *Solid State Technology*, pp.175-182, April 1986.

[59] P.E. Riley, "Development of a Highly Uniform Silicon Dioxide Etching Process Using Response-Surface Methodology," *Journal of Electrochemical Society*, vol.133, no.9, pp.1971-1972, September 1986.

[60] G.S. May, J. Huang, and C.J. Spanos, "Statistical Experimental Design in Plasma Etch Modeling," *IEEE Transactions on Semiconductor Manufacturing*, vol.4, no.2, pp.83-96, May 1991.

[61] P.E. Riley and D.A. Hanson, "Study of Etch Rate Characteristics of SF_6/He Plasmas by Response-Surface Methodology: Effects of Interelectrode Spacing," *IEEE Transactions on Semiconductor Manufacturing*, vol.2, no.4, pp.178-182, November 1989.

[62] P.E. Riley, A.P. Turley, and W.J. Malkowski, "Development of a Multistep SiO_2 Plasma Etching Process in a Minibatch Reactor Using Response-Surface Methodology," *Journal of Electrochemical Society*, vol.136, no.4, pp.1112-1119, April 1989.

[63] P.E. Riley, M. Chang, S.G. Ghanayem, and A. Mak, "Development of a Magnetron-Enhanced Plasma Process for Tungsten Etchback with Response-Surface Methodology," *IEEE Transactions on Semiconductor Manufacturing*, vol.3, no.3, pp.142-144, August 1990.

[64] D.W. Daniel, R. Bloom, and J.E. Reece, "Identifying an Etch Process Window Using Response Surface Methodology," *Solid State Technology*, pp.117-120, September 1988.

[65] G.G. Barna, "Automatic Problem Detection and Documentation in a Plasma Etch Reactor," *IEEE Transactions on Semiconductor Manufacturing*, vol.5, no.1, pp.56-59, February 1992.

[66] S.W. Butler, K.J. McLaughlin, T.F. Edgar, and I. Trachtenberg, "Development of Techniques for Real-Time Monitoring and Control in Plasma Etching," *Journal of Electrochemical Society*, vol.138, no.9, pp.2727-2735, September 1991.

[67] B.N. Chapman and T.A. Hansen, "The Implication of Flow-Rate Dependencies in Plasma Etching," *Journal of Applied Physics*, vol.51, no.7, pp.3608-3613, July 1980.

[68] T.J. Boardman and E.C. Boardman, "Don't Touch That Funnel!," *Quality Progress*, pp.65-69, December 1990.

[69] C.H. Brekel and L.J. Bollen, "Low Pressure Deposition of Polysilicon from Silane," *Journal of Crystal Growth*, vol.54, pp.310-322, 1981.

[70] C.T. Gabriel and J.P. McVittie, "How Plasma Etching Damages Thin Gate Oxides," *Solid State Technology*, pp.81-87, June 1992.

[71] P.P. Apte and C. Saraswat, "Rapid Thermal Processing Uniformity Using Multivariable Control of a Circularly Symmetric 3 Zone Lamp," *IEEE Transactions on Semiconductor Manufacturing*, vol.5, no.3, pp.180-188, August 1992.

[72] J.F. MacGregor, "A Different View of the Funnel Experiments," *Journal of Quality Technology*, vol.22, no.4, pp.255-259, October 1990.

[73] G. Taguchi, Personal Communication, June 1992.

[74] M. Phadke, Personal Communication, November 1992.

APPENDIX A

EQUATION OF QUALITY LOSS

$$QL = K \sum_{i=1}^{m} \sum_{j=1}^{n} (Y_{ij} - T)^2$$

$$= K \sum_{i=1}^{m} \sum_{j=1}^{n} (Y_{ij}^2 - 2TY_{ij} + T^2)$$

$$= K \sum_{i=1}^{m} \sum_{j=1}^{n} (Y_{ij}^2 - 2TY_{ij} + T^2 + 2\overline{Y}_{..}^2 - 2\overline{Y}_{..}^2)$$

$$= K \sum_{i=1}^{m} \sum_{j=1}^{n} (Y_{ij}^2 - 2T\overline{Y}_{..} + T^2 + \overline{Y}_{..}^2 + \overline{Y}_{..}^2 - 2Y_{ij}\overline{Y}_{..}) \quad \cdots\cdots\cdots\cdots (*)$$

$$= K \sum_{i=1}^{m} \sum_{j=1}^{n} \left[(Y_{ij}^2 - 2T\overline{Y}_{..} + \overline{Y}_{..}^2) + (\overline{Y}_{..}^2 - 2Y_{ij}\overline{Y}_{..} + T^2) \right]$$

$$= K \sum_{i=1}^{m} \sum_{j=1}^{n} \left[(Y_{ij} - \overline{Y}_{..})^2 + (\overline{Y}_{..} - T)^2 \right]$$

$$= K \left[\{ \sum_{i=1}^{m} \sum_{j=1}^{n} (Y_{ij} - \overline{Y}_{..})^2 \} + \{ m\, n\, (\overline{Y}_{..} - T)^2 \} \right]$$

$$= K\left[\{ n \sum_{i=1}^{m} [\sigma_{i\bullet}^2 + (\bar{Y}_{i\bullet} - \bar{Y}_{\bullet\bullet})^2] \} + \{ m\, n\, (\bar{Y}_{\bullet\bullet} - T)^2 \} \right] \quad \cdots\cdots\cdots (**)$$

$$= n\, K\left[\{ \sum_{i=1}^{m} [\sigma_{i\bullet}^2 + (\bar{Y}_{i\bullet} - \bar{Y}_{\bullet\bullet})^2] \} + \{ m\, (\bar{Y}_{\bullet\bullet} - T)^2 \} \right]$$

(*)

$$\sum_{i=1}^{m}\sum_{j=1}^{n} 2TY_{ij} = 2T \sum_{i=1}^{m}\sum_{j=1}^{n} Y_{ij} = 2\,T\,m\,n\,\bar{Y}_{\bullet\bullet} = 2\,T \sum_{i=1}^{m}\sum_{j=1}^{n} \bar{Y}_{\bullet\bullet} = \sum_{i=1}^{m}\sum_{j=1}^{n} (\,2\,T\,\bar{Y}_{\bullet\bullet})$$

$$\sum_{i=1}^{m}\sum_{j=1}^{n} 2\bar{Y}_{\bullet\bullet}^2 = 2\sum_{i=1}^{m}\sum_{j=1}^{n} (\bar{Y}_{\bullet\bullet}\bar{Y}_{\bullet\bullet}) = 2\bar{Y}_{\bullet\bullet}\sum_{i=1}^{m}\sum_{j=1}^{n} \bar{Y}_{\bullet\bullet} = 2\bar{Y}_{\bullet\bullet}\sum_{i=1}^{m}\sum_{j=1}^{n} Y_{ij} = \sum_{i=1}^{m}\sum_{j=1}^{n} (2Y_{ij}\bar{Y}_{\bullet\bullet})$$

(**)

$$\sum_{i=1}^{m}\sum_{j=1}^{n} (\,Y_{ij} - \bar{Y}_{\bullet\bullet})^2 = \sum_{i=1}^{m}\sum_{j=1}^{n} (\,Y_{ij}^2 - 2Y_{ij}\bar{Y}_{\bullet\bullet} + \bar{Y}_{\bullet\bullet}^2) = \sum_{i=1}^{m}\left[\sum_{j=1}^{n} Y_{ij}^2 - 2\bar{Y}_{\bullet\bullet}(\sum_{j=1}^{n} Y_{ij}) + n\bar{Y}_{\bullet\bullet}^2 \right]$$

$$= \sum_{i=1}^{m}\left[n\,(\sigma_{i\bullet}^2 + \bar{Y}_{i\bullet}^2) - 2\bar{Y}_{\bullet\bullet}(n\bar{Y}_{i\bullet}) + n\bar{Y}_{\bullet\bullet}^2 \right] = n \sum_{i=1}^{m}\left[\sigma_{i\bullet}^2 + \bar{Y}_{i\bullet}^2 - 2\bar{Y}_{i\bullet}\bar{Y}_{\bullet\bullet} + \bar{Y}_{\bullet\bullet}^2 \right]$$

$$= n \sum_{i=1}^{m}\left[\sigma_{i\bullet}^2 + (\bar{Y}_{i\bullet} - \bar{Y}_{\bullet\bullet})^2 \right]$$

APPENDIX B
OXIDE ETCHING PROCESS EXPERIMENT DATA

B.1 Single Tuning Factor Experiments

B.1.1 2^2 Designed Experiments

[experiment 1]

site	thickness (Å) before	thickness (Å) after	etching rate (Å/min)	relative deviation
1	7181	2830	6526.5	0.043
2	7149	2792	6535.5	0.044
3	7127	2752	6562.5	0.049
4	7167	2799	6552.0	0.047
5	7185	2937	6372.0	0.018
6	7159	2886	6409.5	0.024
7	7072	2789	6424.5	0.027
8	7190	2918	6408.0	0.024
9	7034	3192	5763.0	-0.079
10	7253	3353	5850.0	-0.065
11	7038	3140	5847.0	-0.066
12	7199	3302	5845.5	-0.066
robustness			1154.5	
slope			-5.735	

[experiment 2]

site	thickness (Å) before	thickness (Å) after	etching rate (Å/min)	relative deviation
1	7323	3954	5053.5	-0.013
2	7279	3932	5020.5	-0.019
3	7307	3947	5040.0	-0.015
4	7346	3994	5028.0	-0.018
5	7349	3763	5379.0	0.051
6	7212	3563	5473.5	0.069
7	7324	3671	5479.5	0.071
8	7362	3739	5434.5	0.062
9	7346	4156	4785.0	-0.065
10	7185	3857	4992.0	-0.025
11	7444	4163	4921.5	-0.039
12	7208	3997	4816.5	-0.059
robustness			158.5	
slope			-1.531	

[experiment 3]

site	thickness (Å)		etching rate (Å/min)	relative deviation
	before	after		
1	7492	6331	1741.5	-0.009
2	7471	6325	1719.0	-0.022
3	7491	6343	1722.0	-0.020
4	7494	6341	1729.5	-0.016
5	7492	6399	1639.5	-0.067
6	7447	6332	1672.5	-0.048
7	7515	6408	1660.5	-0.055
8	7469	6356	1669.5	-0.050
9	7501	6245	1884.0	0.072
10	7475	6214	1891.5	0.076
11	7637	6411	1839.0	0.046
12	7278	5996	1923.0	0.094
robustness			202.5	
slope			4.448	

[experiment 4]

site	thickness (Å)		etching rate (Å/min)	relative deviation
	before	after		
1	6331	4874	2185.5	0.103
2	6325	4864	2191.5	0.106
3	6343	4857	2229.0	0.125
4	6341	4863	2217.0	0.119
5	6399	5050	2023.5	0.021
6	6332	5026	1959.0	-0.011
7	6408	4869	2308.5	0.165
8	6356	5003	2029.5	0.024
9	6245	5102	1714.5	-0.135
10	6214	5143	1606.5	-0.189
11	6411	5257	1731.0	-0.126
12	5996	4943	1579.5	-0.203
robustness			100.2	
slope			-13.826	

[experiment 5]

site	thickness (Å)		etching rate (Å/min)	relative deviation
	before	after		
1	6813	2295	6777.0	0.062
2	6806	2284	6783.0	0.063
3	6832	2324	6762.0	0.059
4	6833	2326	6760.5	0.059
5	6753	2421	6498.0	0.018
6	6688	2330	6537.0	0.024
7	6641	2312	6493.5	0.017
8	6790	2487	6454.5	0.011
9	6532	2609	5884.5	-0.078
10	6754	2796	5937.0	-0.070
11	6465	2553	5868.0	-0.081
12	6679	2780	5848.5	-0.084
robustness			1928.4	
slope			-6.941	

[experiment 6]

site	thickness (Å)		etching rate (Å/min)	relative deviation
	before	after		
1	7608	4379	4843.5	-0.053
2	7602	4420	4773.0	-0.067
3	7580	4323	4885.5	-0.045
4	7598	4360	4857.0	-0.051
5	7598	3960	5457.0	0.066
6	7639	3987	5478.0	0.071
7	7548	3873	5512.5	0.077
8	7577	3927	5475.0	0.070
9	7426	4083	5014.5	-0.020
10	7764	4424	5010.0	-0.021
11	7524	4144	5070.0	-0.009
12	7507	4155	5028.0	-0.017
robustness			130.2	
slope			1.865	

[experiment 7]

site	thickness (Å) before	thickness (Å) after	etching rate (Å/min)	relative deviation
1	6274	5099	1762.5	-0.017
2	6324	5138	1779.0	-0.008
3	6327	5137	1785.0	-0.004
4	6278	5091	1780.5	-0.007
5	6204	5070	1701.0	-0.051
6	6353	5197	1734.0	-0.033
7	6383	5208	1762.5	-0.017
8	6201	5048	1729.5	-0.035
9	5961	4739	1833.0	0.022
10	6275	5016	1888.5	0.053
11	6512	5238	1911.0	0.066
12	6074	4841	1849.5	0.032
robustness		453.5		
slope		2.614		

[experiment 8]

site	thickness (Å) before	thickness (Å) after	etching rate (Å/min)	relative deviation
1	5099	3668	2146.5	0.109
2	5138	3700	2157.0	0.115
3	5137	3680	2185.5	0.129
4	5091	3643	2172.0	0.122
5	5070	3732	2007.0	0.037
6	5197	3871	1989.0	0.028
7	5208	3831	2065.5	0.067
8	5048	3700	2022.0	0.045
9	4739	3698	1561.5	-0.193
10	5016	3961	1582.5	-0.182
11	5238	4116	1683.0	-0.130
12	4841	3739	1653.0	-0.146
robustness		241.5		
slope		-14.086		

B.1.2 On-line Control Experiments

run 1

[optimization-only]

site	thickness (Å) before	thickness (Å) after	etching rate (Å/min)
1	7345	5884	2191.5
2	7302	5843	2188.5
3	7250	5795	2182.5
4	7291	5838	2179.5
5	7415	6085	1995.0
6	7297	5935	2043.0
7	7119	5713	2109.0
8	7237	5858	2068.5
9	7431	6057	2061.0
10	7261	5863	2097.0
11	6843	5437	2109.0
12	7014	5630	2076.0
slope		-2.366	
overall uniformity		2.94 %	

[on-line control]

site	thickness (Å) before	thickness (Å) after	etching rate (Å/min)
1	7508	6062	2169.0
2	7545	6094	2176.5
3	7498	6043	2182.5
4	7454	6005	2173.5
5	7504	6148	2034.0
6	7603	6223	2070.0
7	7487	6066	2131.5
8	7309	5895	2121.0
9	7449	6067	2073.0
10	7586	6178	2112.0
11	7459	6029	2145.0
12	7016	5619	2095.5
slope		-1.625	
overall uniformity		7.80 %	

run 2

[optimization-only]

site	thickness (Å) before	thickness (Å) after	etching rate (Å/min)
1	7900	6426	2211.0
2	7956	6474	2223.0
3	7912	6425	2230.5
4	7848	6377	2206.5
5	7861	6534	1990.5
6	8021	6677	2016.0
7	7911	6560	2026.5
8	7691	6359	1998.0
9	7715	6187	2292.0
10	7998	6445	2329.5
11	7883	6370	2269.5
12	7365	5861	2256.0
slope		1.589	
overall uniformity		5.53 %	

[on-line control]

site	thickness (Å) before	thickness (Å) after	etching rate (Å/min)
1	8050	6871	1768.5
2	8091	6904	1780.5
3	8042	6858	1776.0
4	7992	6814	1767.0
5	8051	6907	1716.0
6	8143	6987	1734.0
7	8032	6862	1755.0
8	7825	6679	1719.0
9	8015	6798	1825.5
10	8114	6880	1851.0
11	8010	6768	1863.0
12	7522	6315	1810.5
slope		1.811	
overall uniformity		2.60 %	

run 3

[optimization-only]

site	thickness (Å) before	thickness (Å) after	etching rate (Å/min)
1	8217	6761	2184.0
2	8262	6804	2187.0
3	8223	6761	2193.0
4	8164	6705	2188.5
5	8214	6858	2034.0
6	8322	6949	2059.5
7	8242	6854	2082.0
8	7988	6630	2037.0
9	8190	6773	2125.5
10	8331	6893	2157.0
11	8262	6811	2176.5
12	7596	6166	2145.0
slope		-0.871	
overall uniformity		2.77 %	

[on-line control]

site	thickness (Å) before	thickness (Å) after	etching rate (Å/min)
1	9262	7683	2368.5
2	9525	7958	2350.5
3	9475	7913	2343.0
4	9209	7639	2355.0
5	8954	7516	2157.0
6	9722	8270	2178.0
7	9594	8122	2208.0
8	8780	7336	2166.0
9	8424	6903	2281.5
10	9677	8136	2311.5
11	9504	7978	2289.0
12	8052	6552	2250.0
slope		-1.568	
overall uniformity		3.29 %	

run 4

[optimization-only]

site	thickness (Å) before	thickness (Å) after	etching rate (Å/min)
1	8262	6765	2245.5
2	8278	6781	2245.5
3	8266	6762	2256.0
4	8240	6742	2247.0
5	8245	6867	2067.0
6	8297	6900	2095.5
7	8275	6864	2116.5
8	8132	6744	2082.0
9	8144	6647	2245.5
10	8305	6780	2287.5
11	8295	6765	2295.0
12	7780	6288	2238.0
slope		0.409	
overall uniformity		3.69 %	

[on-line control]

site	thickness (Å) before	thickness (Å) after	etching rate (Å/min)
1	8388	7210	1767.0
2	8403	7225	1767.0
3	8393	7211	1773.0
4	8367	7188	1768.5
5	8378	7244	1701.0
6	8412	7249	1744.5
7	8403	7227	1764.0
8	8253	7097	1734.0
9	8335	7111	1836.0
10	8406	7162	1866.0
11	8408	7164	1866.0
12	7931	6713	1827.0
slope		2.238	
overall uniformity		2.82 %	

run 5

[optimization-only]

site	thickness (Å) before	thickness (Å) after	etching rate (Å/min)
1	8637	7229	2112.0
2	8666	7252	2121.0
3	8653	7212	2161.5
4	8615	7179	2154.0
5	8607	7334	1909.5
6	8689	7399	1935.0
7	8666	7361	1957.5
8	8492	7204	1932.0
9	8518	7162	2034.0
10	8677	7324	2029.5
11	8652	7280	2058.0
12	8161	6787	2061.0
slope		-2.244	
overall uniformity		4.17 %	

[on-line control]

site	thickness (Å) before	thickness (Å) after	etching rate (Å/min)
1	8721	6996	2587.5
2	8747	7019	2592.0
3	8737	6997	2610.0
4	8701	6979	2583.0
5	8692	7145	2320.5
6	8866	7204	2493.0
7	8745	7172	2359.5
8	8579	7027	2328.0
9	8608	6910	2547.0
10	8758	7040	2577.0
11	8731	7041	2535.0
12	8235	6574	2491.5
slope		-1.109	
overall uniformity		4.10 %	

run 6

[optimization-only]

site	thickness (Å) before	thickness (Å) after	etching rate (Å/min)
1	9659	7098	3841.5
2	9688	7123	3847.5
3	9691	7075	3924.0
4	9641	7074	3850.5
5	9623	7374	3373.5
6	9794	7446	3522.0
7	9687	7417	3405.0
8	9497	7328	3253.5
9	9577	7508	3103.5
10	9646	7479	3250.5
11	9616	7410	3309.0
12	9112	6901	3316.5
slope		-8.872	
overall uniformity		7.89 %	

[on-line control]

site	thickness (Å) before	thickness (Å) after	etching rate (Å/min)
1	9674	7236	3657.0
2	9682	7256	3639.0
3	9686	7263	3634.5
4	9660	7238	3633.0
5	9666	7426	3360.0
6	9669	7424	3367.5
7	9703	7447	3384.0
8	9541	7309	3348.0
9	9692	7462	3345.0
10	9635	7375	3390.0
11	9676	7388	3432.0
12	9183	6937	3369.0
slope		-3.709	
overall uniformity		3.68 %	

run 7

[optimization-only]

site	thickness (Å) before	thickness (Å) after	etching rate (Å/min)
1	6078	3074	4506.0
2	6112	3723	3583.5
3	6061	3690	3556.5
4	6022	3667	3532.5
5	6165	4063	3153.0
6	6239	4149	3135.0
7	6088	3878	3315.0
8	5909	3801	3162.0
9	6081	3851	3345.0
10	6194	3903	3436.5
11	6044	3749	3442.5
12	5629	3412	3325.5
slope		-5.889	
overall uniformity		10.11 %	

[on-line control]

site	thickness (Å) before	thickness (Å) after	etching rate (Å/min)
1	6229	4845	2076.0
2	6269	4886	2074.5
3	6212	4845	2050.5
4	6166	4796	2055.0
5	6380	5082	1947.0
6	6515	5162	2029.5
7	6374	5007	2050.5
8	6186	4859	1990.5
9	6168	4838	1995.0
10	6411	5044	2050.5
11	6246	4886	2040.0
12	5779	4439	2010.0
slope		-0.988	
overall uniformity		1.81 %	

run 8

[optimization-only]

site	thickness (Å) before	thickness (Å) after	etching rate (Å/min)
1	6895	4517	3567.0
2	6929	4548	3571.5
3	6884	4484	3600.0
4	6838	4452	3579.0
5	6934	5080	2781.0
6	7012	5154	2787.0
7	6881	4884	2995.5
8	6699	4786	2869.5
9	6820	4634	3279.0
10	6903	4682	3331.5
11	6794	4533	3391.5
12	6336	4105	3346.5
slope		-3.717	
overall uniformity		9.35 %	

[on-line control]

site	thickness (Å) before	thickness (Å) after	etching rate (Å/min)
1	6942	5599	2014.5
2	7051	5726	1987.5
3	7001	5657	2016.0
4	6878	5540	2007.0
5	7047	5761	1929.0
6	7370	6053	1975.5
7	7210	5855	2032.5
8	6784	5459	1987.5
9	6871	5553	1977.0
10	7274	5948	1989.0
11	7148	5812	2004.0
12	6358	5046	1968.0
slope		-0.546	
overall uniformity		1.31 %	

run 9

[optimization-only]

site	thickness (Å) before	thickness (Å) after	etching rate (Å/min)
1	7023	6340	1024.5
2	7046	6365	1021.5
3	7025	6346	1018.5
4	7008	6324	1026.0
5	7172	6494	1017.0
6	7233	6551	1023.0
7	7198	6498	1050.0
8	7056	6360	1044.0
9	6935	6220	1072.5
10	7066	6346	1080.0
11	7065	6296	1153.5
12	6596	5802	1191.0
slope		4.793	
overall uniformity		5.14 %	

[on-line control]

site	thickness (Å) before	thickness (Å) after	etching rate (Å/min)
1	7030	6800	345.0
2	7053	6823	345.0
3	7042	6814	342.0
4	7006	6780	339.0
5	7534	7306	342.0
6	7583	7359	336.0
7	7406	7182	336.0
8	7334	7102	348.0
9	7224	7002	333.0
10	7144	6928	324.0
11	7089	6861	342.0
12	6675	6444	346.5
slope		-0.938	
overall uniformity		1.91 %	

run 10

[optimization-only]

site	thickness (Å) before	thickness (Å) after	etching rate (Å/min)
1	9283	8503	1170.0
2	9295	8525	1155.0
3	9320	8546	1161.0
4	9309	8503	1209.0
5	9209	8365	1266.0
6	9247	8461	1179.0
7	9349	8516	1249.5
8	9331	8418	1369.5
9	8906	7994	1368.0
10	8939	8074	1297.5
11	9351	8427	1386.0
12	9389	8447	1413.0
slope		7.582	
overall uniformity		7.26 %	

[on-line control]

site	thickness (Å) before	thickness (Å) after	etching rate (Å/min)
1	8503	7837	999.0
2	8525	7862	994.5
3	8546	7877	1003.5
4	8503	7829	1011.0
5	8365	7678	1030.5
6	8461	7778	1024.5
7	8516	7811	1057.5
8	8418	7706	1068.0
9	7994	7292	1053.0
10	8074	7374	1050.0
11	8427	7707	1080.0
12	8447	7733	1071.0
slope		2.966	
overall uniformity		2.79 %	

run 11

[optimization-only]

site	thickness (Å) before	thickness (Å) after	etching rate (Å/min)
1	9868	9130	1107.0
2	9907	9169	1107.0
3	9887	9139	1122.0
4	9851	9103	1122.0
5	9775	9016	1138.5
6	9937	9172	1147.5
7	9879	9085	1191.0
8	9760	8977	1174.5
9	9376	8618	1137.0
10	9887	9103	1176.0
11	9858	9054	1206.0
12	9515	8737	1167.0
slope		2.479	
overall uniformity		2.75 %	

[on-line control]

site	thickness (Å) before	thickness (Å) after	etching rate (Å/min)
1	9130	8391	1108.5
2	9169	8427	1113.0
3	9139	8391	1122.0
4	9103	8354	1123.5
5	9016	8257	1138.5
6	9172	8402	1155.0
7	9085	8298	1180.5
8	8977	8199	1167.0
9	8618	7869	1123.5
10	9103	8314	1183.5
11	9054	8253	1201.5
12	8737	7969	1152.0
slope		2.108	
overall uniformity		2.56 %	

run 12

[optimization-only]

site	thickness (Å) before	thickness (Å) after	etching rate (Å/min)
1	7478	6575	1354.5
2	7587	6704	1324.5
3	7519	6616	1354.5
4	7424	6508	1374.0
5	7079	6112	1450.5
6	7393	6456	1405.5
7	7277	6295	1473.0
8	7039	6056	1474.5
9	6360	5365	1492.5
10	7004	6024	1470.0
11	7073	6074	1498.5
12	6557	5567	1485.0
slope		4.708	
overall uniformity		4.22 %	

[on-line control]

site	thickness (Å) before	thickness (Å) after	etching rate (Å/min)
1	6575	5781	1191.0
2	6704	5909	1192.5
3	6616	5817	1198.5
4	6508	5706	1203.0
5	6112	5291	1231.5
6	6456	5629	1240.5
7	6295	5437	1287.0
8	6056	5227	1243.5
9	5365	4557	1212.0
10	6024	5195	1243.5
11	6074	5211	1294.5
12	5567	4760	1210.5
slope		1.785	
overall uniformity		2.70 %	

run 13

[optimization-only]

site	thickness (Å) before	thickness (Å) after	etching rate (Å/min)
1	9641	8914	1090.5
2	9664	8937	1090.5
3	9662	8925	1105.5
4	9652	8914	1107.0
5	9529	8781	1122.0
6	9676	8920	1134.0
7	9645	8861	1176.0
8	9647	8876	1156.5
9	9200	8457	1114.5
10	9642	8871	1156.5
11	9608	8809	1198.5
12	9677	8909	1152.0
slope		2.514	
overall uniformity		2.92 %	

[on-line control]

site	thickness (Å) before	thickness (Å) after	etching rate (Å/min)
1	8914	8039	1312.5
2	8937	8067	1305.0
3	8925	8043	1323.0
4	8914	8022	1338.0
5	8781	7888	1339.5
6	8920	8020	1350.0
7	8861	7922	1408.5
8	8876	7955	1381.5
9	8457	7577	1320.0
10	8871	7975	1344.0
11	8809	7865	1416.0
12	8909	8009	1350.0
slope		1.404	
overall uniformity		2.54 %	

run 14

[optimization-only]

site	thickness (Å) before	thickness (Å) after	etching rate (Å/min)
1	7013	6203	1215.0
2	7100	6295	1207.5
3	7046	6231	1222.5
4	6975	6150	1237.5
5	6660	5827	1249.5
6	6911	6086	1237.5
7	6793	5927	1299.0
8	6720	5857	1294.5
9	6119	5288	1246.5
10	6674	5809	1297.5
11	6623	5734	1333.5
12	6556	5705	1276.5
slope		2.694	
overall uniformity		3.01 %	

[on-line control]

site	thickness (Å) before	thickness (Å) after	etching rate (Å/min)
1	6203	5131	1608.0
2	6295	5219	1614.0
3	6231	5148	1624.5
4	6150	5061	1633.5
5	5827	4766	1591.5
6	6086	5005	1621.5
7	5927	4807	1680.0
8	5857	4760	1645.5
9	5288	4201	1630.5
10	5809	4688	1681.5
11	5734	4557	1765.5
12	5705	4608	1645.5
slope		1.846	
overall uniformity		2.69 %	

run 15

[optimization-only]

site	thickness (Å) before	thickness (Å) after	etching rate (Å/min)
1	9615	8676	1408.5
2	9654	8728	1389.0
3	9666	8715	1426.5
4	9642	8679	1444.5
5	9474	8490	1476.0
6	9656	8684	1458.0
7	9670	8629	1561.5
8	9636	8616	1530.0
9	9116	8127	1483.5
10	9613	8606	1510.5
11	9630	8566	1596.0
12	9685	8686	1498.5
slope		3.543	
overall uniformity		3.99 %	

[on-line control]

site	thickness (Å) before	thickness (Å) after	etching rate (Å/min)
1	6421	5273	1722.0
2	6544	5414	1695.0
3	6503	5353	1725.0
4	6395	5214	1771.5
5	5894	4745	1723.5
6	6311	5128	1774.5
7	6189	4967	1833.0
8	6058	4853	1807.5
9	5241	4055	1779.0
10	6007	4827	1770.0
11	6009	4784	1837.5
12	5988	4798	1785.0
slope		1.823	
overall uniformity		2.44 %	

B.2 Multiple Tuning Factor Experiments

B.2.1 L18 Designed Experiments

[experiment 1]

site	thickness (Å) before	thickness (Å) after	etching rate (Å/min)
1	7706	6692	1521.0
2	7748	6722	1539.0
3	7809	6771	1557.0
4	7779	6755	1536.0
5	7547	6522	1537.5
6	7714	6667	1570.5
7	7864	6784	1620.0
8	7812	6761	1576.5
9	7263	5267	1494.0
10	7664	6636	1542.0
11	7840	6764	1614.0
12	7854	6825	1543.5
robustness		29.280	
slope		0.326	
curvature		1.056	

[experiment 2]

site	thickness (Å) before	thickness (Å) after	etching rate (Å/min)
1	7872	7545	490.5
2	7923	7565	537.0
3	7978	7625	529.5
4	7936	7621	472.5
5	7709	7303	609.0
6	7907	7335	858.0
7	8034	7505	793.5
8	7942	7594	522.0
9	7427	6919	762.0
10	7869	6981	1332.0
11	8000	7270	1095.0
12	7925	7557	552.0
robustness		8.427	
slope		30.016	
curvature		-1.802	

[experiment 3]

site	thickness (Å) before	thickness (Å) after	etching rate (Å/min)
1	8020	7473	820.5
2	8051	7511	810.0
3	8108	7594	771.0
4	8092	7570	783.0
5	7861	7196	997.5
6	8015	7360	982.5
7	8148	7572	864.0
8	8147	7558	883.5
9	7542	6784	1137.0
10	7984	7220	1146.0
11	8132	7512	930.0
12	8244	7612	948.0
robustness		18.500	
slope		13.228	
curvature		0.742	

[experiment 4]

site	thickness (Å) before	thickness (Å) after	etching rate (Å/min)
1	9087	7982	1657.5
2	9155	8046	1663.5
3	9192	8067	1687.5
4	9135	8012	1684.5
5	8894	7765	1693.5
6	9163	8007	1734.0
7	9251	8048	1804.5
8	9106	7935	1756.5
9	8517	7390	1690.5
10	9115	7911	1806.0
11	9245	7975	1905.0
12	9077	7882	1792.5
robustness		26.249	
slope		3.600	
curvature		0.324	

[experiment 5]

site	thickness (Å)		etching rate (Å/min)
	before	after	
1	8807	7114	2539.5
2	8841	7141	2550.0
3	8858	7124	2601.0
4	8839	7117	2583.0
5	8677	6824	2779.5
6	8843	6922	2881.5
7	8875	6888	2980.5
8	8839	6919	2880.0
9	8364	6415	2923.5
10	8827	6736	3136.5
11	8869	6711	3237.0
12	8846	6842	3006.0
robustness		26.522	
slope		8.928	
curvature		1.026	

[experiment 6]

site	thickness (Å)		etching rate (Å/min)
	before	after	
1	9242	8601	961.5
2	9457	8814	964.5
3	9610	8948	993.0
4	9408	8753	982.5
5	8727	8034	1039.5
6	9456	8729	1090.5
7	9820	9072	1122.0
8	9318	8604	1071.0
9	7960	7235	1087.5
10	9319	8532	1180.5
11	9726	8903	1234.5
12	9178	8420	1137.0
robustness		25.044	
slope		8.605	
curvature		0.612	

[experiment 7]

site	thickness (Å)		etching rate (Å/min)
	before	after	
1	9485	7429	3084.0
2	9510	7473	3055.5
3	9513	7426	3130.5
4	9498	7398	3150.0
5	9376	7178	3297.0
6	9509	7321	3282.0
7	9503	7185	3477.0
8	9476	7193	3424.5
9	9035	6754	3421.5
10	9457	7106	3526.5
11	9459	6941	3777.0
12	9424	7066	3537.0
robustness		26.813	
slope		6.880	
curvature		0.521	

[experiment 8]

site	thickness (Å)		etching rate (Å/min)
	before	after	
1	9432	8574	1287.0
2	9466	8586	1320.0
3	9479	8557	1383.0
4	9460	8551	1353.5
5	9298	8465	1249.5
6	9458	8584	1311.0
7	9483	8523	1440.0
8	9460	8512	1422.0
9	8959	8190	1153.5
10	9409	8577	1248.0
11	9453	8502	1426.5
12	9507	8607	1350.0
robustness		19.788	
slope		-1.650	
curvature		1.474	

[experiment 9]

site	thickness (Å)		etching rate (Å/min)
	before	after	
1	9311	7562	2623.5
2	9338	7556	2673.0
3	9353	7584	2653.5
4	9339	7594	2617.5
5	9187	7262	2887.5
6	9332	7323	3013.5
7	9352	7443	2863.5
8	9343	7448	2842.5
9	8859	817	3063.0
10	9282	7085	3295.5
11	9305	7333	2958.0
12	9383	7435	2922.0
robustness		25.429	
slope		7.284	
curvature		0.889	

[experiment 10]

site	thickness (Å)		etching rate (Å/min)
	before	after	
1	8484	8032	678.0
2	8508	8053	682.5
3	8525	8067	687.0
4	8511	8060	676.5
5	8363	7912	676.5
6	8510	8049	691.5
7	8538	8066	708.0
8	8523	8068	682.5
9	8039	7589	675.0
10	8512	8046	699.0
11	8551	8076	712.5
12	8357	8111	669.0
robustness		30.041	
slope		0.574	
curvature		0.342	

[experiment 11]

site	thickness (Å)		etching rate (Å/min)
	before	after	
1	8375	7702	1009.5
2	8399	7708	1036.5
3	8412	7704	1062.0
4	8403	7711	1038.0
5	8257	7538	1078.5
6	8404	7617	1180.5
7	8421	7583	1257.0
8	8418	7661	1135.5
9	7927	7137	1185.0
10	8409	7486	1384.5
11	8428	7447	1471.5
12	8463	7651	1218.0
robustness		19.386	
slope		11.877	
curvature		-0.544	

[experiment 12]

site	thickness (Å)		etching rate (Å/min)
	before	after	
1	8247	7727	780.0
2	8268	7747	781.5
3	8286	7757	793.5
4	8281	7754	790.5
5	8126	7603	784.5
6	8274	7736	807.0
7	8298	7744	831.0
8	8307	7769	807.0
9	7782	7266	774.0
10	8290	7744	819.0
11	8327	7751	864.0
12	8375	7826	823.5
robustness		27.035	
slope		2.097	
curvature		0.257	

[experiment 13]

site	thickness (Å)		etching rate (Å/min)
	before	after	
1	8437	7837	900.0
2	8525	7928	895.5
3	8629	8025	906.0
4	8556	7958	897.0
5	8155	7539	924.0
6	8489	7858	946.5
7	8745	8113	948.0
8	8589	7974	922.5
9	7699	7117	873.0
10	8436	7823	919.5
11	8729	8112	925.5
12	8641	8051	885.0
robustness		30.991	
slope		0.062	
curvature		1.923	

[experiment 14]

site	thickness (Å)		etching rate (Å/min)
	before	after	
1	8711	7598	1669.5
2	8744	7595	1723.5
3	8758	7601	1735.5
4	8737	7609	1692.0
5	8587	7466	1681.5
6	8749	7521	1842.0
7	8776	7504	1908.0
8	8728	7524	1806.0
9	8276	7159	1675.5
10	8739	7442	1945.5
11	8777	7372	2107.5
12	8718	7431	1930.5
robustness		20.543	
slope		5.792	
curvature		-0.016	

[experiment 15]

site	thickness (Å)		etching rate (Å/min)
	before	after	
1	8618	7626	1488.0
2	8657	7662	1492.5
3	8673	7646	1540.5
4	8647	7617	1545.0
5	8482	7351	1696.5
6	8665	7525	1710.0
7	8698	7397	1951.5
8	8633	7344	1933.5
9	8163	6935	1842.0
10	8658	7399	1888.5
11	8693	7220	2209.5
12	8601	7147	2181.0
robustness		19.461	
slope		14.352	
curvature		1.383	

[experiment 16]

site	thickness (Å)		etching rate (Å/min)
	before	after	
1	9171	8206	1447.5
2	9174	8207	1450.5
3	9185	8206	1468.5
4	9194	8220	1461.0
5	9077	8087	1485.0
6	9152	8138	1521.0
7	9167	8135	1548.0
8	9214	8207	1510.5
9	8767	7814	1429.5
10	9098	8088	1515.0
11	9126	8111	1522.5
12	9253	8301	1428.0
robustness		29.242	
slope		0.569	
curvature		1.714	

[experiment 17]

site	thickness (Å) before	thickness (Å) after	etching rate (Å/min)
1	9099	8058	1561.5
2	9120	8067	1579.5
3	9135	8073	1593.0
4	9127	8078	1573.5
5	8983	7946	1555.5
6	9112	8043	1603.5
7	9136	8037	1648.5
8	9136	8075	1591.5
9	8662	7655	1510.5
10	9075	8027	1572.0
11	9110	8020	1635.0
12	9167	8137	1545.0
robustness		28.756	
slope		-0.356	
curvature		0.902	

[experiment 18]

site	thickness (Å) before	thickness (Å) after	etching rate (Å/min)
1	9149	7745	2106.0
2	9211	7795	2124.0
3	9180	7754	2139.0
4	9107	7687	2130.0
5	9099	7561	2307.0
6	9270	7678	2388.0
7	9191	7605	2379.0
8	8921	7369	2328.0
9	9010	7352	2487.0
10	9262	7501	2641.5
11	9138	7419	2578.5
12	8505	6867	2457.0
robustness		29.695	
slope		8.899	
curvature		0.377	

B.2.2 2^2 Designed Experiments

[experiment 1]

site	thickness (Å) before	thickness (Å) after	etching rate (Å/min)
1	7989	6659	1995.0
2	8054	6701	2029.5
3	8073	6722	2026.5
4	8019	6687	1998.0
5	7772	6587	1777.5
6	8015	6761	1881.0
7	8054	6803	1876.5
8	7942	6738	1806.0
9	7396	6154	1863.0
10	7915	6739	1764.0
11	7981	6678	1954.5
12	7889	6593	1944.0
slope		-3.427	
curvature		-2.921	

[experiment 2]

site	thickness (Å) before	thickness (Å) after	etching rate (Å/min)
1	7125	5241	2826.0
2	7152	5255	2845.5
3	7136	5219	2875.5
4	7129	5231	2847.0
5	6837	5035	2703.0
6	6935	5071	2796.0
7	6901	5006	2842.5
8	6933	5116	2725.5
9	6427	4907	2280.0
10	6746	5082	2496.0
11	6723	5104	2428.5
12	6856	5369	2230.5
slope		-9.213	
curvature		3.069	

[experiment 3]

site	thickness (Å)		etching rate (Å/min)
	before	after	
1	8609	8160	673.5
2	8822	8364	687.0
3	8959	8497	693.0
4	8770	8314	684.0
5	8038	7587	676.5
6	8738	8289	673.5
7	9082	8614	702.0
8	8612	8160	678.0
9	7245	6765	720.0
10	8540	8060	720.0
11	8916	8405	766.5
12	8427	7923	756.0
slope		4.004	
curvature		-2.135	

[experiment 4]

site	thickness (Å)		etching rate (Å/min)
	before	after	
1	6703	6115	882.0
2	6731	6140	886.5
3	6780	6189	886.5
4	6764	6175	883.5
5	6531	5924	910.5
6	6677	6065	918.0
7	6794	6173	931.5
8	6771	6170	901.5
9	6276	5742	801.0
10	6645	6098	820.5
11	6773	6226	820.5
12	6836	6315	781.5
slope		-4.533	
curvature		4.037	

[experiment 5]

site	thickness (Å)		etching rate (Å/min)
	before	after	
1	7551	6268	1924.5
2	7570	6260	1965.0
3	7631	6321	1965.0
4	7627	6341	1929.0
5	7311	6152	1738.5
6	7342	6123	1828.5
7	7510	6298	1818.0
8	7602	6441	1741.5
9	6927	5730	1795.5
10	6986	5838	1722.0
11	7280	6035	1867.5
12	7564	6342	1833.0
slope		-3.833	
curvature		-2.537	

[experiment 6]

site	thickness (Å)		etching rate (Å/min)
	before	after	
1	7481	5788	2539.5
2	7518	5807	2566.5
3	7600	5870	2595.0
4	7577	5869	2562.0
5	7206	5576	2445.0
6	7367	5658	2563.5
7	7580	5838	2613.0
8	7566	5911	2482.5
9	6796	5450	2019.0
10	7228	5751	2215.5
11	7520	6052	2202.0
12	7621	6302	1978.5
slope		-9.631	
curvature		3.987	

[experiment 7]

site	thickness (Å) before	thickness (Å) after	etching rate (Å/min)
1	7845	7390	682.5
2	7933	7472	691.5
3	8035	7570	697.5
4	7964	7509	682.5
5	7547	7087	690.0
6	7866	7409	685.5
7	8122	7651	706.5
8	7983	7518	697.5
9	7122	6635	730.5
10	7829	7340	733.5
11	8120	7610	765.0
12	8058	7553	757.5
slope		4.093	
curvature		-1.598	

[experiment 8]

site	thickness (Å) before	thickness (Å) after	etching rate (Å/min)
1	7611	7033	867.0
2	7607	7011	894.0
3	7613	7016	895.5
4	7622	7030	888.0
5	7477	6886	886.5
6	7533	6925	912.0
7	7517	6898	928.5
8	7536	6939	895.5
9	7170	6654	774.0
10	7455	6903	828.0
11	7384	6848	804.0
12	7443	6935	762.0
slope		-5.464	
curvature		3.864	

B.2.3 On-line Control Experiments

run 1

[optimization-only]

site	thickness (Å) before	thickness (Å) after	etching rate (Å/min)
1	6244	5716	792.0
2	6248	5715	799.5
3	6254	5720	801.0
4	6266	5734	798.0
5	6165	5652	769.5
6	6264	5737	790.5
7	6253	5724	793.5
8	5316	5791	787.5
9	5822	5333	733.5
10	6300	5791	763.5
11	6254	5733	781.5
12	6365	5836	793.5
slope		-1.890	
curvature		0.156	
overall uniformity		2.39 %	

[on-line control]

site	thickness (Å) before	thickness (Å) after	etching rate (Å/min)
1	6383	5868	772.5
2	6400	5882	777.0
3	6427	5907	780.0
4	6425	5908	775.5
5	6297	5796	751.5
6	6478	5967	766.5
7	6521	6009	768.0
8	6526	6017	763.5
9	5689	5218	706.5
10	6441	5933	762.0
11	6455	5939	774.0
12	6437	5920	775.5
slope		-1.423	
curvature		-0.196	
overall uniformity		2.49 %	

run 2

[optimization-only]

site	thickness (Å) before	thickness (Å) after	etching rate (Å/min)
1	7513	6991	783.0
2	7533	7006	790.5
3	7546	7017	793.5
4	7539	7014	787.5
5	7404	6899	757.5
6	7537	7019	777.0
7	7556	7030	789.0
8	7557	7045	768.0
9	7077	6592	727.5
10	7546	7041	757.5
11	7568	7036	798.0
12	7592	7082	765.0
slope		-1.719	
curvature		-0.158	
overall uniformity		2.51 %	

[on-line control]

site	thickness (Å) before	thickness (Å) after	etching rate (Å/min)
1	6644	6174	705.0
2	6643	6171	708.0
3	6636	6161	712.5
4	6652	6180	708.0
5	6518	6055	694.5
6	6578	6111	700.5
7	6538	6059	718.5
8	6634	6170	696.0
9	6115	5667	672.0
10	6473	6013	690.0
11	6410	5923	730.5
12	6626	6162	696.0
slope		-0.801	
curvature		-0.027	
overall uniformity		2.03 %	

run 3

[optimization-only]

site	thickness (Å) before	thickness (Å) after	etching rate (Å/min)
1	6486	5921	847.5
2	6515	5941	861.0
3	6468	5894	861.0
4	6452	5882	855.0
5	6297	5747	825.0
6	6399	5822	865.5
7	6258	5682	864.0
8	6305	5744	841.5
9	5937	5427	765.0
10	6258	5722	804.0
11	6108	5574	801.0
12	6284	5760	786.0
slope		-4.037	
curvature		1.590	
overall uniformity		3.97 %	

[on-line control]

site	thickness (Å) before	thickness (Å) after	etching rate (Å/min)
1	7630	7143	730.5
2	7628	7136	738.0
3	7601	7108	739.5
4	7604	7116	732.0
5	7582	7115	700.5
6	7664	7189	712.5
7	7588	7109	718.5
8	7619	7142	715.5
9	7405	6920	727.5
10	7738	7269	703.5
11	7654	7167	730.5
12	7818	7331	730.5
slope		-0.830	
curvature		-1.193	
overall uniformity		1.71 %	

run 4

[optimization-only]

site	thickness (Å) before	thickness (Å) after	etching rate (Å/min)
1	6643	6112	796.5
2	6623	6084	808.5
3	6647	6114	799.5
4	6670	6141	793.5
5	6403	5874	793.5
6	6420	5882	807.0
7	6532	6004	792.0
8	6575	6052	784.5
9	6021	5507	771.0
10	6236	5721	772.5
11	6517	6004	769.5
12	6668	6164	756.0
slope		-2.049	
curvature		0.691	
overall uniformity		1.99 %	

[on-line control]

site	thickness (Å) before	thickness (Å) after	etching rate (Å/min)
1	7280	6794	729.0
2	7266	6776	735.0
3	7262	6780	723.0
4	7289	6807	723.0
5	7212	6746	699.0
6	7227	6751	714.0
7	7211	6744	700.5
8	7324	6855	703.5
9	7029	6560	703.5
10	7246	6770	714.0
11	7273	6798	712.5
12	7521	7047	711.0
slope		-1.208	
curvature		-1.024	
overall uniformity		1.55 %	

run 5

[optimization-only]

site	thickness (Å) before	thickness (Å) after	etching rate (Å/min)
1	6746	6226	780.0
2	6730	6200	795.0
3	6737	6209	792.0
4	6762	6242	780.0
5	6780	6287	739.5
6	6811	6300	766.5
7	6806	6290	774.0
8	6896	6397	748.5
9	6441	5936	757.5
10	6874	6390	726.0
11	6743	6236	760.5
12	6851	6363	732.0
slope		-2.803	
curvature		-0.541	
overall uniformity		2.86 %	

[on-line control]

site	thickness (Å) before	thickness (Å) after	etching rate (Å/min)
1	5253	4762	736.5
2	5266	4773	739.5
3	5231	4733	747.0
4	5242	4748	741.0
5	5045	4560	727.5
6	5083	4579	756.0
7	5016	4505	766.5
8	5124	4635	733.5
9	4916	4435	721.5
10	5092	4616	714.0
11	5114	4625	733.5
12	5379	4917	693.0
slope		-1.737	
curvature		1.201	
overall uniformity		2.51 %	

run 6

[optimization-only]

site	thickness (Å) before	thickness (Å) after	etching rate (Å/min)
1	6278	5749	793.5
2	6268	5733	802.5
3	6331	5793	807.0
4	6352	5817	802.5
5	6164	5658	759.0
6	6132	5611	781.5
7	6307	5775	798.0
8	6450	5926	786.0
9	5743	5258	727.5
10	5849	5361	732.0
11	6045	5523	783.0
12	6351	5830	781.5
slope		-2.911	
curvature		0.157	
overall uniformity		3.27 %	

[on-line control]

site	thickness (Å) before	thickness (Å) after	etching rate (Å/min)
1	5799	5324	712.5
2	5816	5339	715.5
3	5879	5402	715.5
4	5877	5403	711.0
5	5586	5132	681.0
6	5667	5205	693.0
7	5847	5384	694.5
8	5920	5455	697.5
9	5461	4992	703.5
10	5758	5285	709.5
11	6058	5579	718.5
12	6313	5822	736.5
slope		0.239	
curvature		-1.683	
overall uniformity		1.97 %	

run 7

[optimization-only]

site	thickness (Å) before	thickness (Å) after	etching rate (Å/min)
1	7401	6889	768.0
2	7484	6964	780.0
3	7581	7066	772.5
4	7520	7004	774.0
5	7098	6617	721.5
6	7419	6901	777.0
7	7661	7145	774.0
8	7530	7020	765.0
9	6648	6151	745.5
10	7349	6849	750.0
11	7619	7097	783.0
12	7564	7059	757.5
slope		-0.957	
curvature		-0.454	
overall uniformity		2.22 %	

[on-line control]

site	thickness (Å) before	thickness (Å) after	etching rate (Å/min)
1	6302	5782	780.0
2	6292	5764	792.0
3	6287	5759	792.0
4	6331	5806	787.5
5	6195	5703	738.0
6	6153	5644	763.5
7	6184	5668	774.0
8	6286	5774	768.0
9	5995	5507	732.0
10	6217	5732	727.5
11	6200	5699	751.5
12	6343	5838	757.5
slope		-2.996	
curvature		-0.270	
overall uniformity		2.86 %	

run 8

[optimization-only]

site	thickness (Å) before	thickness (Å) after	etching rate (Å/min)
1	6550	6034	774.0
2	6455	5921	801.0
3	6564	6039	787.5
4	6532	6009	784.5
5	6274	5767	760.5
6	6413	5891	783.0
7	6286	5762	786.0
8	6297	5777	780.0
9	5918	5419	748.5
10	6374	5870	756.0
11	6177	5665	768.0
12	6146	5633	769.5
slope		-1.694	
curvature		0.242	
overall uniformity		1.86 %	

[on-line control]

site	thickness (Å) before	thickness (Å) after	etching rate (Å/min)
1	6998	6504	741.0
2	7013	6512	751.5
3	7024	6525	748.5
4	7021	6526	742.5
5	6906	6428	717.0
6	7025	6529	744.0
7	7037	6541	744.0
8	7051	6566	727.5
9	6601	6114	730.5
10	7048	6567	721.5
11	7044	6563	721.5
12	7089	6622	700.5
slope		-1.869	
curvature		0.064	
overall uniformity		2.01 %	

run 9

[optimization-only]

site	thickness (Å) before	thickness (Å) after	etching rate (Å/min)
1	3997	2886	1666.5
2	4054	2957	1645.5
3	4079	2963	1674.0
4	4031	2897	1701.0
5	3498	2268	1845.0
6	3798	2636	1743.0
7	3894	2684	1815.0
8	3739	2452	1930.5
9	2820	1596	1836.0
10	3664	2495	1753.5
11	3941	2720	1831.5
12	3765	2400	2047.5
slope		5.455	
curvature		1.785	
overall uniformity		6.34 %	

[on-line control]

site	thickness (Å) before	thickness (Å) after	etching rate (Å/min)
1	5268	4421	1270.5
2	5250	4394	1284.0
3	5302	4448	1281.0
4	5328	4482	1269.0
5	5178	4283	1342.5
6	5118	4207	1366.5
7	5264	4336	1392.0
8	5426	4532	1341.0
9	4791	3867	1386.0
10	4866	3918	1422.0
11	5027	4054	1459.5
12	5339	4408	1396.5
slope		5.177	
curvature		0.534	
overall uniformity		4.52 %	

run 10

[optimization-only]

site	thickness (Å) before	thickness (Å) after	etching rate (Å/min)
1	6018	5021	1495.5
2	6026	5035	1486.5
3	5996	5008	1482.0
4	6006	5009	1495.5
5	5888	4823	1597.5
6	5940	4892	1572.0
7	5876	4846	1545.0
8	5939	4856	1624.5
9	5644	4512	1698.0
10	5927	4869	1587.0
11	5894	4873	1531.5
12	6060	4931	1693.5
slope		4.390	
curvature		0.831	
overall uniformity		4.64 %	

[on-line control]

site	thickness (Å) before	thickness (Å) after	etching rate (Å/min)
1	5704	4145	2338.5
2	5676	4096	2370.0
3	5674	4092	2373.0
4	5712	4143	2353.5
5	5769	4170	2398.5
6	5762	4062	2550.0
7	5733	4069	2496.0
8	5859	4231	2442.0
9	5454	3827	2440.5
10	5867	4106	2641.5
11	5677	3953	2586.0
12	5831	4186	2467.5
slope		3.567	
curvature		0.516	
overall uniformity		3.80 %	

run 11

[optimization-only]

site	thickness (Å) before	thickness (Å) after	etching rate (Å/min)
1	5021	3917	1656.0
2	5035	3934	1651.5
3	5008	3899	1663.5
4	5009	3901	1662.0
5	4823	3647	1764.0
6	4892	3727	1747.5
7	4846	3670	1764.0
8	4856	3680	1764.0
9	4512	3285	1840.5
10	4869	3679	1785.0
11	4873	3686	1780.5
12	4931	3714	1825.5
slope		4.295	
curvature		0.770	
overall uniformity		3.69 %	

[on-line control]

site	thickness (Å) before	thickness (Å) after	etching rate (Å/min)
1	4697	3513	1776.0
2	4719	3534	1777.5
3	4778	3593	1777.5
4	4776	3594	1773.0
5	4475	3203	1908.0
6	4566	3315	1876.5
7	4737	3477	1890.0
8	4803	3572	1846.5
9	4332	3002	1995.0
10	4670	3364	1959.0
11	4942	3645	1945.5
12	5158	3896	1893.0
slope		4.607	
curvature		0.487	
overall uniformity		4.02 %	

run 12

[optimization-only]

site	thickness (Å) before	thickness (Å) after	etching rate (Å/min)
1	4859	3964	1342.5
2	4875	3980	1342.5
3	4891	4005	1329.0
4	4895	4005	1335.0
5	4747	3795	1428.0
6	4898	3948	1425.0
7	4927	3999	1392.0
8	4952	4021	1396.5
9	4123	3164	1438.5
10	4829	3858	1456.5
11	4843	3925	1377.0
12	4859	3911	1422.0
slope		3.102	
curvature		1.079	
overall uniformity		3.08 %	

[on-line control]

site	thickness (Å) before	thickness (Å) after	etching rate (Å/min)
1	5239	4022	1825.5
2	5287	4052	1852.5
3	5302	4059	1864.5
4	5275	4056	1828.5
5	5065	3872	1789.5
6	5243	4002	1861.5
7	5252	3982	1905.0
8	5266	4059	1810.5
9	4676	3512	1746.0
10	5234	4002	1848.0
11	5178	3903	1[illegible]2.5
12	5309	4118	1786.5
slope		-0.531	
curvature		0.235	
overall uniformity		2.54 %	

run 13

[optimization-only]

site	thickness (Å) before	thickness (Å) after	etching rate (Å/min)
1	4003	3131	1308.0
2	4034	3154	1320.0
3	4040	3142	1347.0
4	4036	3150	1329.0
5	3855	2959	1344.0
6	3983	3061	1383.0
7	3962	2975	1480.5
8	4040	3098	1413.0
9	3500	2570	1395.0
10	3982	3041	1411.5
11	3883	2829	1581.0
12	4098	3125	1459.5
slope		4.856	
curvature		0.402	
overall uniformity		5.43 %	

[on-line control]

site	thickness (Å) before	thickness (Å) after	etching rate (Å/min)
1	6121	5070	1576.5
2	6064	5004	1590.0
3	6101	5020	1621.5
4	6154	5091	1594.5
5	6069	5014	1582.5
6	5873	4788	1627.5
7	6007	4891	1674.0
8	6163	5088	1612.5
9	5942	4880	1593.0
10	5568	4465	1654.5
11	5922	4819	1654.5
12	6131	5044	1630.5
slope		1.159	
curvature		0.301	
overall uniformity		1.87 %	

run 14

[optimization-only]

site	thickness (Å) before	thickness (Å) after	etching rate (Å/min)
1	3131	2193	1407.0
2	3154	2205	1423.5
3	3142	2177	1447.5
4	3150	2197	1429.5
5	2959	2008	1426.5
6	3061	2073	1482.0
7	2975	1944	1546.5
8	3098	2096	1503.0
9	2570	1656	1371.0
10	3041	2031	1515.0
11	2829	1753	1614.0
12	3125	2093	1548.0
slope		2.883	
curvature		0.680	
overall uniformity		4.61 %	

[on-line control]

site	thickness (Å) before	thickness (Å) after	etching rate (Å/min)
1	6075	4344	2596.5
2	6179	4417	2643.0
3	6166	4377	2683.5
4	6106	4359	2620.5
5	5874	4199	2512.5
6	6134	4350	2676.0
7	6041	4300	2611.5
8	5982	4253	2593.5
9	5302	3726	2364.0
10	5736	4004	2598.0
11	5859	4017	2763.0
12	5753	4105	2472.0
slope		-1.669	
curvature		0.112	
overall uniformity		3.87 %	

run 15

[optimization-only]

site	thickness (Å) before	thickness (Å) after	etching rate (Å/min)
1	3974	2835	1708.5
2	3989	2840	1723.5
3	4014	2859	1732.5
4	4014	2882	1698.0
5	3805	2549	1884.0
6	3957	2702	1882.5
7	4007	2709	1947.0
8	4028	2809	1828.5
9	3175	1981	1791.0
10	3867	2583	1926.0
11	3931	2603	1992.0
12	3919	2660	1888.5
slope		5.011	
curvature		2.127	
overall uniformity		5.28 %	

[on-line control]

site	thickness (Å) before	thickness (Å) after	etching rate (Å/min)
1	5301	4239	1593.0
2	5444	4380	1596.0
3	5384	4295	1633.5
4	5243	4163	1620.0
5	4776	3718	1587.0
6	5161	4056	1657.5
7	5002	3842	1740.0
8	4886	3791	1642.5
9	4076	3089	1480.5
10	4857	3761	1644.0
11	4813	3653	1740.0
12	4832	3758	1611.0
slope		0.253	
curvature		1.289	
overall uniformity		4.06 %	

APPENDIX C

POLYSILICON ETCHING PROCESS EXPERIMENT DATA

C.1 2^2 Designed Experiments

[experiment 1]

site	thickness (Å) before	thickness (Å) after	etching rate (Å/min)
1	5350	4961	583.5
2	5350	4953	595.5
3	5352	4949	604.5
4	5349	4943	609.0
5	5350	4903	670.5
6	5344	4996	522.0
7	5343	4900	664.5
8	5354	4927	640.5
9	5342	4928	621.0
10	5337	4923	621.0
11	5349	4896	679.5
12	5342	4878	696.0
robustness		81.9	
slope		4.496	

[experiment 2]

site	thickness (Å) before	thickness (Å) after	etching rate (Å/min)
1	5412	3267	3217.5
2	5426	3331	3142.5
3	5404	3331	3109.5
4	5393	3326	3100.5
5	5409	3312	3145.5
6	5438	3294	3216.0
7	5405	3273	3198.0
8	5406	3295	3166.5
9	5415	3239	3264.0
10	5443	3215	3342.0
11	5417	3190	3340.5
12	5407	3221	3279.0
robustness		1911.4	
slope		2.552	

[experiment 3]

site	thickness (Å)		etching rate (Å/min)
	before	after	
1	5413	4250	1744.5
2	5411	4251	1740.0
3	5410	4251	1738.5
4	5408	4254	1731.0
5	5416	4261	1732.5
6	5450	4262	1782.0
7	5420	4285	1702.5
8	5415	4256	1738.5
9	5442	4342	1650.0
10	5408	4344	1596.0
11	5454	4360	1641.0
12	5413	4349	1596.0
robustness		752.2	
slope		-3.465	

[experiment 4]

site	thickness (Å)		etching rate (Å/min)
	before	after	
1	5401	2245	6312.0
2	5398	2258	6280.0
3	5403	2247	6312.0
4	5401	2246	6310.0
5	5402	2255	6294.0
6	5412	2242	6340.0
7	5408	2260	6296.0
8	5406	2259	6294.0
9	5417	2415	6004.0
10	5405	2388	6034.0
11	5412	2467	5890.0
12	5402	2457	5890.0
robustness		1473.4	
slope		-2.820	

[experiment 5]

site	thickness (Å)		etching rate (Å/min)
	before	after	
1	5353	5039	471.0
2	5356	5027	493.5
3	5363	5031	498.0
4	5352	4996	534.0
5	5364	4992	558.0
6	5367	4992	562.5
7	5359	4985	561.0
8	5353	4983	555.0
9	5364	4953	616.5
10	5369	4961	612.0
11	5347	4909	657.0
12	5356	4926	645.0
robustness		323.6	
slope		11.843	

[experiment 6]

site	thickness (Å)		etching rate (Å/min)
	before	after	
1	5395	3288	3160.5
2	5381	3268	3169.5
3	5384	3278	3159.0
4	5388	3286	3153.0
5	5388	3255	3199.5
6	5384	3239	3217.5
7	5363	3224	3208.5
8	5369	3249	3180.0
9	5392	3196	3294.0
10	5392	3133	3388.5
11	5353	3098	3382.5
12	5359	3171	3282.0
robustness		2617.7	
slope		2.726	

[experiment 7]

site	thickness (Å)		etching rate (Å/min)
	before	after	
1	5392	4236	1734.0
2	5397	4208	1783.5
3	5397	4202	1792.5
4	5395	4233	1743.0
5	5399	4244	1732.5
6	5397	4211	1779.0
7	5389	4209	1770.0
8	5394	4233	1741.5
9	5406	4316	1635.0
10	5403	4307	1644.0
11	5388	4319	1603.5
12	5384	4352	1548.0
robustness		503.3	
slope		-4.553	

[experiment 8]

site	thickness (Å)		etching rate (Å/min)
	before	after	
1	5404	2355	6098.0
2	5406	2375	6062.0
3	5404	2359	6090.0
4	5411	2367	6088.0
5	5408	2399	6018.0
6	5403	2367	6072.0
7	5401	2268	6266.0
8	5405	2386	6038.0
9	5408	2459	5898.0
10	5407	2433	5948.0
11	5403	2501	5804.0
12	5404	2488	5832.0
robustness		1578.1	
slope		-1.778	

C.2 On-line Control Experiments

run 1

[optimization-only]

site	thickness (Å)		etching rate (Å/min)
	before	after	
1	3787	1553	4468.0
2	3767	1527	4480.0
3	3774	1546	4456.0
4	3790	1501	4578.0
5	3797	1493	4608.0
6	3765	1480	4570.0
7	3772	1522	4500.0
8	3800	1527	4546.0
9	3801	1510	4582.0
10	3757	1463	4588.0
11	3762	1543	4438.0
12	3817	1606	4422.0
slope		0.133	
overall uniformity		1.40 %	

[on-line control]

site	thickness (Å)		etching rate (Å/min)
	before	after	
1	3759	1508	4502.0
2	3754	1483	4542.0
3	3756	1497	4518.0
4	3753	1514	4478.0
5	3759	1491	4536.0
6	3745	1440	4610.0
7	3745	1475	4540.0
8	3762	1523	4478.0
9	3741	1487	4508.0
10	3707	1405	4604.0
11	3700	1457	4486.0
12	3757	1509	4496.0
slope		0.149	
overall uniformity		0.94 %	

run 2

[optimization-only]

site	thickness (Å) before	thickness (Å) after	etching rate (Å/min)
1	3413	1018	4790.0
2	3411	1007	4808.0
3	3392	1011	4762.0
4	3412	1020	4784.0
5	3380	975	4810.0
6	3358	948	4820.0
7	3367	961	4812.0
8	3383	990	4786.0
9	3371	934	4874.0
10	3336	892	4888.0
11	3372	947	4850.0
12	3416	992	4848.0
slope		0.820	
overall uniformity		0.76 %	

[on-line control]

site	thickness (Å) before	thickness (Å) after	etching rate (Å/min)
1	3220	784	4872.0
2	3226	784	4884.0
3	3205	780	4850.0
4	3216	788	4856.0
5	3201	736	4930.0
6	3199	712	4974.0
7	3204	724	4960.0
8	3202	747	4910.0
9	3203	722	4962.0
10	3197	675	5044.0
11	3205	735	4940.0
12	3222	778	4888.0
slope		0.945	
overall uniformity		1.11 %	

run 3

[optimization-only]

site	thickness (Å) before	thickness (Å) after	etching rate (Å/min)
1	5423	3042	4762.0
2	5418	3044	4748.0
3	5421	3041	4760.0
4	5423	3043	4760.0
5	5427	3027	4800.0
6	5427	3008	4838.0
7	5414	3008	4812.0
8	5415	3014	4802.0
9	5429	3002	4854.0
10	5429	2971	4916.0
11	5428	2992	4872.0
12	5413	3005	4816.0
slope		1.112	
overall uniformity		1.02 %	

[on-line control]

site	thickness (Å) before	thickness (Å) after	etching rate (Å/min)
1	5423	2716	5414.0
2	5421	2716	5410.0
3	5428	2716	5424.0
4	5419	2718	5402.0
5	5434	2688	5492.0
6	5427	2682	5490.0
7	5422	2685	5474.0
8	5407	2690	5434.0
9	5423	2686	5474.0
10	5431	2653	5556.0
11	5415	2696	5438.0
12	5415	2689	5452.0
slope		0.619	
overall uniformity		0.78 %	

run 4

[optimization-only]

site	thickness (Å) before	thickness (Å) after	etching rate (Å/min)
1	3042	618	4848.0
2	3044	613	4862.0
3	3041	611	4860.0
4	3043	619	4848.0
5	3027	574	4906.0
6	3008	545	4926.0
7	3008	555	4906.0
8	3014	576	4876.0
9	3002	531	4942.0
10	2971	474	4994.0
11	2992	527	4930.0
12	3005	567	4876.0
slope		0.827	
overall uniformity		0.87 %	

[on-line control]

site	thickness (Å) before	thickness (Å) after	etching rate (Å/min)
1	5405	2605	5600.0
2	5408	2602	5612.0
3	5454	2605	5698.0
4	5452	2611	5682.0
5	5405	2596	5618.0
6	5405	2583	5644.0
7	5456	2588	5736.0
8	5450	2590	5720.0
9	5408	2607	5602.0
10	5422	2593	5658.0
11	5444	2628	5632.0
12	5427	2634	5586.0
slope		-0.252	
overall uniformity		0.85 %	

run 5

[optimization-only]

site	thickness (Å) before	thickness (Å) after	etching rate (Å/min)
1	5417	3075	4684.0
2	5413	3070	4686.0
3	5412	3072	4680.0
4	5412	3073	4678.0
5	5426	3058	4736.0
6	5422	3042	4760.0
7	5408	3041	4734.0
8	5411	3058	4706.0
9	5424	3037	4774.0
10	5420	3022	4796.0
11	5409	3039	4740.0
12	5409	3058	4702.0
slope		0.752	
overall uniformity		0.81 %	

[on-line control]

site	thickness (Å) before	thickness (Å) after	etching rate (Å/min)
1	5451	2586	5730.0
2	5436	2653	5566.0
3	5423	2641	5564.0
4	5417	2583	5668.0
5	5442	2642	5600.0
6	5444	2633	5622.0
7	5411	2634	5554.0
8	5412	2636	5552.0
9	5442	2650	5584.0
10	5444	2634	5620.0
11	5419	2648	5542.0
12	5407	2642	5530.0
slope		-0.563	
overall uniformity		1.00 %	

run 6

[optimization-only]

site	thickness (Å) before	thickness (Å) after	etching rate (Å/min)
1	5456	3105	4702.0
2	5454	3118	4672.0
3	5414	3116	4596.0
4	5416	3101	4630.0
5	5449	3104	4690.0
6	5443	3101	4684.0
7	5401	3103	4596.0
8	5453	3103	4700.0
9	5460	3104	4712.0
10	5462	3075	4774.0
11	5460	3104	4712.0
12	5454	3118	4672.0
slope		0.721	
overall uniformity		1.04 %	

[on-line control]

site	thickness (Å) before	thickness (Å) after	etching rate (Å/min)
1	5470	2976	4988.0
2	5470	2977	4986.0
3	5454	2972	4964.0
4	5447	2979	4936.0
5	5477	2963	5028.0
6	5479	2955	5048.0
7	5466	2964	5004.0
8	5420	2963	4914.0
9	5479	2970	5018.0
10	5479	2963	5032.0
11	5458	2998	4920.0
12	5405	3004	4802.0
slope		-0.257	
overall uniformity		1.33 %	

run 7

[optimization-only]

site	thickness (Å) before	thickness (Å) after	etching rate (Å/min)
1	5109	2591	5036.0
2	5121	2594	5054.0
3	5115	2585	5060.0
4	5117	2591	5052.0
5	5114	2573	5082.0
6	5127	2563	5128.0
7	5119	2571	5096.0
8	5114	2588	5052.0
9	5115	2584	5062.0
10	5154	2559	5190.0
11	5139	2596	5086.0
12	5113	2617	4992.0
slope		0.315	

[on-line control]

site	thickness (Å) before	thickness (Å) after	etching rate (Å/min)
1	5005	3298	3414.0
2	5007	3282	3450.0
3	5015	3294	3442.0
4	4974	3294	3360.0
5	4965	3279	3372.0
6	5015	3260	3510.0
7	5017	3253	3528.0
8	4967	3286	3362.0
9	4967	3238	3458.0
10	5026	3196	3660.0
11	5026	3220	3612.0
12	4958	3260	3396.0
slope		1.660	

run 8

[optimization-only]

site	thickness (Å)		etching rate (Å/min)
	before	after	
1	4731	2672	4118.0
2	4742	2667	4150.0
3	4736	2668	4136.0
4	4718	2666	4104.0
5	4716	2623	4186.0
6	4745	2586	4318.0
7	4736	2600	4272.0
8	4700	2633	4134.0
9	4711	2584	4254.0
10	4739	2618	4242.0
11	4731	2576	4310.0
12	4688	2639	4098.0
slope		1.180	

[on-line control]

site	thickness (Å)		etching rate (Å/min)
	before	after	
1	4363	3036	2654.0
2	4362	3031	2662.0
3	4358	3035	2646.0
4	4361	3039	2644.0
5	4363	3023	2680.0
6	4333	2967	2732.0
7	4339	2972	2734.0
8	4370	3026	2688.0
9	4357	2950	2814.0
10	4307	2793	3028.0
11	4321	2818	3006.0
12	4339	2956	2766.0
slope		4.574	

run 9

[optimization-only]

site	thickness (Å)		etching rate (Å/min)
	before	after	
1	5208	3166	4084.0
2	5206	3174	4064.0
3	5208	3165	4086.0
4	5202	3166	4072.0
5	5220	3155	4130.0
6	5209	3110	4198.0
7	5204	3125	4158.0
8	5202	3161	4082.0
9	5225	3166	4118.0
10	5218	3075	4286.0
11	5213	3154	4118.0
12	5208	3205	4006.0
slope		0.674	

[on-line control]

site	thickness (Å)		etching rate (Å/min)
	before	after	
1	5187	3256	3862.0
2	5187	3250	3874.0
3	5181	3254	3854.0
4	5181	3252	3858.0
5	5184	3257	3854.0
6	5183	3213	3940.0
7	5175	3214	3922.0
8	5172	3246	3852.0
9	5192	3252	3880.0
10	5170	3173	3994.0
11	5171	3216	3910.0
12	5166	3259	3814.0
slope		0.483	

run 10

[optimization-only]

site	thickness (Å) before	thickness (Å) after	etching rate (Å/min)
1	3783	1712	4142.0
2	3787	1704	4166.0
3	3781	1706	4150.0
4	3780	1710	4140.0
5	3787	1706	4162.0
6	3790	1679	4222.0
7	3787	1690	4194.0
8	3780	1709	4142.0
9	3792	1726	4132.0
10	3791	1677	4228.0
11	3791	1709	4164.0
12	3786	1745	4082.0
slope		0.024	

[on-line control]

site	thickness (Å) before	thickness (Å) after	etching rate (Å/min)
1	3648	1949	2548.5
2	3659	1938	2581.5
3	3655	1936	2578.5
4	3652	1945	2560.5
5	3659	1931	2592.0
6	3685	1893	2688.0
7	3679	1891	2682.0
8	3648	1924	2586.0
9	3685	1951	2601.0
10	3694	1829	2797.5
11	3694	1828	2799.0
12	3644	1932	2568.0
slope		2.358	

run 11

[optimization-only]

site	thickness (Å) before	thickness (Å) after	etching rate (Å/min)
1	5296	3267	4058.0
2	5289	3263	4052.0
3	5293	3267	4052.0
4	5300	3265	4070.0
5	5296	3259	4074.0
6	5292	3233	4118.0
7	5292	3238	4108.0
8	5300	3258	4084.0
9	5299	3262	4074.0
10	5302	3228	4148.0
11	5304	3261	4086.0
12	5294	3299	3990.0
slope		0.202	

[on-line control]

site	thickness (Å) before	thickness (Å) after	etching rate (Å/min)
1	5298	3808	2980.0
2	5305	3801	3008.0
3	5302	3802	3000.0
4	5301	3804	2994.0
5	5303	3796	3014.0
6	5308	3778	3060.0
7	5301	3771	3060.0
8	5295	3794	3002.0
9	5309	3773	3072.0
10	5339	3734	3210.0
11	5306	3766	3080.0
12	5290	3771	3038.0
slope		1.717	

run 12

[optimization-only]

site	thickness (Å)		etching rate (Å/min)
	before	after	
1	4157	1660	4994.0
2	4162	1656	5012.0
3	4157	1655	5004.0
4	4152	1662	4980.0
5	4179	1665	5028.0
6	4150	1626	5048.0
7	4152	1631	5042.0
8	4177	1661	5032.0
9	4183	1678	5010.0
10	4155	1602	5106.0
11	4162	1644	5036.0
12	4174	1701	4946.0
slope		0.269	

[on-line control]

site	thickness (Å)		etching rate (Å/min)
	before	after	
1	3740	2067	2509.5
2	3751	2046	2557.5
3	3746	2050	2544.0
4	3742	2064	2517.0
5	3749	2039	2565.0
6	3760	2098	2493.0
7	3749	2101	2472.0
8	3739	2032	2560.5
9	3753	2025	2592.0
10	3759	1968	2686.5
11	3753	1981	2658.0
12	3746	2028	2577.0
slope		1.882	

APPENDIX D

LPCVD PROCESS SIMULATION DATA

D.1 L9 Designed Experiments

[experiment 1]

	wafer 1	wafer 2	wafer 3
run 1	48.93	52.37	54.14
run 2	47.35	50.73	52.67
run 3	47.95	50.22	52.82
run 4	47.40	49.98	53.05
run 5	47.52	50.59	54.60
robustness	1568.9		
slope	5.550		

[experiment 2]

	wafer 1	wafer 2	wafer 3
run 1	52.94	52.73	51.71
run 2	51.46	50.00	50.45
run 3	52.58	51.04	50.91
run 4	51.11	48.50	49.53
run 5	51.99	53.75	50.47
robustness	585.3		
slope	-1.367		

[experiment 3]

	wafer 1	wafer 2	wafer 3
run 1	58.48	53.53	46.92
run 2	58.14	54.68	47.52
run 3	59.58	53.90	47.74
run 4	57.09	56.50	48.60
run 5	55.98	55.94	48.66
robustness	485.5		
slope	-9.305		

[experiment 4]

	wafer 1	wafer 2	wafer 3
run 1	49.75	52.72	52.05
run 2	48.81	51.18	50.58
run 3	49.15	50.48	50.40
run 4	48.67	52.18	51.33
run 5	49.36	51.06	52.50
robustness	1022.4		
slope	2.194		

[experiment 5]

	wafer 1	wafer 2	wafer 3
run 1	55.39	56.06	53.82
run 2	57.11	58.7	54.14
run 3	56.62	57.52	52.43
run 4	56.06	56.76	52.59
run 5	55.89	60.19	54.58
robustness	339.9		
slope	-2.419		

[experiment 6]

	wafer 1	wafer 2	wafer 3
run 1	56.09	53.51	52.40
run 2	58.53	54.00	53.32
run 3	57.61	55.00	53.62
run 4	57.98	55.61	53.19
run 5	58.15	56.06	53.50
robustness	1512.2		
slope	-4.043		

[experiment 7]

	wafer 1	wafer 2	wafer 3
run 1	55.04	60.49	59.46
run 2	53.91	58.32	57.63
run 3	54.77	60.43	57.79
run 4	55.52	61.14	55.99
run 5	55.73	61.94	58.30
robustness	238.0		
slope	2.458		

[experiment 8]

	wafer 1	wafer 2	wafer 3
run 1	54.76	54.24	55.54
run 2	55.82	53.76	55.20
run 3	55.53	56.06	54.52
run 4	56.44	57.71	56.33
run 5	55.78	57.08	56.46
robustness	964.1		
slope	-0.050		

[experiment 9]

	wafer 1	wafer 2	wafer 3
run 1	64.75	62.99	56.17
run 2	65.07	62.07	56.23
run 3	65.03	64.43	57.55
run 4	63.42	63.06	55.78
run 5	62.44	61.02	55.76
robustness	540.3		
slope	-6.424		

D.2 Sequential Optimization Experiments

[run 1]

	wafer 1	wafer 2	wafer 3
run 1	46.85	49.50	50.79
run 2	47.48	50.15	52.43
run 3	45.94	49.28	53.18
run 4	46.31	48.86	52.50
run 5	47.25	46.69	52.78
performance index	6.49×10^{-3}		
slope	5.645		
overall uniformity	4.99 %		

[run 2]

	wafer 1	wafer 2	wafer 3
run 1	57.08	54.11	51.16
run 2	55.57	53.98	51.62
run 3	57.51	52.94	50.82
run 4	57.73	53.58	52.35
run 5	56.42	53.65	50.72
performance index	5.30×10^{-3}		
slope	-5.123		
overall uniformity	4.35 %		

[run 3]

	wafer 1	wafer 2	wafer 3
run 1	52.09	50.21	52.20
run 2	51.86	50.78	52.12
run 3	52.64	52.09	49.82
run 4	52.43	52.36	50.70
run 5	51.54	52.65	51.75
performance index	1.20×10^{-4}		
slope	-0.768		
overall uniformity	1.67 %		

[run 4]

	wafer 1	wafer 2	wafer 3
run 1	51.20	51.11	51.70
run 2	48.92	50.38	51.64
run 3	48.84	50.05	52.20
run 4	49.52	48.59	49.62
run 5	50.88	50.89	53.61
performance index	7.88×10^{-4}		
slope	1.859		
overall uniformity	2.66 %		

[run 5]

	wafer 1	wafer 2	wafer 3
run 1	54.94	53.98	51.50
run 2	54.66	52.76	50.87
run 3	55.31	54.09	50.75
run 4	53.61	51.36	51.23
run 5	55.00	51.66	50.66
performance index	2.46×10^{-3}		
slope	-3.504		
overall uniformity	3.20 %		

[run 6]

	wafer 1	wafer 2	wafer 3
run 1	51.77	50.52	52.43
run 2	50.93	51.37	50.06
run 3	52.55	51.10	51.55
run 4	52.52	50.37	51.95
run 5	50.44	52.12	51.92
performance index	6.78×10^{-6}		
slope	-0.058		
overall uniformity	1.57 %		

[run 7]

	wafer 1	wafer 2	wafer 3
run 1	51.77	50.22	51.20
run 2	50.92	51.81	51.81
run 3	50.29	52.31	52.93
run 4	50.42	51.08	51.44
run 5	50.85	52.23	52.09
performance index	2.12×10^{-4}		
slope	1.015		
overall uniformity	1.51 %		

[run 8]

	wafer 1	wafer 2	wafer 3
run 1	53.43	52.72	50.51
run 2	52.04	50.08	50.69
run 3	53.37	51.70	50.93
run 4	53.38	52.05	51.85
run 5	52.58	50.59	50.49
performance index	8.59×10^{-4}		
slope	-1.996		
overall uniformity	2.17 %		

[run 9]

	wafer 1	wafer 2	wafer 3
run 1	50.94	50.68	51.35
run 2	50.70	50.93	51.02
run 3	50.98	51.47	51.81
run 4	51.14	51.12	51.17
run 5	51.08	52.67	52.95
performance index	9.18×10^{-5}		
slope	0.674		
overall uniformity	1.25 %		

APPENDIX E
ON-LINE CONTROL USING MULTIPLE SITE MODELS

E.1 Multiple Response Surfaces and On-line Control

The multiple response surface method is used for the on-line control of uniformity, where each measurement site is modeled as a function of the process parameters. The resulting multiple response surfaces are called *multiple site models*. Uniformity of a process is calculated from the multiple site models. Whenever any changes occur in the process conditions, the multiple site models are adapted to describe the measurements accurately, and as a result the uniformity function is also adapted. On-line control is performed by optimizing the uniformity function. The optimization of the uniformity function generates the optimum process parameter values that will be used for the next run of the process. Since the uniformity function is changing due to the adaptation of multiple site models, the optimum process parameter values also change accordingly, which results in on-line control.

The multiple response surface method has the advantage of fast adaptation, since each response surface is constructed using low-order polynomials, which have a small number of coefficients to be fitted. Because of this fast adaptation capability, the multiple response surface method is appropriate for the on-line control of processes.

E.2 Uniformity in a Single Wafer Plasma Etching Process

The multiple response surface method was applied to the on-line control of within-a-wafer uniformity in a single wafer plasma etching process using the AutoEtch™ 590 single wafer plasma etcher. The experiments were performed in conjunction with the experiments of Section 3.4.1 to compare the on-line control results with the results of the optimization-only experiments.

In the experiments, gap and CHF_3 were the process parameters. Both process parameters were used to model the multiple site models and to control the uniformity, which was calculated using the multiple site models. Using 12 measurements of etching rates of a wafer as shown in Figure 3.6, relative deviations of each site etching rate from the mean etching rate were modeled as first-order linear functions with an interaction term as follows:

$$\frac{Y_i - \overline{Y}_\bullet}{\overline{Y}_\bullet} = C_{0,i} + C_{1,i}\times(\text{gap}) + C_{2,i}\times(CHF_3) + C_{3,i}\times(\text{gap})\times(CHF_3)\,, \qquad \text{(Eq. E.1)}$$

for i = 1, 2, ..., 12, where $\overline{Y}_\bullet$ is the mean etching rate of 12 measured etching rates for each run.

Since it was found that the relative deviation models have a better fit than the absolute etching rate models, the relative deviation models were used to increase model accuracy. The relative deviations are also best suited for representing within-a-wafer non-uniformity patterns. The overall uniformity was represented with *performance index* defined as follows:

$$\text{performance index} = \sum_{i=1}^{12} \left(\frac{Y_i - \overline{Y}_\bullet}{\overline{Y}_\bullet} \right)^2 . \qquad \text{(Eq. E.2)}$$

The performance index was minimized in order to maximize the within-a-wafer uniformity using a non-linear optimizer.

Using the results of 2^2 full factorial experiments (refer to Section 3.4.1.1), the relative deviations of each site were calculated as listed in Table E.1. The experimental data are listed in Appendix B.1.2.

	exp 1	exp 2	exp 3	exp 4	exp 5	exp 6	exp 7	exp 8
gap (cm)	0.4	0.4	0.6	0.6	0.4	0.4	0.6	0.6
CHF_3 (sccm)	0	15	0	15	0	15	0	15
site 1	0.043	-0.013	-0.009	0.103	0.062	-0.053	-0.017	0.109
site 2	0.044	-0.019	-0.022	0.106	0.063	-0.067	-0.008	0.115
site 3	0.049	-0.015	-0.020	0.125	0.059	-0.045	-0.004	0.129
site 4	0.047	-0.018	-0.016	0.119	0.059	-0.051	-0.007	0.122
site 5	0.018	0.051	-0.067	0.021	0.018	0.066	-0.051	0.037
site 6	0.024	0.069	-0.048	-0.011	0.024	0.071	-0.033	0.028
site 7	0.027	0.071	-0.055	0.165	0.017	0.077	-0.017	0.067
site 8	0.024	0.062	-0.050	0.024	0.011	0.070	-0.035	0.045
site 9	-0.079	-0.065	0.072	-0.135	-0.078	-0.020	0.022	-0.193
site 10	-0.065	-0.025	0.076	-0.189	-0.070	-0.021	0.053	-0.182
site 11	-0.066	-0.039	0.046	-0.126	-0.081	-0.009	0.066	-0.130
site 12	-0.066	-0.059	0.094	-0.203	-0.084	-0.017	0.032	-0.146

Table E.1 Relative deviation data from 2^2 full factorial experiments

The multiple site models for 12 sites were the constructed as shown in Table E.2. Whenever new data were available from the previous run, the multiple site models were adapted by updating the constant terms of each model respectively. The model adaptation algorithm explained in Section 3.4.1.2 was used to update the constant terms.

site	model
1	$0.0280 + 0.0185\times(gap) + 0.0085\times(CHF_3) + 0.0511\times(gap)\times(CHF_3)$
2	$0.0264 + 0.0213\times(gap) + 0.0071\times(CHF_3) + 0.0555\times(gap)\times(CHF_3)$
3	$0.0346 + 0.0228\times(gap) + 0.0138\times(CHF_3) + 0.0559\times(gap)\times(CHF_3)$
4	$0.0320 - 0.0226\times(gap) + 0.0112\times(CHF_3)) + 0.0548\times(gap)\times(CHF_3)$
5	$0.0117 - 0.0267\times(gap) + 0.0323\times(CHF_3) + 0.0120\times(gap)\times(CHF_3)$
6	$0.0154 - 0.0316\times(gap) + 0.0237\times(CHF_3) + 0.0008\times(gap)\times(CHF_3)$
7	$0.0440 - 0.0039\times(gap) + 0.0511\times(CHF_3) + 0.0251\times(gap)\times(CHF_3)$
8	$0.0188 - 0.0229\times(gap) + 0.0314\times(CHF_3) + 0.0073\times(gap)\times(CHF_3)$
9	$-0.0595 + 0.0011\times(gap) - 0.0437\times(CHF_3) - 0.0618\times(gap)\times(CHF_3)$
10	$-0.0529 - 0.0077\times(gap) - 0.0514\times(CHF_3) - 0.0738\times(gap)\times(CHF_3)$
11	$-0.0423 + 0.0062\times(gap) - 0.0338\times(CHF_3) - 0.0584\times(gap)\times(CHF_3)$
12	$-0.0562 + 0.0004\times(gap) - 0.0501\times(CHF_3) - 0.0685\times(gap)\times(CHF_3)$

Table E.2 12 site models from 2^2 full factorial experiment data

In order to compare the results of on-line control based on multiple site models, the experiments were performed at the same time as the optimization-only experiments, whose parameter values were fixed. Table E.3 shows the parameter values for the optimization-only experiments and the on-line control experiments, respectively. A total of 15 runs of the experiments were performed with a step change introduced after the 9th run as explained in Section 3.4.1.2. The experimental data are listed in Appendix E.4.

	optimization-only	on-line control
pressure (torr)	3	3
power (watts)	900	900
gap (cm)	0.53	control parameter
He flow rate (sccm)	200	200
CHF_3 flow rate (sccm)	0	control parameter
CF_4 flow rate (sccm)	20	20
process time	40	40

Table E.3 Process parameter values for experiments

Table E.4 lists the historical data of the constant terms of all 12 multiple site models for 15 runs of the experiments.

	run 1	run 2	run 3	run 4	run 5	run 6	run 7	run 8	run 9
site 1	0.0280	0.0711	0.0935	0.0107	0.0607	0.0102	0.0678	0.0577	0.0228
site 2	0.0264	0.0785	0.0946	0.0104	0.0576	0.0298	0.0651	0.0451	0.0130
site 3	0.0346	0.0921	0.1006	0.0181	0.0660	0.0348	0.0755	0.0482	0.0096
site 4	0.0320	0.0804	0.0951	0.0114	0.0600	0.0211	0.0659	0.0374	0.0018
site 5	0.0117	-0.0317	0.0087	0.0308	-0.0273	0.0126	0.0230	-0.0061	-0.0169
site 6	0.0154	-0.0295	-0.0235	0.0353	-0.0296	0.0170	0.0119	-0.0170	-0.0305
site 7	0.0440	0.0077	0.0142	0.0709	0.0013	0.0671	0.0363	0.0571	0.0535
site 8	0.0188	-0.0224	-0.0130	0.0424	-0.0293	0.0274	0.0152	0.0062	0.0290
site 9	-0.0595	-0.0741	-0.0768	-0.0585	-0.0351	-0.0779	-0.1002	-0.1203	-0.0722
site 10	-0.0529	-0.0674	-0.0888	0.0000	-0.0325	-0.0592	-0.0872	-0.1132	-0.0768
site 11	-0.0423	-0.0334	-0.0825	-0.0287	-0.0291	-0.0214	-0.0747	0.0301	0.0370
site 12	-0.0562	-0.0713	-0.1221	-0.0866	-0.0627	-0.0614	-0.0984	-0.0253	0.0297

Table E.4 Adapted constants for on-line control experiments

	run 10	run 11	run 12	run 13	run 14	run 15
site 1	0.0228	-0.0838	-0.2340	-0.2618	-0.2100	-0.2085
site 2	0.0130	-0.1446	-0.3054	-0.2732	-0.2647	-0.2164
site 3	0.0096	-0.0879	-0.2840	-0.2451	-0.2481	-0.2278
site 4	0.0018	-0.0516	-0.2293	-0.2458	-0.2038	-0.2281
site 5	-0.0169	0.0226	0.0587	-0.0691	0.0216	0.0034
site 6	-0.0305	-0.0483	-0.0768	-0.0214	-0.0582	0.0706
site 7	0.0535	0.0404	-0.1300	-0.0109	-0.1174	-0.0987
site 8	0.0290	0.0652	0.0390	-0.0113	0.0259	-0.0904
site 9	-0.0722	0.0757	0.4245	0.1731	0.3382	0.2641
site 10	-0.0768	0.0507	0.2722	0.3219	0.2335	0.4927
site 11	0.0370	0.0839	0.1195	0.3953	0.1361	0.1683
site 12	0.0297	0.0775	0.3456	0.2484	0.3469	0.0708

Table E.4 Adapted constants for on-line control experiments (continued)

Figure E.1 shows the contour plots of the performance index function that is calculated from the multiple site models. The contour plots were constructed to show the optimum process parameter values for each run using the multiple site models adapted using the data of the previous run. In the figures, the black dots indicate the position of the optimum process parameter values for the next run.

As explained in Section 3.4.1.2, a step change was introduced after the 9th run to check the effectiveness of on-line control. It is shown in Figure E.1 that the effect of the step change on the multiple site models was so large that the contour of the performance index changed significantly before and after the step change.

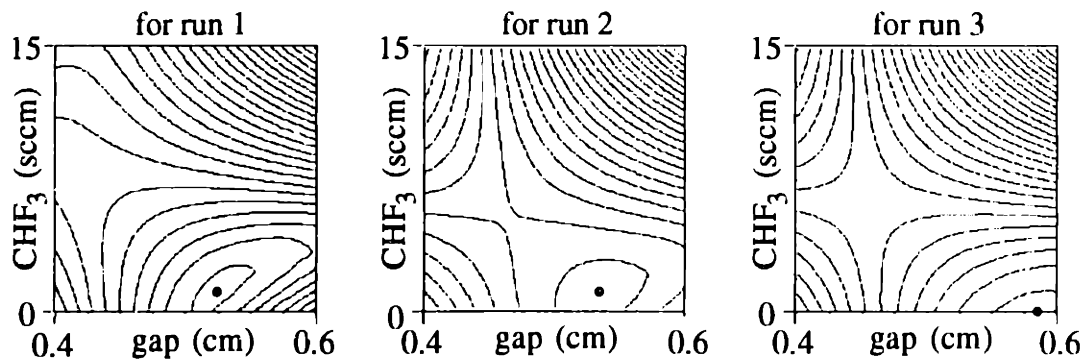

Figure E.1 Performance index contours
and optimizing process parameter values for each run

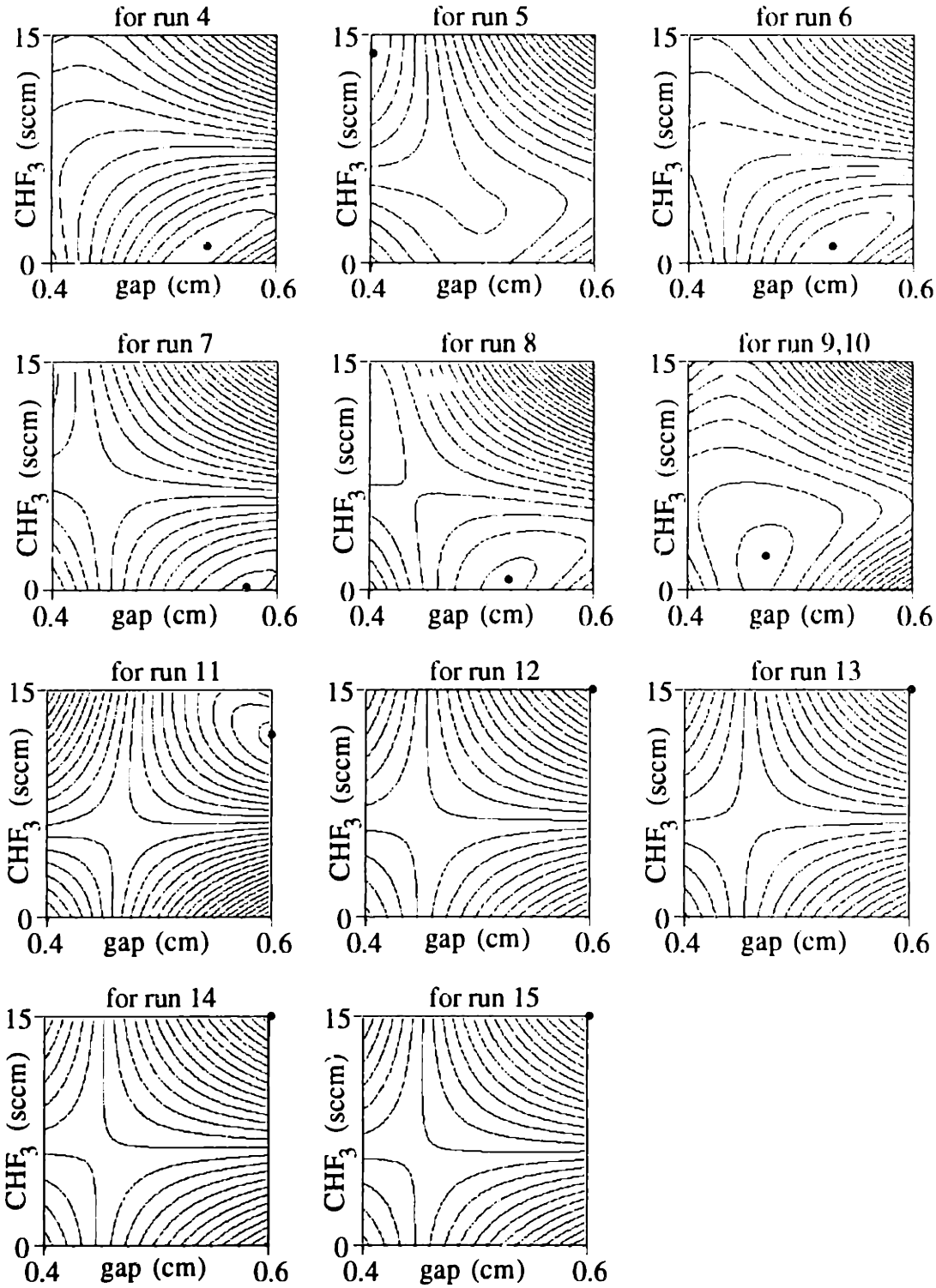

Figure E.1 Performance index contours
and optimizing process parameter values for each run (continued)

Figure E.2 shows the historical data of overall uniformity defined in Eq. 3.9. It is noted that the on-line control using the multiple site models was effective in controlling the process uniformity before the step change (from 1st run to 9th run), while the optimization-only experiments showed large variations. The on-line control using the multiple site models, however, resulted in worse overall uniformity than the optimization-only experiments after the step change was introduced (from after 11th run).

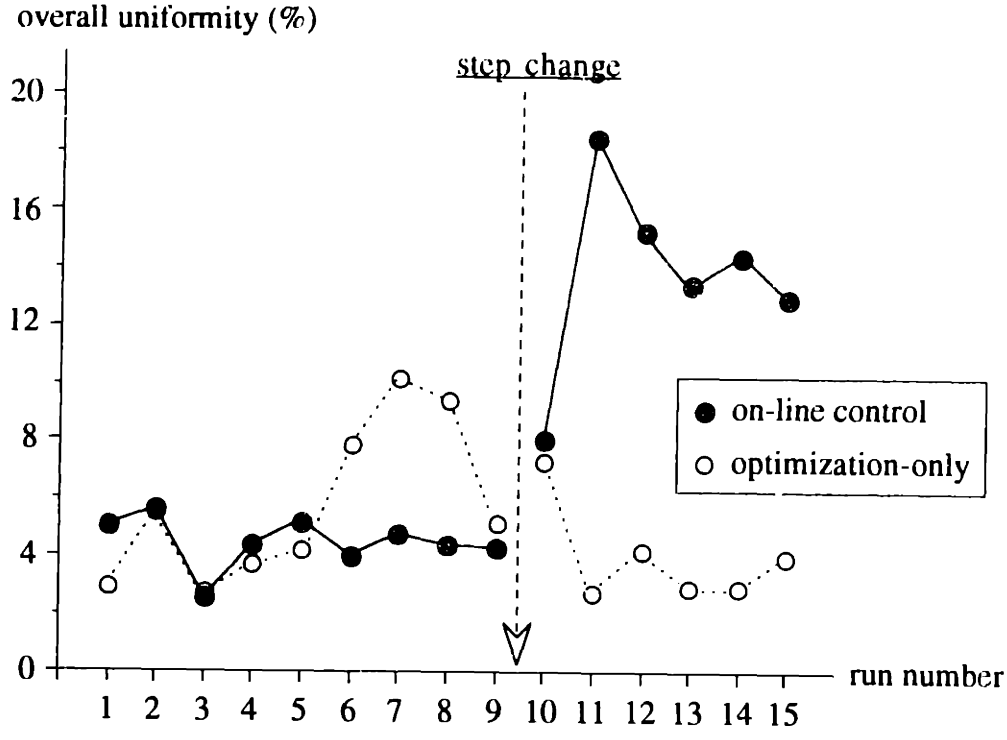

Figure E.2 Historical data of the overall uniformity

E.3 Discussions

The application of the multiple response surface method to the on-line control of uniformity in a single wafer plasma etching process showed that the on-line control improved the overall uniformity by a factor of 1.3 when no step change was introduced. However, when there was a step change in process conditions, control based or multiple site models was unable to control the overall uniformity properly. Figure E.3 shows the overall uniformity of the optimization-only experiments and on-line control

experiments before and after the step change. In the figure, the error bars represent the magnitude of two standard deviations of the average overall uniformity values.

The on-line control using the multiple site models was effective when the process was relatively stable. When the process condition experienced a step change, the multiple site models were not robust enough to describe the process condition correctly. Since the multiple site models describe both non-tunable variability and tunable variability, it is difficult to expect robust prediction capability of the models when the process conditions experience a stepwise change.

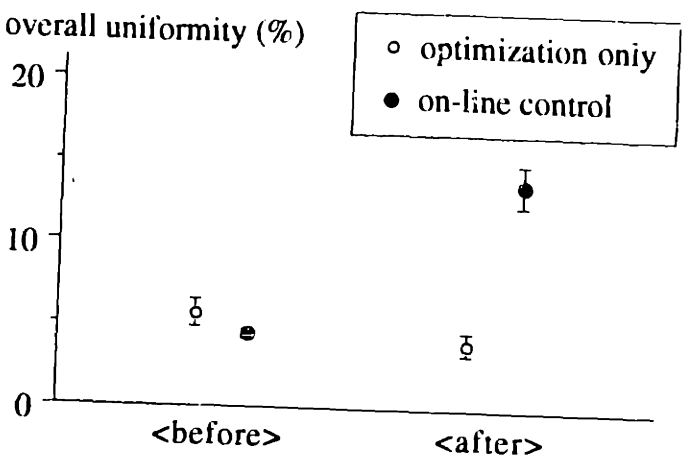

Figure E.3 Average overall uniformity before and after the step change

E.4 Experiment Data

[run 1]

site	thickness (Å) before	thickness (Å) after	etching rate (Å/min)	relative deviation
1	7732	6211	2281.5	0.054
2	7786	6253	2299.5	0.063
3	7738	6194	2316.0	0.070
4	7679	6148	2296.5	0.061
5	7697	6360	2005.5	-0.073
6	7853	6499	2031.0	-0.061
7	7731	6358	2059.5	-0.048
8	7523	6168	2032.5	-0.061
9	7569	6149	2130.0	-0.016
10	7835	6394	2161.5	-0.001
11	7695	6229	2199.0	0.016
12	7201	5766	2152.5	-0.005
overall uniformity			5.10 %	

[run 2]

site	thickness (Å) before	thickness (Å) after	etching rate (Å/min)	relative deviation
1	8488	6915	2359.5	0.077
2	8608	7032	2364.0	0.079
3	8550	6974	2364.0	0.079
4	8420	6848	2358.0	0.076
5	8435	7022	2119.5	-0.033
6	8718	7338	2070.0	-0.055
7	8585	7185	2100.0	-0.042
8	8156	6770	2079.0	-0.051
9	8280	6846	2151.0	-0.018
10	8681	7253	2142.0	-0.022
11	8543	7130	2119.5	-0.033
12	7718	6339	2068.5	-0.056
overall uniformity			5.60 %	

[run 3]

site	thickness (Å) before	thickness (Å) after	etching rate (Å/min)	relative deviation
1	8257	7139	1677.0	-0.021
2	8288	7170	1677.0	-0.021
3	8270	7150	1680.0	-0.019
4	8226	7110	1674.0	-0.022
5	8233	7124	1663.5	-0.029
6	8325	7196	1693.5	-0.011
7	8289	7148	1711.5	-0.001
8	8072	6942	1695.0	-0.010
9	8165	6990	1762.5	0.029
10	8365	7176	1783.5	0.042
11	8319	7120	1798.5	0.050
12	7642	6487	1732.5	0.012
overall uniformity			2.58 %	

[run 4]

site	thickness (Å) before	thickness (Å) after	etching rate (Å/min)	relative deviation
1	8495	6659	2754.0	0.052
2	8515	6682	2749.5	0.050
3	8504	6668	2754.0	0.052
4	8475	6645	2745.0	0.049
5	8473	6832	2461.5	-0.060
6	8527	6875	2478.0	-0.053
7	8512	6854	2487.0	-0.050
8	8363	6724	2458.5	-0.061
9	8387	6627	2640.0	0.009
10	8521	6743	2667.0	0.019
11	8508	6755	2629.5	0.005
12	8023	6300	2584.5	-0.013
overall uniformity			4.43 %	

[run 5]

site	thickness (Å) before	thickness (Å) after	etching rate (Å/min)	relative deviation
1	8821	4693	6192.0	-0.040
2	8848	4666	6273.0	-0.027
3	8834	4617	6325.5	-0.019
4	8798	4644	6231.0	-0.033
5	8787	4256	6796.5	0.054
6	8867	4288	6868.5	0.065
7	8840	4155	7027.5	0.090
8	8675	4085	6885.0	0.068
9	8672	4657	6022.5	-0.066
10	8856	4709	6220.5	-0.035
11	8820	4563	6385.5	-0.010
12	8312	4222	6135.0	-0.048
overall uniformity			5.14 %	

[run 6]

site	thickness (Å) before	thickness (Å) after	etching rate (Å/min)	relative deviation
1	9907	7143	4146.0	0.056
2	9930	7170	4140.0	0.055
3	9895	7125	4155.0	0.058
4	9865	7113	4128.0	0.051
5	9903	7320	3874.5	-0.013
6	9959	7381	3867.0	-0.015
7	9827	7256	3856.5	-0.018
8	9756	7189	3850.5	-0.019
9	9891	7405	3729.0	-0.050
10	9897	7356	3811.5	-0.029
11	9439	6912	3790.5	-0.035
12	9396	6887	3763.5	-0.041
overall uniformity			4.03 %	

[run 7]

site	thickness (Å) before	thickness (Å) after	etching rate (Å/min)	relative deviation
1	6780	6103	1015.5	0.030
2	6794	6125	1003.5	0.017
3	6778	6111	1000.5	0.014
4	6755	6093	993.0	0.007
5	6885	6268	925.5	-0.062
6	6917	6299	927.0	-0.060
7	6883	6233	975.0	-0.011
8	6754	6125	943.5	-0.043
9	6653	6021	948.0	-0.039
10	6792	6149	964.5	-0.022
11	6776	6051	1087.5	0.103
12	6303	5602	1051.5	0.066
overall uniformity			4.81 %	

[run 8]

site	thickness (Å) before	thickness (Å) after	etching rate (Å/min)	relative deviation
1	7233	6423	1215.0	0.008
2	7248	6445	1204.5	-0.001
3	7237	6442	1192.5	-0.011
4	7212	6421	1186.5	-0.016
5	7268	6510	1137.0	-0.057
6	7274	6519	1132.5	-0.061
7	7251	6450	1201.5	-0.003
8	7121	6324	1195.5	-0.008
9	7131	6340	1186.5	-0.016
10	7183	6389	1191.0	-0.012
11	7188	6317	1306.5	0.084
12	6733	5854	1318.5	0.094
overall uniformity			4.43 %	

[run 9]

site	thickness (Å) before	thickness (Å) after	etching rate (Å/min)	relative deviation
1	6340	5456	1326.0	0.067
2	6365	5486	1318.5	0.061
3	6346	5481	1297.5	0.044
4	6324	5467	1285.5	0.035
5	6494	5703	1186.5	-0.045
6	6551	5758	1189.5	-0.043
7	6498	5693	1207.5	-0.028
8	6360	5563	1195.5	-0.038
9	6220	5437	1174.5	-0.055
10	6346	5538	1212.0	-0.025
11	6296	5438	1287.0	0.036
12	5802	4982	1230.0	-0.010
overall uniformity			4.33 %	

[run 10]

site	thickness (Å) before	thickness (Å) after	etching rate (Å/min)	relative deviation
1	7837	6609	1842.0	-0.084
2	7862	6714	1722.0	-0.144
3	7877	6660	1825.5	-0.093
4	7829	6561	1902.0	-0.054
5	7678	6324	2031.0	0.010
6	7778	6512	1899.0	-0.056
7	7811	6457	2031.0	0.010
8	7706	6297	2113.5	0.051
9	7292	5825	2200.5	0.094
10	7374	5933	2161.5	0.075
11	7707	6240	2200.5	0.094
12	7733	6259	2211.0	0.099
overall uniformity			8.08 %	

[run 11]

site	thickness (Å) before	thickness (Å) after	etching rate (Å/min)	relative deviation
1	8391	7470	1381.5	-0.174
2	8427	7580	1270.5	-0.240
3	8391	7513	1317.0	-0.212
4	8354	7418	1404.0	-0.160
5	8257	7072	1777.5	0.063
6	8402	7389	1519.5	-0.091
7	8298	7273	1537.5	-0.081
8	8199	7036	1744.5	0.043
9	7869	6362	2260.5	0.352
10	8314	7002	1968.0	0.177
11	8253	7070	1774.5	0.061
12	7969	6561	2112.0	0.263
overall uniformity			18.43 %	

[run 12]

site	thickness (Å) before	thickness (Å) after	etching rate (Å/min)	relative deviation
1	5781	4892	1333.5	-0.184
2	5909	5026	1324.5	-0.189
3	5817	4894	1384.5	-0.153
4	5706	4788	1377.0	-0.157
5	5291	4258	1549.5	-0.052
6	5629	4571	1587.0	-0.029
7	5437	4281	1734.0	0.061
8	5227	4133	1641.0	0.004
9	4557	3393	1746.0	0.069
10	5195	3900	1942.5	0.189
11	5211	3785	2139.0	0.309
12	4760	3529	1846.5	0.130
overall uniformity			15.22 %	

[run 13]

site	thickness (Å) before	thickness (Å) after	etching rate (Å/min)	relative deviation
1	8039	7009	1545.0	-0.132
2	8067	7095	1458.0	-0.181
3	8043	7041	1503.0	-0.156
4	8022	6972	1575.0	-0.115
5	7888	6655	1849.5	0.039
6	8020	6911	1663.5	-0.065
7	7922	6789	1699.5	-0.045
8	7955	6719	1854.0	0.042
9	7577	6113	2196.0	0.234
10	7975	6669	1959.0	0.101
11	7865	6619	1869.0	0.050
12	8009	6551	2187.0	0.229
overall uniformity			13.44 %	

[run 14]

site	thickness (Å) before	thickness (Å) after	etching rate (Å/min)	relative deviation
1	5131	3884	1870.5	-0.130
2	5219	3975	1866.0	-0.132
3	5148	3908	1860.0	-0.135
4	5061	3827	1851.0	-0.139
5	4766	3302	2196.0	0.021
6	5005	3480	2287.5	0.063
7	4807	3411	2094.0	-0.026
8	4760	3433	1990.5	-0.075
9	4201	2538	2494.5	0.160
10	4688	2738	2925.0	0.360
11	4557	3005	2328.0	0.082
12	4608	3242	2049.0	-0.047
overall uniformity			14.35 %	

[run 15]

site	thickness (Å) before	thickness (Å) after	etching rate (Å/min)	relative deviation
1	7597	6421	1764.0	-0.114
2	7668	6544	1686.0	-0.153
3	7638	6503	1702.5	-0.145
4	7561	6395	1749.0	-0.121
5	7360	5894	2199.0	0.105
6	7585	6311	1911.0	-0.040
7	7448	6189	1888.5	-0.051
8	7413	6058	2032.5	0.021
9	6966	5241	2587.5	0.300
10	7430	6007	2134.5	0.072
11	7323	6009	1971.0	-0.010
12	7493	5988	2257.5	0.134
overall uniformity			12.94 %	

APPENDIX F
SEQUENTIAL OPTIMIZATION USING ALL PARAMETERS

F.1 Introduction

Process uniformity was optimized by applying the sequential optimization method. In the optimization, the objective function was modeled as a function of all the process parameters of a process. Optimization was performed using a commercial software package called Ultramax® [15].

All the process parameters were used in the sequential optimization, with the expectation that the process behavior would be described more accurately with all the process parameters. The objective function to be optimized was constructed using multiple response surfaces so that model adaptation would be performed quickly and efficiently as the sequential optimizer approached the optimum point. Multiple process output characteristics were modeled as linear functions of all the process parameters, and the objective function was calculated using the multiple response surface models to evaluate the uniformity of the process output characteristics.

F.2 Uniformity in a Single Wafer Plasma Etching Process

Sequential optimization, using all the process parameters was performed to optimize within-a-wafer uniformity in a single wafer plasma etching process using the AutoEtch™ 590 single wafer plasma etcher. Included first in the characterization

experiments of the process were all the process parameters, i.e., RF plasma power (power), pressure of the reaction chamber (pressure), gap spacing between the top and bottom electrodes (gap), He gas flow rate (He), CHF_3 gas flow rate (CHF_3), and CF_4 gas flow rate(CF_4). In the characterization experiments, 9 sites of a wafer were selected as measurement sites as shown in Figure F.1. From the understanding that the equipment has an axisymmetric configuration, it was decided to model the output characteristics of the process, $\overline{Y}_1$, $\overline{Y}_2$, and $\overline{Y}_3$, as follows:

$$\overline{Y}_1 = Y_1 \ , \qquad \text{(Eq. F.1)}$$

$$\overline{Y}_2 = \frac{Y_2 + Y_3 + Y_4 + Y_5}{4} \ , \qquad \text{(Eq. F.2)}$$

and

$$\overline{Y}_3 = \frac{Y_6 + Y_7 + Y_8 + Y_9}{4} \ , \qquad \text{(Eq. F.3)}$$

where Y_i's are etching rates at measurement site i (for i = 1, 2, ..., 9).

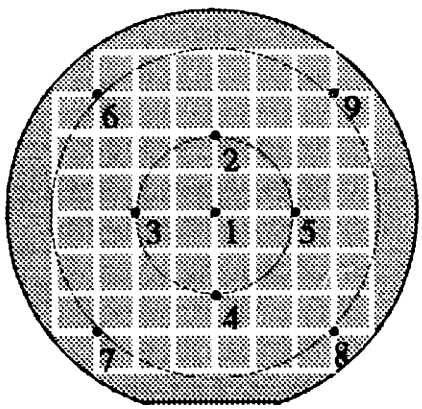

• : measurement site

Figure F.1 Positions of 9 measurement sites on a wafer

During the modeling of $\overline{Y}_1$, $\overline{Y}_2$, and $\overline{Y}_3$, it was found that pressure does not have a significant effect on the models, and the output characteristics were modeled as first order linear functions of power, gap, He, CHF_3, and CF_4 as follows:

$$\overline{Y}_1 = C_0 + C_1\times(\text{power}) + C_2\times(\text{gap}) + C_3\times(\text{He}) + C_4\times(CHF_3) + C_5\times(CF_4) \ , \qquad \text{(Eq. F.4)}$$

$$\overline{Y}_2 = D_0 + D_1\times(\text{power}) + D_2\times(\text{gap}) + D_3\times(\text{He}) + D_4\times(CHF_3) + D_5\times(CF_4) \ , \qquad \text{(Eq. F.5)}$$

and

$$\overline{Y}_3 = E_0 + E_1\times(\text{power}) + E_2\times(\text{gap}) + E_3\times(\text{He}) + E_4\times(CHF_3) + E_5\times(CF_4)\ . \quad \text{(Eq. F.6)}$$

The coefficients of the models above were first decided by the sequential optimizer according to the measurement data and were updated as new data became available in order to describe the process conditions more correctly.

After the output characteristics were modeled, an objective function called *performance index* was defined to represent the uniformity of the process as follows:

$$\text{performance index} = \sqrt{\left(\frac{\overline{Y}_1 - \overline{Y}_\bullet}{\overline{Y}_\bullet}\right)^2 + \left(\frac{\overline{Y}_2 - \overline{Y}_\bullet}{\overline{Y}_\bullet}\right)^2 + \left(\frac{\overline{Y}_3 - \overline{Y}_\bullet}{\overline{Y}_\bullet}\right)^2}\ , \quad \text{(Eq. F.7)}$$

$$\text{where} \quad \overline{Y}_\bullet = \sum_{i=1}^{9} Y_i\ . \quad \text{(Eq. F.8)}$$

The performance index defined above represents the radial uniformity.

Sequential optimization experiments were performed using the process parameter values that were designed by the sequential optimizer. The process parameter values were chosen so the performance index may be optimized using the output characteristic functions, whose coefficients were updated using the measurement data up to that point. The process parameter values for each run are listed in Table F.1. The experimental data are listed in Appendix F.4.

run number	pressure (torr)	gap (cm)	He flow rate (sccm)	CHF_3 flow rate (sccm)	CF_4 flow rate (sccm)
1	500	0.30	100	15	45
2	677	0.34	133	28	50
3	762	0.39	123	26	82
4	794	0.31	129	36	79
5	646	0.34	146	34	105
6	667	0.34	124	44	76
7	692	0.30	135	39	78
8	508	0.32	131	38	73
9	626	0.32	149	38	62
10	627	0.30	139	44	82

Table F.1 Process parameter values in sequential optimization experiments

The results of the sequential optimization experiments are shown in Figure F.2, where the performance index is shown to be improved sequentially as the optimization sequence continued. The fluctuations of the performance index in the sequential optimization are due to the exploration of the parameter space.

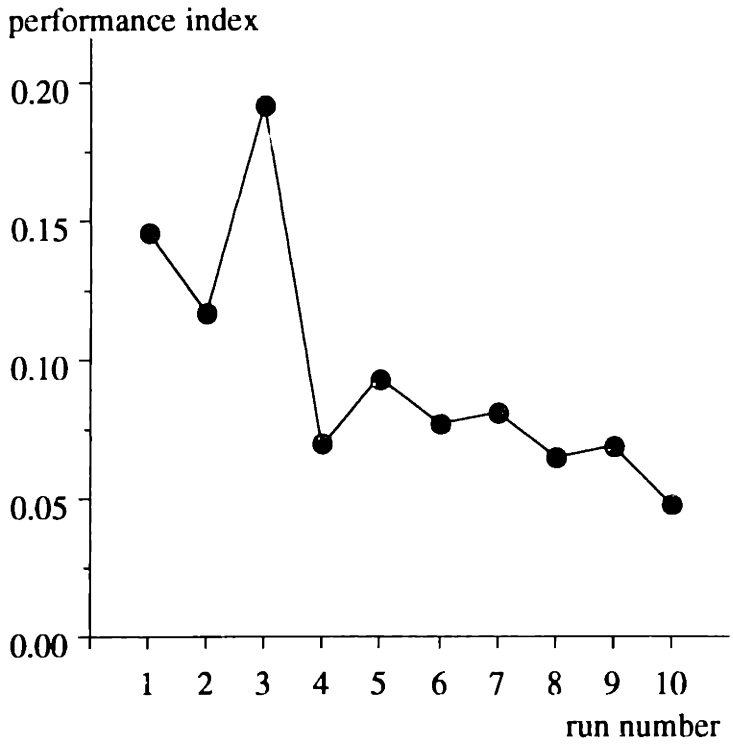

Figure F.2 Performance index in sequential optimization

F.3 Discussions

Within-a-wafer uniformity in a single wafer plasma etching process was optimized using a sequential optimization method. The performance index, which was defined to represent within-a-wafer uniformity, was shown to be optimized sequentially.

The performance index was calculated using the output characteristics defined in Eqs. F.1, F.2, and F.3. It is noted that the output characteristics represent only the radial etching rate profile, and information on the magnitudes of circumferential variation was not included in modeling the output characteristics. The process

parameters were not classified either. Therefore, it was shown that the actual within-a-wafer uniformity, which is defined as in Eq. 3.9, was not improved even though the performance index was shown to be improved. The historical data of overall uniformity is shown in Figure F.3; little improvement is indicated because improvement of the performance index was offset by the degraded circumferential uniformity.

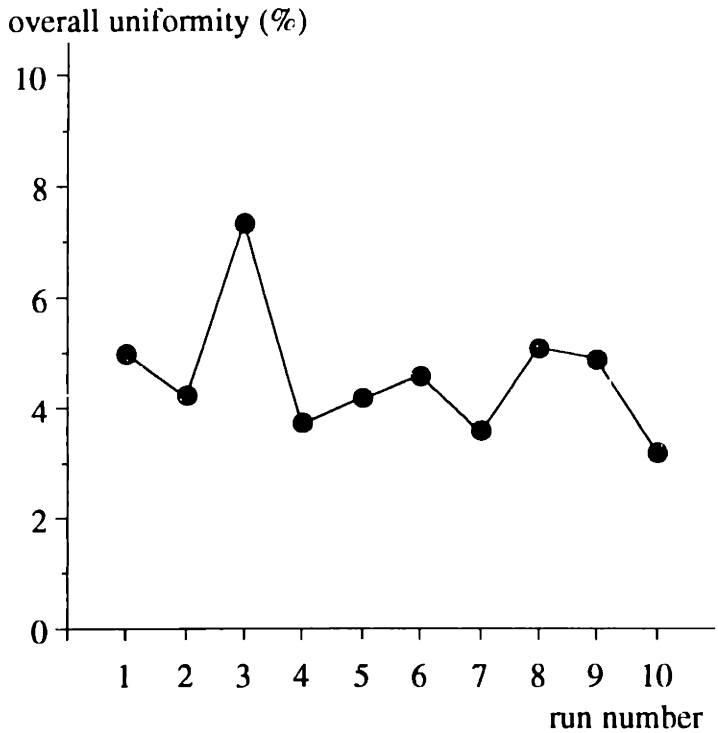

Figure F.3 Overall uniformity in sequential optimization

Therefore it is concluded that it is necessary to optimize the radial uniformity as well as the circumferential uniformity to improve overall uniformity in the single wafer plasma etching process. It is also shown that the use of all the process parameters for the optimization of the radial uniformity can deteriorate the circumferential uniformity. Hence, it is necessary to select a as small as possible number of process parameters for the effective control of the radial uniformity without degrading the circumferential uniformity.

F.4 Experiment Data

[run 1]

site	thickness (Å) before	thickness (Å) after	etching rate (Å/min)
1	6299	4270	6087.0
2	6412	4287	6375.0
3	6271	4101	6510.0
4	6234	4090	6432.0
5	6266	4144	6366.0
6	6323	4399	5772.0
7	6032	4050	5946.0
8	6308	4390	5754.0
9	6331	4432	5697.0
performance index		0.146	
overall uniformity		5.00 %	

[run 2]

site	thickness (Å) before	thickness (Å) after	etching rate (Å/min)
1	6359	3562	8391.0
2	6522	3558	8892.0
3	6328	3337	8973.0
4	6266	3260	9018.0
5	6329	3299	9090.0
6	6435	3737	8094.0
7	6079	3234	8535.0
8	6331	3510	8463.0
9	6515	3812	8109.0
performance index		0.117	
overall uniformity		4.24 %	

[run 3]

site	thickness (Å) before	thickness (Å) after	etching rate (Å/min)
1	6399	3158	9723.0
2	6528	3216	9936.0
3	6368	2910	10374.0
4	6315	2914	10203.0
5	6363	3152	9633.0
6	6423	3419	9012.0
7	6096	3078	9054.0
8	6369	3369	9000.0
9	6463	3785	8034.0
performance index		0.192	
overall uniformity		7.34 %	

[run 4]

site	thickness (Å) before	thickness (Å) after	etching rate (Å/min)
1	6300	3389	8733.0
2	6429	3430	8997.0
3	6288	3221	9201.0
4	6221	3128	9279.0
5	6267	3325	8826.0
6	6408	3467	8823.0
7	6051	3037	9042.0
8	6324	3456	8604.0
9	6383	3680	8109.0
performance index		0.070	
overall uniformity		3.75 %	

[run 5]

site	thickness (Å)		etching rate (Å/min)
	before	after	
1	6583	3935	7944.0
2	6677	3893	8352.0
3	6593	3763	8490.0
4	6518	3785	8199.0
5	6525	3871	7962.0
6	6633	3925	8124.0
7	6406	3797	7827.0
8	6415	3881	7602.0
9	6639	4186	7359.0
performance index		0.093	
overall uniformity		4.22 %	

[run 6]

site	thickness (Å)		etching rate (Å/min)
	before	after	
1	6346	4227	6357.0
2	6475	4306	6507.0
3	6323	4028	6885.0
4	6265	3921	7032.0
5	6332	4128	6612.0
6	6406	4205	6603.0
7	6278	4055	6669.0
8	5928	3734	6582.0
9	6520	4553	5901.0
performance index		0.077	
overall uniformity		4.60 %	

[run 7]

site	thickness (Å)		etching rate (Å/min)
	before	after	
1	6332	3795	7611.0
2	6443	3807	7908.0
3	6294	3633	7983.0
4	6261	3565	8088.0
5	6345	3757	7764.0
6	6259	3743	7548.0
7	6446	3822	7872.0
8	5866	3396	7410.0
9	6448	4056	7176.0
performance index		0.081	
overall uniformity		3.61 %	

[run 8]

site	thickness (Å)		etching rate (Å/min)
	before	after	
1	6500	4572	5784.0
2	6630	4688	5826.0
3	6480	4446	6102.0
4	6412	4255	6471.0
5	6462	4423	6117.0
6	6579	4688	5673.0
7	6399	4305	6282.0
8	6070	4010	6180.0
9	6627	4807	5460.0
performance index		0.065	
overall uniformity		5.08 %	

[run 9]

site	thickness (Å)		etching rate (Å/min)
	before	after	
1	6574	4261	6939.0
2	6703	4351	7056.0
3	6531	4108	7269.0
4	6488	3958	7590.0
5	6550	4142	7224.0
6	6605	4357	6744.0
7	6437	3958	7437.0
8	6095	3669	7278.0
9	6696	4566	6390.0
performance index		0.069	
overall uniformity		4.89 %	

[run 10]

site	thickness (Å)		etching rate (Å/min)
	before	after	
1	6622	4266	7068.0
2	6777	4351	7278.0
3	6560	4080	7440.0
4	6509	4063	7338.0
5	6621	4249	7116.0
6	6618	4250	7104.0
7	6447	3986	7383.0
8	6056	3679	7131.0
9	6769	4562	6621.0
performance index		0.048	
overall uniformity		3.22 %	